AD-774 851

# SUMMARY OF PROPELLER DESIGN PROCEDURES AND DATA. VOLUME I. AERODYNAMIC DESIGN AND INSTALLATION

Henry V. Borst

Henry V. Borst and Associates

Prepared for:

Army Air Mobility Research and Development Laboratory

November 1973

DISTRIBUTED BY:

NTIS

National Technical Information Service
U. S. DEPARTMENT OF COMMERCE
5285 Port Royal Road, Springfield Va. 22151

## DISCLAIMERS

The findings in this report are not to be construed as an official Department of the Army position unless so designated by other authorized documents.

When Government drawings, specifications, or other data are used for any purpose other than in connection with a definitely related Government procurement operation, the United States Government thereby incurs no responsibility nor any obligation whatsoever; and the fact that the Government may have formulated, furnished, or in any way supplied the said drawings, specifications, or other data is not to be regarded by implication or otherwise as in any manner licensing the holder or any other person or corporation, or conveying any rights or permission, to manufacture, use, or sell any patented invention that may in any way be related thereto.

Trade names cited in this report do not constitute an official endorsement or approval of the use of such commercial hardware or software.

## DISPOSITION INSTRUCTIONS

Destroy this report when no longer needed. Do not return it to the originator.

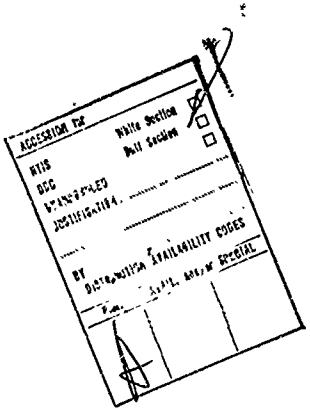

Unclassified

Security Classification

AD-774831

## DOCUMENT CONTROL DATA - R & D

*(Security classification of title, body of abstract and indexing annotation must be entered when the overall report is classified)*

| 1. ORIGINATING ACTIVITY (Corporate author) | 2a. REPORT SECURITY CLASSIFICATION |
|---|---|
| Henry V. Borst & Associates<br>353 Yorkshire Road<br>Rosemont, Pennsylvania | Unclassified<br>2b. GROUP |

3. REPORT TITLE

SUMMARY OF PROPELLER DESIGN PROCEDURES AND DATA
VOLUME I - AERODYNAMIC DESIGN AND INSTALLATION

4. DESCRIPTIVE NOTES (Type of report and inclusive dates)

5. AUTHOR(S) (First name, middle initial, last name)

Henry V. Borst

| 6. REPORT DATE | 7a. TOTAL NO. OF PAGES | 7b. NO. OF REFS |
|---|---|---|
| November 1973 | ~~319~~ 323 | 68 |

| 8a. CONTRACT OR GRANT NO. | 9a. ORIGINATOR'S REPORT NUMBER(S) |
|---|---|
| DAAJ02-72-C-0033<br>b. PROJECT NO.<br>c. Task 1G162207AA7203<br>d. | USAAMRDL Technical Report 73-34A<br>9b. OTHER REPORT NO(S) (Any other numbers that may be assigned this report) |

10. DISTRIBUTION STATEMENT

Approved for public release; distribution unlimited.

| 11. SUPPLEMENTARY NOTES | 12. SPONSORING MILITARY ACTIVITY |
|---|---|
| Volume I of a 3-volume report | Eustis Directorate<br>U.S. Army Air Mobility R&D Laboratory<br>Fort Eustis, Virginia |

13. ABSTRACT

The technology needed for the design and installation of propellers is presented and summarized in three volumes.

Volume I (Aerodynamic Design and Installation) contains the basic theory and necessary design procedures for establishing the external geometry and performance of any propeller. The procedures and data which apply for both single and dual rotation propellers are established for the entire range of flight conditions. The performance of propellers operating at off design condition, high values of shaft angle of attack and negative thrust condition is given.

Reproduced by
NATIONAL TECHNICAL
INFORMATION SERVICE
U.S Department of Commerce
Springfield VA 22151

DD FORM 1 NOV 68 1473 REPLACES DD FORM 1473, 1 JAN 64, WHICH IS OBSOLETE FOR ARMY USE.

Unclassified

Security Classification

323

Unclassified

Security Classification

| 14. KEY WORDS | LINK A | | LINK B | | LINK C | |
|---|---|---|---|---|---|---|
| | ROLE | WT | ROLE | WT | ROLE | WT |
| Propellers - Design | | | | | | |
| Dual-Rotation Propellers | | | | | | |
| Controls - Propellers | | | | | | |
| Aerodynamics - Propellers | | | | | | |
| Propeller Performance | | | | | | |
| Blades - Propellers | | | | | | |
| Propulsion | | | | | | |
| Turboprops | | | | | | |
| Aircraft | | | | | | |
| V/STOL Aircraft Propellers | | | | | | |
| STOL Aircraft Propellers | | | | | | |
| Composite Structure Blades | | | | | | |
| Propeller Deicing | | | | | | |
| Propeller Maintenance | | | | | | |

Unclassified

Security Classification

AD-774831

DEPARTMENT OF THE ARMY
U. S. ARMY AIR MOBILITY RESEARCH & DEVELOPMENT LABORATORY
EUSTIS DIRECTORATE
FORT EUSTIS, VIRGINIA 23604

## ERRATUM

USAAMRDL Technical Report 73-34A
TITLE: Summary of Propeller Design Procedures and Data, Volume I - Aerodynamic Design and Installation

On Figures 121 - 133, the broken line curves are $C_T$ and the solid line curves are $C_P$.

12

DEPARTMENT OF THE ARMY
U. S. ARMY AIR MOBILITY RESEARCH & DEVELOPMENT LABORATORY
EUSTIS DIRECTORATE
FORT EUSTIS, VIRGINIA 23604

This report was prepared by Henry V. Borst & Associates under the terms of Contract DAAJ02-72-C-0033. It describes and summarizes available propeller design and performance methods and data needed for the design and installation of propellers for conventional and V/STOL airplanes.

The technical manager for this contract was Mr. James Gomez, Technology Applications Division.

Id

Task 1G162207AA7203
Contract DAAJ02-72-C-0033
USAAMRDL Technical Report 73-34A
November 1973

# SUMMARY OF PROPELLER DESIGN PROCEDURES AND DATA

## VOLUME I

## AERODYNAMIC DESIGN AND INSTALLATION

By

Henry V. Borst

Prepared by

HENRY V. BORST & ASSOCIATES
Rosemont, Pennsylvania

for

EUSTIS DIRECTORATE
U.S. ARMY AIR MOBILITY RESEARCH AND DEVELOPMENT LABORATORY
FORT EUSTIS, VIRGINIA

Approved for public release;
distribution unlimited.

## SUMMARY

This report describes and summarizes the technology needed for the design and installation of propellers for conventional and V/STOL airplanes. The report is contained in three volumes. Only the theory, methods and data that are representative of current design practice are presented.

Volume I (Aerodynamic Design and Installation) contains data on the general design considerations, criteria, installation and qualification requirements of propellers. Also given in Volume I are the basic momentum, the vortex and compressible flow propeller theories. These theories are developed to apply for the operating ranges of zero to those corresponding to Mach numbers in excess of one. Two-dimensional airfoil data for use with the theories are also presented. Included are data for NACA 16 and 6 series sections covering thickness ratios from 4% to 21%. Data for thick airfoil sections and circular cylinders are also given.

The detailed strip analysis procedures for calculating the performance and designing the propellers are also presented. Included is a method for calculating the optimum propeller, short methods of analysis and the necessary material for a computer method. Comparison of the calculated performance with wind-tunnel test data shows excellent agreement, especially when operating in the usual speed range. The details and actual test data are given for calculating the forces and moments at high shaft angles of attack along with the methods for finding performance at the negative thrust and feather conditions. Material is given for the design of spinners, engine inlets and cowlings for the proper installation of the propeller.

Volume II (Structural Analysis and Blade Design) contains the theory and data for the detailed structural and vibration analysis of propellers. Included are estimating procedures for initial design purposes. The details for designing solid, hollow and composite blades are included. With the discussion of the blades are the manufacturing techniques used.

Volume III (Hub, Actuator, and Control Design), the final volume, contains material on the design of the hub and actuator systems. Comparisons of the various types of blade actuators are given along with their description. The theories of propeller controls are presented with the details of the types used with conventional and V/STOL airplanes. A brief discussion of past and future propeller installations is given along with recommendations for future work. The material given in the appendixes contains the design criteria, airfoil data and basics for a computer program to calculate performance.



Best Available Copy

## FOREWORD

The report completes the work summarizing the basic technology of propellers and was done under Contract No. DAAJ02-72-C-0033. The objective of the work was to retain for future use as much of the basic propeller design and analysis technology as possible. The material was prepared from the basic reports contained in the literature and material gathered through working in the field for a number of years. The material presented is based on the experience of individuals who were experts in their particular fields.

The writer acknowledges with thanks the support and help of Messrs. William Amatt, William F. Bates, Edward Sand and Douglas Elliott, Jr., who prepared the sections on propeller structures, blade design, hub and actuator design and control design respectively. It is hoped that the work contained in this report can serve as the basis for future propeller developments and will eliminate repetition of engineering efforts that have already been completed.



Preceding page blank

TABLE OF CONTENTS


| | Page |
|---|---|
| SUMMARY | iii |
| FOREWORD | v |
| LIST OF ILLUSTRATIONS | x |
| LIST OF TABLES | xxi |
| LIST OF SYMBOLS | xxii |
| INTRODUCTION | 1 |
| GENERAL PROPELLER DESIGN CONSIDERATIONS | 4 |
| DESIGN CRITERIA | 4 |
| INSTALLATION CONSIDERATIONS | 5 |
| Aircraft and Engine Characteristics | 5 |
| Performance Requirements | 7 |
| Structural Requirements | 7 |
| Dynamic Characteristics | 10 |
| Noise | 10 |
| Propeller Control Considerations | 11 |
| Weight | 11 |
| Operational Requirements | 12 |
| PROPELLER DESIGN PARAMETERS | 13 |
| OPERATING CONDITIONS - PROPELLER TYPES | 17 |
| PROPELLER SELECTION | 18 |
| DETAILED FINAL PROPELLER DESIGN | 22 |
| Optimum Propeller | 22 |
| Propeller Design | 23 |
| QUALIFICATION PROCEDURES UNDERTAKEN | 24 |
| PRESENT QUALIFICATION REQUIREMENTS | 25 |
| Commercial Propeller Qualifications | 26 |
| Recommendations | 27 |




Preceding page blank

TABLE OF CONTENTS (Continued)


| | Page |
|---|---|
| MAINTENANCE, RELIABILITY AND SAFETY | 28 |
| PROPELLER AERODYNAMICS | 30 |
| INTRODUCTION | 30 |
| BASIC PROPELLER THEORY | 31 |
| Propeller Momentum Theory | 32 |
| Momentum Theory Static Condition | 35 |
| Vortex Theory of Propellers, V > 0 | 37 |
| Vortex Theory - Theodorsen, V > 0 | 40 |
| Propeller Strip Theory, Single Rotation, V > 0 | 42 |
| EQUATIONS FOR STRIP ANALYSIS - DUAL-ROTATION PROPELLERS | 63 |
| Compressibility Considerations | 67 |
| THEORY OF PROPELLERS AT ZERO VELOCITY | 119 |
| Ideal Performance, V = 0 | 120 |
| Basis for Calculating Induced Velocity, V = 0 | 124 |
| Equations for Strip Analysis, V = 0 Single-Rotation Propellers | 125 |
| TWO-DIMENSIONAL AIRFOIL SECTION DATA | 128 |
| Data for Propeller Strip Analysis Calculation. | 128 |
| Data Correlation - Subsonic Range | 130 |
| Lift & Drag Divergence Mach Numbers | 133 |
| Data Correlation - Supersonic Range | 136 |
| Data Correlation - Transonic Range | 137 |
| Data at High Angles of Attack | 138 |
| Performance of Thick Airfoils | 140 |
| Trailing-Edge Extension | 141 |
| Airfoil Moment Data | 144 |
| PROPELLER PERFORMANCE CALCULATION PROCEDURES | 150 |
| Introduction | 150 |
| Installed Propeller Efficiency | 152 |
| Strip Analysis Procedure - Single Rotation, V = 0 | 152 |
| Strip Analysis Procedure - Single Rotation, V > 0 | 156 |

TABLE OF CONTENTS (Continued)


| | Page |
|---|---|
| Strip Analysis Procedure - Single Rotation, V > 0, M < 1.0 | 160 |
| Strip Analysis Procedure - Single Rotation, M > 1 | 161 |
| Strip Analysis Procedures - Dual Rotation, V > 0 | 161 |
| OPTIMUM PROPELLER DESIGN | 166 |
| Optimum Blade Loading | 166 |
| Aerodynamic Balancing - Strip Analysis | 172 |
| SHORT OR SINGLE-POINT METHODS OF ANALYSIS | 173 |
| Single-Point Method - Efficiency Maps | 173 |
| Single-Point Method Theory, V > 0 | 175 |
| Single-Point Method Theory, V = 0 | 180 |
| Application of the Single-Point Method | 181 |
| OFF-DESIGN AND FAILURE CONDITIONS | 199 |
| Malfunction Conditions | 200 |
| Negative Thrust Propeller Calculations | 200 |
| Feathered Propeller Performance | 205 |
| Feather Blade Angle | 207 |
| Vortex Ring State | 208 |
| Performance at Shaft Angles Above Zero | 211 |
| Method of Calculation, Shaft Angle > 0 | 214 |
| ACCURACY OF ANALYSIS METHODS | 219 |
| PROPELLER TEST DATA, A = 0 TO 180° | 244 |
| Propeller Tests | 245 |
| RESULTS | 245 |
| COWLINGS AND PROPELLER SPINNERS | 275 |
| Spinner Types and Selection | 275 |
| Ram Pressure Recovery for Propeller Spinners | 284 |
| Nacelle Flow Field and Propeller Design | 285 |
| CONCLUSIONS | 289 |
| LITERATURE CITED | 290 |
| DISTRIBUTION | 296 |

## LIST OF ILLUSTRATIONS


| Figure | | Page |
|---|---|---|
| 1 | Operating Aq - Typical Tractor Airplane ..... | 9 |
| 2 | Propeller Parametric Study ..... | 20 |
| 3 | Propeller Selection Study ..... | 21 |
| 4 | Propeller/Airplane Design Relationship ..... | 21 |
| 5 | Selection of Section Design Lift Coefficient - $C_{Li}$ ..... | 23 |
| 6 | Propeller in an Axial Flow Stream ..... | 33 |
| 7 | Mass Coefficient - k, Single Rotation Propeller ..... | 43 |
| 8 | Propeller Circulation Function - K(x) Two-Blade Single Rotation ..... | 44 |
| 9 | Propeller Circulation Function - K(x) Three-Blade Single Rotation ..... | 45 |
| 10 | Propeller Circulation Function - K(x) Four-Blade Single Rotation ..... | 46 |
| 11 | Propeller Circulation Function - K(x) Six-Blade Single Rotation ..... | 47 |
| 12 | Propeller Circulation Function - K(x) Eight-Blade Single Rotation ..... | 48 |
| 13 | Propeller Circulation Function - $K(x,\theta)$ Four-Blade Dual Rotation ..... | 49 |
| 14 | Propeller Circulation Function - $K(x,\theta)$ Six-Blade Dual Rotation ..... | 50 |
| 15 | Propeller Circulation Function - $K(x,\theta)$ Eight-Blade Dual Rotation ..... | 51 |
| 16 | Propeller Circulation Function - $K(x,\theta)$ Ten-Blade Dual Rotation ..... | 52 |
| 17 | Propeller Circulation Function - $K(x,\theta)$ Twelve-Blade Dual Rotation ..... | 53 |

## LIST OF ILLUSTRATIONS (Continued)


| Figure | | Page |
|---|---|---|
| 18 | Mass Coefficient - k, Dual-Rotation Propeller | 54 |
| 19 | Axial Loss Ratio - Single-Rotation Propeller | 55 |
| 20 | Axial Loss Ratio - Dual-Rotation Propeller | 56 |
| 21 | Propeller Velocity and Force Diagram - Single-Rotation Propeller | 58 |
| 22 | Typical Thrust or Torque Loading Curve | 62 |
| 23 | Propeller Velocity and Force Diagram - Dual-Rotation Propellers | 65 |
| 24 | Propeller Vortex Lines and Relative Positions | 69 |
| 25 | Mach Wave Caused by Propeller Tip, Forward Mach No. = .9 Tip, Mach No. = 2.13 | 70 |
| 26 | Propeller Vortex Lines and Position | 72 |
| 27 | Compressible Flow/Inflow Velocity Correction - B = 2, x = .2 and .3 | 80 |
| 28 | Compressible Flow/Inflow Velocity Correction - B = 2, x = .4 and .5 | 81 |
| 29 | Compressible Flow/Inflow Velocity Correction - B = 2, x = .6 | 82 |
| 30 | Compressible Flow/Inflow Velocity Correction - B = 2, x = .7 | 83 |
| 31 | Compressible Flow/Inflow Velocity Correction - B = 2, x = .8 | 84 |
| 32 | Compressible Flow/Inflow Velocity Correction - B = 2, x = .9 | 85 |
| 33 | Compressible Flow/Inflow Velocity Correction - B = 2, x = .95 | 86 |

LIST OF ILLUSTRATIONS (Continued)


| Figure | | Page |
|---|---|---|
| 34 | Compressible Flow/Inflow Velocity Correction - B = 3, x = .2 and .3 | 87 |
| 35 | Compressible Flow/Inflow Velocity Correction - B = 3, x = .4 and .5 | 88 |
| 36 | Compressible Flow/Inflow Velocity Correction - B = 3, x = .6 | 89 |
| 37 | Compressible Flow/Inflow Velocity Correction - B = 3, x = .7 | 90 |
| 38 | Compressible Flow/Inflow Velocity Correction - B = 3, x = .8 | 91 |
| 39 | Compressible Flow/Inflow Velocity Correction - B = 3, x = .9 | 92 |
| 40 | Compressible Flow/Inflow Velocity Correction - B = 3, x = .95 | 93 |
| 41 | Compressible Flow/Inflow Velocity Correction - B = 4, x = .2 and .3 | 94 |
| 42 | Compressible Flow/Inflow Velocity Correction - B = 4, x = .4 | 95 |
| 43 | Compressible Flow/Inflow Velocity Correction - B = 4, x = .5 | 96 |
| 44 | Compressible Flow/Inflow Velocity Correction - B = 4, x = .6 | 97 |
| 45 | Compressible Flow/Inflow Velocity Correction - B = 4, x = .7 | 98 |
| 46 | Compressible Flow/Inflow Velocity Correction - B = 4, x = .8 | 99 |
| 47 | Compressible Flow/Inflow Velocity Correction - B = 4, x = .9 | 100 |
| 48 | Compressible Flow/Inflow Velocity Correction - B = 4, x = .95 | 101 |

LIST OF ILLUSTRATIONS (Continued)


| Figure | | Page |
|---|---|---|
| 49 | Compressible Flow/Inflow Velocity Correction - B = 6, x = .2 and .3 ..... | 102 |
| 50 | Compressible Flow/Inflow Velocity Correction - B = 6, x = .4 and .5 ..... | 103 |
| 51 | Compressible Flow/Inflow Velocity Correction - B = 6, x = .6 ..... | 104 |
| 52 | Compressible Flow/Inflow Velocity Correction - B = 6, x = .7 ..... | 105 |
| 53 | Compressible Flow/Inflow Velocity Correction - B = 6, x = .8 ..... | 106 |
| 54 | Compressible Flow/Inflow Velocity Correction - B = 6, x = .9 ..... | 107 |
| 55 | Compressible Flow/Inflow Velocity Correction - B = 6, x = .95 ..... | 108 |
| 56 | Comparison of Induced Velocity Compressibility Correction for Betz and Constant Load Distributions ..... | 110 |
| 57 | Tip Compressibility Correction to Airfoil Characteristics, $M_t$ = 1.2 ..... | 111 |
| 58 | Tip Compressibility Correction to Airfoil Characteristics, $M_t$ = 1.4 ..... | 112 |
| 59 | Tip Compressibility Correction to Airfoil Characteristics, $M_t$ = 1.5 ..... | 113 |
| 60 | Tip Compressibility Correction to Airfoil Characteristics, $M_t$ = 1.75 ..... | 114 |
| 61 | Tip Compressibility Correction to Airfoil Characteristics, $M_t$ = 2.0 ..... | 115 |
| 62 | Tip Compressibility Correction to Airfoil Characteristics, $M_t$ = 2.25 ..... | 116 |
| 63 | Tip Compressibility Correction to Airfoil Characteristics, $M_t$ = 2.50 ..... | 117 |

LIST OF ILLUSTRATIONS (Continued)


| Figure | | Page |
|---|---|---|
| 64 | Propeller Figure of Merit Comparison for Static Thrust Condition ..... | 122 |
| 65 | Propeller Slipstream Contraction Coefficient - k' - Velocity = 0 ..... | 123 |
| 66 | Velocity and Force Diagram, V = 0, Static Condition ..... | 126 |
| 67 | Comparison of $M_{CR}$ With Lift and Drag Divergence NACA 16-206 Section ..... | 135 |
| 68 | Angle of Extension vs. Design $C_L$ NACA 16 Section ..... | 142 |
| 69 | Change in Blade Angle Due to Addition of Trailing-Edge Strip ..... | 143 |
| 70 | Airfoil Center of Pressure Location, NACA 16 Sections $C_{Li}$ = 0.0 ..... | 145 |
| 71 | Airfoil Center of Pressure Location, NACA 16 Sections $C_{Li}$ = 0.3 ..... | 146 |
| 72 | Airfoil Center of Pressure Location, NACA 16 Sections $C_{Li}$ = 0.5 ..... | 147 |
| 73 | Airfoil Center of Pressure Location, NACA 16 Sections Effect of Thickness Ratio ..... | 148 |
| 74 | Propeller Profile Loss Chart, V = 0 ..... | 183 |
| 75 | Propeller Thrust to Power Coefficient Ratio, Static Condition - Two Blades ..... | 184 |
| 76 | Propeller Thrust to Power Coefficient Ratio, Static Condition - Three Blades ..... | 185 |
| 77 | Propeller Thrust to Power Coefficient Ratio, Static Condition - Four Blades ..... | 186 |
| 78 | Propeller Unit Loading - $C_{Li}$ = 0 ..... | 187 |
| 79 | Propeller Unit Loading - $C_{Li}$ = .25 ..... | 188 |
| 80 | Propeller Unit Loading - $C_{Li}$ = .5 ..... | 189 |

LIST OF ILLUSTRATIONS (Continued)


| Figure | | Page |
|---|---|---|
| 81 | Propeller Efficiency, B = 2, $\gamma = 0^{\circ}$ ..... | 190 |
| 82 | Propeller Efficiency, B = 2, $\gamma = 5^{\circ}$ ..... | 191 |
| 83 | Propeller Efficiency, B = 2, $\gamma = 10^{\circ}$ ..... | 192 |
| 84 | Propeller Efficiency, B = 3, $\gamma = 0^{\circ}$ ..... | 193 |
| 85 | Propeller Efficiency, B = 3, $\gamma = 5^{\circ}$ ..... | 194 |
| 86 | Propeller Efficiency, B = 3, $\gamma = 10^{\circ}$ ..... | 195 |
| 87 | Propeller Efficiency, B = 4, $\gamma = 0^{\circ}$ ..... | 196 |
| 88 | Propeller Efficiency, B = 4, $\gamma = 5^{\circ}$ ..... | 197 |
| 89 | Propeller Efficiency, B = 4, $\gamma = 10^{\circ}$ ..... | 198 |
| 90 | Force and Velocity Diagrams for a Windmilling Propeller ..... | 201 |
| 91 | Flow Diagrams, Propeller in Vortex Ring State ..... | 203 |
| 92 | Propeller Performance at 0 Rotation ..... | 206 |
| 93 | Vortex Ring and Windmill Brake State - Propellers and Rotors ..... | 209 |
| 94 | Rate of Descent for a Propeller for Start of Vortex Ring State ..... | 210 |
| 95 | Propeller Force and Moment Diagram - Shaft Angle Greater Than Zero ..... | 212 |
| 96 | Propeller Velocity Diagram at Shaft Angles Above Zero ..... | 213 |
| 97 | Propeller Total Lift and Thrust Force, $A = 0$ to $90^{\circ}$ ..... | 215 |
| 98 | Comparison of Test and Calculated Propeller Loading, M = .35 ..... | 221 |
| 99 | Comparison of Test and Calculated Propeller Loading, M = .60 ..... | 222 |

LIST OF ILLUSTRATIONS (Continued)


| Figure | | Page |
|---|---|---|
| 100 | Comparison of Test and Calculated Propeller Loading, M = .60 | 223 |
| 101 | Comparison of Test and Calculated Propeller Loading, M = .70 | 224 |
| 102 | Comparison of Test and Calculated Propeller Loading, M = .7 | 225 |
| 103 | Comparison of Test and Calculated Propeller Loading, M = .7 | 226 |
| 104 | Comparison of Test and Calculated Propeller Loading, M = .7 | 227 |
| 105 | Comparison of Test and Calculated Propeller Loading, M = .8 | 228 |
| 106 | Comparison of Test and Calculated Propeller Loading, M = .925 | 229 |
| 107 | Comparison of Test and Calculated Propeller Loading, M = .925 | 230 |
| 108 | Comparison of Test and Calculated Efficiency | 231 |
| 109 | Comparison of Propeller Wind Tunnel Test and Calculated Performance | 232 |
| 110 | Comparison of Propeller Wind Tunnel Test and Calculated Performance | 233 |
| 111 | Comparison of Propeller Wind Tunnel Test and Calculated Performance | 234 |
| 112 | Comparison of Propeller Wind Tunnel Test and Calculated Performance | 235 |
| 113 | Comparison of Propeller Wind Tunnel Test and Calculated Performance | 236 |
| 114 | Comparison of Propeller Wind Tunnel Test and Calculated Performance | 237 |

LIST OF ILLUSTRATIONS (Continued)


| Figure | | Page |
|---|---|---|
| 115 | Comparison of Propeller Wind Tunnel Test and Calculated Performance ..... | 238 |
| 116 | Comparison of Propeller Wind Tunnel Test and Calculated Performance ..... | 239 |
| 117 | Comparison of Propeller Wind Tunnel Test and Calculated Performance ..... | 240 |
| 118 | Comparison of Propeller Wind Tunnel Test and Calculated Performance ..... | 241 |
| 119 | Comparison of Propeller Wind Tunnel Test and Calculated Performance ..... | 242 |
| 120 | Characteristic Curves, 109652 Blade ..... | 246 |
| 121 | Performance at 0-Degree Shaft Angle, Three-Blade Propeller, Blade No. 109652 .... | 247 |
| 122 | Performance at 20-Degree Shaft Angle, Three-Blade Propeller, Blade No. 109652 .... | 248 |
| 123 | Performance at 40-Degree Shaft Angle, Three-Blade Propeller, Blade No. 109652 .... | 249 |
| 124 | Performance at 60-Degree Shaft Angle, Three-Blade Propeller, Blade No. 109652 .... | 250 |
| 125 | Performance at 75-Degree Shaft Angle, Three-Blade Propeller, Blade No. 109652 .... | 251 |
| 126 | Performance at 85-Degree Shaft Angle, Three-Blade Propeller, Blade No. 109652 .... | 252 |
| 127 | Performance at 90-Degree Shaft Angle, Three-Blade Propeller, Blade No. 109652 .... | 253 |
| 128 | Performance at 95-Degree Shaft Angle, Three-Blade Propeller, Blade No. 109652 .... | 254 |
| 129 | Performance at 105-Degree Shaft Angle, Three-Blade Propeller, Blade No. 109652 .... | 255 |

LIST OF ILLUSTRATIONS (Continued)


| Figure | | Page |
|---|---|---|
| 130 | Performance at 120-Degree Shaft Angle, Three-Blade Propeller, Blade No. 109652 .... | 256 |
| 131 | Performance at 140-Degree Shaft Angle, Three-Blade Propeller, Blade No. 109652 .... | 257 |
| 132 | Performance at 160-Degree Shaft Angle, Three-Blade Propeller, Blade No. 109652 .... | 258 |
| 133 | Performance at 180-Degree Shaft Angle, Three-Blade Propeller, Blade No. 109652 .... | 259 |
| 134 | Normal Force at 20-Degree Shaft Angle, Three-Blade Propeller, Blade No. 109652 .... | 260 |
| 135 | Normal Force at 40-Degree Shaft Angle, Three-Blade Propeller, Blade No. 109652 .... | 260 |
| 136 | Normal Force at 60-Degree Shaft Angle, Three-Blade Propeller, Blade No. 109652 .... | 261 |
| 137 | Normal Force at 75-Degree Shaft Angle, Three-Blade Propeller, Blade No. 109652 .... | 261 |
| 138 | Normal Force at 85-Degree Shaft Angle, Three-Blade Propeller, Blade No. 109652 .... | 262 |
| 139 | Normal Force at 90-Degree Shaft Angle, Three-Blade Propeller, Blade No. 109652 .... | 262 |
| 140 | Normal Force at 95-Degree Shaft Angle, Three-Blade Propeller, Blade No. 109652 .... | 263 |
| 141 | Normal Force at 105-Degree Shaft Angle, Three-Blade Propeller, Blade No. 109652 .... | 263 |
| 142 | Pitching Moment at 20-Degree Shaft Angle, Three-Blade Propeller, Blade No. 109652 .... | 264 |
| 143 | Pitching Moment at 40-Degree Shaft Angle, Three-Blade Propeller, Blade No. 109652 .... | 264 |
| 144 | Pitching Moment at 60-Degree Shaft Angle, Three-Blade Propeller, Blade No. 109652 .... | 265 |

LIST OF ILLUSTRATIONS (Continued)


| Figure | | Page |
|---|---|---|
| 145 | Pitching Moment at 75-Degree Shaft Angle, Three-Blade Propeller, Blade No. 109652 .... | 265 |
| 146 | Pitching Moment at 85-Degree Shaft Angle, Three-Blade Propeller, Blade No. 109652 .... | 266 |
| 147 | Pitching Moment at 90-Degree Shaft Angle, Three-Blade Propeller, Blade No. 109652 .... | 266 |
| 148 | Pitching Moment at 95-Degree Shaft Angle, Three-Blade Propeller, Blade No. 109652 .... | 267 |
| 149 | Pitching Moment at 105-Degree Shaft Angle, Three-Blade Propeller, Blade No. 109652 .... | 267 |
| 150 | Pitching Moment at 120-Degree Shaft Angle, Three-Blade Propeller, Blade No. 109652 .... | 268 |
| 151 | Pitching Moment at 140-Degree Shaft Angle, Three-Blade Propeller, Blade No. 109652 .... | 268 |
| 152 | Pitching Moment at 160-Degree Shaft Angle, Three-Blade Propeller, Blade No. 109652 .... | 268 |
| 153 | Yawing Moment at 20Degree Shaft Angle, Three-Blade Propeller, Blade No. 109652 .... | 269 |
| 154 | Yawing Moment at 40-Degree Shaft Angle, Three-Blade Propeller, Blade No. 109652 .... | 269 |
| 155 | Yawing Moment at 60-Degree Shaft Angle, Three-Blade Propeller, Blade No. 109652 .... | 270 |
| 156 | Yawing Moment at 75-Degree Shaft Angle, Three-Blade Propeller, Blade No. 109652 .... | 270 |
| 157 | Yawing Moment at 85-Degree Shaft Angle, Three-Blade Propeller, Blade No. 109652 .... | 271 |
| 158 | Yawing Moment at 90-Degree Shaft Angle, Three-Blade Propeller, Blade No. 109652 .... | 271 |
| 159 | Yawing Moment at 95-Degree Shaft Angle, Three-Blade Propeller, Blade No. 109652 .... | 272 |

LIST OF JLLUSTRATIONS (Continued )


| Figure | | Page |
|---|---|---|
| 160 | Yawing Moment at 105-Degree Shaft Angle, Three-Blade Propeller, Blade No. 109652 .... | 272 |
| 161 | Yawing Moment at 120-Degree Shaft Angle, Three-Blade Propeller, Blade No. 109652 .... | 273 |
| 162 | Yawing Moment at 140-Degree Shaft Angle, Three-Blade Propeller, Blade No. 109652 .... | 273 |
| 163 | Yawing Moment at 160-Degree Shaft Angle, Three-Blade Propeller, Blade No. 109652 .... | 274 |
| 164 | Ram Pressure Recovery Effects on Shaft Horsepower and Specific Fuel Consumption for a Typical Turboprop Engine ..... | 276 |
| 165 | Typical Symmetrical Cowling and Spinner Types ..... | 277 |
| 166 | NACA Series 1 Cowling Ordinates ..... | 280 |
| 167 | Selection Chart for NACA 1-Series Cowlings . | 281 |
| 168 | Selection Chart for NACA 1-Series Cowlings With NACA 1-6-080 Spinner Propeller Removed ..... | 282 |
| 169 | Pressure Recovery at Cowl Inlet ..... | 286 |
| 170 | Radial Variation of Axial Velocity at Propeller Plane for "D" and "E" Type Cowls ..... | 287 |

## LIST OF TABLES


| Table | | Page |
|---|---|---|
| I | Range of 1xP Excitation Factors | 8 |
| II | Summary of Airfoil Data, NACA-16 Sections | 132 |
| III | Strip Analysis Calculation Procedure, Forward Velocity = 0 | 153 |
| IV | Procedure for Calculating $C_L$ and $C_D$ Forward Velocity = 0 | 154 |
| V | Strip Analysis Calculation, Single-Rotation Propellers | 157 |
| VI | Strip Analysis Calculation Procedure, Single-Rotation Propellers, V > 0 | 158 |
| VII | Procedure for Calculating $C_L$ and $C_D$, Single-Rotation Propellers, Forward Velocity V > 0 | 159 |
| VIII | Strip Analysis Calculation, Dual-Rotation Propellers | 162 |
| IX | Strip Analysis Calculation Procedure, Dual-Rotation Propellers | 163 |
| X | Procedure for Calculating $C_L$ and $C_D$, Dual-Rotation Propellers, Velocity V > 0, $M_T$ < 1.0 | 164 |
| XI | Procedure for Calculating $C_L$ and $C_D$, Dual-Rotation Propellers, Velocity V > 0, $M_T$ < 1.0 | 165 |

## LIST OF SYMBOLS

| | |
|---|---|
| A | area - $ft^2$ |
| A | angle of propeller inflow - deg |
| AR | aspect ratio = $(\text{Wing Span})^2/\text{Wing Area}$ |
| AF | blade activity factor |
| a | speed of sound - ft/sec |
| B | blade number |
| b | blade chord - ft |
| $C_c$ | chordwise force coefficient |
| $C_D$ | drag coefficient |
| $C_{Di}$ | induced drag coefficient |
| $C_{DP}$ | profile drag coefficient |
| $C_L$ | lift coefficient |
| $C_{Li}$ | section design lift coefficient |
| $C_M$ | moment coefficient |
| $C_N$ | normal force coefficient |
| $C_P$ | power coefficient |
| $C_P$ | pressure coefficient |
| $C_Q$ | torque coefficient |
| $C_T$ | thrust coefficient |
| D | propeller diameter - ft |
| D | wake diameter |
| d | distance |
| FM | figure of merit |
| H | total pressure head - lb/sq ft |

## LIST OF SYMBOLS (Continued)

| | |
|---|---|
| h | maximum blade thickness - ft |
| hp | horsepower |
| J | advance ratio = V/nD |
| K(x) | circulation function - single rotation propellers |
| $K(x,\theta)$ | circulation function - dual rotation propellers |
| L | lift - lb |
| M | Mach number |
| $M_{CR}$ | critical Mach number |
| m | mass |
| mph | miles per hour |
| N | propeller rotational speed - rpm |
| $N_R$ | Reynolds number |
| n | propeller rotational speed - rps |
| P | power |
| p | pressure - psf |
| Q | torque - ft-lb, sec |
| q | dynamic pressure - psf |
| R | propeller radius - ft |
| r | propeller radius at any station - ft |
| T | thrust - lb |
| u | axial inflow velocity - fps |
| V | airplane velocity - fps |
| $V_i$ | indicated airspeed - fps |

## LIST OF SYMBOLS (Continued

| | |
|---|---|
| $V_{NE}$ | never-exceed velocity - fps |
| $V_o$ | free-stream velocity - fps |
| $V_p$ | velocity at propeller disc - momentum - fps |
| $V_w$ | velocity in final wake - fps |
| W | true wind velocity - fps |
| w | displacement velocity - fps |
| $\bar{w}$ | displacement velocity ratio = w/V |
| x | fractional radius at any station = r/R |
| $\alpha$ | angle of attack - deg |
| $\alpha_i$ | induced angle of attack - deg |
| $\beta$ | blade angle - deg |
| $\Gamma$ | strength of circulation |
| $\gamma$ | drag lift angle = $\tan^{-1} C_D/C_L$ |
| $\delta$ | angle between blades |
| $\epsilon$ | energy function |
| $\eta$ | propeller efficiency |
| $\lambda$ | advance ratio = J/$\pi$ |
| $\rho$ | mass density of air - slugs/cu ft |
| $\sigma$ | propeller solidity |
| $\phi$ | helical pitch angle |
| $\phi_o$ | apparent wind angle |
| $\omega$ | rotational velocity - rad/sec |

SUBSCRIPTS

| | |
|---|---|
| C | compressible |
| F | front propeller |
| R | rear propeller |
| ref | reference |
| .75 | conditions at $x = .75$ |
| i | incompressible; induced |
| p | profile |

## INTRODUCTION

The technology for designing high-performance lightweight propellers was well developed up to 1958. The procedures and data were formulated over a long period of time, especially from 1946 to 1955. Propellers were designed and built for aircraft using engines producing up to 15,000 horsepower and operating at speeds corresponding to a Mach number of 0.8. The propellers were designed with diameters up to 22 feet and had anywhere from two blades single rotation to eight blades counter rotation. Propellers were tested at tip speeds up to 1.5 Mach number and forward Mach number to 1.1. The propellers were designed to use either solid dural, hollow dural or hollow steel blades in various configurations. Ultra lightweight propellers for V/STOL aircraft were designed to use fiber glass blades of several types. The reliability of the designs and life of the later configurations were excellent, and blades have been built with an operating life of over 30,000 hours.

Up to 1958 the Air Force had been procuring high-performance turboprop aircraft and had been actively supporting advanced propeller development. With the exception of the activity with V/STOL aircraft, propeller development was terminated by the Air Force in 1958. The V/STOL propeller activity did result in a modest R&D effort leading to the lightweight propellers for such aircraft as the X-19, XC-142 and the CL-84 airplanes. Work has also been done by the Air Force in the development of cyclic pitch propellers for tilt-wing type V/STOL airplanes. The Army has supported studies with limited hardware component programs for the development of ultra lightweight propellers, and the Navy has supported work in the variable camber field.

During World War II the propellers were designed using the available technology developed prior to 1940, and as a result it was possible to apply only the available data for new designs. The only real advances made in technology were to improve cooling, and to develop reverse thrust propellers for dive breaking and water handling. The research to improve the performance of propellers was by flight testing, using speed/power techniques, and the development and use of a thrust meter for a reciprocating engine.

During the early forties the general propeller design and method of analysis used were on the whole quite crude. For instance, the selection of propellers for a new airplane was done largely using single-point methods of analysis. The blade geometry was determined by scalings from other blades of known performance characteristics.

In the areas of blade design and structural analysis, the methods used were quite crude. The development of new blade designs during the period was done based on experience and

empirical approaches. Little was known about problems involved from flow angularity, flutter, engine-mount stiffness, or other problems as a result of engine vibration. The suitability of a new propeller installation was determined from extensive installation testing, including blade vibration stress surveys and component testing.

After World War II there was a considerable interest shown in propeller development, and large expenditures of engineering time and money were made to improve propellers for the B-36 airplane as well as for high-powered turboprop engines. This work was planned by the Propeller Laboratory of the Air Force, who worked closely with industry and the NACA. The Propeller Laboratory sponsored a number of programs including the development of several new propellers, engineering research and flight test programs. The NACA conducted a large number of wind tunnel tests in the 8-foot and 16-foot tunnels covering the Mach number range up to a forward Mach number of .975. They tested a number of two-blade, 4- and 10-foot-diameter propellers for a large variation of blade design configurations.

The flight test programs funded by the Propeller Laboratory included flight tests of a P47 airplane equipped with thrust and torque meters. Tests were made at climb, cruise and high speed and included dive tests to a forward Mach number of 0.8. Included in the program were tests of three- and four-blade propellers, swept-back blades, ultra-thin blades and blades using sections other than the standard NACA 16 normally used. See Reference 1.

Supporting these programs of flight and wind tunnel testing were applied research programs for developing and refining the techniques of design and analysis of the performance of propellers. This included applied research in developing suitable tables of lift, drag and moment characteristics of two-dimensional airfoils. Also included were the methods of application of these airfoil data for calculating the performance of propellers. This required the development of suitable methods for calculating the induced efficiency of propellers. A great deal of time was spent on correlating the results of the calculations with propeller test data, making adjustments in the airfoil data until good accuracy was obtained. The methods of calculating the performance were refined until the accuracy was excellent over the entire range.

The quest for ever-increasing speed led to the question of best propeller type, i.e., subsonic, transonic or supersonic. Because of the large efficiency losses with propellers operating at high tip Mach numbers, it was of major concern to reduce these losses. Two approaches were taken: (1) the use of very large slow-turning propellers and in some cases counterrotating slow-turning propellers, or (2) the use of thin low-camber

blades with much of the blade operating at transonic speeds. Also considered were supersonic propellers. These propellers used blades with very thin airfoils: thickness ratios of 2% at the tip and 6% inboard. A considerable amount of time was spent investigating the supersonic propeller with theoretical structural aerodynamic studies, propeller design, fabrication work and performance testing in wind tunnels.

The results of much of the propeller work accomplished during the time period of 1945 to the present are still valid and therefore provide an excellent base for any future propeller developments. In this report the material will be detailed in the light of present technology with the objective of preserving the data and technology where possible. The areas where additional research and development will be necessary are to be discussed. In this way a firm technology base will be established for future developments of propellers for any application.

## GENERAL PROPELLER DESIGN CONSIDERATIONS

During the time period 1945 to the present, the propeller selected for a given installation was specifically designed to satisfy the requirements of the airplane. The aircraft designer, after selecting an engine configuration, could only obtain a competitive airplane design by demanding peak propeller efficiency at all the critical flight conditions and minimum installed weight. These demands in performance, along with demands for minimum weight and cost, and good reliability and maintenance in all but a few unusual cases, resulted in the design of new propellers for each new installation.

As the engine was generally in existence for the new airplane when the propeller was selected, the time required to develop a new propeller for each installation was extremely small. This was true as the airplane was generally well along in its design prior to the selection of the propeller contractor. This lack of time imposed special problems on the propeller design and development program. As a result of the short development time, many problems were encountered due to the lack of proper lead time for engineering, designing, testing and qualifying the propeller.

The need for developing a new propeller for each installation is apparent when one considers the many variables involved which influence the final design. These include:

a) Airplane performance requirements
b) Airplane geometric considerations
c) Engine characteristics and design parameters
d) Propeller design factors

With the recognition of the need of increased lead time for necessary engineering and development, it will be possible to properly consider all the factors for successful installations.

### DESIGN CRITERIA

To assure that proper consideration is given to all the factors which influence the design of a propeller, it is necessary to develop a design procurement specification based on a complete design criterion. To establish the design criteria, detailed consideration must be given to the airplane design objectives, including:

a) Mission
b) Takeoff, cruise and climb performance
c) Operational Environment
d) Maneuverability

e) Size & Geometry
f) Noise
g) Cost

In preparing the propeller design criteria, it is necessary to select suitable engines for final evaluation, as the power available, rotational speed characteristics, specific fuel consumption and weight have a considerable influence on the propeller design. Also influencing the design criteria will be the overall airplane configuration developed to satisfy the mission. Its layout and geometric configuration will have an important bearing on the overall propeller design.

An outline of the topics and factors of a complete propeller design criterion procurement specification is given in Appendix I of Volume III. Completion of all the major topics given will allow the propeller designer to prepare a specification from which required propellers can be designed, built, fabricated, qualified and delivered. The many topics listed in the criteria in Appendix I, Volume III, are dependent on the airplane operating requirements and installation considerations. These items are discussed as follows as an aid for preparing the required criteria.

## INSTALLATION CONSIDERATIONS

Early in the initial design of a new propeller-driven airplane, careful consideration must be given to the engine selection and overall propeller installation to obtain the best configuration. This is especially important, as the operating requirements for the propeller can be quite diverse. For instance, for peak takeoff performance of V/STOL aircraft, large-diameter propellers with light disc loadings will give high ratios of thrust to horsepower. Such large propellers can lead to long, narrow, flexible helicopter-like blades that must be installed on the wing tips to obtain fuselage clearance. These large propellers must be thoroughly designed and analyzed to avoid severe overall dynamic problems. On the other hand, smaller propellers with a higher disc loading could be used to obtain the same performance, but higher powered engines would be required. Such an installation could lead to problems involving downwash velocity and high overall fuel consumption.

### Aircraft and Engine Characteristics

The airplane geometric characteristics influencing the installation of the propeller and its size limit must be established. Geometric factors affecting the maximum diameter such as ground clearance and fuselage tip clearance are therefore especially important. The airplane geometric characteristics that determine the flow field into the propeller disc must also be

established, as these determine the performance and the required propeller structural characteristics. If the flow axial velocity into the propeller is uniform, the structural requirements are much less severe than for the case where the velocity is higher on one quadrant of the disc than the other.

The structural stiffness and aeroelastic characteristics of the airplane are also of great importance to the design of the propeller, as they can directly determine the propeller weight.

The engine performance characteristics influence the design of the propeller, especially its variation of output shaft rotational speed as a function of power and altitude. For instance, certain coupled turbine engines run at only one rotational speed. Because of this fixed rotational speed, it is difficult to establish a blade design that is optimum for more than one operating condition. When the engine rotational speed is a variable as in the case of a free turbine turboprop engine, it is possible to improve the overall design significantly. This is done by operating at high rotational speeds at high loadings and low rpm's at light loadings. This is especially necessary when there are two important operating conditions such as takeoff and cruise, as in the case of V/STOL aircraft.

Based on the aircraft geometric characteristics, the engine operating parameters, and the overall performance requirements, the best engine/propeller output shaft gear ratio can be established. The factors influencing the gear ratio selection are:

a) Performance
b) Noise (Tip Speed)
c) Weight
d) Compressibility considerations
e) Propeller diameter

A parametric analysis of these factors in terms of selected design criteria is then used to select the best gear ratio.

After the engine/propeller gear ratio is selected, the propellers must be analyzed in terms of the engine rotational speed and specific fuel consumption characteristics to find the best overall operating conditions. Generally, free-turbine engines operate at the minimum specific fuel consumption over a relatively narrow range of rotational speeds. For this reason, unless the airplane flight conditions lead to requirements for propellers operating at a wide range of loadings, the operating engine speed used may be quite narrow. In any case, the higher rotational speed would be selected for takeoff and climb, with a low value used at cruise to improve efficiency and reduce noise level.

If the aircraft thrust requirements at the design flight conditions lead to wide variations in propeller loading, it may become desirable to operate the engine at rotational speeds below that for minimum specific fuel consumption. In this case the engine speed will be chosen to give the maximum miles per pound of fuel for the combination, and neither the propeller efficiency loss nor the specific fuel consumption will be a minimum.

Performance Requirements

The propeller characteristics needed depend directly on the aircraft installation and performance requirements. Thus the aircraft performance in terms of speed and altitude must be known along with the associated engine performance output characteristics. These characteristics must be known for the series of critical flight conditions of the airplane, and to establish the propeller it is necessary to know the aircraft thrust requirements for each condition. Therefore, the information presented below must be tabulated prior to the start of the propeller design analysis.

| AIRCRAFT DESIGN CONDITIONS | | | | | | |
|---|---|---|---|---|---|---|
| Condition | Velocity | Altitude | Temp. | hp | Eng rpm | T req'd |
| T.O.<br>Climb<br>Cruise<br>V Max<br>Reverse | | | | | | |

Structural Requirements

The propeller of course must be designed with structural integrity at all flight conditions. The structure required to accomplish this is directly influenced by the propeller-airplane installation. For instance, the blade cyclic load is influenced by the flow field into the disc. If the propeller is operating in a uniform airstream with the shaft parallel to the free-stream velocity, the cyclic load distribution will be low and the vibratory blade stresses will be low. In this case the blades can be designed mainly for the steady stresses with a corresponding weight saving.

The operating characteristics of the airplanes also influence the flow angle at the propeller disc. Due to the high angle of attack of the airplane necessary for the low-speed flight conditions, the propeller shaft will operate at an angle of attack, A, with respect to the free-stream velocity. The flow around the fuselage and the wing will also influence the angle of the velocity vector into the propeller. As discussed in Volume II, Structural Design Methodologies, this angle times the dynamic pressure based on the free-stream velocity directly influences the level of the cyclic stress in the blade. This stress becomes a peak once per revolution and is known as 1xP blade stress. The 1xP stress is thus a function of Aq, the inflow angle times the dynamic pressure.

Because the vibratory stresses of the blade are proportioned to the value of Aq and because this factor is independent of the propeller characteristics, it is called an "excitation factor". The Aq curve for a typical tractor airplane is shown in Figure 1. From this figure it will be noted that typically for a conventional airplane the highest values of Aq are obtained at maximum gross weight and at the "never exceed" dive speed. Table I gives the range of magnitude of Aq for evaluating the initial structural requirements of conventional propeller blades.

TABLE I. RANGE OF 1xP EXCITATION FACTORS

| Value of Aq | Relative Magnitude |
|---|---|
| Less than 1000 | Low |
| 1000 - 1500 | Moderate |
| 1500 - 2000 | Moderate High |
| Above 2000 | High |

Under certain conditions the propeller will operate at flow conditions where blades are subjected to a peak stress two times per revolution, such as when operating behind a thick wing as pusher propeller. In this case the vibratory stress is known as the 2xP stress and can also be a designing condition. In any case, all multiples of the rotation speed must be examined to find the peak vibratory stress and the blade designed accordingly. Also, steps should be taken in the installation design to eliminate the forcing function.

With certain high-power installations using high disc loadings, blade flutter has been encountered. These flutter conditions are usually encountered at zero velocity, the static condition. Because of the high blade stresses associated with flutter, it cannot be accepted at any operating condition. For this

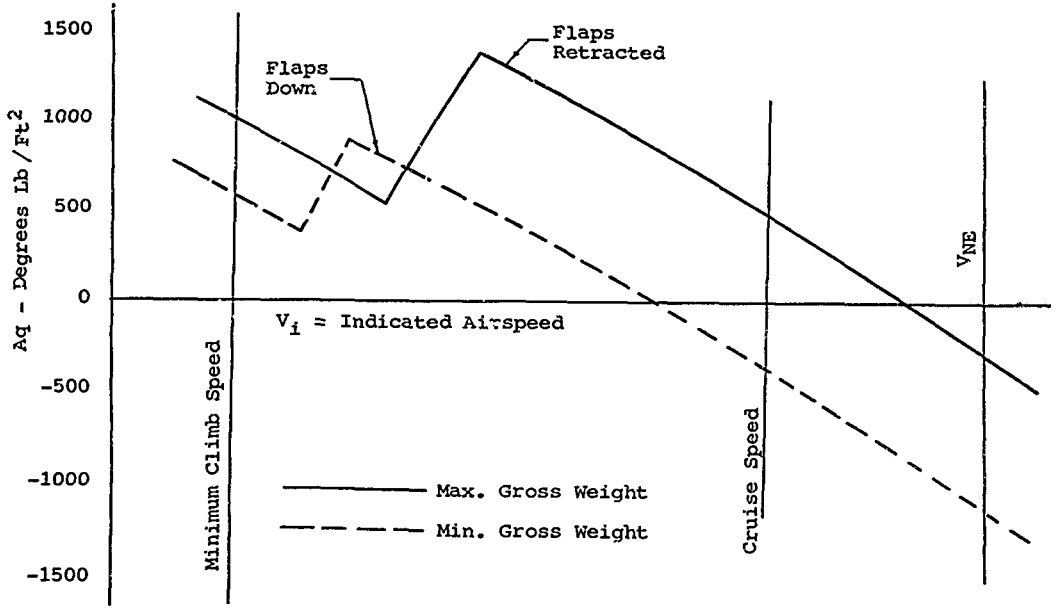


Figure 1. Operating Aq - Typical Tractor Airplane.

reason, the blade, including its control flexibility, must be designed to be flutter free when installed on the airplane. In the past, operating restrictions have been placed on the system to avoid conditions where flutter would be encountered, but this is not an acceptable solution.

Dynamic Characteristics

The propeller is generally mounted on a wing of a given stiffness characteristic along with an engine mount of another stiffness. This stiffness combined with the associated mass characteristic of the system influences the overall dynamics of the propeller and its frequency response.

The propeller when mounted on the elastic system of the airplane must be designed so that at least the first three coupled flap/chord/torsion natural frequencies are displaced at least +0.15/rev from an integer harmonic at the operating rpm with a ±6%. Also, no natural frequency can be encountered within an operational frequency band determined by blade number and rotational speed.

The propeller and its mounting system must be designed to be free of all aeroelastic instabilities with the operating range, including the zero rpm feathering conditions, all combinations of design thrust values, and reverse thrust conditions. All environmental conditions encompassed by the flight operating envelope must be considered.

Noise

Of major importance with any propeller installation is the overall noise level. Both the near-field and far-field levels of noise are of great importance. The noise level generated by the propeller is dependent on the rotational speed, tip speed, disc loading and blade load distribution. The noise level generated within the airplane is critically dependent upon the distance of the propeller tip from the fuselage and its fore/aft location with respect to the observer.

Quiet propellers can be designed which operate at high levels of efficiency and using large blades operating at low tip speeds. In fact, propellers can be the quietest form of propulsion in the subsonic speed range.

## Propeller Control Considerations

The propeller control requirements are directly influenced by the airplane, engine, and engine control characteristics. In conjunction with the engine control, the propeller control must be designed so that the required thrust response is obtained at all flight conditions. Additionally, the control system must protect the airplane from unwanted values of negative thrust in cases of failures of the engine or propeller control system.

The propeller control system for the turboprop engine requires a much higher rate of pitch change than in the case of the reciprocating engine. This is especially true when fixed turbine engines are used. In this case, pitch change rates up to six times that required for reciprocating engines are sometimes necessary. With the free-turbine turboprop engine, the pitch change rates required are reduced, but control and its protective system are still more complex than was necessary with the older installations.

Since high rates of pitch change directly affect the weight and the complexity of a new propeller, it is important that the new installation be completely analyzed to find the overall requirements. With the complete analysis, the best overall configuration can be designed without excessive weight or complexity.

## Weight

Propeller weight is a direct function of the installation configuration, installed power and design rotational speed. This is apparent, as the size is influenced by the power, thrust required, flight speed, the design Aq, the propeller placement, and the operating environment. The design rotational speed is of course important, as the centrifugal stresses and loads vary directly with the square of the rotational speed. The installation of the propeller can be designed to minimize the angular flow conditions that directly influence the blade stress and so minimize the weight. To accomplish significant improvements in the propeller installation, changes must be accomplished early in the design.

With an integration of the propeller/airplane design, important weight advantages can also be had. These advantages are possible in addition to those possible with advanced materials, composite structures, etc. One of the most important improvements was the development of the integral gearbox propeller. By combining the function of the propeller and hub into a single unit, important weight advantages were made possible.

The propellers designed for conventional airplanes during the time period of 1940 to 1955 had a specific weight of 0.3 pound per horsepower for 1000-horsepower engines and a specific weight as low as .17 pound per horsepower in the range of 8000 horsepower. The development of composite structures using fiber glass and other new materials plus new design and fabrication techniques will result in significant weight reductions. Reductions in weight of over 50% are projected for new propellers compared with the propellers of the 1950's.

Operational Requirements

In developing the propeller for a new airplane, the requirements of high reliability and good maintainability must receive high design priority. Because of the importance of maintaining the required thrust, especially with V/STOL airplanes, the probability of a loss of control or other shutdown must be very small. The value assigned to the probability value for failure will depend on the type of airplane and the mission time.

With the techniques of design and analysis available today, a new propeller should be designed for on-condition maintenance during its service life. The practice of scheduled overhaul used in the past will not be used. Along with an on-condition repair, the design should have a mean time between unscheduled maintenance of at least 50 flight hours.

The time required for any given maintenance task must be minimized, compared with past propeller designs. For instance, field replacement of a blade should be possible without the requirement for complete propeller removal, rebalance, etc. It should also be possible to remove and replace other major items in the field with a minimum of maintenance time.

The design operating life of a propeller is defined as the period of flight time during which it is economically feasible to conduct necessary repairs. The design operating life specified for a propeller is a function of the installation of the operating environment and the expected life of the airplane. For instance, a transport type airplane would have a higher operating life than a combat airplane.

The environment in which a propeller must operate is dependent on the airplane type and its uses. On certain airplane types, short takeoffs and landings must be made at unimproved forward bases where the propeller blades will be subjected to all types of sand, rocks, etc. On propeller-driven seaplanes, the blades must be designed to withstand the forces of green or solid water ingestion. It is therefore apparent that the operating environmental condition can have a large effect on the overall

propeller design.

If the airplane is operating under battlefield conditions, the chances of survival after a severe hit must be reasonable. Experience with steel blades, for instance, has shown that a remarkable amount of damage can be sustained without loss of a blade. The new designs being considered should also have a high degree of survivability.

## PROPELLER DESIGN PARAMETERS

To satisfy the requirements of a given installation with the best overall propeller configuration, a large number of design parameters must be considered and analyzed at all flight conditions. These parameters include:

1. Propeller diameter
2. Blade number
3. Single or dual rotation
4. Blade activity factor and width distribution
5. Thickness ratio distribution
6. Design lift distribution
7. Blade angle distribution
8. Blade section type

These parameters influence both the induced and profile efficiency of the propeller. The induced efficiency is the efficiency generated as a result of the production of thrust with blades operating at zero profile drag. The profile efficiency is a measure of the profile drag produced by the blades and is a peak when the blade sections are operating at the best overall lift/drag ratio.

When considering the propeller design parameters, the most important is the diameter. The propeller diameter not only determines the overall disc loading but also influences the remainder of the design parameters.

As shown from momentum considerations (page 33), the disc loading directly determines the velocity increase in the final wake and is an indication of mass of air handled by the propeller, since

$$\frac{T}{A} = \rho (V_o + u/2)u \qquad (1)$$

and the mass of air handled by the propellers is equal to

$$m = \rho A(V_o + u/2)u \qquad (2)$$

where T = The propeller thrust
A = The disc area = $\pi D^2/4$
$\rho$ = The density of air - slugs/cu ft
$V_o$ = The free-stream velocity
u = The axial velocity increase in the final wake

Also, from momentum considerations the efficiency equals

$$\eta = \frac{V_o}{V_o + u/2} \qquad (3)$$

Thus it is apparent from equations (1) to (3) that for peak efficiency, the velocity imparted to the air in the final wake must be small. Also, to obtain high levels of thrust at high efficiency, the mass handled by the propeller must be high. The disc loading must therefore be low to obtain high levels of efficiency.

Since the mass of air handled by a propeller increases with increasing forward speed, the velocity increment necessary for the production of the same level of thrust decreases and the ideal efficiency will increase with increased speed. Likewise, to obtain high levels of induced efficiency at low speeds such as takeoff and climb, large-diameter propellers are required to obtain a high level of mass flow. For these reasons, the propeller diameter required for a given efficiency is dependent on the operating requirements, speed and altitude. Also, as the speed increases, the requirement for low disc loading decreases.

For a given operating condition, the total solidity required is a function of the disc loading and therefore the propeller diameter selected.

Blade number and blade solidity (activity factor) are interrelated, and the combination is established so that the propeller will operate at a lift coefficient close to that for peak lift/drag ratio and thus peak profile efficiency. The peak lift/drag ratio that can be achieved is dependent on the section thickness ratio, section type and blade camber (design $C_L$).

Once the total solidity is established, the choice of number of blades vs blade solidity is dependent on both structural and induced efficiency considerations. As the induced efficiency is a function of the velocity and its uniformity in the final wake, propellers with a large number of blades will have the highest induced efficiency. However, if the disc loading is not too high, propellers with three or four blades usually operate very near the peak value of induced efficiency. If the

disc loading is very high and the speeds low, the designer would have to select a propeller with a greater number of blades.

In those cases where the disc loading is high, and a critical low-speed condition is encountered such as takeoff or early climb, six- and eight-blade propellers are required. These propellers will have high rotational induced losses unless half the total blades are operating in the opposite direction of rotation. When this is done, the rear set of blades of the dual rotation unit recovers the rotational energy losses of the front propeller.

Dual rotation propellers may therefore increase the overall efficiency whenever high rotation energy losses are encountered. The Soviet "Bear" bomber and the AM-22 transports, for instance, use dual rotation propellers, as the primary operating condition is a high-advance-ratio condition where high rotational losses are encountered.

To eliminate the torque reaction, dual rotation propellers have also been used for a number of experimental VTOL airplanes. The Navy XFY and XFV VTOL airplanes were primary examples. These tail-sitters used one dual rotation propeller for lift and propulsion. Low-speed control was obtained from the propeller flow over the tail surface.

For a given solidity, the actual blade planform is generally chosen for ease of manufacture except at the inboard end of the blade. Here structural and manufacturing considerations would result in high thickness ratios and low chord widths. These blades are unsatisfactory and would produce high engine losses. For this reason special fairings are installed on the blades inboard to obtain good thickness ratios and reduce the inlet losses.

On the remainder of the blade, including the tip, the planform shape required for manufacturing reasons can be obtained by adjusting the design $C_L$ and blade angle distribution. The blade chord can be increased or decreased while maintaining the same overall loading by decreasing or increasing the camber. This can be done without a loss of efficiency with practical limits.

From the manufacturing point of view, there is a considerable advantage in using a square tip. When this is done, the blade angle and design lift coefficient are reduced to obtain the desired loading. Tests with round- and square-tip propellers designed for the same load distribution indicated no significant change in performance. The only advantage identified with round-tip propellers is a reduction of near-field noise in the cabin of multiengine airplanes.

The design lift coefficient or camber of an airfoil is an important parameter in the practical design of a propeller. For low-speed operation, a high design $C_L$ in the range of .5 to .7 is generally best, as the lift/drag ratio peaks at these levels of camber. The operating lift coefficient is high at the peak lift/drag ratio for high design lift coefficient airfoils. This reduces the blade solidity required for a given load with a corresponding reduction in the overall weight.

The blade camber and blade angle distribution are generally established together so that the optimum load distributions are obtained. With the proper selection of these, it is often possible to obtain optimum efficiency at more than one blade station.

Since the load on the blade is approximately normal to the blade chord, the blade is effectively a cantilever beam; thus its strength is directly dependent on its absolute thickness. Thus for a given thickness ratio, the wider, higher solidity blades generally have better strength characteristics than propellers with narrow blades. For this reason it is possible that the propeller with the lower number of blades will have a lower thickness ratio. If compressibility losses are important, the overall improvement in the lift/drag ratio as a result of the reduction in thickness ratio may offset the increase in the induced efficiency obtained from the use of the extra blade. A complete aerodynamic and structural analysis is required to find the best configuration in this case.

The detailed choice of section type is dependent on the propeller application. Generally, the section choice depends on the spread of the operating lift coefficient, the thickness ratio and the peak section Mach number. Some airfoil sections such as NACA 65 sections have a better range of peak L/D than others. Whereas NACA 16 series sections tend to operate at higher section Mach numbers without encountering the drag rise due to compressibility than the 6 series sections. The detailed procedures for calculating the optimum distribution of the blade design parameters are covered in the aerodynamics section. Here the procedures for calculating the optimum configuration are given based on the theory of the Calculus of Variations.

## OPERATING CONDITIONS - PROPELLER TYPES

The selection of the propeller and its design parameters are directly dependent on the operating conditions. For instance, a propeller selected for a low-power, low-speed airplane will be very different from that for a high-speed installation. In this case the blade section would be chosen to favor the maximum lift coefficient whereas the sections of the high-speed prop would be chosen to avoid compressibility losses.

Compressibility losses on the propellers can be avoided either by the use of the blade sections designed to operate at the highest possible Mach numbers or by designing the blades to operate at low rotational speeds to keep the section Mach number low. In either case the objective to delay the onset of compressibility losses is achieved. The propeller types to achieve the various design objectives are defined as follows:

| | |
|---|---|
| Subsonic | Single rotation |
| Subsonic | Dual rotation |
| Transonic | Single rotation |
| Transonic | Dual rotation |
| Supersonic | Single rotation |
| Ducted | Single & dual rotation |

The term subsonic propeller refers to the maximum operating section Mach number. In this report the term subsonic propeller is a propeller where blade sections are all operating below their critical section Mach number.

Subsonic single-rotation propellers will use from two to eight or more blades and may even have two or more rows of blades. The majority of subsonic propellers will use two to four blades. The blade number and width depend on the power input, disc loading and details of the blade such as camber and thickness ratio. The propeller for a low-disc-loading application will have three or four long, narrow blades, whereas a high-disc-loading propeller installation will have four or more wide blades. The maximum blade width is determined by the solidity, which must be less than 1.0 at any blade station. The propeller solidity is defined by Equation (4):

$$\sigma = \frac{bB}{\pi x D} \qquad (4)$$

where $\sigma$ = total solidity
$b$ = blade chord
$B$ = blade number
$x$ = fractional radius
$D$ = diameter

If the total solidity exceeds one, a second row of blades is required if the blades are to rotate over the full range of blade angles.

If the solidity does exceed one and a second row of blades is required, it is generally desirable to reverse the direction of rotation of the second row and then have a dual-rotation propeller. The dual-rotation propeller has the advantage in recovering the rotation losses of the front row. Properly designed, the dual-rotation propeller will have only an axial outflow velocity and the torque reaction on the airplane will be zero. Like the subsonic single-rotation propeller, the dual-rotation propeller will have the blade sections operating below their critical Mach number.

Transonic propellers, whether single or dual rotating, will have blade sections operating above their critical Mach number at some design flight conditions. The forward Mach number of transonic type propellers will be less than one. Tip Mach numbers as high as 1.1 can be obtained with transonic propellers at some operating conditions; however, these propellers will be very noisy. For this reason transonic propellers are usually designed to operate at tip speeds below .95.

Because of the promise of high efficiency, supersonic propellers were considered for high-speed aircraft. Supersonic propellers are designed for operation at a forward Mach number above one so that with the rotational velocity of the blade component, each section on the propeller is operating at Mach numbers much higher than that of the airplane.

Ducted propellers are designed to reduce the noise level and the diameter. The disc loading used for these propellers is generally higher than conventional propellers, and the blade number used must therefore be greater. The duct design is critical and determines the speed range where peak performance will be obtained.

## PROPELLER SELECTION

As was previously noted, the selection of the best propeller for a given airplane configuration depends on the design mission of the airplane, the available engines, and factors such as payload size that affect the overall box size and fuselage geometry. Also, because of the interaction and number of design variables involved, the process of propeller selection is an iterative procedure to find the best overall configuration.

During the initial selection process, it is desirable to evaluate the effects of changes on the airplane configuration as

well as the changes in the basic propeller. Propeller diameter is one of the most important factors influencing performance; it also has a large influence on the airplane configuration because of difficulties in mounting, etc. For instance, large-diameter propellers must be mounted far out on the wing to clear the fuselage, and this influences the wing span, its loading, and therefore the performance of the airplane. Ground clearance also becomes a problem with large-diameter propellers and can lead to excessively long and heavy landing gears.

Because of the large influence of diameter on the overall airplane characteristics, it is desirable early in the design phase to conduct parametric performance studies for the airplane over a large range of propeller design parameters. This is especially important if there is a low-speed performance requirement as well as a high-speed requirement.

To conduct these parametric studies, propeller efficiency data is required for evaluating the effects of the design changes on the overall aircraft performance. Because of the lack of data for designing complete propellers and the extensive time required for each configuration, estimating procedures must be used to establish the necessary performance data. These procedures have been established for blades which are representative structurally of an average installation. The aerodynamic design parameters at each condition are established to give the peak performance at the condition considered, so in effect the load distribution is an optimum. The estimating procedures used are presented in the section on performance methods.

To estimate the performance of a propeller for a given condition for the parametric studies, the diameter is usually assumed. Based on the diameter and an assured tip speed, usually between 650 and 950 feet per second, the total blade solidity can be found that will give peak performance for any desired blade camber. The choice of blade number, camber and activity factor of the propeller is dependent on the flight condition. Usually the smallest number of blades are used, with blades having activity factor not exceeding 200 to 230. Unless the propeller is operating at high speeds where compressibility losses are a major factor, the highest blade section camber is chosen, as this gives the smallest propeller and thus the minimum weight. With all the blade design characteristics known, the efficiency of the propeller is found using the data presented in the performance section.

A typical parametric study could be an analysis of the variation of payload and airplane gross weight as a function of propeller diameter for the three-engine climb condition. As the diameter is increased, the propeller efficiency will increase, allowing an increase in gross weight. If the gross

weight increases at a rate higher than the increase in weight required for the propeller, then there is a net increase in payload; see Figure 2. It should also be noted from Figure 2 that there is probably a propeller diameter for peak load.

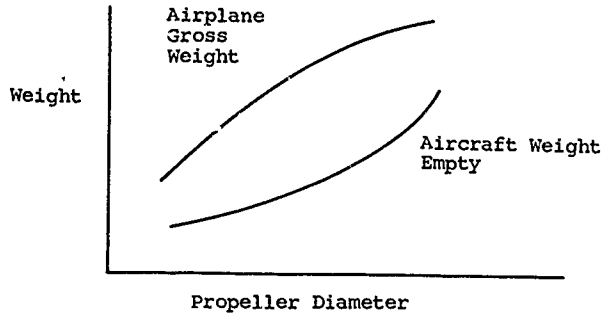


Figure 2. Propeller Parametric Study.

Because of the large effect of disc loading on the hover and cruise performance of V/STOL airplanes, parametric studies for selecting the best diameter and therefore disc loading are extremely valuable. These studies are usually done for the critical-hover and extended-range cruise conditions. Analysis of the performance at these two conditions in terms of diameter, solidity and propeller camber levels will establish the propeller design characteristics needed for peak overall performance. The desired propeller characteristics are generally found from plots of cruise efficiency as a function of takeoff efficiency (see Figure 3).

The propeller diameter and disc loading have a large effect on the overall design and performance characteristics of STOL aircraft. This is caused by the action of the propeller slipstream, as it is generally used to augment free-stream slipstream to give increased levels of lift. For this reason the wing span of the aircraft is a function of the propeller diameter, with the result that wing loading and disc loading are directly connected. To find the best configuration, then, the aircraft characteristics must be varied as well as the propeller diameter. From parametric studies of wing loading as a function of propeller diameter as shown on Figure 4, the areas for peak performance are identified. It will then be

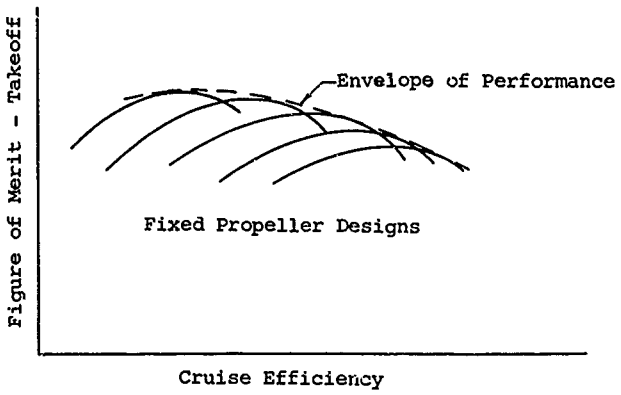


Figure 3. Propeller Selection Study.

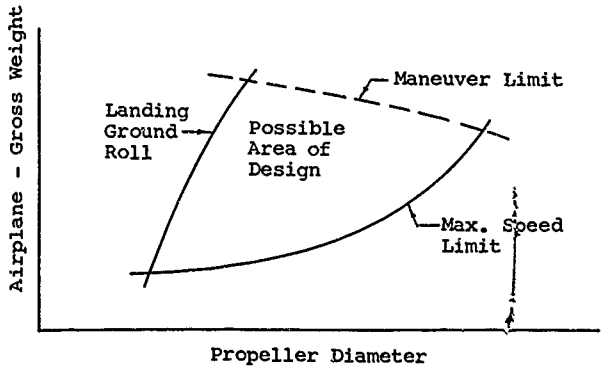


Figure 4. Propeller/Airplane Design Relationship.

possible to optimize further within these areas to find the best overall propeller.

## DETAILED FINAL PROPELLER DESIGN

The propeller characteristics required for a new airplane installation are established from parametric analyses such as those discussed in the previous section. A complete in-depth design analysis of each propeller considered in these parametric analyses could not be done at this time due to lack of detailed design data. The accuracy of characteristics of the propeller established will be dependent on the accuracy of the estimating procedure used. For propeller installations similar to existing installations, these estimates have been found to be very accurate. However, if propellers are required for large increases of size and power above current experience, the accuracy of estimates is reduced. If the complete design analysis shows that the details of the propeller differ greatly from the propeller characteristics estimated for the parametric analysis, it will be necessary to redo the analysis and establish a new overall airplane configuration.

Once the propeller's general design characteristics in terms of diameter, blade number and activity factor are found with satisfactory accuracy from the parametric studies, an in-depth analysis is done to completely define the propeller parameters for design release. This is done through a series of design studies considering all aspects of aerodynamics, structures, and blade design. Only through a large number of design tradeoff analyses, considering all the aspects of the design problem, can the best and lightest propeller configuration be obtained.

### Optimum Propeller

To establish the detailed blade characteristics, it is necessary to find the optimum configuration and performance at each important airplane operating condition. This is done by determining the optimum load distribution for a blade with a given chord and thickness ratio distribution. The blade width and thickness ratio distributions are established from the parametric analysis and estimating procedures given in the Structures and Blade sections. The optimum load or blade lift distribution is found using the theory of the "Calculus of Variation" presented in the Aerodynamics section. The load distribution obtained using this method will not necessarily correspond to either that for peak-induced efficiency or that for the maximum lift/drag ratio of each blade station. The load distribution calculated using the "Calculus of Variation" will correspond to the best combination of the profile and

induced loading to give peak efficiency.

After the optimum load distributions are found for each operating condition, the design $C_L$ and blade angle required to satisfy the optimum loading are determined. At each blade station, the design $C_L$ required has a fairly wide range. For instance, design lift coefficients in the range of .3 to .5 will often be the same drag, and thus the same lift/drag ratio. This wide range of $C_{Li}$ for a given drag $C_D$ makes it possible to select a distribution that is nearly optimum for two or more flight conditions, and thus have a propeller that is best over a much wider range of operating conditions. This is illustrated in Figure 5.

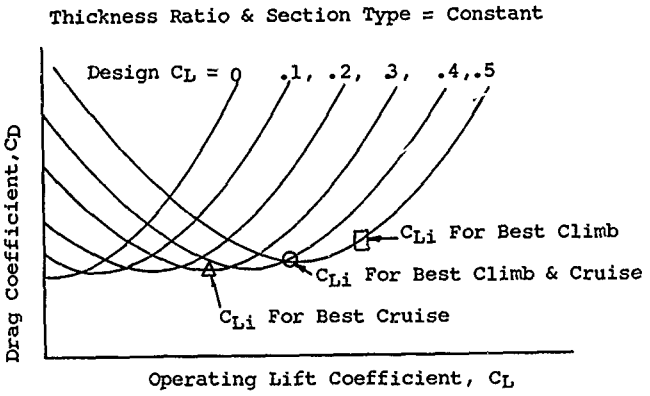


Figure 5. Selection of Section Design Lift Coefficient - $C_{Li}$.

With the selection of the design $C_L$ and blade angle distributions for optimum performance, all the blade aerodynamic characteristics required are known.

## Propeller Design

The details of the blade required for manufacture, including its structure and construction, are established from the required aerodynamic properties using the procedures as described in the section on Structures and Blade Design. This is an iterative process to establish the lightest design and depends on the characteristics of the installation as well as

aerodynamic requirements for establishing the final blade design. During this design analysis phase, problems are often encountered where deviations in the previously established aerodynamic characteristics are necessary to meet structural and design requirements without excessive weight penalties. Aerodynamic analysis of design change required to satisfy these structural or manufacturing requirements generally shows that design changes can be made with little or no loss of performance.

The hub, blade retention, blade angle actuator and control system are dependent on the blade design and required installation characteristics. The design considerations for these are covered in later sections of the report, and again consideration must be given to the entire system to obtain the best propeller. For instance, the integration of the engine, gearbox and propeller can result in elimination of parts and thus important weight savings.

During the design phase of the entire propeller, a considerable amount of component tests should be done to assure a successful design and completion of the qualification testing without costly redesign. The testing necessary will include, as a minimum, material fatigue, blade vibration, blade actuator, control system and hub load testing. These tests must be planned early in the development to assure the results are available prior to design release, so that the necessary corrective action can be taken before the propeller is completely released for manufacturing.

## QUALIFICATION PROCEDURES UNDERTAKEN

The current requirements for qualifying a new propeller for a military installation are outlined in Reference 2. These qualifying procedures have been made more concise and more stringent compared with those in force during the early 1950's.

To qualify a propeller in the early 1950's, it was only necessary to demonstrate performance of 1 hour at 110% maximum speed, 20 hours at a load corresponding to 200% normal power, and a 105% overspeed centrifugal load proof test. Feathering and reverse testing requirements were dependent on those specified by the procuring agency. The engine endurance test required a 50-hour run at maximum continuous power and 50 hours at a high stress condition selected on the basis of a vibration survey during the stand testing. Functional tests consisted of 500 manual pitch cycles and 1500 automatic pitch cycles.

Also, as a part of the propeller type test, it was calibrated at the zero-speed condition on an electric motor dynamometer. For the zero-speed calibration, the propeller was usually run

at a series of blade angles from -25 degrees to +50 degrees in increments of 3 to 5 degrees over the range of rotational speed up to the maximum. Power and thrust were measured at all operating conditions and corrected to standard conditions.

It was recognized during the 1950's that the tests as described above are done only at the zero speed and therefore do not necessarily simulate all the conditions along with the critical stress condition that may be encountered in service. Thus, service experience was relied upon to judge the acceptability of a new propeller installation, and if unfavorable, could be sufficient for its rejection even though it passed the type test.

Experience with propellers certified in this manner was not good, especially on aircraft with higher powered reciprocating and turbine engines. As the engine power and the propeller diameter increased, a number of new unknown problems were encountered. Although there was a considerable amount of component testing done by the contractors in developing new propellers during this time, the work was not adequate to isolate all the problems. To prevent design problems and unknowns, experience has shown that proper qualification testing must be done which duplicates the conditions to be encountered on the installation to obtain the degree of reliability and safety needed. Coupled with this testing must be an adequate engineering program to account for secondary structural and dynamic problems which may become of major importance.

## PRESENT QUALIFICATION REQUIREMENTS

To qualify a new propeller for production, extensive testing is now required (Reference 2). Before the propeller can be certificated for flight operation under controlled testing conditions, it must pass a preliminary flight release test (PFRT). The testing required is similar to that used for previous qualification procedures. However, before the endurance testing can be undertaken, a vibration stress summary to establish flutter characteristics of the hub and blade is first required before these data are used for determining the test operational limits for further testing.

The propeller is then to be calibrated with the measurements of thrust and power up to rotational speeds of 120% of the maximum rated speed. With the propeller blade angle set for normal rated power and rpm, it shall be run at 150% of maximum rated horsepower for 20 hours.

After the structural proof testing is complete and teardown inspection shows no problems, the propeller is reassembled and functionally tested. The overspeed feather test not only

confirms the propeller's ability to feather from a severe overspeed condition, but it also tests the blade retention at conditions of twice centrifugal force. The propeller, in demonstrating the ability to feather at 141% maximum rated rpm at low pitch and at 120% maximum rated rpm at 45 degrees blade angle and above, must have a high reserve pitch change capacity. These tests are more fully described in Reference 2.

In addition to the above test, a 50-hour engine test is required. This test series is designed to show engine/propeller compatibility and requires running at representative operating conditions such as takeoff, Military, normal, maximum reverse, etc., for a total of 50 hours. This test simulates the torque conditions expected and some propeller control activity, but does not subject the propeller to the critical flight loads. The engine/propeller 50-hour test also does not simulate the vibratory loads on the propeller.

To duplicate flight conditions, preliminary aircraft tests are required. These tests are conducted on an aircraft test bed or a suitable aircraft having a nacelle configuration similar to the proposed application. The objectives of these tests are to prove compatibility and check vibratory stress levels. This program usually takes place during the initial flight test program, and the propeller is carefully monitored at all times.

After the PFRT has been completed and production is undertaken, a very extensive test program is required. This program, known as accreditation tests, is necessary to assure the propeller can demonstrate adequate safety at all flight conditions. Basically, the accreditation tests are extensions of the PFRT. An additional 150 hours of engine/propeller testing is to be accomplished with 150 successive 1-hour cycle tests duplicating the same conditions of the 50 twin-engine propeller tests. The ice control system shall be cycled during these tests. As part of the accreditation tests, the propeller is to be subjected to environmental tests, component and accessory tests, and durability tests. The durability tests are to establish an overhaul period of at least 1500 hours. A complete description of the test requirements, including records, test conditions and inspections, is given in Reference 2.

Commercial Propeller Qualifications

A type certificate for a new propeller can be obtained from the FAA by completing vibration tests, centrifugal load tests, endurance tests and functional tests. Information specifying operational limits, instruction manuals, design features, materials and durability characteristics of the blade must also

be provided.

The testing requirements listed are similar to those required by MIL Specs. A vibration test to determine areas of high stress in all components is required. The propeller must also demonstrate its strength by operating at a condition equal to twice the centrifugal force of normal operation for a period of 1 hour. This requirement can be completed by rotational test or a pull test.

Endurance testing is necessary corresponding to a 100-hour engine test at maximum continuous power and rpm except where the vibration test showed a critical rotational speed condition.

In this case, up to 50 hours of the 100-hour test must be made at this critical speed. Also, if the takeoff rating is greater than the maximum continuous rating, an additional 10 hours of block testing must be made at this rating. The propeller must also be endurance tested with the intended engine for a period of 150 hours. This running must be made at conditions simulating actual operation, and is detailed in Reference 3.

The functional test requirements consist of 500 manually controlled cycles, 1500 complete cycles of automatic control through the range, 50 feather cycles, and 200 reverse cycles. After completing these tests, the propeller must pass an inspection after being disassembled. Complete details are given in Reference 3.

Recommendations

The tests outlined to first qualify the propeller for flight testing, and finally for production, come at a time during the program where problems will cause costly delays. To minimize such problems, a better definition of the expected environment is required. For instance, the airplane, engine and propeller must be integrated so that the structure is of the proper mounting stiffness and impedance. Also, the frequency of the wing and engine propeller mounts must be matched to the propeller weight, strength and rpm range. The flow field should be completely defined so that the blades can be designed for the proper level of Aq. In addition, the propeller control requirements and safety features must be completely specified to eliminate as many surprises as possible during the qualification program.

To minimize problems and surprises during qualification, it is therefore recommended that the propeller design criteria as outlined in Appendix I of volume III be completely specified well in advance of the initiation of the design. Further

component testing of all the important components must be completed as early as possible to allow for any necessary redesign.

## MAINTENANCE, RELIABILITY AND SAFETY

The maintenance requirements of propellers in use during the 1940's and early 1950s were specified in the service manuals. Generally, daily visual inspections were specified which called for a visual inspection of the blades, hub and power unit. These inspections did not call for the removal of covers. Preflight checks of operation were also specified to prevent takeoff with a nonoperating propeller. The visual inspections call for removing grease and dirt and looking for cracks, scratches, nicks and corrosion and taking the necessary corrective action.

Maintenance inspections calling for removal of covers, lubrication and visual inspection were required at 100-hour intervals. Included in this maintenance work was the inspection and cleaning of electrical points.

Complete propeller removal with complete teardown and inspection during this period was usually specified by the operator as the requirement, especially during wartime, depending on the operation. This teardown and inspection was a complete overhaul of the propeller and included magnaflux of all critical steel parts including steel blades, replacement of bearings, seals, etc.

The success of the maintenance program described above depended largely on the diligence of the maintenance crew and the accessibility of critical parts. Primary structural components covered by aerodynamic surfaces, critical parts hidden within the propeller, and incomplete service information were other causes of maintenance difficulties. Thus, many of the maintenance problems of this period were caused by basic design errors as well as human errors.

The propellers of the 1950's were designed with primary emphasis on maximum performance, minimum weight and protection from mechanical failures. Little attention was given to maintenance considerations, and therefore many of the propellers were overcomplicated and complex. Removal of blades of some propellers, for instance, would require the complete teardown of the complete propeller involving many man-hours. In addition, such a teardown would involve disturbing assemblies prematurely. Thus, if it were necessary to change a blade due to foreign-object damage, excessive disassembly would be required.

The multiplicity of propeller parts used in past designs has

tended to encourage a high frequency of maintenance actions, and it was difficult to identify troublesome items. The complexity of some of the propellers, particularly those used on turboprop engines, required the employment of highly trained and equipped personnel to handle the troubleshooting, removal and repair required.

To be competitive from the standpoint of maintenance, the propeller of the future must employ the concept of modular construction used on some of the earlier Curtiss Electric propellers, and one of the recent Hamilton Standard propellers used on the AH-56 (AAFSS) helicopter. These propellers offered the advantage of easy blade replacement in the field, and separate power units and speed controls allowing replacement without disturbing other assemblies. The blades, control unit and all other propeller components must be designed with an overhaul life exceeding the engine, so that the only maintenance action required would be a result of foreign-object damage. Thus, items would be replaced as a result of condition only and complete overhaul. Also required will be easy access to the critical parts required for inspection, so that excessive time is not required to perform preflight inspection tasks.

Further, it is desirable to design the propeller using the concept of on-condition maintenance only. Then the propeller becomes less important in determining the downtime of the airplane.

## PROPELLER AERODYNAMICS

### INTRODUCTION

The aerodynamics of propellers have been developed over the years so that there are many design and evaluation procedures available for determining their characteristics. These procedures run from short single-point methods of analysis to the more extensive complete strip methods. The short method of analysis considers the propeller as a whole and is useful for preliminary design analysis and evaluating propeller performance data. The strip analysis procedures consider each section of the propeller blade from root to tip and are the most accurate calculation methods for finding the performance.

In this section the aerodynamics theory and data will be presented so that methods will be available for designing and analyzing any type of propeller. The theory and data presented are limited to those needed for the practical design and the evaluation of the performance of the propellers operating over the speed, power, altitude and angle range of conventional and V/STOL airplanes. In the development of the design and performance evaluation procedures, empirical corrections have been avoided where possible. The empirical corrections and data are only applied where the theory is not available; for instance, at negative thrust and other off-design operating conditions. It is considered important to stay close to the theory wherever possible to provide information for improving the design and correcting any deficiencies.

The primary function of a propeller is the conversion of shaft torque to shaft thrust in an efficient manner. If the propeller is operating at a given free-stream velocity V and is producing a thrust T, the efficiency becomes

$$\eta = \frac{\text{Power output}}{\text{Power input}} = \frac{TV}{550\,(hp)} = \frac{TV}{P} \qquad (5)$$

where $\eta$ = propulsive efficiency
T = thrust
P = power
V = free-stream velocity
hp = shaft power absorbed by the propeller

Equation (5) is the usual definition of efficiency and is used at all conditions where V is greater than zero. At zero velocity, the performance or efficiency of a propeller is measured by the term Figure of Merit, FM, which is defined by the

equation

$$FM = \frac{T\ D_p}{\sqrt{53.64}\ hp\ D_w} \sqrt{\frac{T}{A_p \sigma}} \qquad (6)$$

where $D_p$ = propeller diameter

$D_w$ = wake diameter

$A_p$ = propeller disc area = $\frac{\pi D_p^2}{4}$

$\sigma$ = density ratio

The efficiency of a given propeller at any condition depends on the losses due to friction and those losses due to the acceleration of the fluid.

The efficiency loss due to the production of thrust as a result of the acceleration of the fluid is known as the induced loss. The induced efficiency, a measure of the induced loss, is the efficiency of the propeller when the profile drag of the blade sections is zero. If the propeller were moving through the air with zero slip, the induced efficiency would be 100%. However, as the propeller must accelerate the fluid to produce thrust, the induced efficiency is always less than 100%. The induced efficiency accounts for all the losses due to the acceleration of the fluid, including the axial, tangential and radial losses. Thus the energy expended as a result of flow about the blade tip and between blades is accounted for as well as the axial velocity when the induced efficiency is found.

The profile efficiency of a propeller, a measure of the losses due to friction, depends on the drag of the two-dimensional airfoil sections used for the blades, the operating lift, Reynolds number, Mach number and their distribution along the radius. The section drag of the blade will reduce the thrust and increase the power required, and is therefore a direct loss. The profile efficiency is then a measure of the losses due to drag of the blade section. To determine the profile losses of propellers, a large amount of two-dimensional airfoil data is required. The airfoil data are needed as a function of thickness ratio, section type, design lift coefficient, Mach number and Reynolds number.

## BASIC PROPELLER THEORY

The theory of propellers has been developed so that it is now possible, using suitable two-dimensional airfoil data, to

design highly efficient propellers and predict their performance over a wide variety of operating conditions. The theory has developed from the very simple momentum theory concept, which allows a prediction of the overall highly idealized performance of a propeller, to the more complex vortex theory, which enables the prediction of the induced losses and the application of two dimensional airfoil data for calculating the profile losses. By knowing both the induced and profile losses, the total propeller efficiency is thus determined.

There have been many approaches used to develop a theory of propellers suitable for designing and evaluating them over a wide range of operating conditions. However, only those theories which have been applied to calculate propeller performance will be discussed in this report. These will include the simple momentum theory and the vortex theory propeller given by Goldstein and Theodorsen and their modifications for practical application.

The basic theory of propellers applies only for the case when propellers are operating in an incompressible fluid under steady-state conditions. Modifications to the theory are therefore necessary when performance is required for the compressible flow case. Where the flow is effectively unsteady, as when the propeller is operating at high shaft angle of attack, also requires modification to the basic theory. The other theoretical approaches available may be found in References 14 and 15.

## Propeller Momentum Theory

As the thrust of a propeller is produced from the acceleration of the fluid, an understanding of the flow process is important in the development of the theory and the design analysis of new propellers. The classical axial momentum theory gives the basis for describing the flow process and for finding the peak efficiency. For this reason and the fact that the momentum theory is basically the foundation of all propeller theory, it is presented here. The basic or simple momentum theory was developed by Rankine & Froude for ship propellers and has been presented by many others, including Glauret, Reference 4.

Consider a propeller with an infinite number of blades, each capable of imparting an increase of axial velocity to the air. The propeller has a disc area $A_D$ and is advancing with a velocity $V_o$ in a fluid with a density $\rho$. The propeller is assumed to produce a thrust T and is absorbing power P. As the fluid passes through the propeller, it is continuous. The velocity is identical on either side of the disc, but the pressure increases by a factor T/A. The pressure decreases in the final wake to that of the free stream, with a corresponding increase

in velocity and a decrease of area. The pressure in the fluid far upstream and far downstream is equal to the ambient pressure $p_o$. The general type of flow for the propeller is shown on Figure 6.

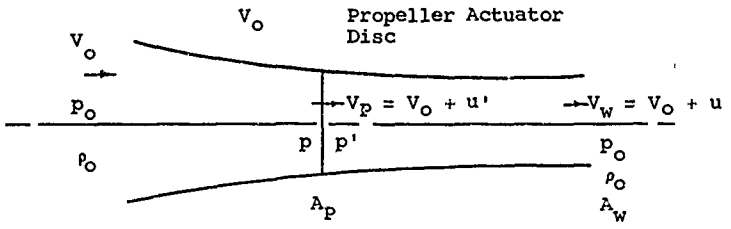


Figure 6. Propeller in an Axial Flow Stream.

If the propeller is handling a mass of air of m pounds per second and the velocity in the final wake has been increased to $V_w$, the force is equal to the change in momentum. Thus

$$T = m\ (V_w + V_o) = mu \qquad (7)$$

where
- $T$ = the thrust produced
- $m$ = the mass of air handled
- $V_o$ = initial velocity
- $V_p$ = velocity at disc = $V_o + u_p$
- $V_w$ = velocity in final wake = $V_o + u$
- $u'$ = the velocity increase through the propeller disc
- $\rho$ = the mass density of the air
- $u$ = the velocity increase in final slipstream

The increase of kinetic energy in the slipstream is

$$KE = \tfrac{1}{2}\ m\ (V_w^2 - V_o^2) \qquad (8)$$

Since power is equal to the change in kinetic energy, the power is

$$P = \tfrac{1}{2}\, m\, (V_w^2 - V_o^2) \tag{9}$$

As the propeller is advancing with a velocity $V_o$, the power output is

$$\text{Power out} = T\, V_o \tag{10}$$

Since efficiency is the ratio of power out to power in, or

$$\eta = \frac{\text{Power out}}{\text{Power in}} = \frac{m(V_w - V_o)V_o}{\tfrac{1}{2}m(V_w^2 - V_o^2)} \tag{11}$$

Equation 11 reduces to

$$\eta = \frac{V_o}{V_o + u'} \tag{12}$$

Since the energy is only added at the propeller disc, the total head upstream is constant and the total head downstream of the propeller is constant. The difference in head across the disc represents the pressure rise due to thrust since there is no change of velocity through the disc.

Thus $$H_1 - H_o = p \tag{13}$$

$$H_o = p_o + \tfrac{1}{2}\rho V_o^2 = \tfrac{1}{2}\rho(V + u')^2 + p' \tag{14}$$

$$H_1 = p + p' + \tfrac{1}{2}\rho(V + u')^2 \tag{15}$$

$$p' = H_1 - H_o = \rho(V + \tfrac{1}{2}\, u)u = T/A \tag{16}$$

Since $$T = \rho A(V + u')u \tag{17}$$

then $$u' = \tfrac{1}{2}\, u \tag{18}$$

Thus the momentum theory gives the propeller designer a measure of the peak efficiency that can be expected for any propeller disc area or diameter. The momentum theory also provides information as to the increment of velocity through the propeller disc in relationship to the velocity in the final wake. This conclusion is of major importance in the application of the more complex vortex theory of propellers to be covered later in this section. The momentum theory only provides average information on the flow of a propeller with

an infinite number of blades. Further, since there is rotation in the final stream, the solution of the momentum equations represents the case of a highly idealized propeller. This is of interest only as it gives information with respect to the peak efficiency.

Momentum Theory Static Condition

When the forward velocity is zero, as at the start of takeoff or hover, the efficiency as described by the above is zero since the free-stream velocity is zero. To assess the overall worth of a propeller at these conditions, the level of thrust to power could be used as measured. Thus, from Equation (11) at $V = 0$,

$$T/P = \frac{2}{u} \tag{19}$$

The term T/P does not have any particular significance when considered alone, as in the case of efficiency. That is, a maximum value of thrust or efficiency is not apparent. For this reason the term Figure of Merit was developed for measure of relative performance or efficiency of propellers and rotors operating at the static condition. The figure of merit of a propeller is a measure of power in the slipstream to the power input. If the process were 100% efficient, the power in the slipstream would equal the power input. Since all the input or shaft power is not converted into slipstream power and likewise this slipstream power is not converted to thrust, the flow process is not equal to 100% as in the case if the process were adiabatic. Thus the term Figure of Merit can be thought of as the efficiency of the adiabatic process. Thus,

$$FM = \frac{\text{Power out}}{\text{Power in}} = \frac{\frac{1}{2} m(V_w^2 - V_o^2)}{550 \text{ hp}} \tag{20}$$

at the static condition $V_o = 0$ & $V_w = u$

$$T = mu \tag{21}$$

$$FM = \frac{Tu}{1100 \text{ hp}} \tag{22}$$

From Equation (18) and noting that

$$M = A_p u_p \text{ and } u' = u/2 \tag{23}$$

$$u' A_p = A_w u \tag{24}$$

the velocity increase in the final wake becomes

$$u = \frac{T}{m} = \frac{T}{A_p w u_p} \quad \frac{A_p}{A_w} \tag{25}$$

and $$u^2 = \frac{T}{\rho A_p} \quad \frac{D_p^2}{D_w^2 \ .002378} \tag{26}$$

$$u = \frac{D_p}{D_w} 20.5 \sqrt{\frac{T}{A_p} \frac{1}{\sigma}} \tag{27}$$

Substituting Equation (27) in (21), the Figure of Merit becomes

$$FM = \frac{T}{hp} \quad \frac{D_p}{D_w} \quad \frac{1}{53.64} \sqrt{\frac{T}{A_p}} \tag{28}$$

Since at the static condition by momentum consideration $D_p/D_w = \sqrt{2}$,

$$FM = \frac{T^{3/2}}{38.94 hp \sqrt{\sigma A_p}} \tag{29}$$

Substituting the standard propeller thrust and power coefficients in Equation (29), the Figure of Merit in coefficient form becomes

$$FM = \frac{.798 \left[C_T\right]^{3/2}}{C_p} \tag{30}$$

With the equations for calculating the ideal efficiency of propellers by momentum considerations and efficiency at zero velocity using the concept of Figure of Merit, the tools are available for evaluating the relative merits of any configuration. When evaluating a given propeller, it is useful to find the peak value as represented by the ideal efficiency and compare this efficiency with that of the actual configuration to determine if changes should be made to improve the performance.

It is particularly useful to compare the performance measured by test to that of the ideal efficiency. Many times the measured propeller efficiency has been above the ideal due to test errors. By comparing with the ideal, the errors have been found.

The ideal efficiency of a given configuration is an excellent

measure for the assessment of the performance requirements of a new installation. For instance, when thrust requirements for a new installation are compared with the ideal performance for the given power, velocity and diameter problems can be quickly determined with the overall design.

It is therefore important to determine the ideal efficiency of a new propeller early in the design evaluation to assure that the required performance is below the ideal. Otherwise, an impossible situation will exist and a new configuration will have to be developed.

Vortex Theory of Propellers $V > 0$

Although the momentum theory of propellers provides certain basic information that is suitable in determining the upper limits of performance, the assumptions used in the theory are too gross to be practical for actual propellers with a finite number of blades. With a practical propeller, the axial, radial and tangential velocity losses must be found instead of only the axial loss as is found for the actuator disc considered in the momentum theory. Also, with practical propellers having a finite number of blades, the axial velocity is not uniform across the disc, further increasing the losses. For these reasons, a more extensive theory is required to find the induced losses and velocity field of the actual propeller than is possible using the simple momentum theory.

The actual induced velocity at any blade station is required so that the total induced losses may be found as well as the flow corresponding to two-dimensional conditions. Knowing the induced losses, the induced efficiency can of course be found. Also, with the true induced velocity known, the true two-dimensional conditions at any blade station can be determined. This makes it possible to apply two-dimensional airfoil data for finding the drag, lift/drag ratio, and so the profile efficiency. The combination of the induced efficiency and profile efficiency of course makes it possible to determine the total efficiency of the propeller.

The problem of determining the inflow velocity for an actual propeller with any load distribution resolves itself with determining the positions of the vortices in the final wake. Since the vortices proceed downstream with a velocity equal to the free-stream velocity plus the induced velocity and the induced velocity is dependent on the load, the position of the vortices in the final wake is not directly known. Thus, if the induced velocity is calculated directly for a given load distribution, it will be necessary to assume the position of the vortices in the final wake, calculate the induced velocity at the propeller, find a new vortex wake, and recalculate the velocity at the

propeller until convergence is obtained. Since the vortices produced by all the blade stations on each blade of the propeller influence the induced velocity at each blade station, the procedure described is very lengthy and has not been successfully accomplished. This is especially true at the static case, V = 0, where the induced velocity determines the position of the vortices in the final wake only (Reference 5).

Using a vortex theory similar to wing theory, Goldstein (Reference 6) developed the first practical solution for calculating the induced velocity for a propeller with a finite blade number operating in incompressible flow. He assumed that the circulation at the root and the tip of each blade is zero; the blade is represented by a lifting line with the strength $\delta\Gamma/\delta r$ equal to the change in circulation between stations. These vortex lines are assumed to form helical vortex sheets that extend from the blade to infinity.

Goldstein formulated the problem for calculating the induced velocity at the propeller by using the concept of rigid vortex sheets. This approach was used as Betz and others, who showed that when the blade loading is equal to that for minimum power, the vortex sheets behind the propeller will be rigid. Thus, using the idea of optimum load distribution, the vortex sheets are rigid behind the propeller and a practical solution becomes possible.

Goldstein solved the problem by placing the rigid vortex sheets in a potential stream and calculated the conditions at the propeller. In this calculation it was assumed that the helical pitch angle is equal to

$$\phi = \tan^{-1} \frac{V}{\pi nD} \tag{31}$$

where V = the free-stream velocity
n = rotational speed, rps
D = propeller diameter

Thus it is assumed that the induced velocity is very small in relation to the free-stream velocity and can be neglected. This is the assumption of light loading and assumes the propeller is moving through the air with zero slip. By using this assumption, Goldstein then solved the potential flow problem with Bessel function and generated coefficients that could be used to find the induced velocity as a function of advance ratio.

Goldstein related the strength of the circulation to the velocity of the screw surface w by the relationship shown in Equation (32), which was calculated as a function of advance ratio for two- and four-blade propellers.

$$K(x) = \frac{B \Gamma \omega}{2\pi V w} \qquad (32)$$

where B = blade number
$\omega = 2\pi n$
V = the forward velocity
w = the velocity of the screw surface on its axis

By using the relation that the induced velocity in wake is twice that at the propeller and assuming zero slipstream contraction, the total induced velocity at any blade station can be found using the values of K(x) calculated by Goldstein, Reference 6.

Propeller theory is similar to wing theory in that both use the concept of the surface of discontinuity within a potential flow field to determine the velocity change due to the generation of lift. As was noted previously, the propeller sheds a series of vortices which form a vortex surface. The strength of the vortices shed at each point is dependent on the change in lift or circulation along the span. Since no flow can theoretically penetrate the vortex surface formed by the shed vortices, the velocity normal to the surface is identical on both sides. This means the surface must be moving downstream from the propeller with a velocity equal to the free-stream velocity plus a velocity represented by w, the displacement velocity. Within the field, the flow can pass around the edges of the surface of discontinuity; as a result of this flow, the tangential velocity difference at any point on the vortex surface is equal to the strength of the surface. In reality the difference in the tangential velocity is equal to the net effect of all the elements of vortices in the field which were formed due to change in circulation along the blade span.

Thus, if the tangential velocity is determined on either side of the vortex sheet, the change is equal to the effect of all the lift changes produced by the propeller. Now these lift changes represent the difference between the two-dimensional ideal case and the actual three-dimensional propeller. For this reason, if the change in velocity is determined based on the flow around the vortex sheets at the propeller disc, it is exactly the velocity change necessary to apply two-dimensional airfoil data. An integration of this velocity also represents the efficiency loss due to three-dimensional effects, i.e., the effects of the shed vortices due to lift changes. Thus the potential solution developed by Goldstein was a major step development of the theory of propellers, as it provided the data required for the application of two-dimensional airfoil data.

Lock, Reference 7, expanded the work of Goldstein and published

suitable working charts for two-, three-, four- and six-blade single-rotating propellers. These charts were found to give satisfactory results when applied for calculating the performance of propellers operating at the usual climb, cruise and high-speed conditions.

The working charts developed by Lock using the Goldstein theory were found to give accurate results for propellers operating at the usual cruise and climb conditions. When operating at low advance ratios and high loadings, it was believed that the assumption of light loading used by Goldstein was leading to inaccurate results. Since power loading was also increasing and dual-rotation propellers were being considered, an improvement in the basic Goldstein theory was found to be necessary.

Vortex Theory - Theodorsen - $V \geq 0$

The vortex theory of propellers developed by Goldstein was extended to the case of heavy loading by Theodorsen using the same basic concepts of the rigid helical surface, zero circulation at the tip and root, and a circulation whose strength is equal to $\partial\Gamma/\partial r$ at a given blade station. Since the basic potential flow solution is the same for any loading as long as the blade number and helix angle are the same, the main difference between the basic Goldstein theory and that of Theodorsen is the handling of the results of the potential flow solution. Reference 8.

Theodorsen showed that the wake or pitch of the helical screw surface is dependent not only by the advance ratio but also by the term displacement velocity, w. The displacement velocity (w) is defined by Goldstein as the velocity of the screw surface in the direction of its axis. Thus, when the term K(x) was found from the potential flow solution to relate the strength of the circulation to the displacement velocity, it was shown that helix angle should be equal to

$$\phi_w = \tan^{-1} \frac{V + w}{\pi n D} \tag{33}$$

rather than

$$\phi_w = \tan^{-1} \frac{V}{\pi n D} \tag{34}$$

as was used by Goldstein, which is the assumption of light loading.

The effect of finding K(x) at the higher helix angle is to lower its value and increase the magnitude of the displacement velocity for a given loading. Thus the induced efficiency is reduced as a result of using the concept of heavy loading.

The use of the helix angle in the final wake based on its actual pitch leads to a new definition of the term K(x). Theodorsen uses

$$K(x) = \frac{B\,\Gamma\,\omega}{2\pi(V + w)w} \qquad (35)$$

where B = the blade number
$\Gamma$ = the strength of circulation
$\omega$ = rotational speed
V = free-stream velocity
w = displacement velocity

rather than the definition used by Goldstein, Equation (32). This change in the definition of K(x) tends to reduce the displacement velocity. Therefore, any errors in the efficiency as a result of the use of the concept of light loading tend to compensate.

The error of the displacement velocity obtained using the Goldstein assumption of light loading will cause an error in the calculation of the induced velocity. More serious, however, are the errors in determining blade design characteristics using Equation (34) rather than (33). A small error in the displacement velocity can lead to errors in blade angle distribution that may reduce the efficiency, especially at the low-advance-ratio conditions. For this reason, the Theodorsen theory should be used rather than the Goldstein theory for finding the induced efficiency, the flow conditions at the propeller, and in the final wake and the detailed design.

In addition to modifying the Goldstein theory to apply at the heavy loading condition, Theodorsen extended the theory and data to apply for both single- and dual-rotation propellers.

Using the electrical analogy technique with actual models of helical vortices instead of Bessel functions, Theodorsen found values of K(x) for single- and dual-rotation propellers at the blade stations from hub to tip and advance ratios 1 to 6. These measured values of K(x) agreed very closely with the Goldstein values when compared at the same helix angle.

An integration of K(x) and K(x,$\theta$), where $\theta$ represents the angle with respect to the helix necessary for dual-rotation propellers, gives the mass coefficient k (equation (34)

$$k = \frac{1}{\pi}\int_0^{2\pi}\int_0^1 K(x,\theta)\;\; d\theta \times dx \qquad (36)$$

for dual-rotation propellers and

$$k = 2\int_0^1 K(x)\, x\, dx \qquad (37)$$

for single-rotation propellers.

The quantity k in equations defined is the mass coefficient and can be thought of as the modifier for correcting the momentum equation to the three-dimensional case. The mass coefficient is actually

$$k = \frac{w'}{w} \qquad (38)$$

where $w'$ = mean displacement velocity over the wake
$w$ = rearward displacement velocity at the vortex

Another interpretation of the mass coefficient is that the full interference or displacement velocity is imparted to the air of cross section k times the cross section of the wake helix. The mass coefficient is particularly useful when calculating the performance of dual-rotation propellers. It is also useful when assessing the source of the slipstream losses and determining the true interference velocity at the propeller.

The values of K(x) and k originally published by Theodorsen were found to be somewhat in error. Crigler, Reference 9, corrected the values of K(x) and k needed to calculate the performance of propellers by strip analysis. The corrected values of K(x) and k required are presented in Figures 7 through 18 as a function of the advance ratio in the final wake $J(1 + \bar{w})$. The axial loss coefficients $\epsilon/k$ are given in Figures 19 and 20.

Propeller Strip Theory - Single Rotation - $V \geq 0$

Propeller strip theory has been developed to use the data from the vortex theory of propellers to determine the induced efficiency and the induced velocity for the application of two-dimensional airfoil data for calculating the profile efficiency. The strip theory is used to find the performance as it makes possible a complete analysis of all the details of the propeller blade. Thus, the effects of detailed changes of any sections of the blade can be determined for any operating condition. This is of course a very effective procedure, as it enables the designer to evaluate detailed design changes until an optimum is obtained.

The determination of the induced velocity using the vortex

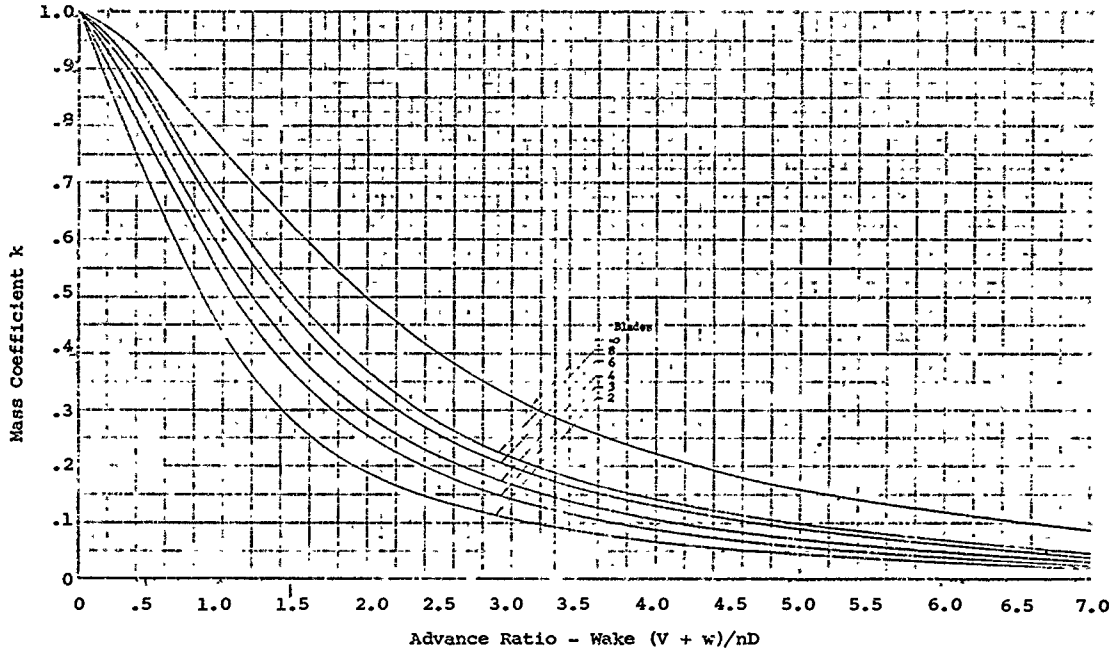


Figure 7. Mass Coefficient - k,
Single-Rotation Propeller.

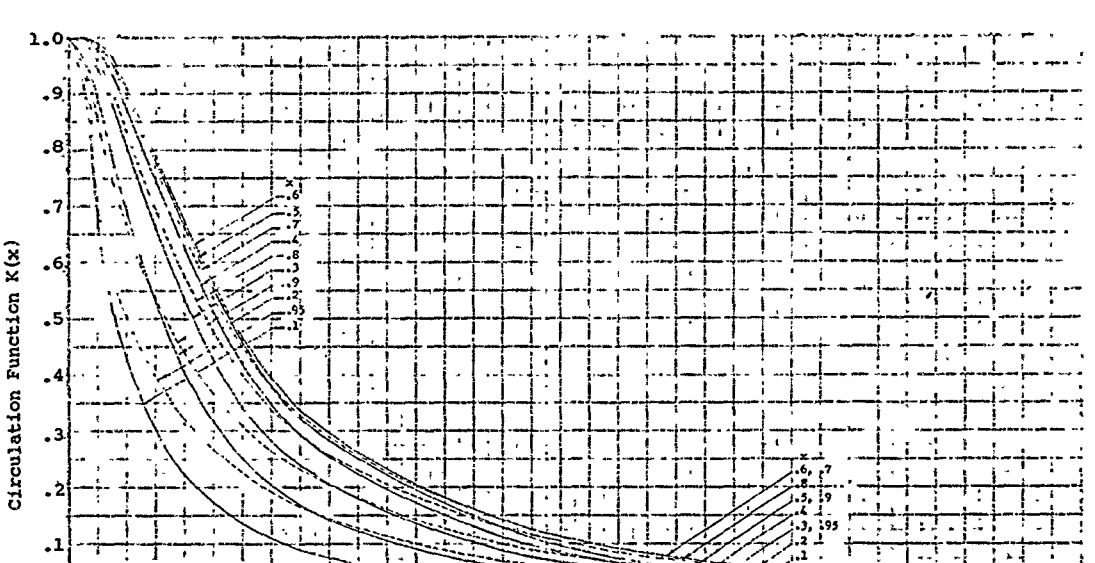


Figure 8. Propeller Circulation Function - Two-Blade Single Rotation.

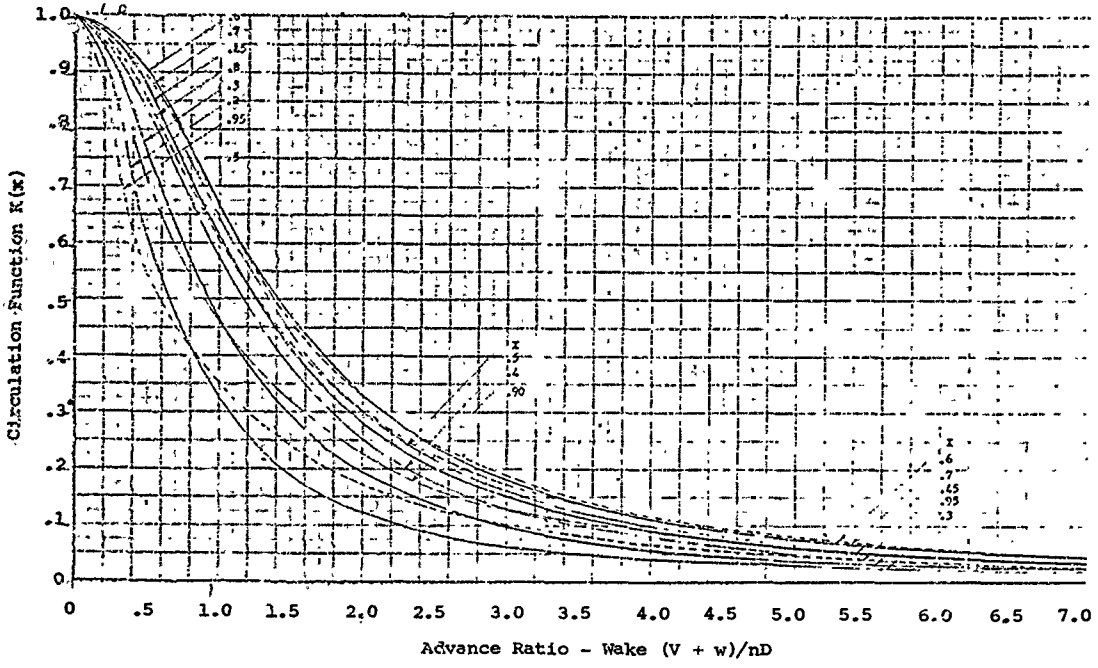


Figure 9. Propeller Circulation Function - Three-Blade Single Rotation.

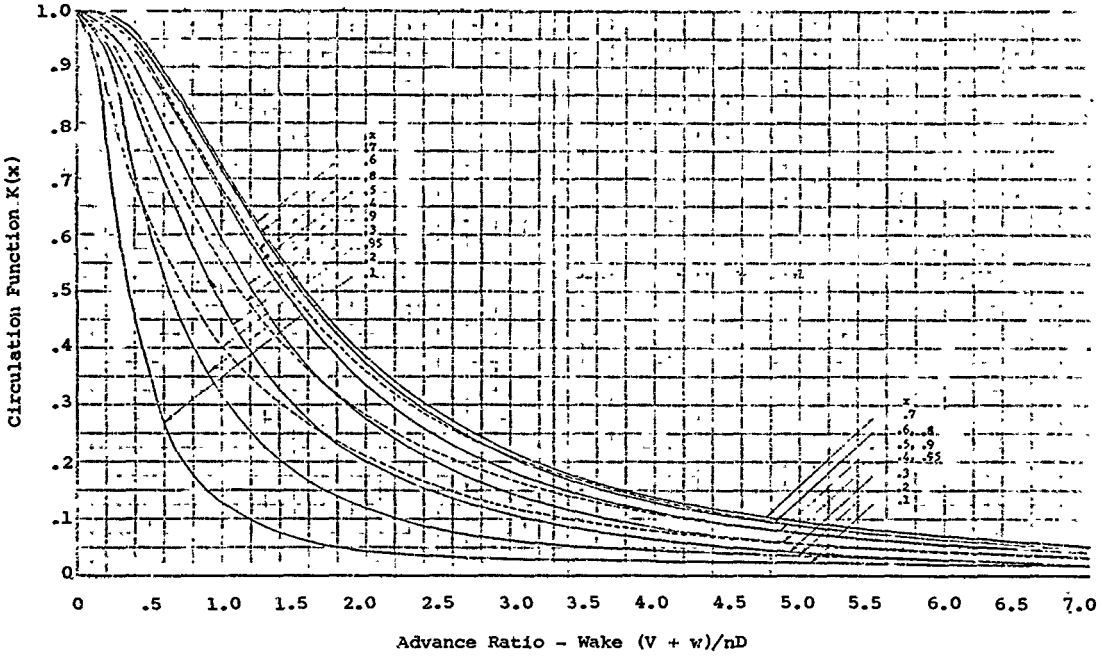


Figure 10. Propeller Circulation Function - Four-Blade Single Rotation.

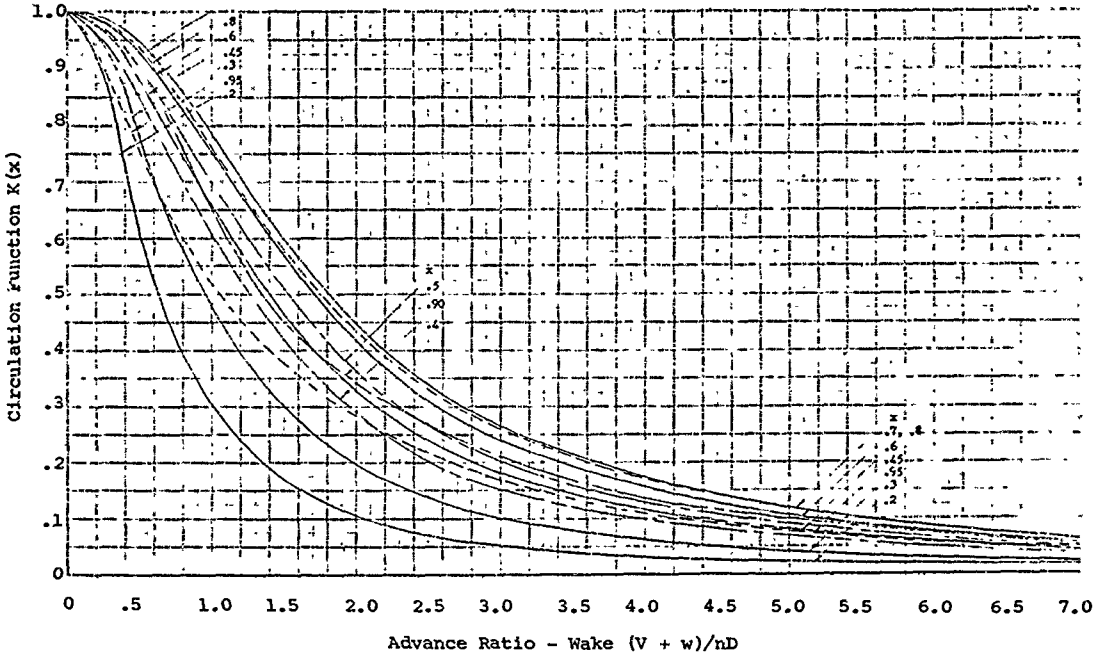


Figure 11. Propeller Circulation Function - Six-Blade Single Rotation.

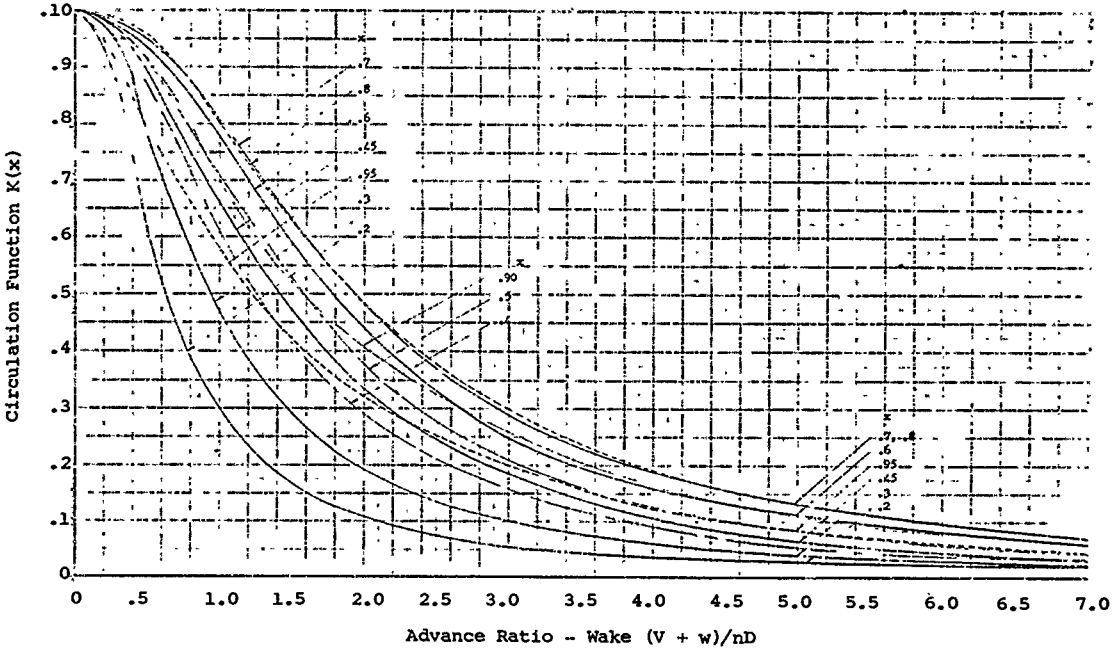


Figure 12. Propeller Circulation Function - Eight-Blade Single Rotation.

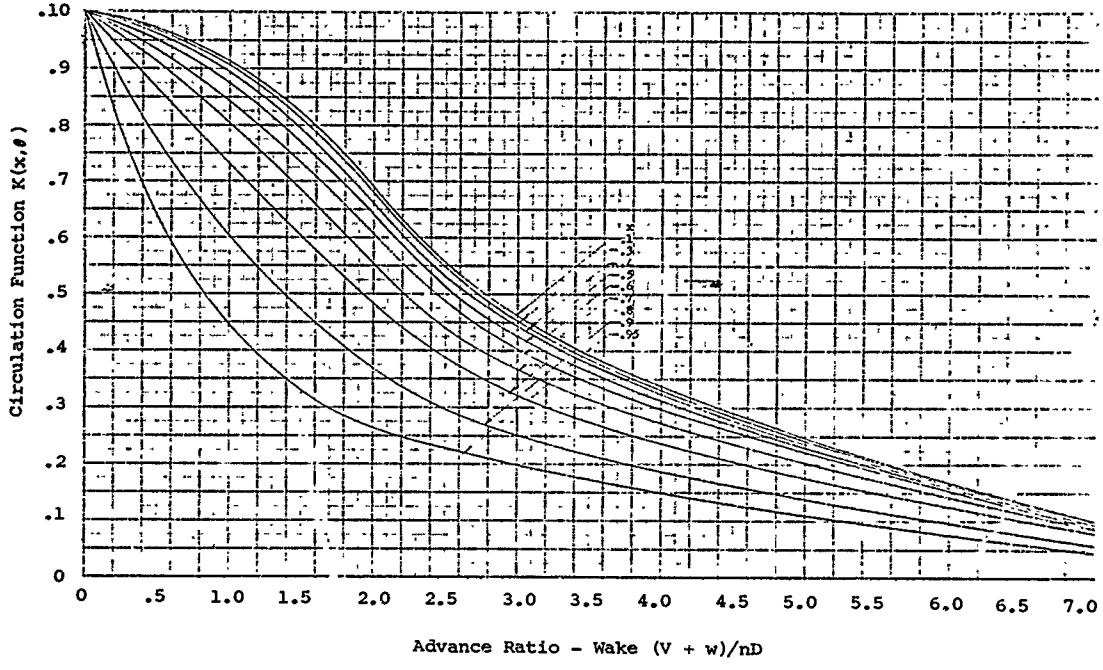


Figure 13. Propeller Circulation Function - Four-Blade Dual Rotation.

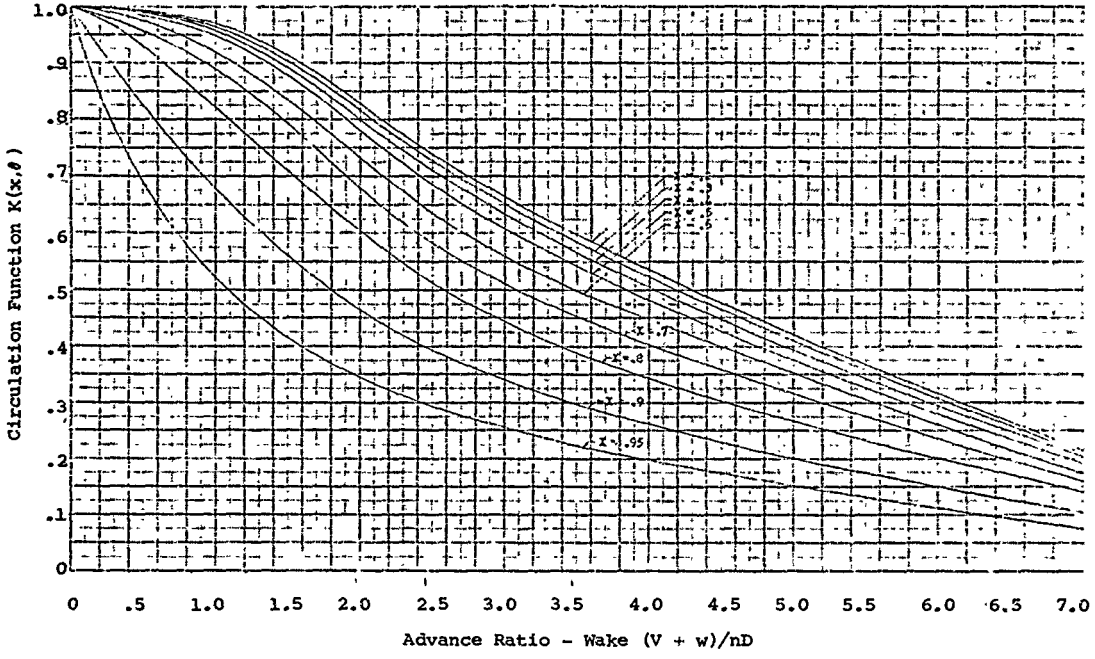


Figure 14. Propeller Circulation Function - Six-Blade Dual Rotation.

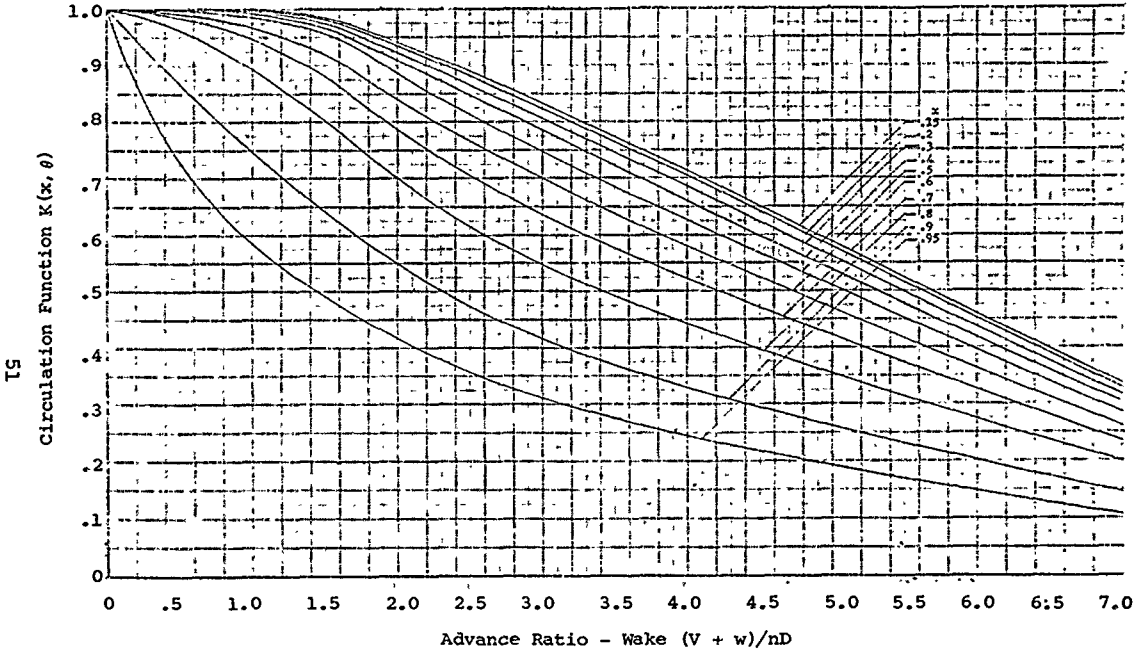


Figure 15. Propeller Circulation Function - Eight-Blade Dual Rotation.

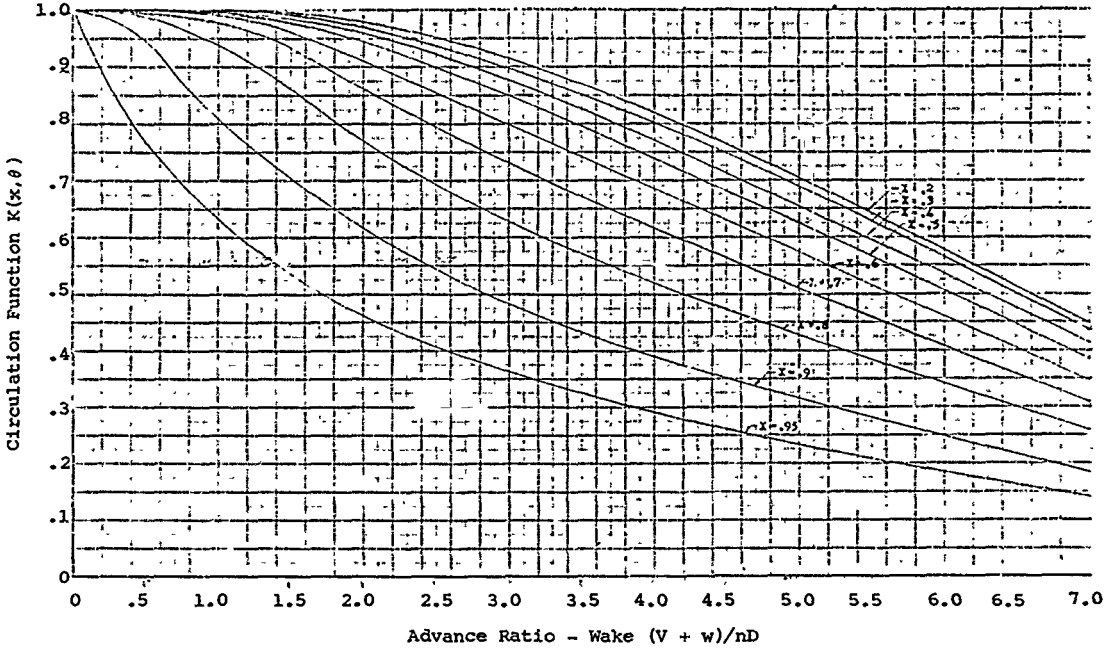


Figure 16. Propeller Circulation Function - Ten-Blade Dual Rotation.

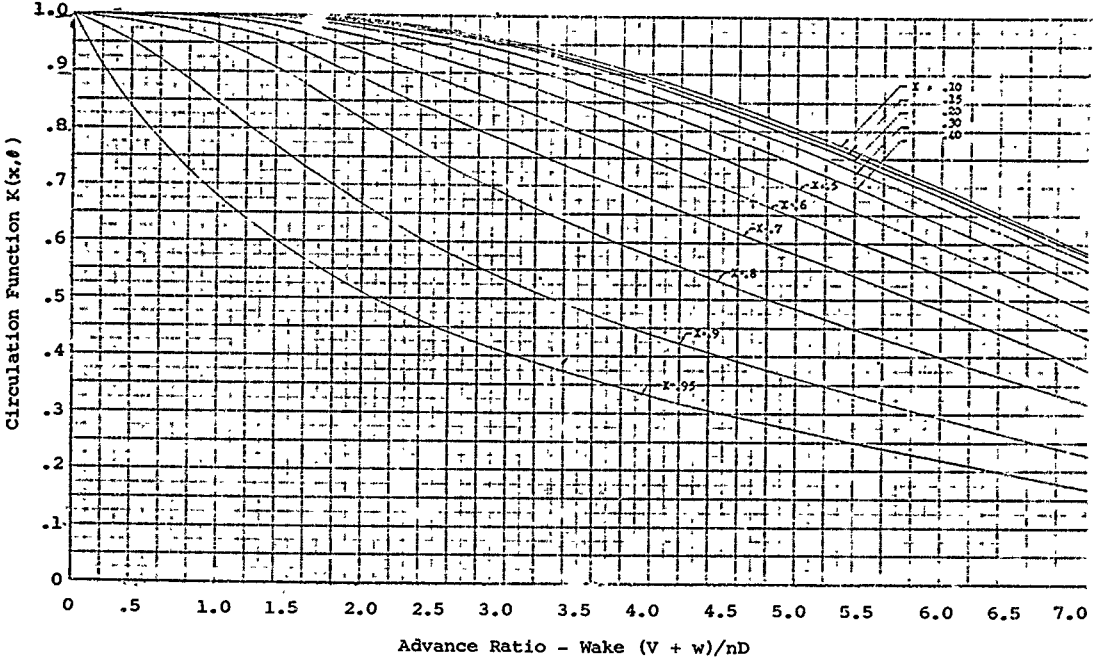


Figure 17. Propeller Circulation Function - Twelve-Blade Dual Rotation.

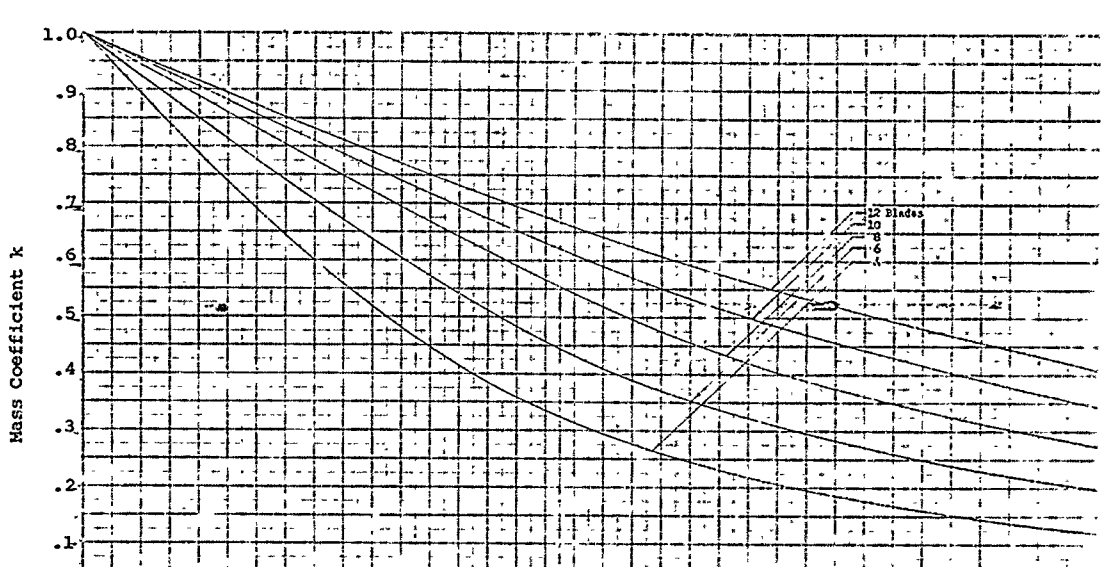


Figure 18. Mass Coefficient - k
Dual-Rotation Propeller.

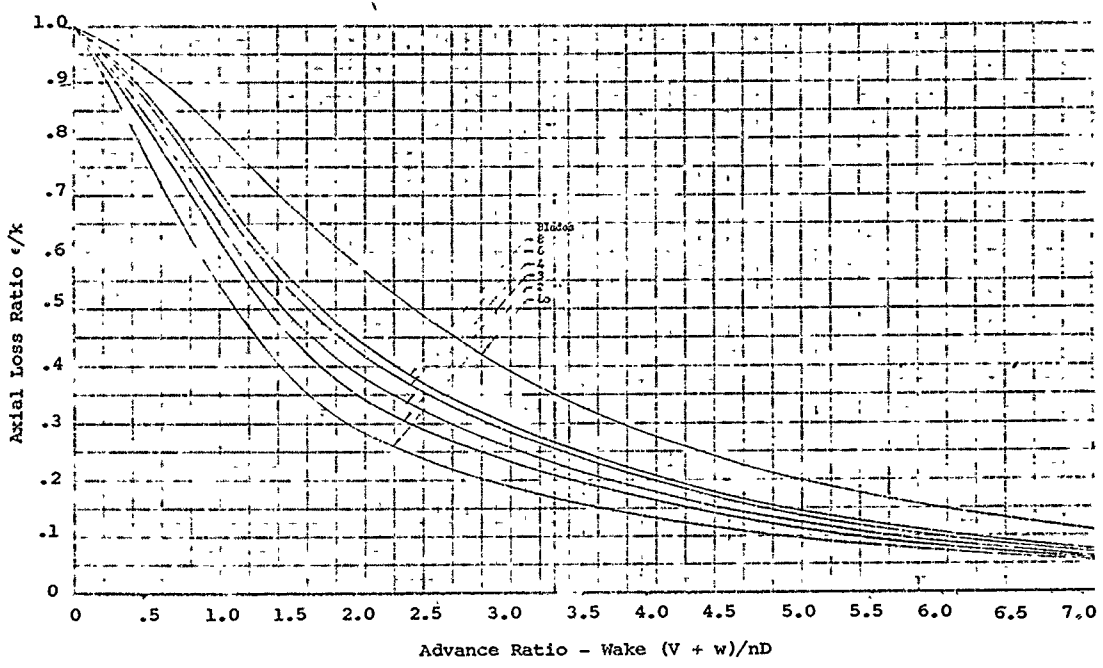


Figure 19. Axial Loss Ratio - Single-Rotation Propeller.

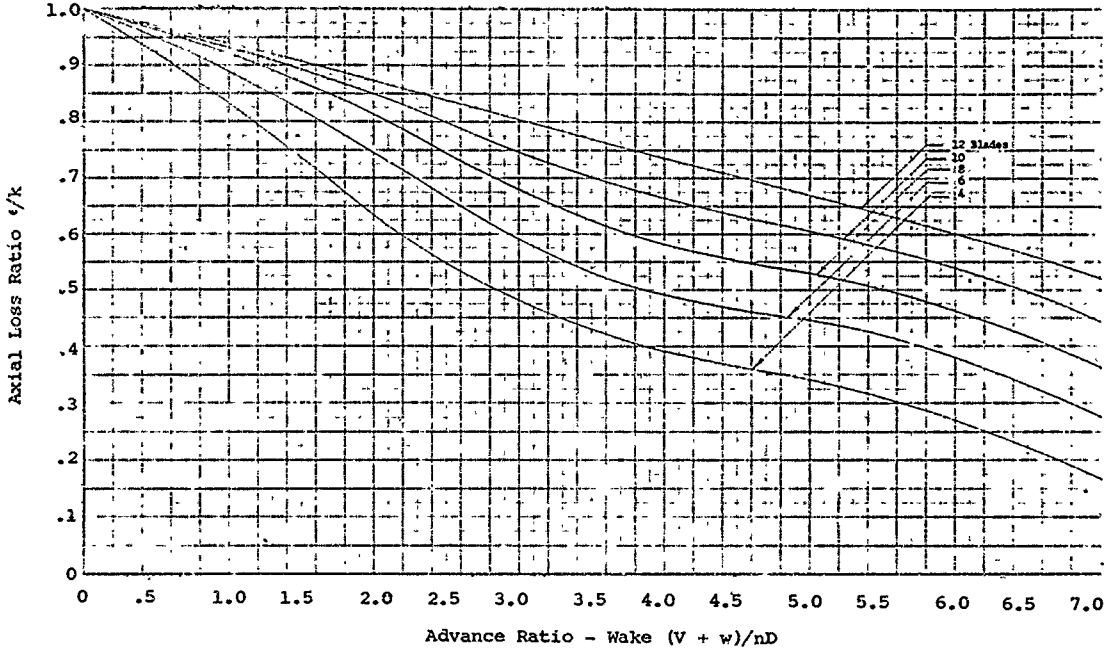


Figure 20. Axial Loss Ratio - Dual-Rotation Propeller.

theory also makes it possible to find the true two-dimensional flow conditions for the application of two-dimensional airfoil data. When calculating the induced velocity at the propeller disc at any station, it is assumed that the blade is operating at the optimum load distribution so that the influence of the vortices shed at each station corresponds to this case. Near peak efficiency, this assumption leads to very small errors as the loading approaches the optimum. At off-design conditions the error is larger, and if the induced efficiency is very high, the procedure outlined by Theodorsen, Reference 8, should be used to calculate the induced velocity.

At each blade station, then, the performance of the particular airfoil section used is determined from the two-dimensional data for that section found from wind tunnel test. The lift and drag of the section are resolved in the thrust and torque directions for each blade station. Then the differential thrust and torque are integrated to find the total thrust and torque produced by the propeller. Knowing the thrust and torque, the efficiency and horsepower absorbed are easily found.

As the name implies, two-dimensional sections are tested in the wind tunnel under conditions where only the section in one plane influences the flow field. Under these conditions the forces can be measured and the angle of attack determined based on the free-stream flow conditions. When sections are tested, great care is taken to prevent leakage at ends of the airfoil so that three-dimensional effects are eliminated.

The true or equivalent velocity at any given section on the blade must then be found by eliminating the three-dimensional effects from the vector diagram. This is done using the vortex theory for calculating the induced velocity produced as a result of tip effect changes in loading on the blade.

The equations necessary to find the thrust and torque by strip analysis are developed as follows for the case of $V > 0$: Consider a blade section at a radius r from the axis of rotation, Figure 21. Then

$$\frac{dQ}{r} = B\, dR \sin(\phi + \gamma) = B \frac{dL}{\cos\gamma} (\sin(\phi + \gamma)) \tag{39}$$

Since $$dL = \frac{C_L \rho W^2 b}{2} dr\ ,\ x = r/R,\ \sigma = \frac{dB}{\pi x D} \tag{40}$$

and $$dC_Q = \frac{dQ}{\rho n^2 D^5} \tag{41}$$

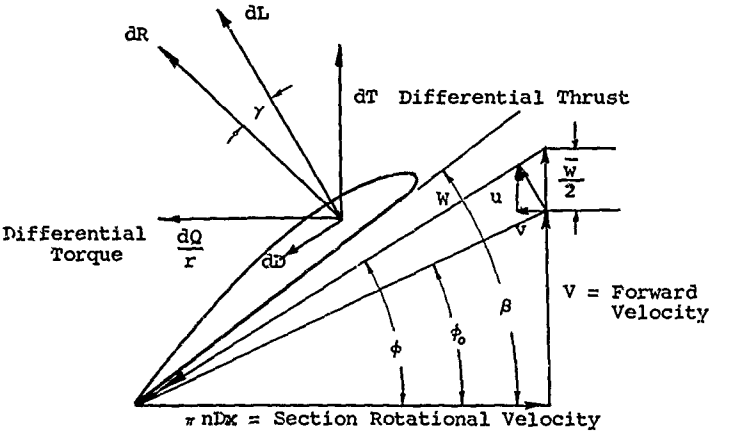


dQ/r = Section Torque
dL = Section Lift
dD = Section Drag
$\beta$ = Blade Angle
$\phi$ = True Wind Angle
$\phi_o$ = Apparent Wind Angle
$\bar{w}/2$ = Displacement Velocity
W = Apparent Velocity

Figure 21. Propeller Velocity and Force Diagram - Single-Rotation Propellers.

Equation (41) becomes

$$\frac{dC_Q}{dx} = \sigma\, C_L\, \frac{x^2}{8}\left(\frac{W}{nD}\right)^2 (\sin\phi + \tan\gamma\cos\phi) \qquad (42)$$

From Figure 21,

$$\frac{W}{nD} = \frac{\frac{V + w/2}{\sin\phi} - \frac{W}{2}\sin\phi}{nD} \qquad (43)$$

and by definition $\bar{w} = w/V$ and $J = \frac{V}{nD}$.

Combining equations,

$$\frac{dC_Q}{dx} = \frac{\pi x^2}{8} J^2 \left[\frac{1 + \frac{\bar{w}}{2}(1 - \sin^2\phi)}{\sin\phi}\right]^2 \sigma\, C_L \sin\phi\left[1 + \frac{\tan\gamma}{\tan\phi}\right] \qquad (44)$$

For convenience let the quantity

$$\frac{\pi x^2 J^2}{8}\left[\frac{1 + \frac{\bar{w}}{2}(1 - \sin^2\phi)}{\sin\phi}\right]^2 \sin\phi = Z \qquad (45)$$

Then Equation (44) becomes

$$\frac{dC_Q}{dx} = \sigma\, C_L Z\left(1 + \frac{\tan\gamma}{\tan\phi}\right) \qquad (46)$$

Also from Figure 21,

$$dT = B\, dR \cos(\phi + \gamma) \qquad (47)$$

since

$$\frac{dC_T}{dx} = \frac{dT}{dx}\,\frac{1}{\rho n^2 D^4} \qquad (48)$$

and making the same substitutions for dL, x and Z as above, Equation (47) becomes

$$\frac{dC_T}{dx} = \frac{x\,\pi J^2}{4}\left[\frac{1 + \frac{\bar{w}}{2}(1 - \sin^2\phi)}{\sin\phi}\right]^2 \sigma\, C_L \sin\phi\,(\cot\phi - \tan\gamma) \qquad (49)$$

Using the Z term to simplify Equation (49),

$$\frac{dC_T}{dx} = \sigma C_L \frac{2Z}{x}(\cot\phi - \tan\gamma) \tag{50}$$

Before Equations (46) and (50) can be solved, the two-dimensional angle of attack must be determined so that the lift and drag coefficients can be found from the two-dimensional airfoil data. The two-dimensional angle of attack is equal to

$$\alpha = \beta - \phi \tag{51}$$

where $\beta$ = the blade angle at each station
$\phi$ = the true wind angle, and is found from the equation

$$\phi = \tan^{-1} \frac{J}{x}(1 + \frac{\bar{w}}{2}) \tag{52}$$

Thus it is necessary to relate $\bar{w}$ to the section operating $C_L$ to find $\phi$. The operating $C_L$ is also dependent on the blade angle which is known or assumed for each condition.

From the Kutta-Joukowski theory,

$$\frac{dL}{dr} = \rho W \Gamma = C_L \frac{\rho}{2} W^2 b \tag{53}$$

Also from Equation (35),

$$\Gamma = \frac{(V + w)w}{Bn} K(x) \tag{54}$$

Substituting for $\Gamma$ and recalling by definition $\sigma = bB/(\pi x D)$, Equation (53) becomes

$$C_L = \frac{2(V + w)w}{xDnW} K(x) \tag{55}$$

From Figure 21 it will be noted that the apparent velocity W at a given blade is

$$W = \frac{V + w/2}{\sin\phi} - \frac{w}{2}\sin\phi \tag{56}$$

which becomes

$$W = \frac{V}{\sin \phi}\left(1 - \frac{\bar{w}}{2} \cos \phi\right) \tag{57}$$

Thus, substituting the expression for W in Equation (57), we have

$$\sigma C_L = \frac{(1 + \bar{w})\bar{w}\ 2\ K(x)}{(1 + \bar{w}/2)(1 + \bar{w}/2 \cos^2\phi \cos \phi} \frac{\sin^2 \phi}{} \tag{58}$$

Since $\bar{w}$ is dependent on $C_L$, which is dependent on $\alpha$ and $\bar{w}$, it is necessary to solve Equations (51) and (58) in terms of the airfoil characteristic to find the operating $C_L$ for each blade section with a given blade angle. This procedure must be carried out at each blade station, after which the differential thrust and torque coefficients can be calculated using Equations (46) and (50). To determine the total thrust and torque coefficients, the differential values are integrated along the blade span.

There are many methods available for integrating the differential values to find the total, including plots with the area found mechanically with a planimeter. Mechanical methods have poor repeatability, and therefore a simple summation method was adopted. This method has the advantage of allowing for fast repeatable integrations and is well adapted for computers.

Consider a typical thrust or torque loading curve as shown in Figure 22. This curve is divided into Y stations with corresponding ordinates. The area may be written

$$A = \sum_{n=1}^{n=q-1} \frac{h_n + h_{n+1}}{2} \left(x_{n+1} - x_n\right) \tag{59}$$

Upon expanding,

$$A = \frac{h_1 + h_2}{2}(x_2 - x_1) + \left(\frac{h_2 + h_3}{2}\right)(x_3 - x_2) \ldots .$$

$$+ \frac{h_n + h_{n+1}}{2}\ (x_{n+1} - x_n) \tag{60}$$

$$A = h_1 \frac{(x_2 - x_1)}{2} + h_2\ \frac{(x_3 - x_1)}{2} + h_3 \frac{(x_4 - x_2)}{2}\ \ldots . \tag{61}$$

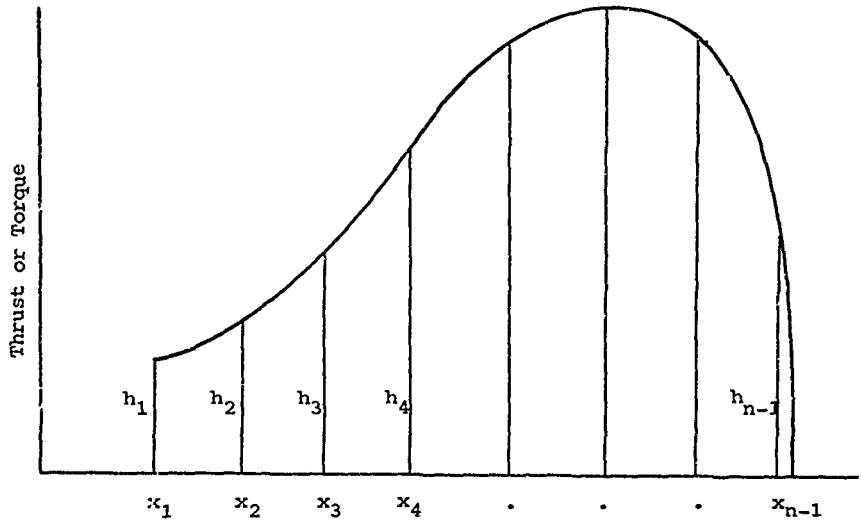


Figure 22. Typical Thrust or Torque Loading Curve.

From Equation (59), note that the area may be expressed as the ordinate times half the distance between the preceding and the following stations. This holds for every ordinate except the first. In this case, the increment of area is the ordinate times half the distance between the first and second stations. The distance factor $(x_2 - x_1)/2, (x_3 - x_1)/2, (x_{n+1} - x_{n-1})/2$ will be termed $\Delta x$ for the strip analysis calculations.

Thus, to find the total thrust and torque, Equations (46) and (50). become

$$C_Q = \sum_{n=0}^{n=1} \sigma C_L Z \left(1 + \frac{\tan \gamma}{\tan \phi}\right) \Delta x \qquad (62)$$

$$C_T = \sum_{n=0}^{n=1} \sigma C_L \frac{2Z}{x} (\cot\phi - \tan\gamma)\, x \qquad (63)$$

Now, $$C_P = 2\pi C_Q \qquad (64)$$

and the propeller efficiency is

$$\eta = \frac{C_T}{2\pi C_Q} J = \frac{C_T}{C_P} J \qquad (65)$$

EQUATIONS FOR STRIP ANALYSIS - DUAL-ROTATION PROPELLERS

The same technique for calculating the performance of dual-rotation propellers may be used as was used for single rotation. However, because of the interaction between the front and rear units, modifications must be made to the differential thrust and torque equations as well as the equations for finding the true wind angle, $\phi$, and the resultant velocity. These qualities are dependent on $K(x,\theta)$ and $k$.

Values of $K(x,\theta)$ and $k$ were found for dual-rotation propellers using the same techniques as were used to determine $K(x)$ and $k$ for single-rotation propellers. The electrical analogy technique used by Theodorsen for this purpose is especially effective for the complex flow field produced by dual-rotation propellers. In the case of dual-rotation propellers, the dimensionless quantity $K(x,\theta)$ is used rather than $K(x)$ as in the case of single-rotation propellers, as $K(x,\theta)$ is a function of not only $x$ but also $\theta$. The angle $\theta$ varies from zero to 360 degrees and at zero $K(x,\theta)$ is on the blade vortex for which conditions are being calculated. When using $K(x,\theta)$ for calculating the flow conditions, the assumption is made that $\theta$ equals zero. This assumption is necessary as

sufficient data was not available to use the average value. The error is small, however, at normal blade loadings. Values of $K(x, \theta)$ and $k$ for dual-rotation propellers obtained from Reference 9 are given in Figures 13 through 20.

Based on the theory of dual-rotation propellers developed by Theodorsen, the velocity and vector diagrams for the front and rear units are shown on Figure 23. When calculating the flow vectors based on the Theodorsen data and theory, the following assumptions are made:

1. The front and rear components operate in the same plane.
2. The propellers are operating at the optimum loading condition.
3. The torque absorbed by the front and rear units is equal.

The resultant sectional velocity on the front and rear units may be calculated from the equations derived in Reference 8:

$$W_f = \frac{V}{\sin \phi_o} \left(1 + \frac{1}{4} k \bar{w} \sin^2 \phi_o\right) \tag{66}$$

$$W_R = \frac{V}{\sin \phi_o} \left(1 + \frac{3}{4} k \bar{w} \sin^2 \phi_o\right) \tag{67}$$

The differential thrust and torque coefficient for the front unit of a dual rotation may be derived in the same manner as for single-rotation propellers, Equations (46) and (50). Thus

$$\frac{dC_Q}{dx} = \frac{\pi x^2}{8} J \left(\frac{V}{\sin \phi_o}\right)^2 \left[1 + \frac{1}{4} k \bar{w} \sin^2 \phi_o\right]^2 \sigma C_L (\sin \phi + \tan \gamma \cos \phi) \tag{68}$$

$$\frac{dC_T}{dx} = \frac{\pi x}{4} J^2 \left(\frac{V}{\sin \phi_o}\right)^2 \left[1 + \frac{1}{4} k \bar{w} \sin^2 \phi_o\right]^2 \sigma C_L (\cos \phi - \tan \gamma \sin \phi) \tag{69}$$

For the rear unit, the differential thrust and torque coefficients may be determined using Equations 68 and 69 by substituting

$$\left[1 + 3/4 (k \bar{w} \sin^2 \phi)\right] \text{ for } \left[1 + 1/4 (k \bar{w} \sin^2 \phi_o)\right] \tag{70}$$

Before Equations (67) and (68) can be solved at each blade station, the operating lift coefficients for the front and rear propellers are found in the same manner as was used for single-

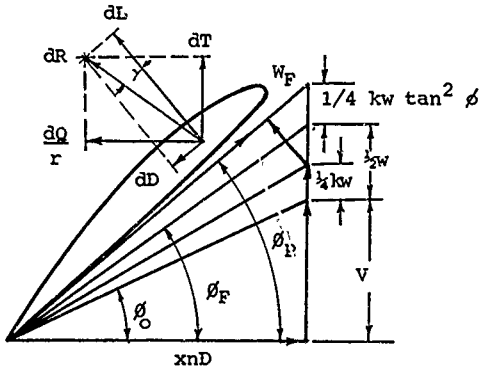


Front Propeller

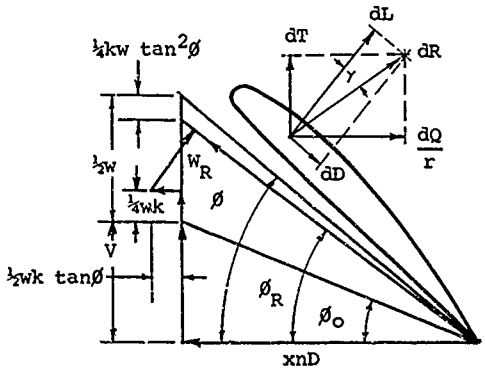


Rear Propeller

Figure 23. Propeller Velocity and Force Diagram Dual-Rotation Propellers.

rotating propellers by using the proper values for $W_F$ and $W_R$ (Equations (66) and (67).

$$\sigma C_{L,F} = \frac{V \quad \bar{w} \ (1 + \bar{w}) \ \sin \phi_o}{D \quad x(1 + 1/4 \quad \bar{w} \sin^2\phi_o)} K(x, \theta) \qquad (71)$$

$$\sigma C_{LR} = \frac{V \quad \bar{w} \ (1 + \bar{w}) \ \sin \phi_o}{D \quad x(1 + 3/4 \quad \bar{w} \sin^2\phi_o)} K(x, \theta) \qquad (72)$$

The section angle of attack used to find the operating lift coefficient from two-dimensional airfoil data is found from the equation

$$\alpha_F = \beta_F - \phi_F \qquad (73)$$

$$\alpha_R = \beta_R - \phi_R \qquad (74)$$

The true wind angle for front and rear propellers may be calculated from the equations derived by Crigler, Reference 9, which are based on the results given by Theodorsen.

$$\phi_F = \tan^{-1} \frac{J}{\pi x} \left[1 + \frac{\bar{w}}{2} (1 + \tfrac{1}{2} k \tan^2\phi)\right] \qquad (75)$$

$$\phi_R = \tan^{-1} \frac{J}{\pi x} \left[1 + \frac{\bar{w}}{2} (1 - \tfrac{1}{2} k \tan^2\phi)\right] \qquad (76)$$

where $$\phi = \tan^{-1} \frac{J}{\pi x} (1 + \frac{\bar{w}}{2}) \qquad (77)$$

To find the operating lift coefficient for the front and rear discs, $C_L$ is found as a function of w using Equations (71) and 72) and two-dimensional airfoil data with Equations (73) and (74). After solving for operating $C_L$, the drag may be found from the airfoil data, and the differential thrust and torque may be calculated from Equations (67) and (68). The efficiency of the propeller can then be determined from the equation

$$\eta = \frac{C_T}{2\pi C_Q} J \qquad (78)$$

## Compressibility Considerations

The efficiency of propellers operating at high Mach numbers has often been calculated by correcting the performance determined for the incompressible flow case with an empirical correction based on the operating tip Mach number. This procedure depends on a reduction of test propeller data and neglects many important interacting variables. Further, the procedure is not suitable for calculating the effects of detailed changes of the blade design and thus finding ways of minimizing the compressibility losses. For these reasons the empirical approach was not used for calculating the propeller performance losses due to compressibility.

When the performance of two-dimensional airfoils is found from the airfoil data, the effects of compressibility are included, as the data is plotted as a function of Mach number. Thus when the section Mach number is known, the actual lift and drag can be determined using the data given in Appendix II of Volume III. To use these airfoil data for the case where the propeller is operating at high forward Mach numbers, compressibility effects on the induced velocity must also be determined. This is especially true when any section of the propeller is operating above a section helical Mach number of one. The compressibility effects must be considered for the cases:

1. Forward and tip Mach numbers less than one
2. Forward Mach number less than one and the tip Mach number greater than one
3. Forward and tip Mach numbers greater than one

Frankel, Reference 10, considered case 1 where the forward and tip Mach numbers are less than one. This was done using the concept of the retarded potential which accounts for the finite speed of the pressure disturbances. As was explained by Ginzel, Reference 11, the concept of the retarded potential was added to the incompressible flow propeller theory in the form of a correction. The results of this work indicate that up to a forward Mach number of 0.7, incompressible flow propeller theory can be used without compressibility corrections if the lift and drag coefficients at each blade station are found at the correct section helical Mach number.

Under a separate investigation, K. Kondo (Reference 12) also analyzed propeller theory for the compressible flow case using the concept of the retarded potential. Based on this analysis he concluded: "The induced velocity of a symmetric propeller at the position of the blade line is independent of sound velocity and equals that of the propeller working in an incompressible fluid with the same lift distribution and working condition as the given one". Based on these analyses, it appears that as

long as the entire propeller is operating at subsonic speeds, the incompressible theory of Theodorsen and Goldstein can be used to calculate the induced velocity without compressibility corrections. The actual load distribution used is based on the characteristics of the airfoil at the given section Mach number.

When calculating the inflow velocity of a propeller operating in a compressible fluid with some of the sections operating at section helical Mach numbers above one, it is necessary to consider the finite speed of the pressure disturbances in comparison with the speed of the blade section being analyzed. This leads to the rule of forbidden signals and the zone action as discussed by Von Karman, Reference 13. Thus the effects of the line vortex shed from a section operating at a helical Mach number above one will be considered only in the region of its aft Mach cone, where the apex of the Mach cone is on the propeller blade. It is apparent that the trailing vortices will have an influence in front of the propeller and thus cause an inflow velocity at each point on the vortex line, as the influence of the vortex is being propagated in all directions with at least sonic velocity, and the propeller is moving forward at less than sonic velocity. This can be illustrated by considering Figure 24.

In Figure 24 the path of the tip of a one-blade propeller operating at a forward Mach number less than one and a tip Mach number over one is plotted to scale as viewed from above. Point A represents time equal to zero. After time equal to that for 1/4, 1/2, 3/4 and 1.0 revolution, the tip of the propeller is at points A, B, C and D respectively. The loci of the pressure disturbances created by the tip of the propeller after time equal to 1/4, 1/2, 3/4 and 1.0 revolution are also shown in Figure 24. It is observed from this figure that the propeller is not influenced by the disturbances created at time equal to zero until after a period corresponding to approximately one revolution. Thus, due to the geometry of the configuration, it is observed that when the tip Mach number is over one, the sections move away from the disturbances produced by themselves until a certain percentage of a revolution has been passed, at which time the section comes back into the zone of the original disturbance. Thus, instead of the trailing vortices influencing the inflow on a propeller immediately, as in incompressible flow, there is in the compressible case a reduction which decreases the inflow velocity as compared to that calculated for the incompressible flow case. This effect can be visualized in three dimensions by inspection of Figure 25.

To calculate the inflow velocity of a propeller operating at a tip Mach number exceeding one and a forward Mach number less than one, it is necessary to evaluate the effects of the

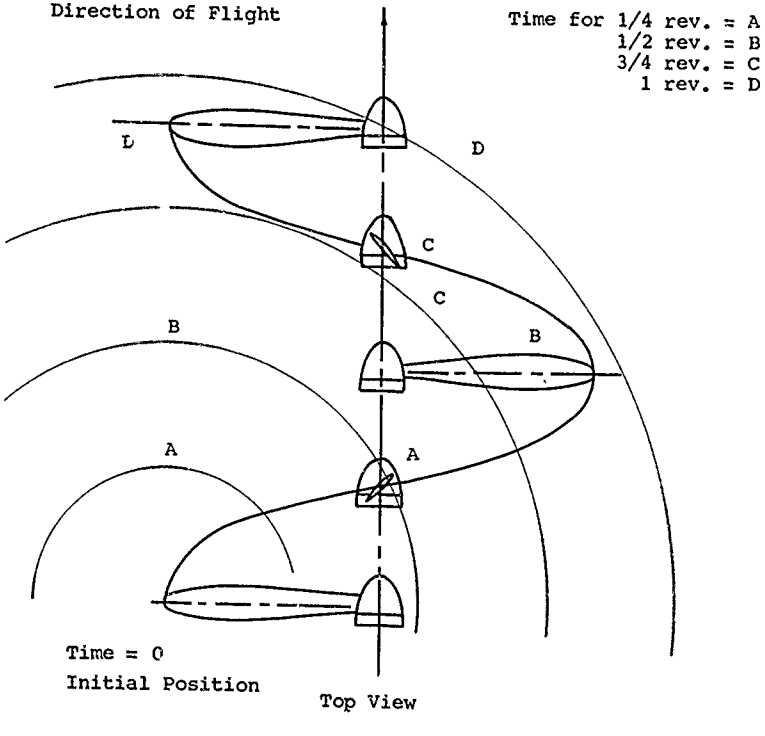


Figure 24. Propeller Vortex Lines and Relative Positions.

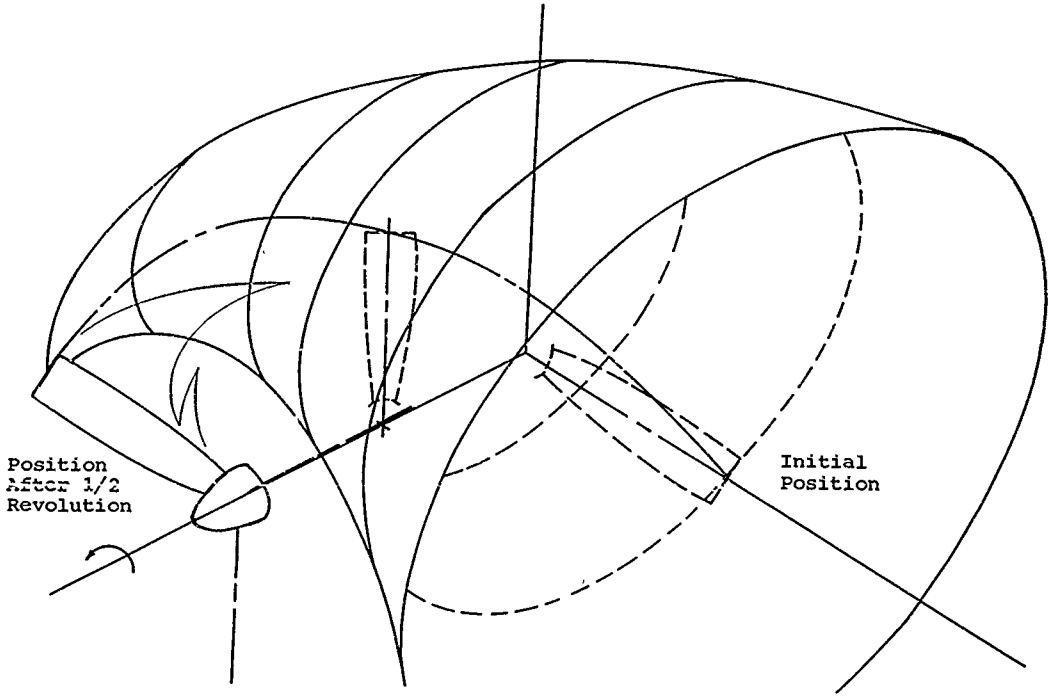


Figure 25. Mach Wave Caused by Propeller Tip Operating at Forward Mach No. = .9, Tip Mach No. = 2.13.

trailing vortices that lie in the zone of influence only. Thus, unlike the incompressible flow case where effects of the vortices are considered from the propeller plane to infinity, it becomes necessary to discriminate against the effects of the vortices outside the zone of influence or the Mach cone as shown on Figure 25.

The inflow velocity at the propeller disc can be calculated using the Biot-Savart law as was done by Moreya, Hirsch and S. Kawata (Reference 14) for the incompressible flow case. The inflow velocity calculated in this manner agrees closely with the results found by Theodorsen and Goldstein for the same operating condition. The advantage of using the Biot-Savart law to calculate the inflow velocity is that the lower limit of the integral can be modified to account for the zone of action as is necessary in the compressible flow case.

The equations for calculating the inflow velocity can therefore be derived from the Biot-Savart law Equation (79):

$$V_{(x,y,z)} = \frac{1}{4\pi} \int \frac{\Gamma \, d\bar{S} . \bar{R}}{d^3} \qquad (79)$$

where $\Gamma$ = the strength of circulation

$\bar{R}$ = the vector distance between the point being considered x', y', z' and the vector filament x, y, z

$d\bar{S}$ = the differential length of the vector filament

d = the absolute distance from point x', y', z' and the vector filament x, y, z

D = the induced velocity, which is normal to the plane formed by the vortex filament and the line to the vortex filament

To apply the Biot-Savart law to find the inflow velocity, consider a propeller with B blades rotating about and moving along the x axis. The propeller disc is in the y, z axis. The forward direction of the propeller is assumed to be negative along the x axis. At each blade station r, vortices having a strength $\frac{dr}{dr} dr$ are assumed to be shed. The vortex lines produced at each station will form a helical vortex sheet which remains stationary behind the propeller. Assume blade number (0) is on the y axis and it is desired to find the axial inflow velocity at this blade due to the helical vortex sheet produced by the entire propeller. The general configuration of the above is shown on Figure 26.

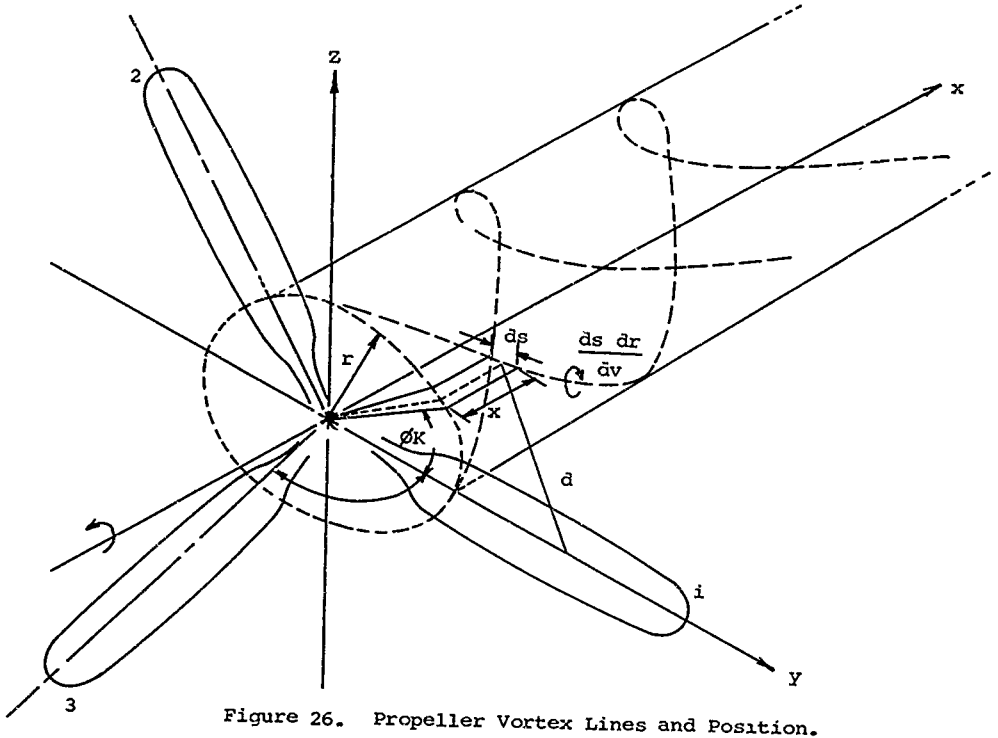


Figure 26. Propeller Vortex Lines and Position.

The general equation of the Biot-Savart law can be rewritten for finding the inflow velocity in the x direction in Cartesian coordinates in the following form:

$$u = -\frac{1}{4\pi}\int \frac{\Gamma\left[(z - z')dy - (y - y')dz\right]}{d^3} \qquad (80)$$

where the primes refer to points on the vortex surface.

Since $d^2 = (x - x')^2 + (y - y')^2 + (z - z')^2$ (81)

Equation (80) becomes

$$u = -\frac{1}{4\pi}\int \frac{\Gamma\left[(z - z')dy - (y - y')dz\right]}{\left[(x-x')^2 + (y-y')^2 + (z-z')^2\right]^{3/2}} \qquad (82)$$

Equation (82) will now be applied to find the induced velocity in the x direction at point o, y, o as shown in Figure 26.

The element ds on any one of the line vortices is located at x', y', z'. This point is a function of $\phi$, the angle in the y, z plane (see Figure 26), which is measured positive in the counterclockwise direction from the y axis. Then the following transformation can be made:

$$\begin{aligned} y' &= r\ \cos\phi; & dy' &= -r\ \sin\phi\ d\phi \\ z' &= r\ \sin\phi; & dz' &= r\ \cos\phi\ d\phi \end{aligned} \qquad (83)$$

In a unit time,

$$V = x' \text{ and } 2\pi n = \phi \qquad (84)$$

then $$\frac{x'}{\phi R} = \lambda_o \qquad (85)$$

or $$x' = \lambda_o\ \phi\ R \qquad (86)$$

The above transformations hold only when considering the effect of one blade on itself. If $\delta$ is the angular distance between blades and p is the blade number equal to 0, 1, 2, 3 . . . (B-1), then the above transformation becomes

$$\begin{aligned} y' &= r\cos(\phi + p\delta); & dy &= -r\sin(\phi + p\delta)d\phi \\ z' &= r\sin(\phi + p\delta); & dz &= r\cos(\phi + p\delta)d\phi \end{aligned} \qquad (87)$$

Equation (82) can be rewritten as follows by making the above transformation and letting $(\phi + p) = \phi_K$:

$$u = -\frac{1}{4\pi}\int_0^R \frac{d\Gamma}{dr}\,dr \sum_{p=0}^{p=B-1} \int_0^\infty \frac{(r^2 - yr\cos\phi_K)\,d\phi}{\left[\lambda^2 R^2\phi^2 + y^2 + r^2 - 2ry\cos\phi_K\right]^{3/2}} \tag{88}$$

It is convenient to let $r = Rx$ and $y = x_1 R$ and rewrite Equation (88).

Thus

$$u = -\frac{1}{4\pi R}\int_0^1 \frac{d\Gamma}{dx}\,dx \sum_{p=0}^{p=B-1} \int_0^\infty \frac{(x^2 - x_1 x\cos\phi_K)\,d\phi}{\left[\lambda^2\phi^2 + x_1^2 + x^2 - 2x_1 x\cos\phi_K\right]^{3/2}} \tag{89}$$

where $x_1$ = the fractional radius at which the inflow velocity is desired

$x$ = the fractional radius at which the vortex lines are being shed.

From Equation (89) it will be noted that the inflow velocity at $x_1$ is produced by the effects of trailing vortices of strength $d\Gamma/dx$ leaving each station of all the blades of the propeller. Equation (89) is the general equation for finding the axial inflow velocity u.

The equations for calculating the radial inflow velocity and rotational inflow velocity w can be developed in the same manner as was used for Equation (89). These are:

$$v = -\frac{1}{4\pi R}\int_0^1 \frac{d\Gamma}{dx}\,dx \sum_{p=0}^{p=B-1} \int_0^\infty \frac{\lambda(\phi\cos\phi_K - \sin\phi_K)\,d\phi}{(\lambda^2\phi^2 + x_1^2 + x^2 - 2x_1 x\cos\phi_K)^{3/2}} \tag{90}$$

$$w = -\frac{1}{4\pi R}\int_0^1 \frac{d\Gamma}{dx}\,dx \sum_{p=0}^{p=B-1} \int_0^{\infty} \frac{\lambda_o(x_1 - x\,\phi\,\sin\phi_K + \cos\phi_K)\,d\phi}{(\lambda^2\phi^2 + x_1^2 + z^2 - 2x_1 x\cos\phi_K)^{3/2}} \tag{91}$$

When the assumption is made that the propeller is operating in an incompressible fluid, the effects of the vortices on the components of the inflow velocity are found by integration from the propeller disc to infinity or for values of $\phi$ from 0 to $\infty$. Thus, strictly, Equations (89) to (91) apply only for the subsonic incompressible flow case.

As stated previously for the case where the propeller is operating at section helical Mach numbers above one and at a forward Mach number less than one, the trailing vortices influence the inflow velocity produced at a given point and the propeller disc is affected only by those vortices within the region of the fore Mach cone of the point being considered.

The values of the second integral of Equations (89) to (91) for the compressible flow case will be a function of the number of revolutions through which the propeller turns.

Thus, for the steady incompressible flow case, the inflow velocity is found for a vortex system produced by a propeller which has gone through an infinite number of revolutions. For the compressible flow case where the effects of the vortices are considered only within the fore Mach cone, it is desirable to find the solution of Equations (89) to (91) for the propeller going through revolutions from $\phi_L$ equal to the angular distance the propeller has turned in the period required for the trailing vortices to make themselves felt at the propeller disc.

Evaluation of Lower Limit: Thus, to find $\phi_L$, the lower limit of Equations (89) to (91) it is necessary to find the part of the revolution that the propeller turns through before the effects of the trailing vortices are felt at the propeller disc. As $\phi_L$ is a function of where the vortex is produced on the propeller, it is necessary to find $\phi_L$ for the following cases:

1. The limit for the vortex produced at the same station for the same blade as that where the inflow velocity is desired.
2. The limit for the vortex produced at other stations for the same blades as that where the inflow velocity is desired.
3. The limit for the vortex produced at the same station on

other blades of the propeller than that at which the inflow velocity is desired.

4. The limit for the vortex produced at other stations on other blades than that at which the inflow velocity is desired.

It must be noted that the limits hold only if the section Mach number of the station at which the vortex is being shed is over one, as the disturbances are "trapped" within the Mach cones only for this case. The general equations for finding the lower limit to be used in Equations (89) to (91) can be found by determining the time required for the expanding sphere produced by the disturbance to intersect the path of station on the propeller at which the inflow velocity is desired. After the period of time is determined, the angle that the propeller turns through in this period is easily found.

The equation of an expanding sphere produced at r on the blade at which the vortex is being shed is initia on the y axis can be written in the form

$$x^2 + (y - r)^2 + z^2 = a^2 t^2 \tag{92}$$

where $a$ = the speed of sound
$t$ = the time

Now, at any time t, the path of the station $r_1$ at which the inflow is desired must satisfy the equations

$$\begin{aligned} x &= -Vt \\ y &= r_1 \cos \phi_k \\ z &= r_1 \sin \phi_k \end{aligned} \tag{93}$$

where $\phi_k = \phi + p\delta'$
$\phi$ = the angle between the y axis and the blade, positive in the direction of rotation = wt
$p$ = blade number, equals 0 to (B - 1)
$\delta'$ = the angular distance between blades

Letting $x = r/R$ and $x_1 = r_1/R$, Equations (92) and (93) can be combined to give

$$\frac{1 + \left(\frac{x_1}{x}\right)^2 - 2\left(\frac{x_1}{x}\right) \cos \phi_k}{\phi_L^2} - \frac{1 - M_a^2}{M_r^2} \tag{94}$$

where $M_r = \frac{2\pi rn}{a}$ = the rotational Mach number of the station at which the vortex is shed

$$\phi_k = \phi_L + p \tag{95}$$

The angle $\phi$ becomes $\phi_L$ when Equations (92) and (93) are combined. For Equation (94) to be satisfied, the section Mach number at which the vortex is shed must be over one, as only in this case will the effects of vortex be limited to the region within the Mach cone of this vortex. When the section Mach number at which a vortex is shed is less than one, the vortex can influence the entire blade immediately.

Thus, in the compressible flow case, stations operating at helical Mach numbers less than one are influenced to a lesser extent by the stations which operate at helical Mach numbers above one.

As a result, the inflow velocity at these stations is less than would be calculated for the incompressible flow case. Thus, for Equation (94) to apply,

$$M_r^2 + M_a^2 > 1 \tag{96}$$

or

$$\frac{1 - M_a^2}{M_{r_1}^2} \left(\frac{x_1}{x}\right)^2 < 1 \tag{97}$$

Calculation of Inflow Velocity: To find the inflow velocity for any given condition, it is thus necessary to solve Equations (89) to (96) using the proper limits. Unfortunately, the second integrals of Equations (89) to (91) cannot be evaluated by exact methods. Therefore, it was necessary to use a numerical method for evaluating these integrals.

Actually, the second integrals of Equations (89) to (91) have been evaluated by Moriya and Hirsch, References 14 and 15, respectively. However, the values of inflow velocity can be found only for the lower limit equal to zero. As a variable lower limit is required, it was still necessary to evaluate the integrals of Equations (89) to (91). The results of Moriya and Hirsch, however, were useful for checking purposes.

When the assumption is made that the slipstream contraction can be neglected, the resultant inflow velocity is normal to the true resultant velocity at any section on the propeller.

Because of this, it is only necessary to calculate the axial inflow velocity using Equation (89). The rotational inflow velocity can then be calculated from the equations

$$v = u \tan \phi \tag{98}$$

$$u = \pi n D x \sin \phi \cos \phi - V \cos^2 \phi \tag{99}$$

where $u$ = the axial inflow velocity
$v$ = the rotational inflow velocity
$D$ = the propeller diameter
$x$ = $r/R$
$\phi$ = the true wind angle

To evaluate the second integral of Equation (89) by numerical methods, IBM machines were used. To simplify the problem for these machines, Equation (89) was rewritten by dividing through by $x$. Thus

$$u = -\frac{1}{4\pi R} \int_0^1 \frac{d\Gamma}{dx}\, dx \sum_{p=0}^{p=B-1} \frac{1}{x} \int_0^{\infty} \frac{\left(1 - \frac{x_1}{x} \cos\phi_k\right) d\phi}{\left[\frac{\lambda^2}{x^2}\phi^2 + \left(\frac{x_1}{x}\right)^2 + 1 - 2\frac{x_1}{x}\cos\phi_k\right]^{3/2}} \tag{100}$$

Letting $\frac{x_1}{x} = X$ and $\frac{\lambda}{x} = \frac{J}{\pi x} = \frac{J_1}{\pi}$, Equation (94) becomes

$$u = -\frac{1}{4\pi R} \int_0^1 \frac{d\Gamma}{dx}\, dx \sum_{p=0}^{p=B-1} \frac{1}{x} \int_0^{\infty} \frac{(1 - X\cos\phi_k) d\phi}{\left[\left(\frac{J}{\pi}\right)^2 \phi^2 + X^2 + 1 - 2X\cos\phi_k\right]^{3/2}} \tag{101}$$

The second integral of equation (101), designated as $I$, was evaluated by numerical methods between the limit 0 to $4\pi$. The remainder from the limit $4\pi$ to $\infty$ was found by assuming that $\cos\phi_k$ was small compared to $\phi$, and thus the integral $I$ in this range was approximately equal to

$$I \cong \int \frac{d\phi}{\frac{J}{\pi}\phi^3} \tag{102}$$

Knowing the values of I and the lower limit, the inflow velocity can be calculated for any given flight condition and any load distribution. Furthermore, the inflow velocity can be calculated for the incompressible flow case if desired. Unfortunaely, the method of calculation is very time consuming, and therefore for routine calculations a simpler approach is needed.

Method for Routine Analysis: To eliminate the large amount of time required to calculate the inflow velocity for the case where the propeller is operating in a subsonic stream with a supersonic section Mach number, it was necessary to make the assumption that the blades are operating at constant circulation. On the basis of this approximation, it was possible to determine the ratio of the inflow velocity for the compressible flow case to the inflow velocity for the incompressible flow case. Then, knowing this ratio, the incompressible flow/inflow velocity determined by the method of Reference 8 could be corrected for compressibility effects.

When the assumption is made that the circulation is constant, the lower limits of Equations (89) to (91) apply only for cases 1 and 3. These cases correspond to X = 1.0 on the limit curves. For the condition of constant circulation, the ratio of the compressible inflow velocity to the incompressible value may be found by finding the ratio of I using the proper value of the lower limit $\phi_L$ to the value of I at $\phi_L = 0$. This will give the ratio $u_c/u_i$, where $u_c$ is the compressible value of axial inflow velocity and $u_i$ is the incompressible value of inflow velocity. The ratio of $u_c/u_i$ is assumed equal to $W_c/W_i$ since

$$\frac{w_c}{w_i} = \frac{u_c \cos^2 \phi_i}{u_i \cos^2 \phi_c} = \frac{u_c}{u_i} \qquad (103)$$

where $w_c$ = the displacement velocity in final wake for the compressible flow case

$w_i$ = the displacement velocity in final wake for the incompressible flow case

$u_c$ and $u_i$ = the axial inflow velocity for the compressible and incompressible flow cases respectively

$\phi_i, \phi_c$ = the true wind angle for the incompressible flow and compressible flow cases respectively.

The ratios of $w_c/w_i$ are plotted versus Mach number on Figures 27 to 55 for the required range of J and x so that effects of compressibility can be determined for 2-, 3-, 4-, and 6-bladed

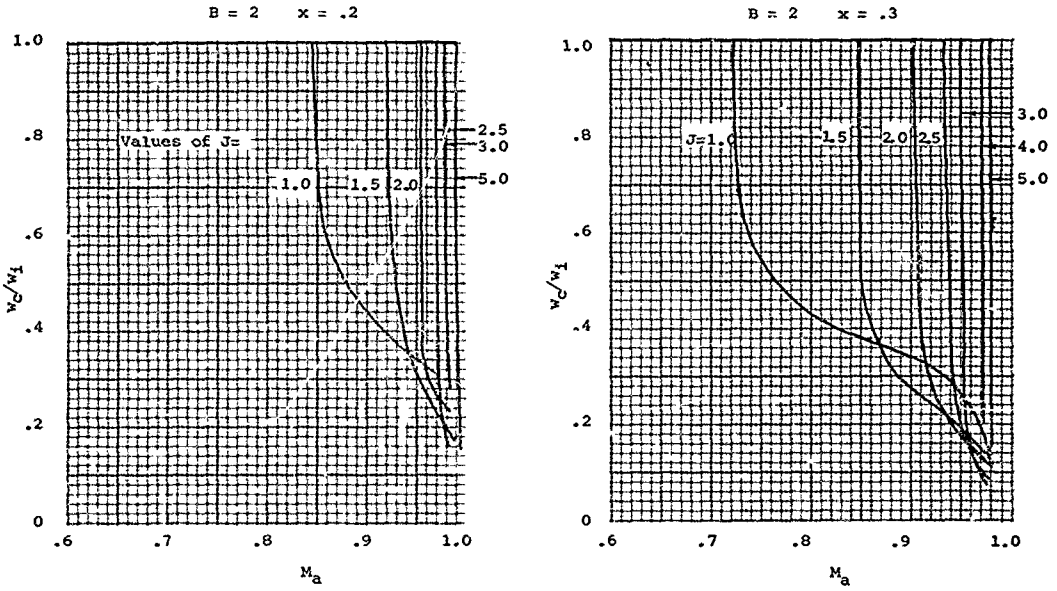


Figure 27. Compressible Flow/Inflow Velocity Correction - B = 2, x = .2 and .3.

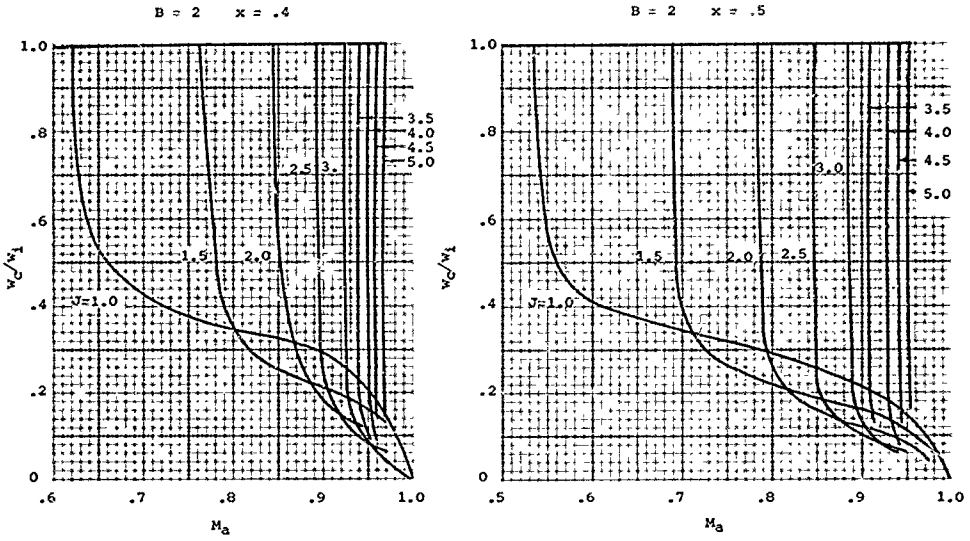


Figure 28. Compressible Flow/Inflow Velocity Correction - B = 2, x = .4 and .5.

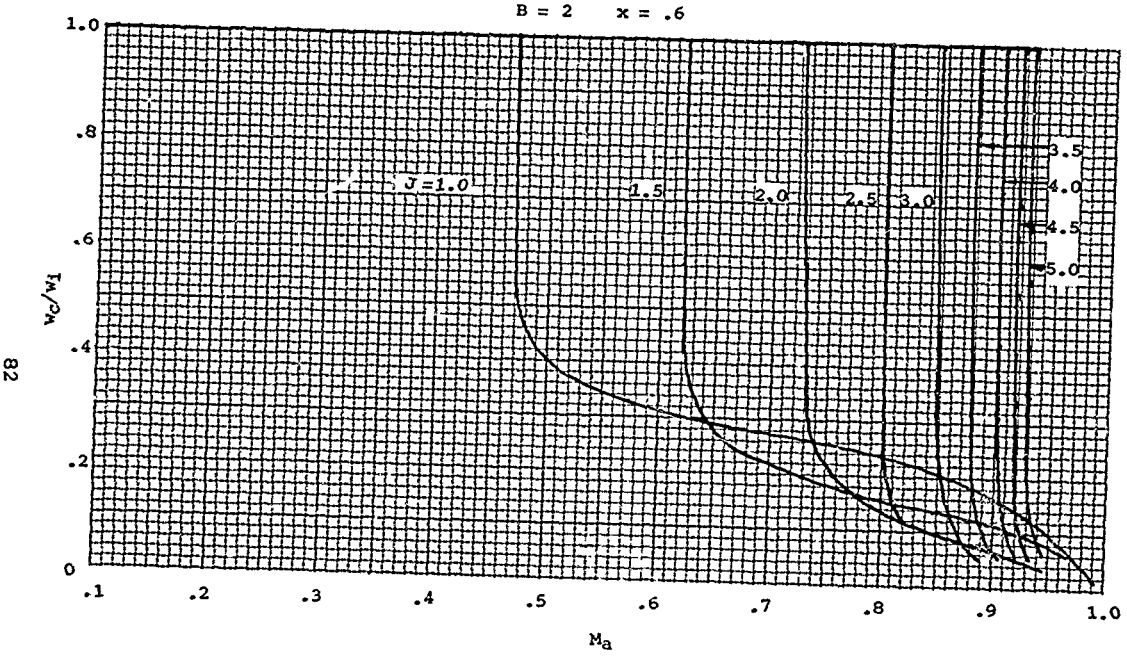


Figure 29. Compressible Flow/Inflow Velocity Correction - B = 2, x = .6.

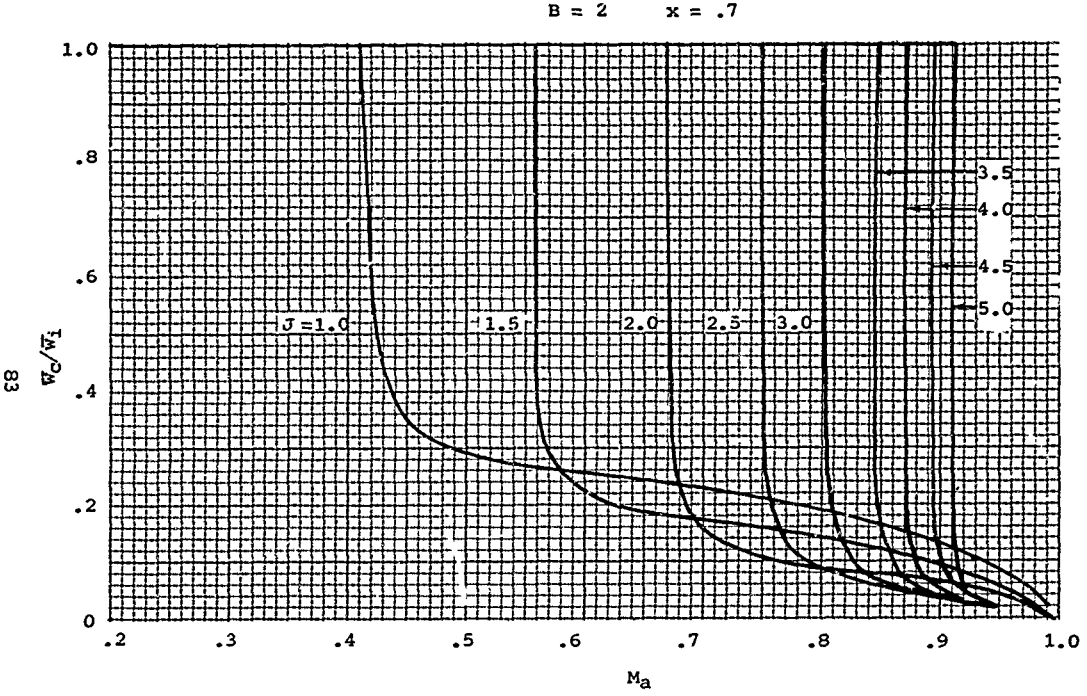


Figure 30. Compressible Flow/Inflow Velocity Correction - B = 2, x = .7.

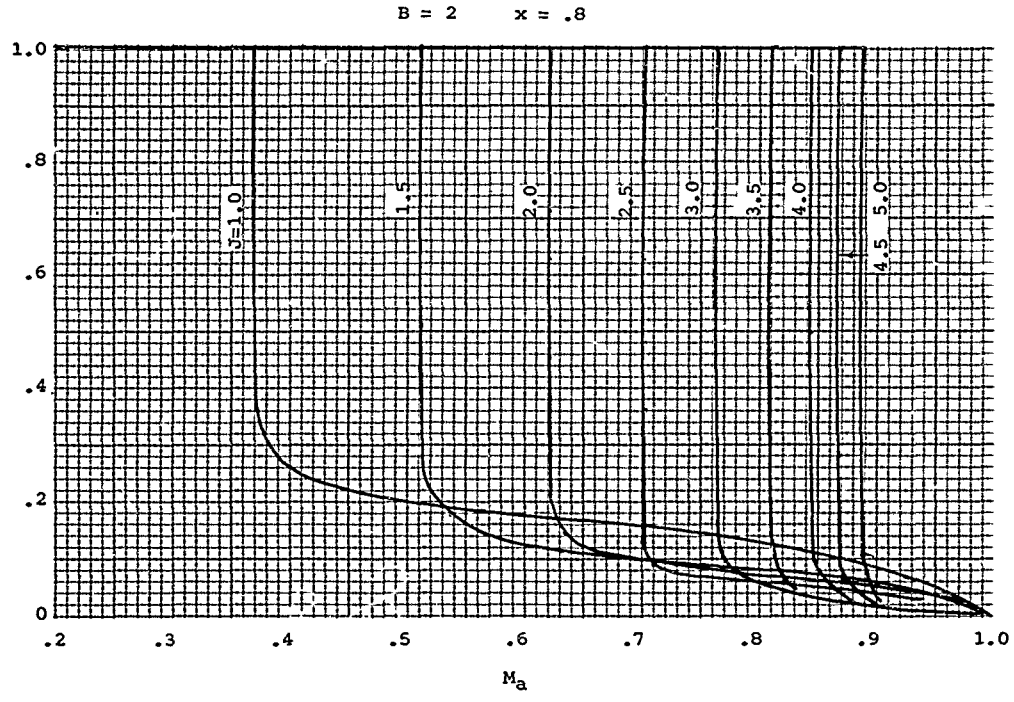


Figure 31. Compressible Flow/Inflow Velocity Correction - B = 2, x = .8.

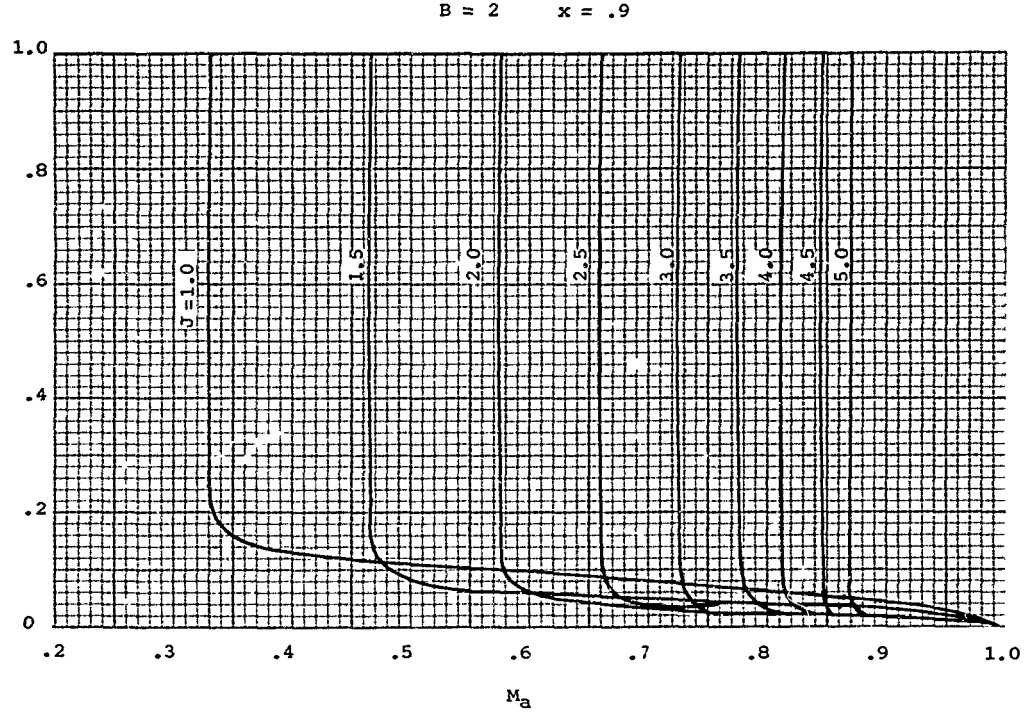


Figure 32. Compressible Flow/Inflow Velocity Correction - B = 2, x = .9.

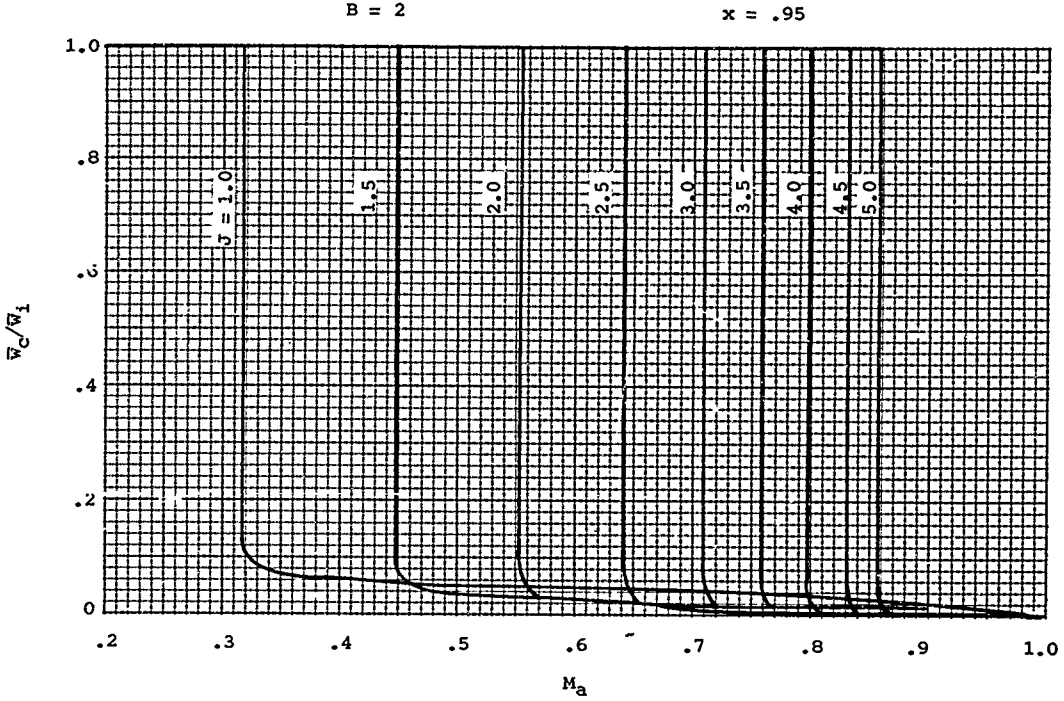


Figure 33. Compressible Flow/Inflow Velocity Correction - B = 2, x = .95.

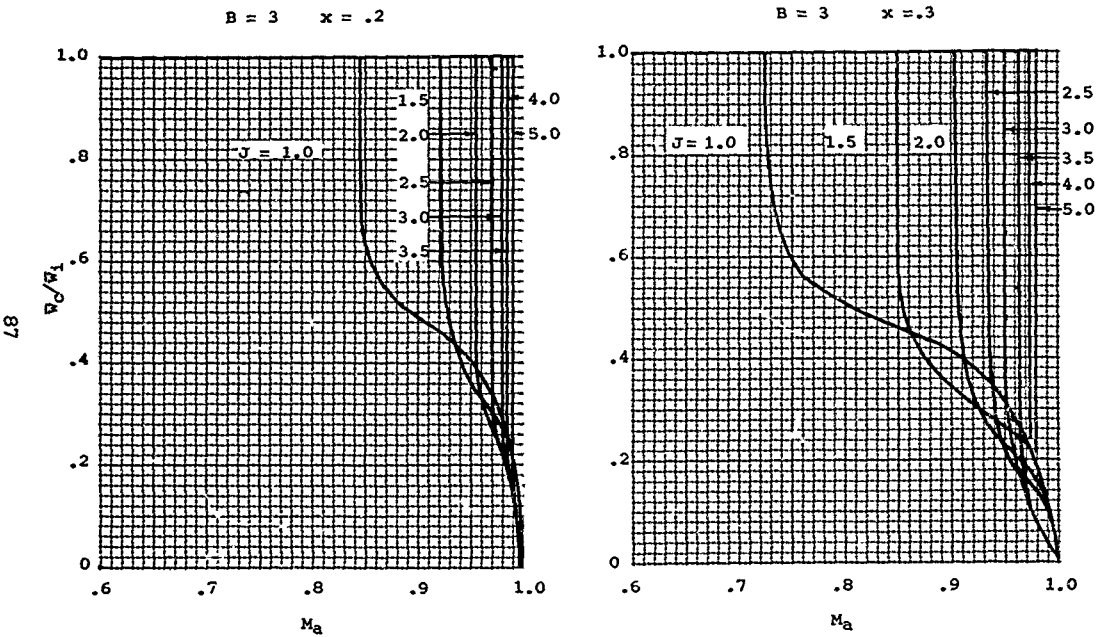


Figure 34. Compressible Flow/Inflow Velocity Correction - B = 3, x = .2 and .3.

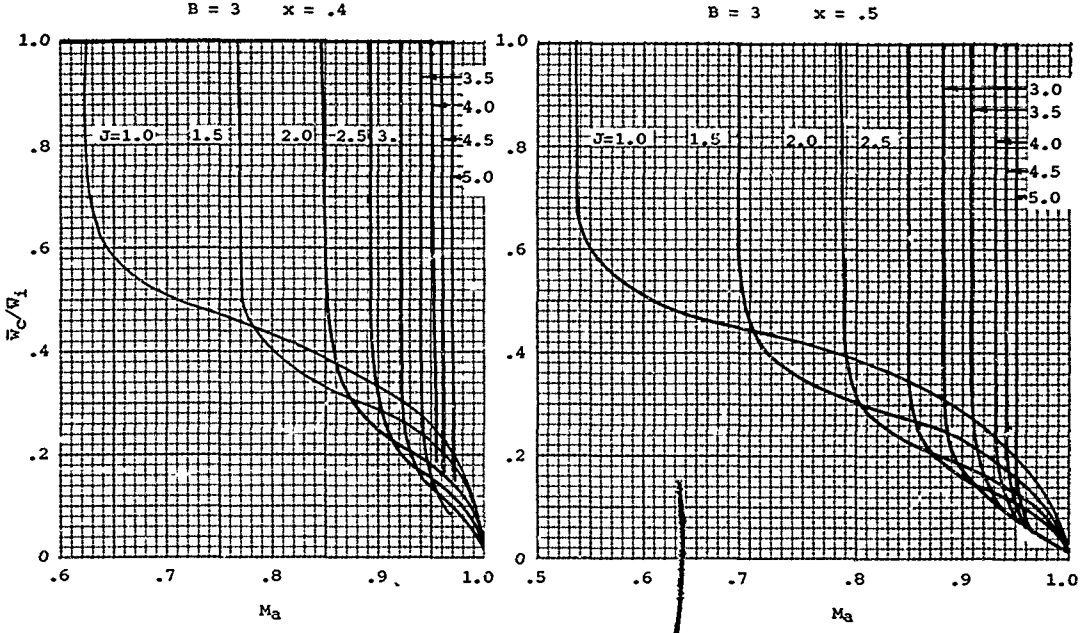


Figure 35. Compressible Flow/Inflow Velocity Correction - B = 3, x = .4 and .5.

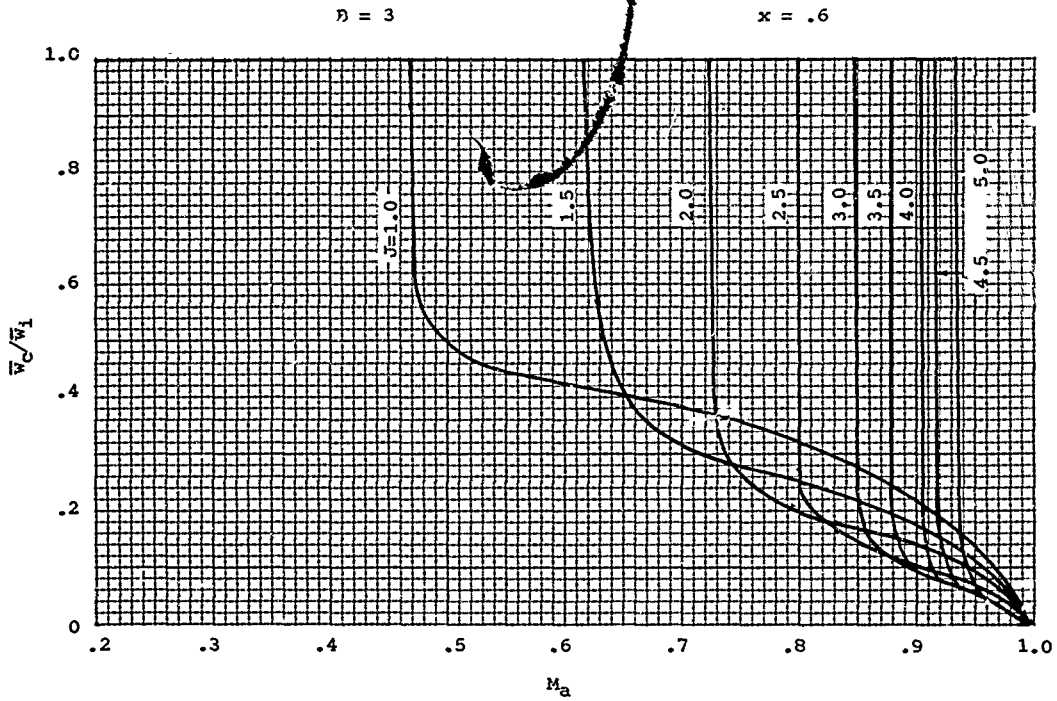


Figure 36. Compressible Flow/Inflow Velocity Correction - B = 3, x = .6.

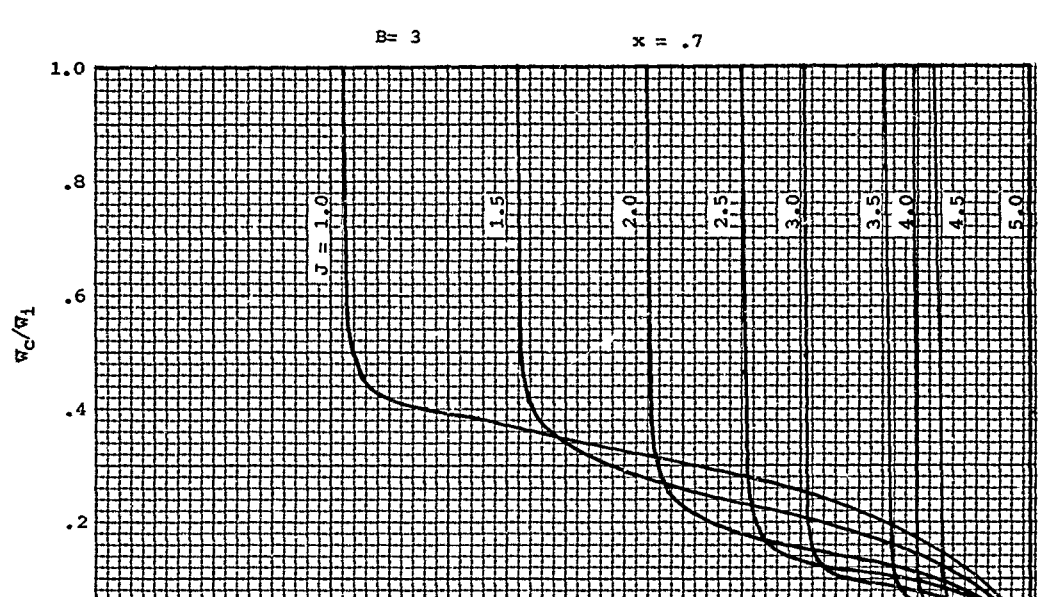


Figure 37. Compressible Flow/Inflow Velocity Correction - B = 3, x = .7.

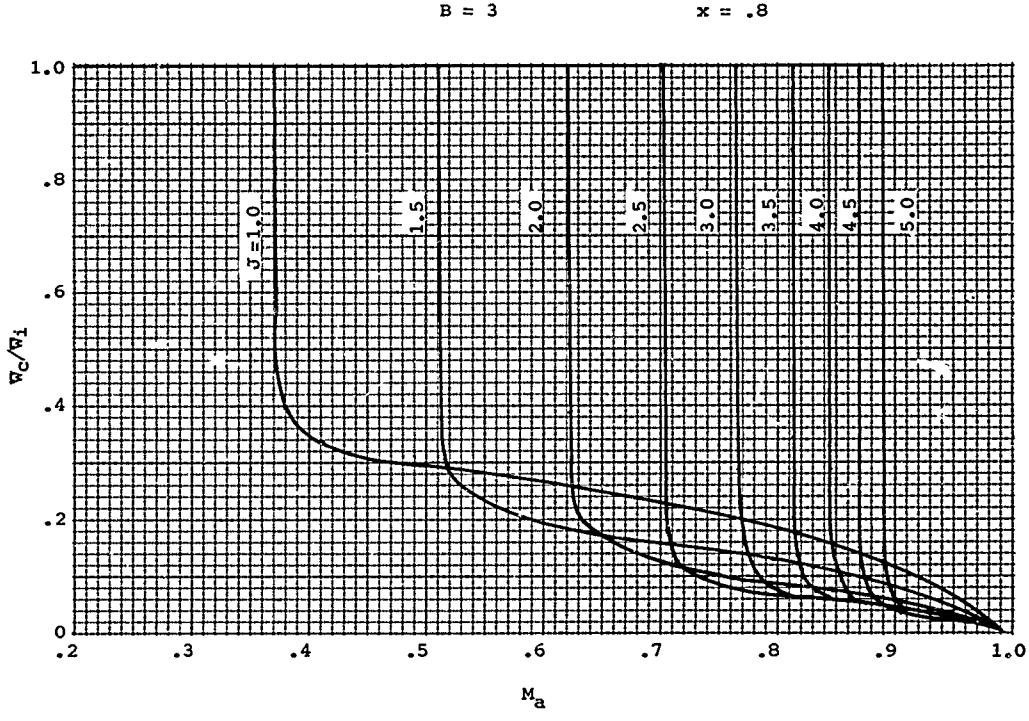


Figure 38. Compressible Flow/Inflow Velocity Correction - B = 3, x = .8.

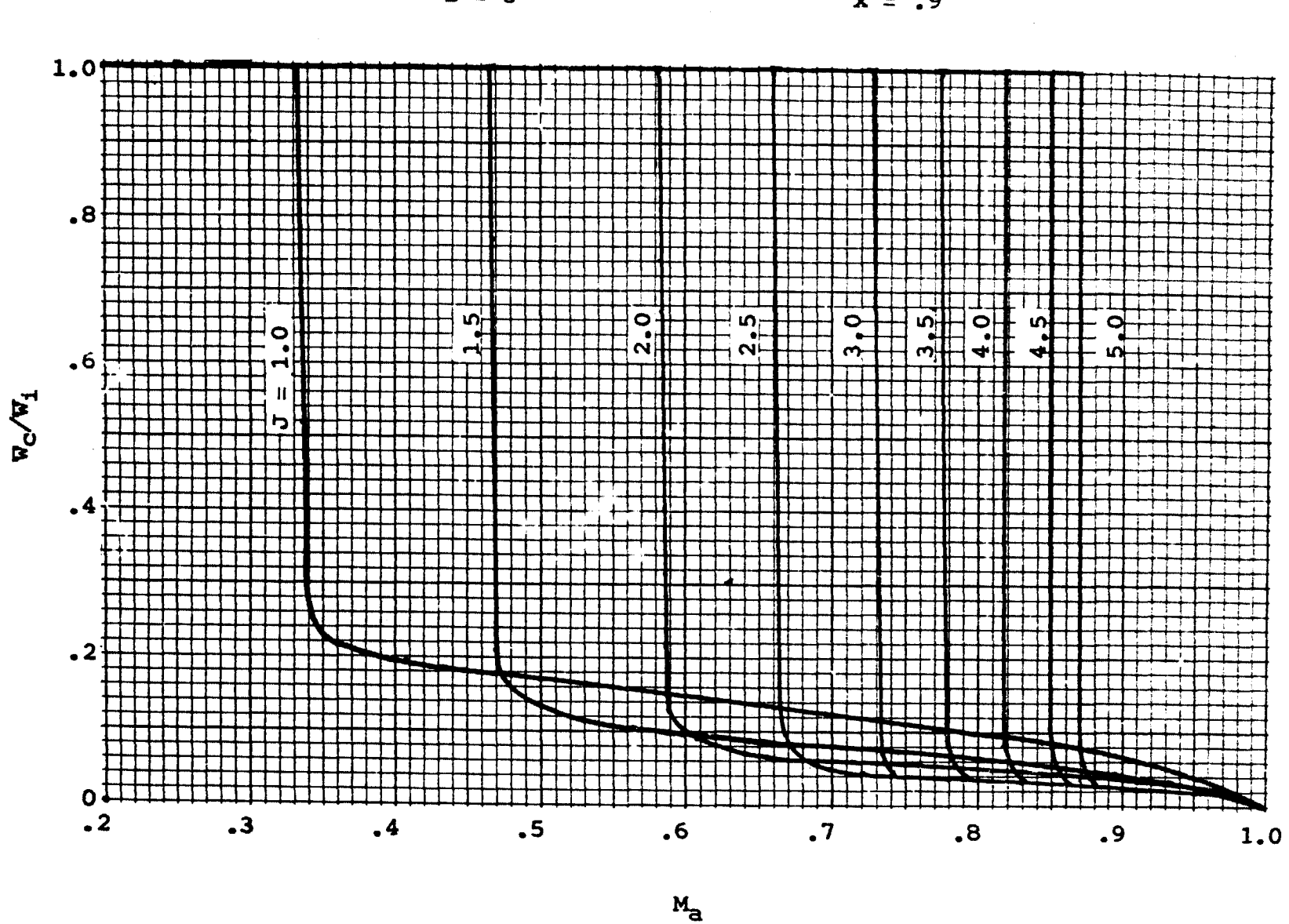


Figure 39. Compressible Flow/Inflow Velocity Correction - B = 3, x = .9.

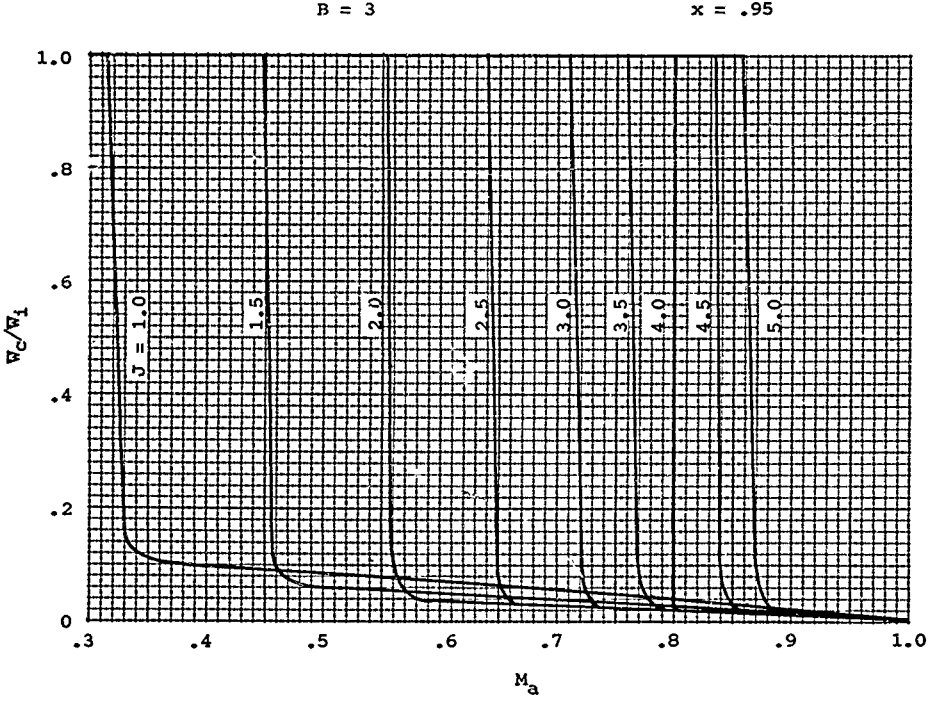


Figure 40. Compressible Flow/Inflow Velocity Correction - B = 3, x = .95.

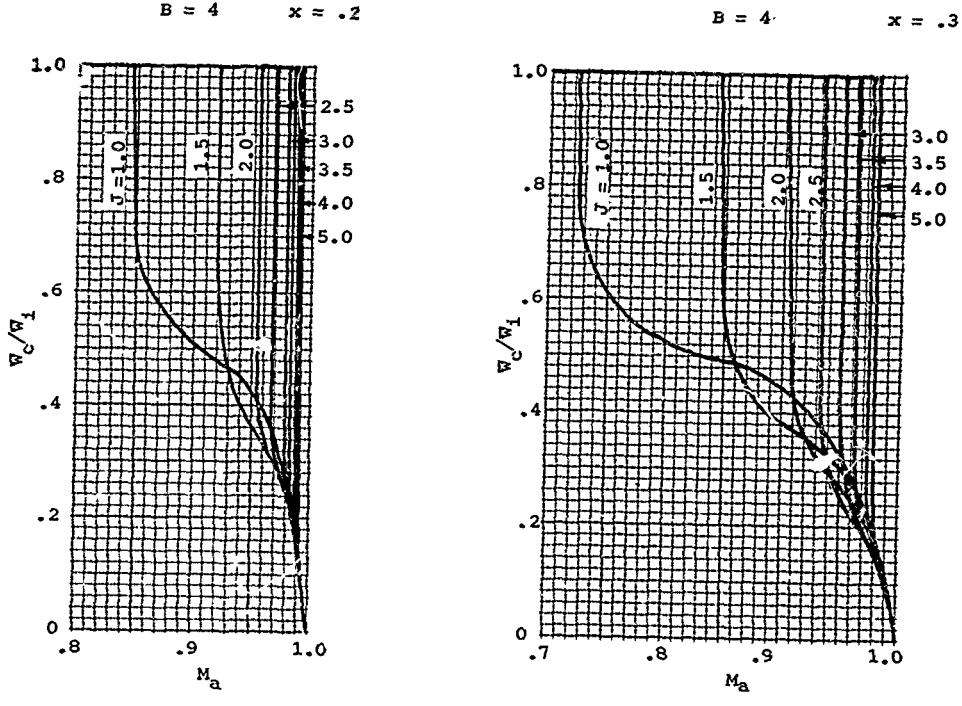


Figure 41. Compressible Flow/Inflow Velocity Correction - B = 4, x = .2 and .3.

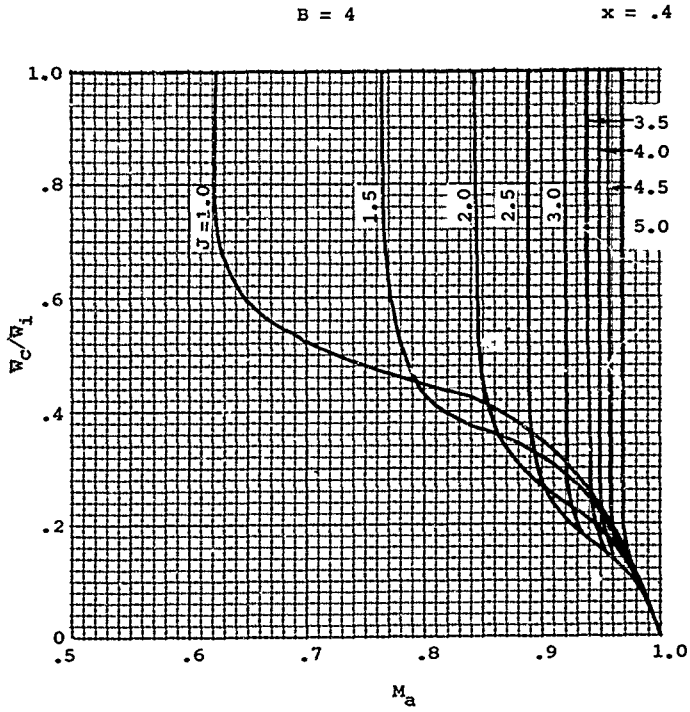


Figure 42. Compressible Flow/Inflow Velocity Correction - B = 4, x = .4.

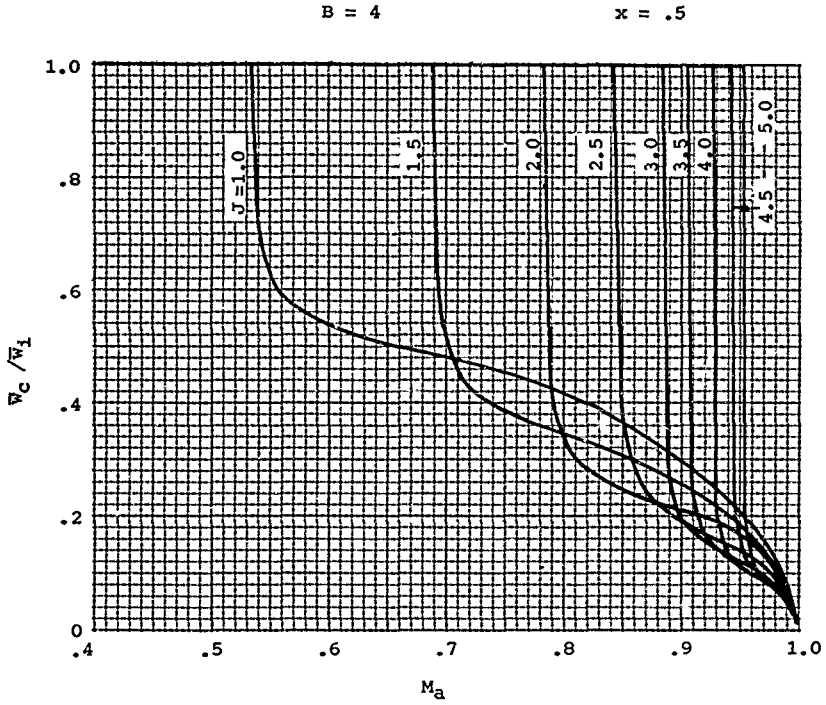


Figure 43. Compressible Flow/Inflow Velocity Correction - B = 4, x = .5.

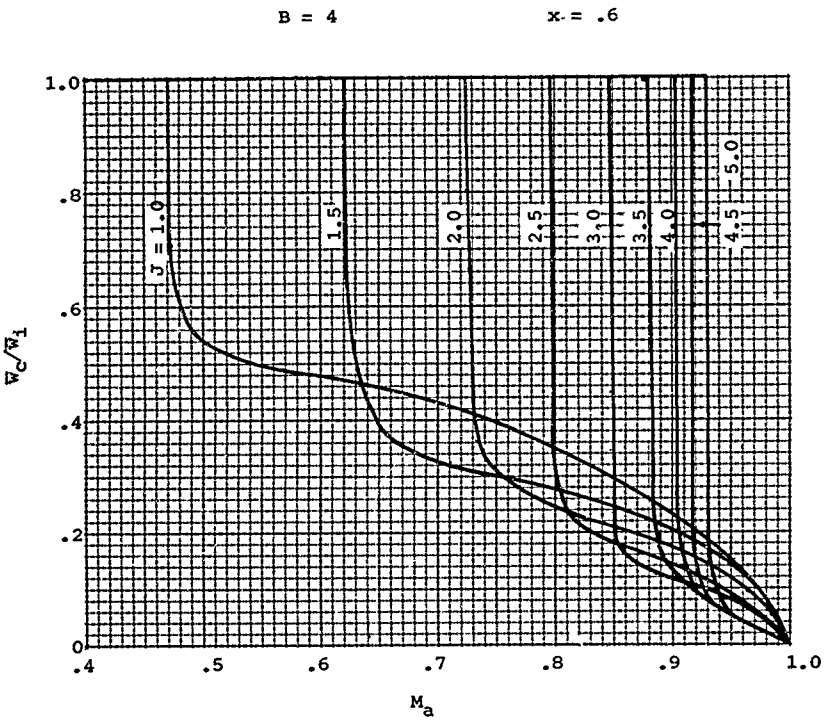


Figure 44. Compressible Flow/Inflow Velocity Correction - B = 4, x = .6.

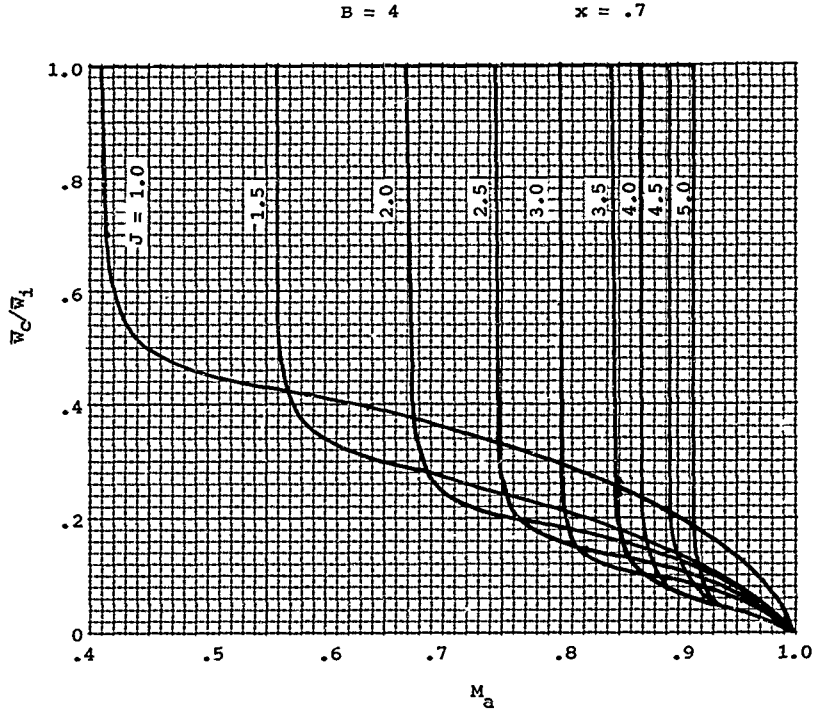


Figure 45. Compressible Flow/Inflow Velocity Correction - B = 4, x = .7.

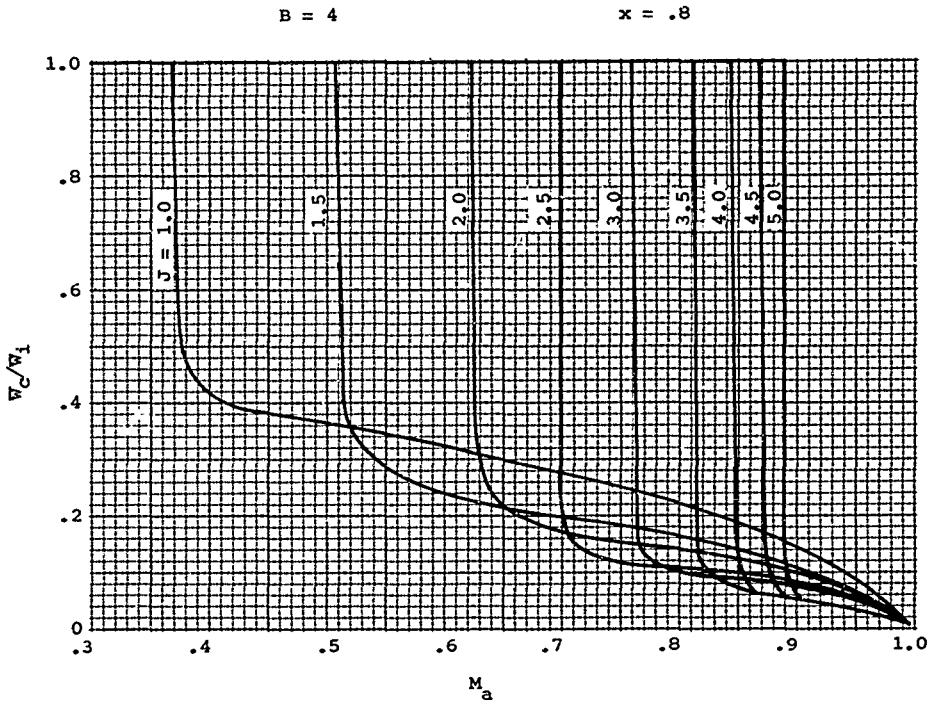


Figure 46. Compressible Flow/Inflow Velocity Correction - B = 4, x = .8.

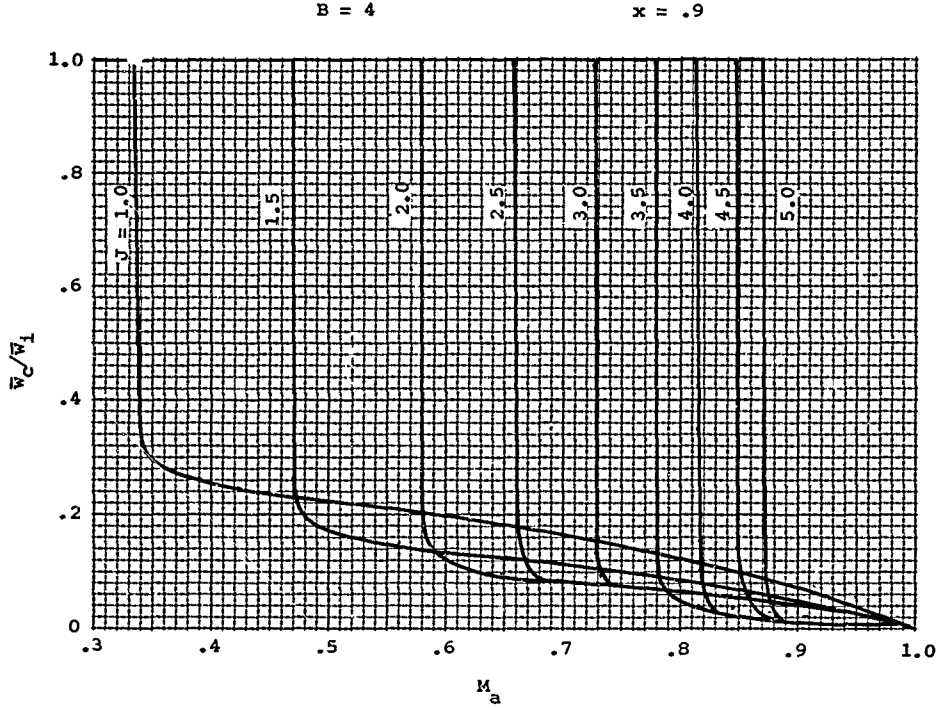


Figure 47. Compressible Flow/Inflow Velocity Correction - B = 4, x = .9.

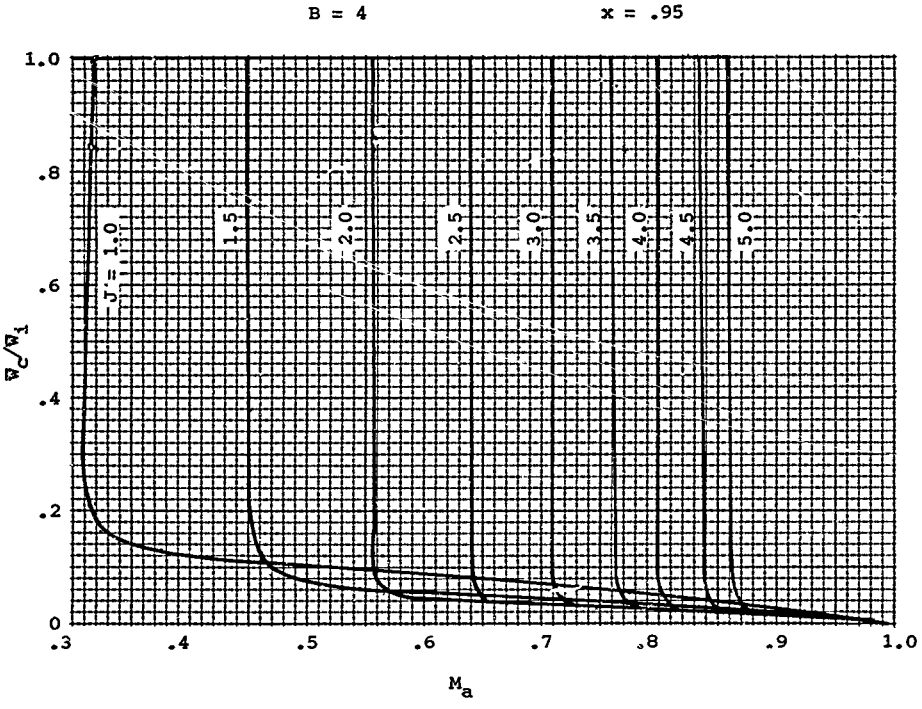


Figure 48. Compressible Flow/Inflow Velocity Correction - B = 4, x = .95.

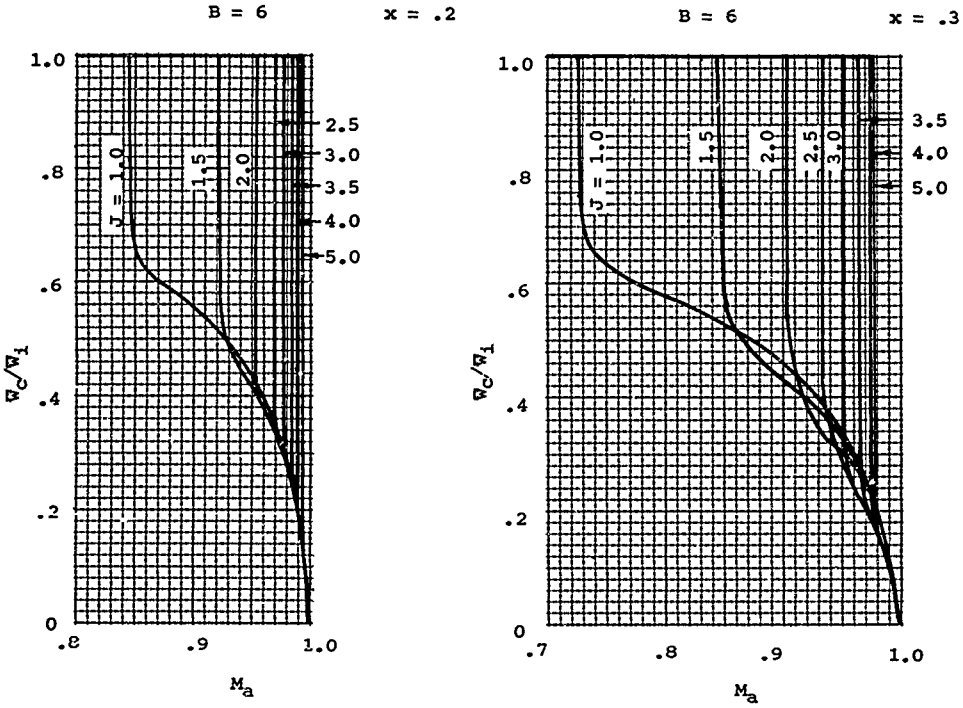


Figure 49. Compressible Flow/Inflow Velocity Correction - B = 6, x = .2 and .3.

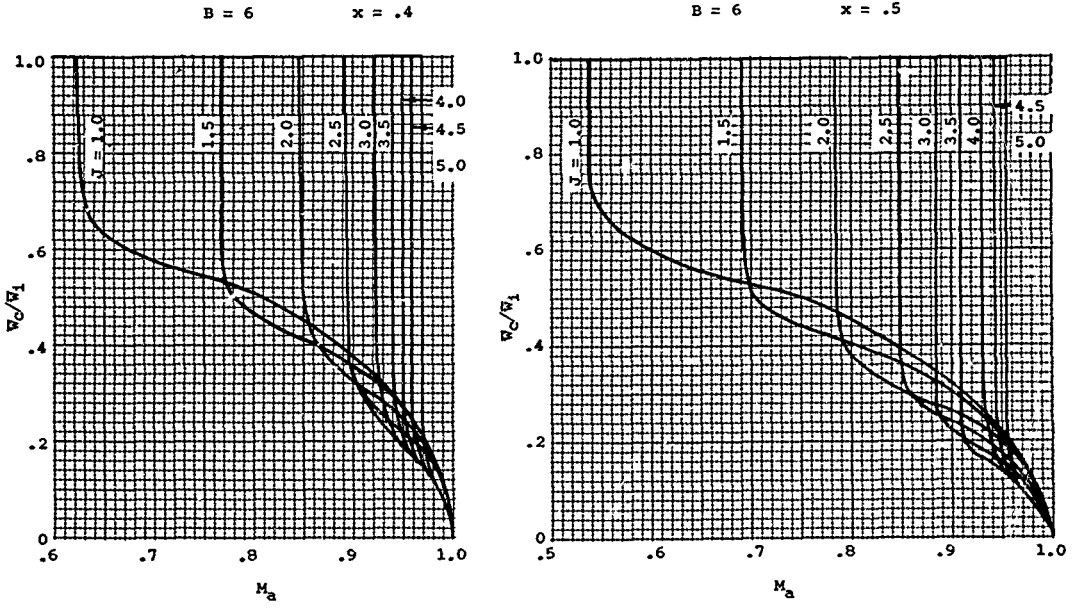


Figure 50. Compressible Flow/Inflow Velocity Correction - B = 6, x = .4 and .5.

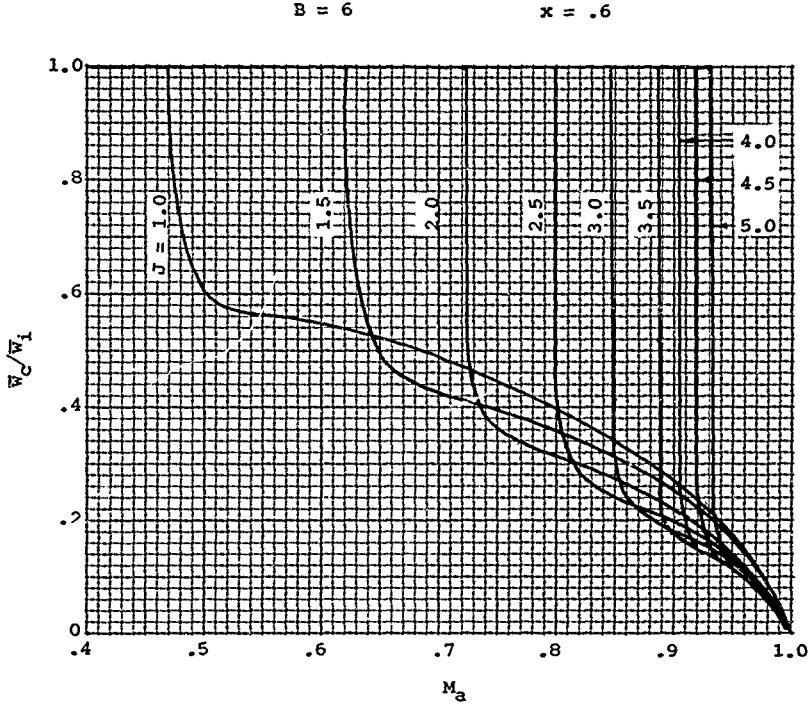


Figure 51. Compressible Flow/Inflow Velocity Correction - B = 6, x = .6.

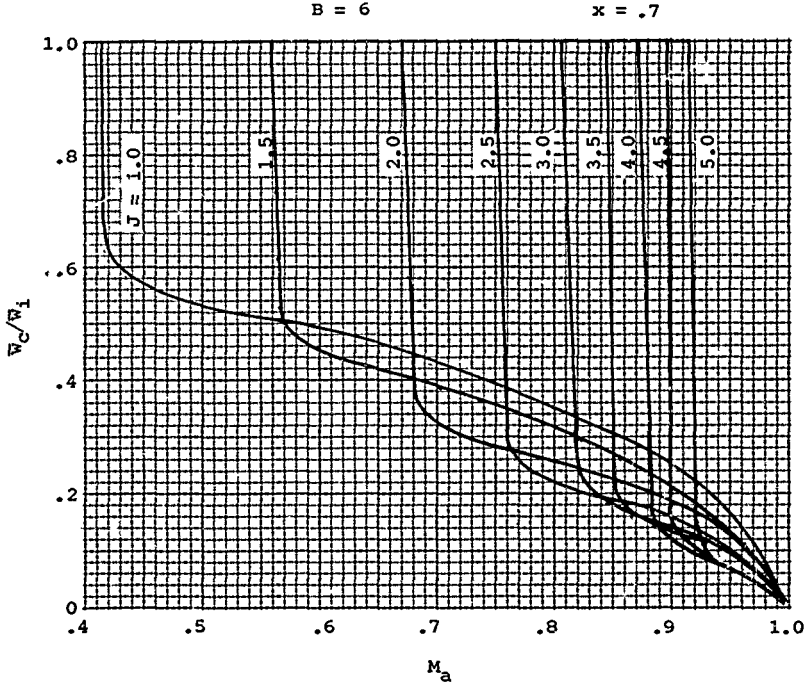


Figure 52. Compressible Flow/Inflow Velocity Correction - B = 6, x = .7.

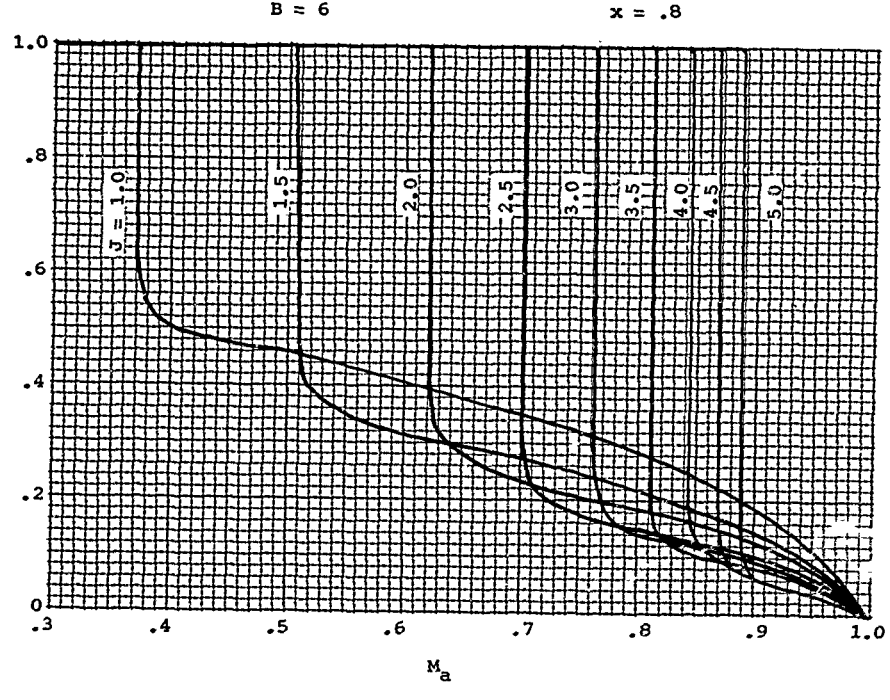


Figure 53. Compressible Flow/Inflow Velocity Correction - B = 6, x = .8.

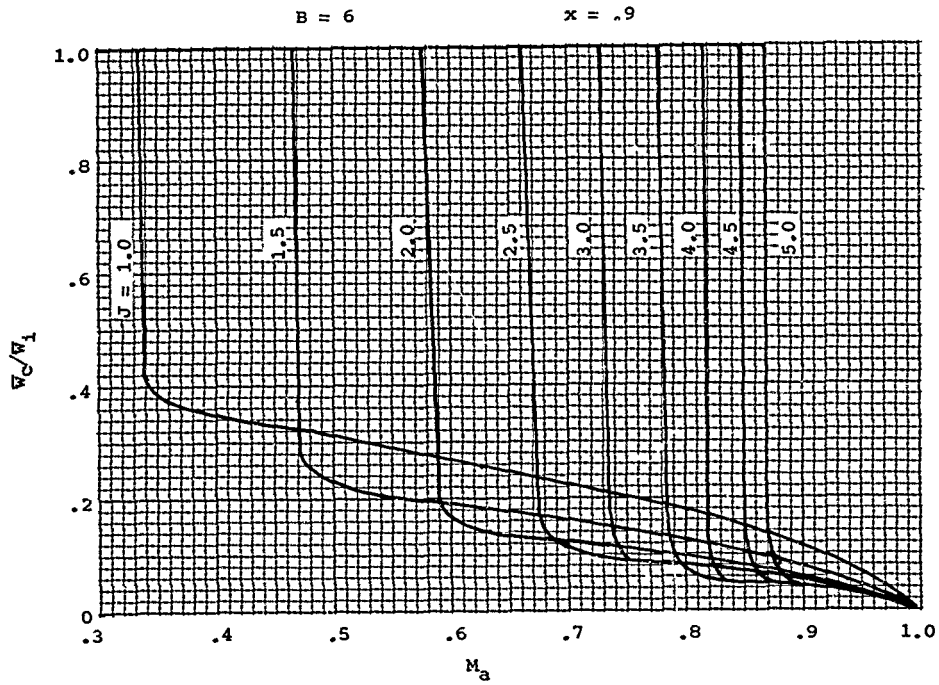


Figure 54. Compressible Flow/Inflow Velocity Correction - B = 6, x = .9.

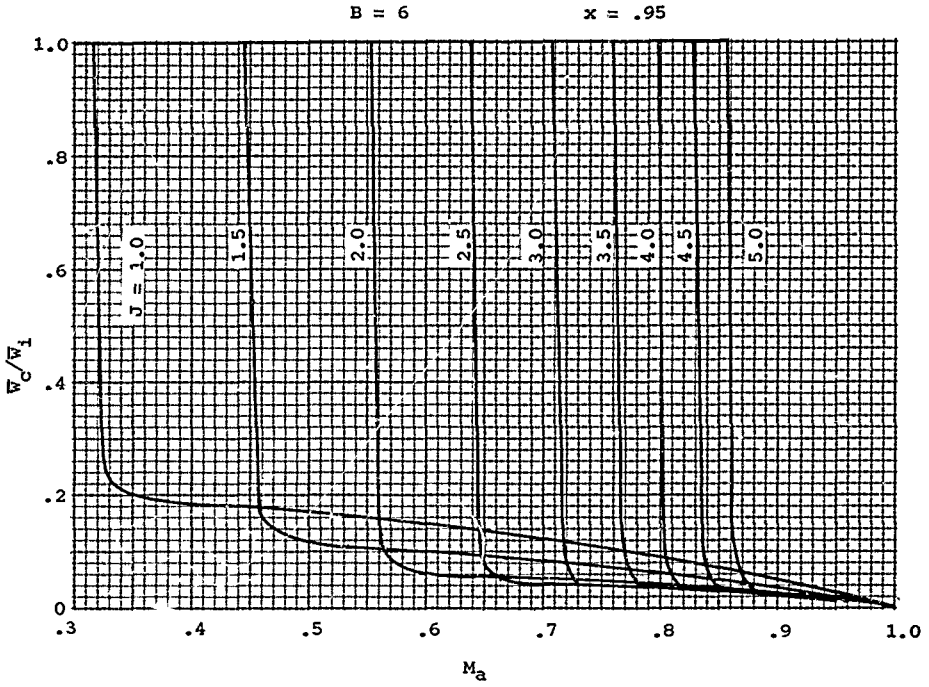


Figure 55. Compressible Flow/Inflow Velocity Correction - B = 6, x = .95.

single-rotation propellers. It will be noted from Figures 27 to 55 that $w_c/w_i$ are equal to one until a certain forward Mach number is obtained, at which point the value of ratio becomes very much lower. This value of forward Mach number corresponds to a section Mach number of one. The sudden drop of the ratio $\bar{w}'_c/\bar{w}'_i$ shown is due to the simplifying assumption of constant loading as described above.

If the case of optimum circulation is taken as was done by Goldstein and Theodorsen and the proper limits are used, i.e., cases 1 to 4 described previously, the sudden drop shown on Figures 27 to 55 will not be obtained. An example of this is shown on Figure 56 for an x of .7, a J of 2.0 and a two-bladed propeller. In this case the drop of $\bar{w}_c/\bar{w}_i$ begins below the section Mach number of one, which indicates that the full effects of the outboard tailing vortices are not felt at this condition. This would be expected as the outboard trailing vortices are trapped within their Mach cones for a certain period of time.

From the results of the sample calculation given on Figure 56, it will be noted that the inflow velocity calculated at the stations operating at section Mach numbers just below one will be too high. This will result in a slightly lower efficiency than indicated by the more exact calculation. Actually, however, the load distribution will probably be between the Betz and the constant load distributions considered herein; therefore, the error should prove to be small for normal type propellers.

Tip Correction: When the compressible flow value of the inflow velocity is found for a propeller operating at a forward Mach number less than one and tip Mach number over one, it is necessary to apply the supersonic tip Mach number correction developed for wings by Evvard, Reference 16 . This correction applies only in the tip Mach cone and reduces the drag due to lift and the lift by a factor K. The method of applying this correction was described in Reference 16. From this reference, charts have been developed, so that, knowing the tip Mach number, the blade chord, and the blade diameter, the value of K is easily determined. The values of K and the method of application are shown on Figures 57 to 62. It should be noted that this correction does not apply at stations within the tip Mach cone where the section Mach number is less than one.

To calculate the inflow velocity of a propeller when the forward Mach number is less than one and the tip Mach number is over one requires the calculation of the inflow velocity as described above and then correcting this value according to the charts presented herein. The correction depends on the advance ratio, forward Mach number, and the number of blades. After finding the inflow velocity for this case, it is necessary to

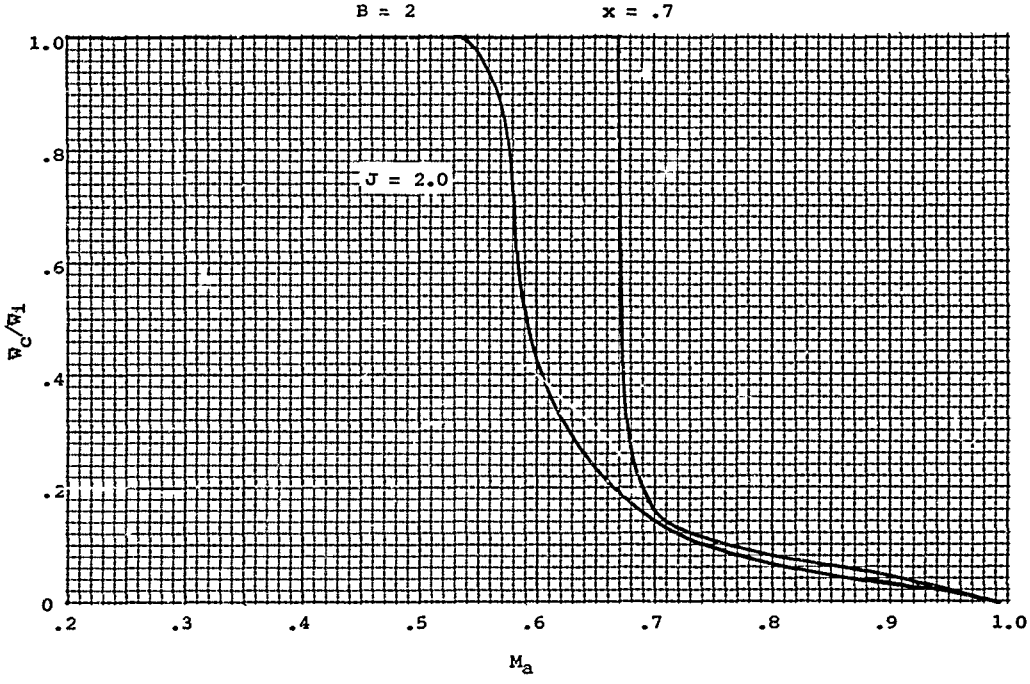


Figure 56. Comparison of Induced Velocity Compressibility Correction for Betz And Constant Load Distributions.

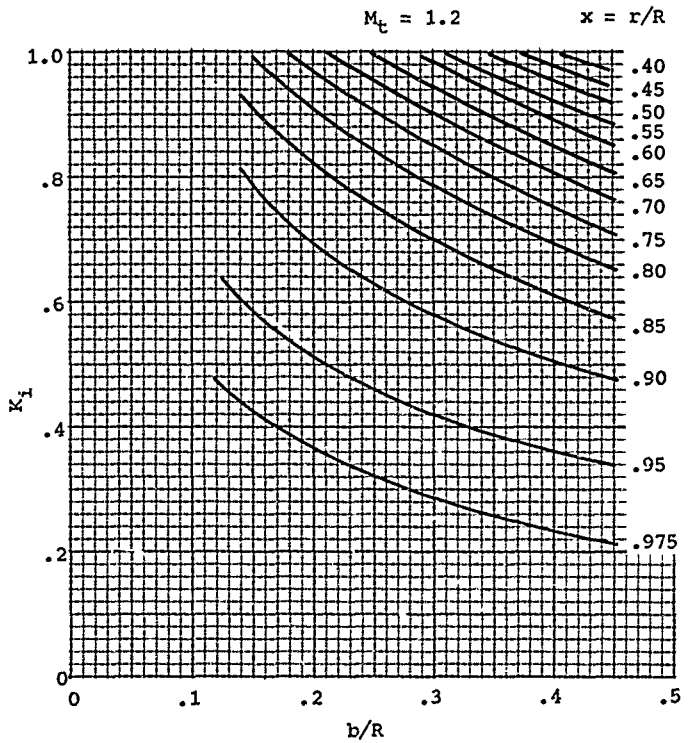


Figure 57. Tip Compressibility Correction to Airfoil Characteristics.

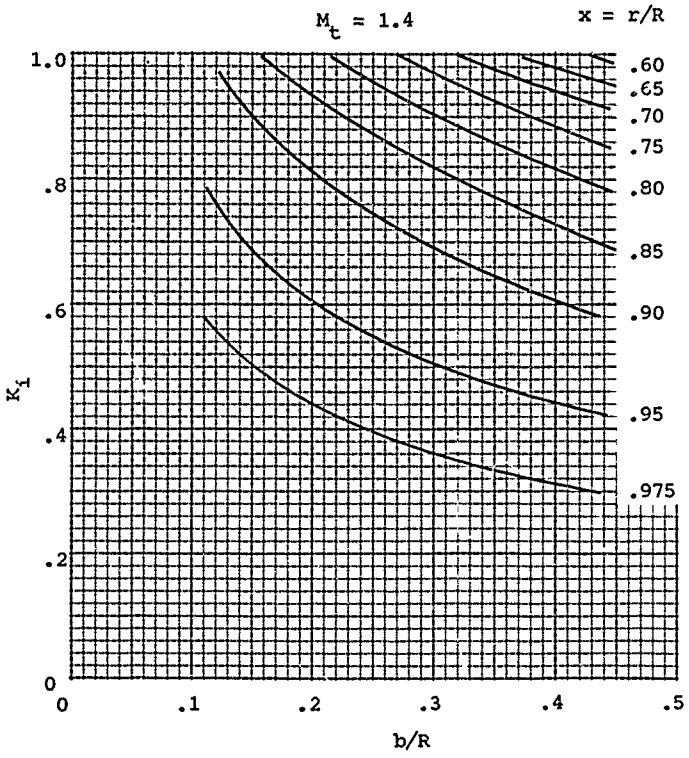


Figure 58. Tip Compressibility Correction to Airfoil Characteristics.

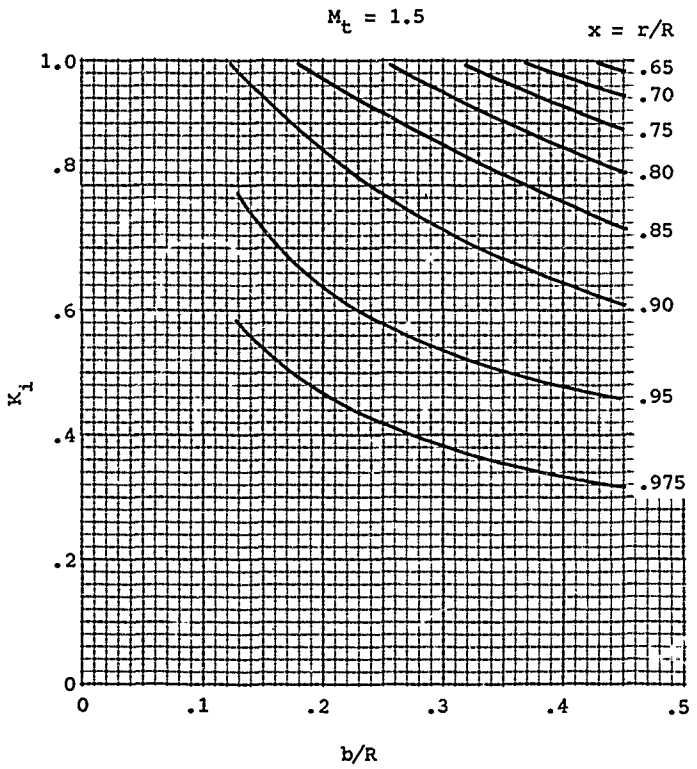


Figure 59. Tip Compressibility Correction to Airfoil Characteristics.

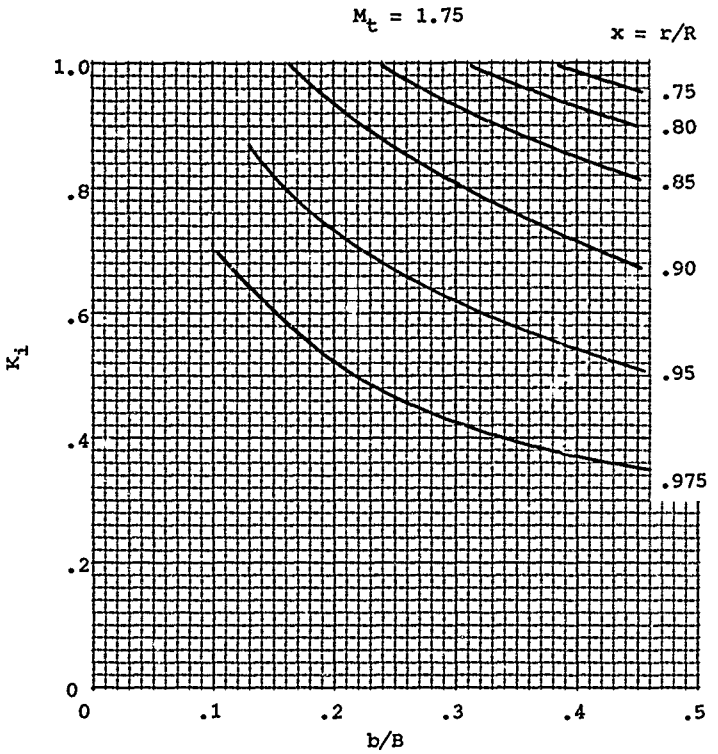


Figure 60. Tip Compressibility Correction to Airfoil Characteristics.

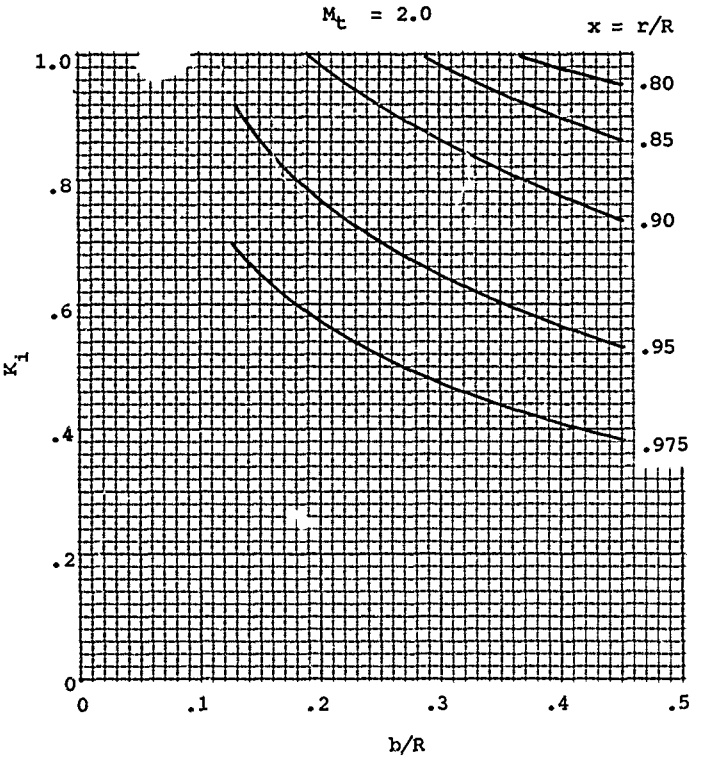


Figure 61. Tip Compressibility Correction to Airfoil Characteristics.

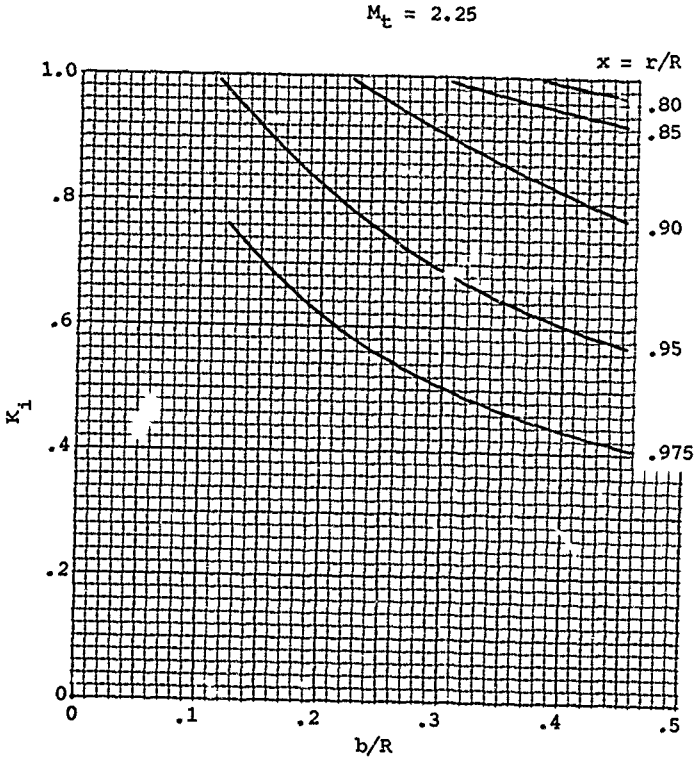


Figure 62. Tip Compressibility Correction to Airfoil Characteristics.

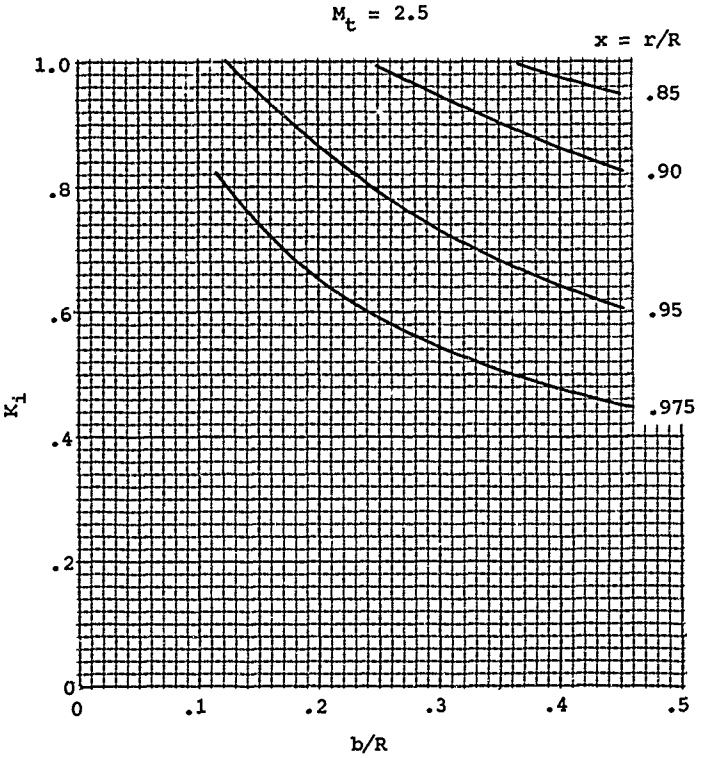


Figure 63. Tip Compressibility Correction to Airfoil Characteristics.

correct the drag due to lift and the lift for the tip relief effect. This is easily done knowing the tip Mach number, blade width, and propeller diameter.

When the propeller is operating at a forward Mach number over one, the inflow velocity is zero and the only correction necessary to apply two-dimensional airfoil data to strip analysis calculations is the tip relief effect described above and plotted on Figures 57 to 63 . Thus, all the data and theory to find the performance of propellers at all operating conditions have been established.

## THEORY OF PROPELLERS AT ZERO VELOCITY

The vortex theory of propellers developed and presented previously applies only to the case where the forward velocity is large with respect to the induced velocity. For this case any errors of the induced velocity which determine the position of the vortices in the final wake along with the free-stream velocity will have a small effect on the final results. The position accuracy of the vortices in the wake is influenced by errors in the load distribution and slipstream contraction as well as the errors of the induced velocity. These effects are small for the forward flight condition, as the position of the vortices is mainly determined by the free-stream velocity. In the case of a propeller operating at zero velocity, the slipstream contraction, load distribution, and induced velocity are of major importance, as these directly influence the position of the vortices in the wake.

The direct interdependence of the wake position and the induced velocity at the disc has lead to considerable problems in developing a satisfactory theory. Attempts have been made to modify the existing Goldstein and Theodorsen's theory for calculating the induced velocity, but these methods have proved to be unsatisfactory. As a result, attempts to design and predict the performance of propellers operating at the static condition using strip theory have failed. The performance calculated for propellers designed by these methods has been well above the actual measured values.

The accurate measurement of the performance of propellers operating at the static condition has been difficult also. This has caused problems in evaluating the accuracy of the calculated performance, and is therefore of importance. Because of the direct relation of the wake position on the induced velocity, and therefore the angle of attack of the blade section, effects of the external air currents on performance are large. Thus, when testing propellers operating at zero velocity, extreme care must be used to eliminate the effects of external wind force. Testing should be done under calm wind conditions only, and only these data should be used for performance comparisons of test and calculated results.

The performance of propellers calculated at zero velocity using modifications of the Goldstein or Theodorsen theory greatly overestimated the thrust at a given power. Since the profile drag losses have been found to be accurately predicted for the flight conditions from two-dimensional airfoil data, the error appears to be in the induced efficiency.

Several attempts have been made to develop a theory to calculate accurately the induced velocity, and therefore the induced

losses for any load distribution, References 17 and 18. Generally, closed solutions to the problem have not been found except as a result of extremely long computer runs. Even these results have not been considered a final solution to the problem because of the complexity and the interdependence of the wake on the induced velocity, Reference 18.

Ideal Performance V = 0

The ideal performance of a propeller with a finite number of blades operating at the static or hover condition is of great importance in assessing a blade design. Like propellers operating at a forward velocity condition, knowledge of the peak induced efficiency at hover gives a target value of peak performance and indicates those areas where improvements can be made.

Until recently the only knowledge of the ideal performance at the static condition was that based on momentum considerations for an ideal propeller with an infinite number of blades. For the case of a propeller with a finite blade number, Theodorsen, Reference 19, showed that the ideal performance is obtained only when the surface of discontinuity in the final wake is displaced rearward with a constant axial velocity w and is a rigid structure. This is exactly the same condition determined for an optimum propeller operating at the forward velocity condition. Thus, at the static condition, the load distribution for peak efficiency will give a vortex distribution that forms a surface of discontinuity which moves rearward in the final wake at a constant axial velocity.

In his book "Theory of Propellers" (Reference 8), Theodorsen relates the thrust and power to energy functions. These energy functions were called loss functions, $\epsilon$, but are more of a measure of the energy for thrust. For this reason, Theodorsen in Reference 19 refers to $\epsilon$ as an energy function. The energy function and mass coefficient can be related to find the peak thrust to power coefficient ratio for a finite blade number. From Reference 19 it was shown that

$$\frac{C_T^{3/2}}{C_P} = \frac{(\epsilon + \tfrac{1}{2} k)^{3/2}}{\epsilon} \frac{k'}{2}\sqrt{\pi} \qquad (104)$$

where $\epsilon$ = energy function
$k$ = mass coefficient
$k'$ = the contraction ratio
$T$ = thrust
$P$ = power

Now from page 36, the Figure of Merit, FM, is equal to

$$FM = \frac{.565}{k'} \frac{C_T^{3/2}}{C_p} \tag{105}$$

$$FM = \frac{(\epsilon + \frac{1}{2} k)^{3/2}}{\epsilon} \frac{\sqrt{\pi}}{2} .565 \tag{106}$$

$$FM = \frac{(\epsilon + \frac{1}{2} k)^{3/2}}{2\epsilon} \tag{107}$$

The optimum Figure of Merit for two- and four-bladed propellers as calculated from the data of Reference 19 is shown as a function of power of coefficient in Figure 64. Also shown here is the Figure of Merit based on the assumption that the wake contraction ratio is equal to 0.707 or the induced velocity in the wake is equal to twice the velocity at the propeller. This comparison shows that the peak Figure of Merit for propellers operating at the static condition is much below the level previously considered possible.

When calculating the Figure of Merit from test data for comparison with the ideal value, the constant representing a slipstream contraction ratio corresponding to a change of velocity of 2 from the propeller disc to the final wake should not be used. This velocity change gives an area ratio of 0.707 and the constant of 0.798.

The proper equation of Figure of Merit for the comparison of test data with the ideal value for propellers is

$$FM = \frac{.565}{k'} \frac{C_T^{3/2}}{C_p} \tag{108}$$

The contraction ratio $k'$ is a function of $C_p$ and is found from Figure 65.

A comparison of the available test data of propellers operating at the static condition shows that the optimum value as predicted with the Theodorsen data is not exceeded with any of the cases examined. Although this does not prove the theory, at least it appears that a valid measurement is now available

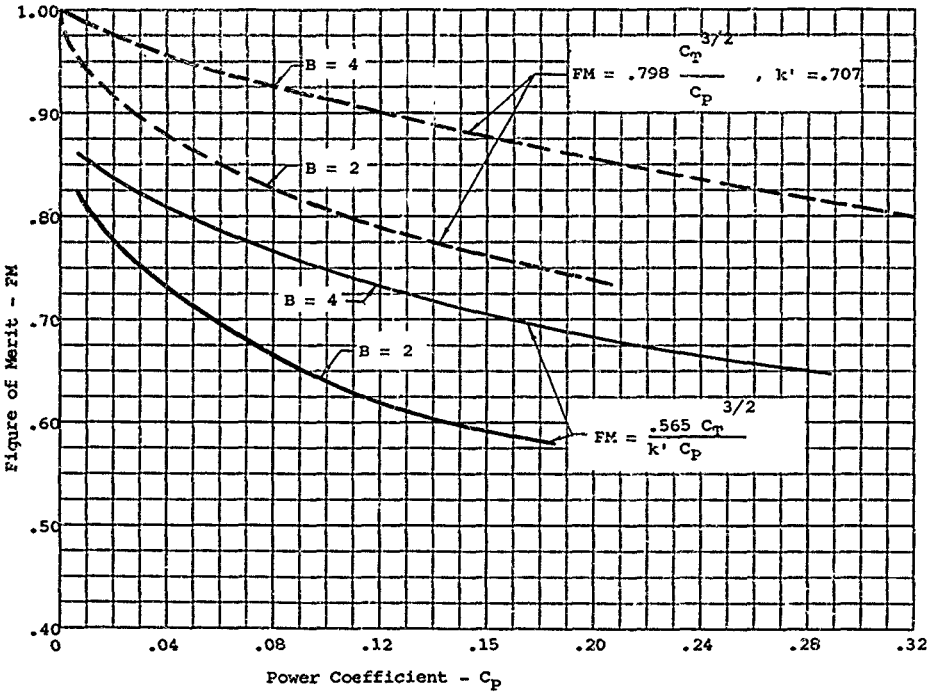


Figure 64. Propeller Figure of Merit Comparison for Static Thrust Condition.

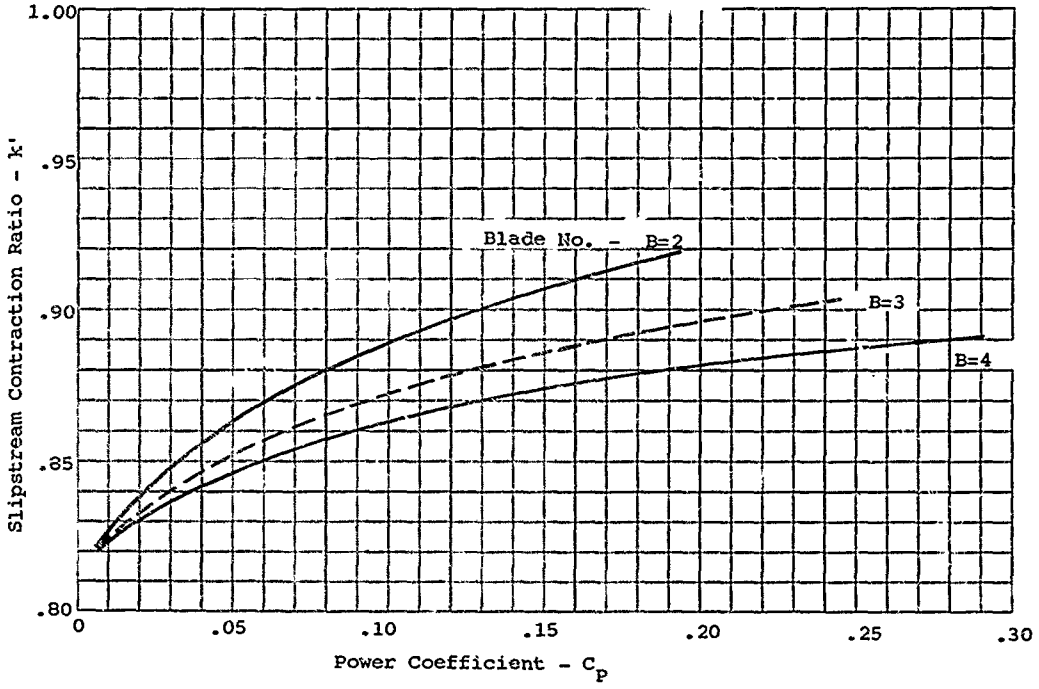


Figure 65. Propeller Slipstream Contraction Coefficient - k'
Velocity = 0.

for finding the optimum performance at the static condition.

Basis for Calculating Induced Velocity V = 0

As previously stated, the induced velocity at the flight conditions is found with satisfactory accuracy based on the assumption that optimum load distribution for the entire blade determined the induced velocity at the station of interest, rather than actual load distribution. Since procedures of first assuming the load distribution, calculating the induced velocity based on that distribution, and then iterating with a new distribution have not given satisfactory results for the static condition, the assumption of optimum load distribution is also assumed to apply for the static condition for calculating the induced losses.

The accuracy of the assumption of the optimum load distribution improves as the Figure of Merit approaches a peak as, of course, this is the load distribution required for peak performance. As noted previously, Theodorsen proved that the wake must be rigid when the load distribution is an optimum. Based on the rigid wake concept, the necessary data for calculating the induced velocity at any radius in the final wake is available by using the values of K(x) at the proper wake angle.

If the slipstream contraction is zero or small, it would be possible to convert the induced velocity in the final wake to the propeller disc with good accuracy. However, when the propeller is operating at the static condition, the contraction is large and takes place close to the propeller disc. As a result of this contraction, the induced velocity on the outboard station will be different from that found in the wake, and converted back to a similar station at the propeller by the continuity equation. In fact, since the outboard section of the blade is outside the diameter of much of the wake, the velocity will be different than if it were all within the wake. The magnitude of this change is not known, but could be found with further research.

Until this additional research is accomplished, it will be necessary to assume that the velocity at the same fractional radius in the final wake corrected to the propeller disc using the continuity equation is the inflow velocity. When the continuity equation is used to find the velocity at the propeller disc, the contraction ratio found from Figure 65 is used. This contraction ratio is a function of the power coefficient.

## Equations for Strip Analysis - V=0 - Single-Rotation Propellers

As in the case of a propeller operating at a forward velocity, the thrust and power may be found by strip analysis procedure by determining the differential forces at each blade station and then integrating to find the total. When the free-stream velocity is zero, the equations developed previously for finding the thrust and torque coefficient must be modified to eliminate J. From Figure 66,

$$\left(\frac{W}{nD}\right)^2 = \frac{(x\pi nD)^2 \cos^2\phi}{(nD)^2} = (x\pi)^2\cos^2\phi \qquad (109)$$

Thus, Equations (46) and (50) become, for the case V = 0,

$$\frac{dC_Q}{dx} = \sigma C_L \frac{x^4 \pi^3}{8} \cos^2\phi \ (\sin\phi + \tan\gamma \cos\phi) \qquad (110)$$

and

$$\frac{dC_T}{dx} = \sigma C_L \frac{(x\pi)^3}{4} \cos^2\phi \ (\cos\phi - \tan\gamma \sin\phi) \qquad (111)$$

To solve Equations (110) and (111), it is necessary to determine the operating lift coefficient and wind angle $\phi$. The procedure considered to be the best at this time for solving for the operating lift coefficient is the use of the Theodorsen circulation function K(x) (Figures 8 to 12) to calculate the displacement velocity in the final wake, and the use of the proper contraction ratio (Figure 64) for correcting the final wake velocity to the propeller. Although the procedure will be somewhat inaccurate, it should give a better estimate of the performance than is now possible.

Thus, for the static condition $w = 2\pi n$ and V=0, we get from Equation 35

$$\Gamma = \frac{w_w^2 K(x)}{Bn} \qquad (112)$$

$$\frac{dT}{dr} = \rho W \Gamma = \frac{C_L W^2 b}{2} \qquad (113)$$

$$\Gamma = \frac{C_L}{2} Wb = \frac{w_w^2 K(x)}{Bn} \qquad (114)$$

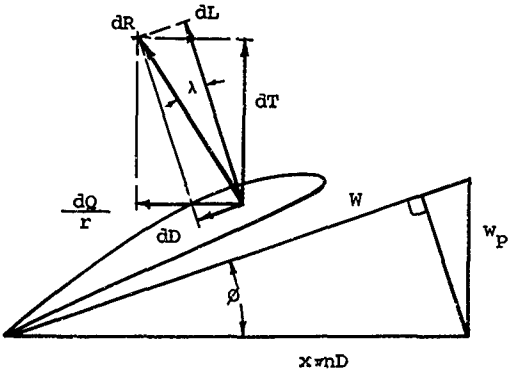


Figure 66. Velocity and Force Diagram, V = 0, Static Condition.

From Reference 19, the displacement velocity at the propeller, $w_p$, is

$$w_p = w_w \left( \frac{\epsilon}{\epsilon + k/2} \right) \tag{115}$$

where $\epsilon$ = the energy function
$k$ = mass coefficient
$w_w$ = the displacement velocity in final wake

Substituting in Equation (114) and rearranging,

$$\sigma C_L = \frac{2 w_p^2 K(x)}{W \pi n D x} \left( \frac{\epsilon + k/2}{\epsilon} \right)^2 \tag{116}$$

which becomes, using the angular relationships of Figure 66,

$$\sigma C_L = \frac{2K(x) \tan \phi \, w_p}{W} \left( \frac{\epsilon + k/2}{\epsilon} \right)^2 \tag{117}$$

Since $\beta = \alpha - \phi$, the lift coefficient that satisfies Equation (117) and the two-dimensional airfoil data can be found.

With the known operating lift coefficient, the torque and thrust coefficients are obtained from Equations (110) and (111), and the results are integrated as described by Equation (61). When finding the performance as described above, the power as calculated from the assumed blade angle setting must agree with the given power within ±3%; otherwise, a new setting must be assumed until agreement is obtained. A step-by-step procedure for calculating the performance using the equations developed above is given in Tables III and IV.

## TWO-DIMENSIONAL AIRFOIL SECTION DATA

Many different types of airfoil sections have been used for propellers. Some of the early propellers used RAF-6 sections, Clark Y, and double cambered Clark Y sections. Propellers using these sections have good operating characteristics, especially for low-speed type airplanes. In fact, some general aviation propellers still use blades which have the older type sections.

Modern propellers are designed using NACA 16 or NACA 6 series airfoil sections. The NACA 16 series sections were specifically designed for propellers. These sections have a flat pressure distribution chosen to delay the onset of shock waves and thus operate at high Mach numbers without encountering the compressibility drag rise. The small leading-edge radius, along with the flat pressure loading used on NACA 16 series sections, gives high values of lift/drag ratios when the sections are operating at low angles of attack. However, at high angles of attack, the small leading-edge radius tends to induce separation which reduces the lift/drag ratio. This causes a reduction in efficiency when the propeller is operating at conditions where the section angle of attack is high, such as at takeoff and climb conditions.

To improve the efficiency at climb and cruise, the NACA 6 series sections have been used for propeller blade sections. One of the early tests of a propeller equipped with identical blades except for airfoil section showed a marked improvement in the takeoff and climb performance when using the blades with NACA 6 series sections, thus proving the advantages of these sections. Unfortunately, the NACA 6 sections do not have as high a critical Mach number as the NACA 16 series, and for this reason propellers designed to operate at high speeds generally will require the use of a combination of sections; outboard where high values of Mach number are encountered, NACA 16 series sections are used, and inboard where high values of angle of attack are obtained, NACA 6 series are used.

### Data for Propeller Strip Analysis Calculation

To calculate the performance of propellers by the procedure of strip analysis, accurate two-dimensional airfoil data are required. Lift, drag and moment coefficients are needed covering a wide range of airfoil parameters such as thickness ratio, camber and section type. The data should cover section Mach numbers to at least 1.2, Reynolds numbers in the range of $2 \times 10^5$ to $9 \times 10^6$, and an angle of attack range of $-4^\circ$ to above the stall angle. The range of thickness ratio required runs from 4% to 21% for normal airfoil sections covering the full range of Mach numbers. Propeller blades also use thick

airfoils at the blade root, and for this reason data are needed for analysis of these airfoils at thickness ratios of 25 to 100%.

Because of the diverse requirements of propellers and range of operation, airfoils with different characteristics are needed. The design requirements can be satisfied by the proper selection of the type of airfoil and design lift coefficient. Generally, for propellers the section data at design lift coefficient from 0 to .7 will meet all the design requirements and cover the range of design experience. Propellers with design $C_L$ above 1.0 may be feasible, but the data is not available for proper evaluation and application.

As many different airfoil sections will be used on a propeller blade, it is important to have accurate and consistent data. Changes in airfoil design parameters should be properly reflected by the data so that modifications and differences between propellers will be properly evaluated. It would also be highly desirable to have the airfoils tested in the same wind tunnel under nearly identical conditions to eliminate problems due to differences in tunnels and to maintain consistency. Unfortunately, with the large amount of data required, this is not possible, and it has been necessary to use data from a number of different sources. All the available airfoil data was used for development of the necessary data for propellers, including that from government, private and foreign sources.

Because of the unknown effects due to centrifugal force or the boundary layer influencing critical Mach number, other separation problems, tip effects, and other installation problems, the airfoil data developed must be checked by calculating the performance and comparing the results with wind tunnel data. Modification must be made to the airfoil data until agreement is obtained with test data before it can be used for analysis. This is especially necessary when the data is to be used for high-speed propellers where the tip and Mach number variation may influence the drag rise due to compressibility. The airfoil data presented in this section has been checked and reformulated so that it is suitable for propeller design purposes.

The airfoil data developed for propeller strip analysis calculations was developed from a compilation of all the data available at the time. This was done during the early 1950's, and the effort was somewhat handicapped by the lack of data throughout the transonic Mach number region. This, however, will not present a serious problem unless the propeller is designed to operate at speeds in excess of a Mach number of 0.75. At speeds below this, the data as applied to strip analysis calculations appears to have sufficient accuracy for the airfoil sections considered. The procedures for developing the basic airfoil data and corrections are presented in the following

paragraphs.

The airfoil data compiled and checked for use in strip analysis calculations consists of a basic set of data for NACA 16 series sections covering a range of Mach numbers from 0.3 to 1.6. The data covers airfoil sections with thickness ratios of 4% to 21% and design lift coefficients 0 to .7. For the range of angle of attack covered, the lift and drag coefficients are assumed to be independent of Reynolds number. These basic data are presented in Appendix II of Volume III, Figures 67 to 166, in the form of plots of lift and drag coefficient as a function of Mach number for a range of values of angle of attack.

For the range of thickness above 21%, four-digit airfoil data in terms of lift and drag coefficients were compiled for strip analysis calculations for sections of suitable operating characteristics. These data are compiled as a function of Reynolds number, as this is the major parameter influencing the performance of the thicker airfoil sections. When the thickness ratio is above 25%, the available data indicates that high-camber airfoils have poor lift/drag characteristics with early flow separation. NACA 16 series airfoils also have undesirable characteristics, when operating at the higher thickness ratios, due to aft position of maximum thickness. For these reasons, the basic data for the thick airfoils strip analysis was developed for NACA four-digit series and elliptical sections. To determine the performance of the thicker airfoils at Mach numbers above the critical, corrections to the low-speed data were developed. These corrections were developed from test data and apply to all sections above a thickness ratio of 25%. The airfoil data for determining the performance of thick sections is also given on Figures 167 to 179, Appendix II, Volume III.

For the case where airfoils are operating above the stall angle, corrections to the basic data of Appendix II, Volume III, have been developed to determine the required variation of the lift and drag coefficients at high angles. These corrections were developed to be used only for sections operating on a propeller blade, as the lift coefficients under these dynamic conditions are much higher than would be estimated from two-dimensional airfoil data. The data also accounts for the difference in performance between NACA 16 and NACA 65 series sections. These corrections are presented in Appendix II, Volume III, Figures 179 to 196.

Data Correlation - Subsonic Range

In the subsonic range there is a large amount of wind tunnel airfoil data available which is suitable for propeller analysis. However, even with the large amount of testing that has been done in the subsonic range, a number of airfoils that are

needed for propeller analysis were not covered. Table II was prepared to show the range of available data for NACA 16 airfoils. From this table it will be noted that the most important omission of the test data for the NACA 16 airfoil sections is that for thickness ratios of 4%.

In Table II it will also be noted that there are several NACA 16 series airfoils for which there is duplicate test data. The reason for this duplication is that the original test data reported in Reference 20 was found to be in error. The error in the test data presented in Reference 20 was caused by end leakage at the junction of the airfoil and the tunnel wall. To correct the drag coefficient data for this end leakage effect required the development of a correction that accounted for the Mach number, the lift coefficient and thickness ratio. These corrections were determined in Reference 21 and have been used to correct all the data reported. Only the corrected data of Reference 21 was used for developing the data for strip analysis calculations.

To determine the performance of the NACA 16 series airfoils where data is lacking as shown in Table II, NACA 66 series are used, as these sections have a similar thickness distribution and the same mean camber line as the NACA 16 series, Reference 22. The airfoil data for the NACA 66 sections, References 22 to 27, were used where NACA 16 series data was lacking. Where both NACA 16 series and NACA 66 series data was lacking, NACA 65 or NACA 64 series data was used as a guide, References 22 to 27. Sufficient data is available so that cross plots can be made to fill in the gaps in the test data for NACA 16 sections. It is also seen that in most cases it was not necessary to extend the cross plots beyond the experimental data except in the case of the 4% thickness sections. To find the characteristics of the airfoils which were not tested and to fair out as many test differences as possible that exist in the data, cross plots of the lift and drag coefficients were made at constant values of free-stream Mach number.

The following cross plots of the available airfoil data were made:

1. $C_L$ vs. $C_{Li}$ for lines of constant angle of attack. These plots were made for the range of thickness ratios at M = .3, .45 and .6.

2. $C_L$ vs. h/b for lines of constant angle of attack. These plots were made for the range of design $C_L$'s at M = .3, .45 and .6.

3. $C_D$ vs. $C_{Li}$ for lines of constant values of operating $C_L$; plots were made for the range of thickness ratios

TABLE II. SUMMARY OF AIRFOIL DATA, NACA-16 SECTIONS

| Design $C_L$ | 0 | .1 | .2 | .3 | .4 | .5 | .6 | .7 | 1.0 |
|---|---|---|---|---|---|---|---|---|---|
| h/b | | | | | | | | | |
| .04 | | | | | | | | | |
| .06 | | L, S | | L | | L, S | | | |
| .09 | L, S | L, S | L, S | L | L | L, S | | L, S | L, S |
| .12 | | | | L | | L, S | | L | L |
| .15 | | L | L | L | | L | | L | |
| .18 | | | | | | | | | |
| .21 | | | | L | | L, S | | | |
| .24 | | | | | | | | | |
| .27 | | | | | | | | | |
| .30 | | L | | | | L, S | | | |

NOTE: The peak test Mach number is approximately 0.8
L - Test data from Reference 21
S - Test data from Reference 20

at M = .3, .45, and .6.

4. $C_D$ vs. h/b for lines of constant values of operating $C_L$; plots were made for the range of design $C_L$'s at M = .3, .45 and .6.

The data faired from the cross plots described above established the basic ariation in the subsonic range of the lift and drag coefficients for the desired range of airfoils. The end of the subsonic range is determined by the lift and drag divergence Mach numbers. Thus the subsonic trends established are valid only up to these Mach numbers.

Lift and Drag Divergence Mach Numbers

Theoretically, the end of the subsonic range can be considered to occur at that free-stream Mach number where the local Mach number at any point on the airfoil is equal to one. This point is defined as the critical Mach number $M_{cr}$. The critical Mach number of the section is very difficult to determine based on the lift and drag characteristics of the airfoil, as there is no apparent change in characteristics which occur exactly at that Mach number. Thus, it has been necessary to define a free-stream Mach number where a change of the lift and drag coefficients does occur to denote the transition from subsonic to transonic flow. The Mach number at which an inflection point occurs in the lift coefficient vs. Mach number curve for lines of constant angle of attack is defined as the lift divergence Mach number ($M_{C_L}$). The drag divergence Mach number ($M_{C_D}$) is taken as that Mach number where the slope of a curve of $C_D$ vs. Mach number of a line of constant operating lift coefficient is equal to 0.1, i.e., $dC_D/dM = 0.1$.

At the time the airfoil data was formulated, problems were being encountered in measuring the lift and drag coefficients at high Mach numbers due to tunnel blockage. When airfoils were tested in closed-throat wind tunnels at high Mach numbers, blockage was obtained after the critical Mach number was reached. This blockage results in inaccuracies in the data, especially with regard to the lift and drag divergent Mach numbers. For this reason, the lift and drag divergent Mach numbers could not be found directly from the experimental airfoil data.

After the critical Mach number is exceeded on an airfoil section, a normal shock wave is formed which increases in strength with increasing Mach number. When the shock wave has sufficient strength, the lift and drag are influenced and the corresponding Mach number is the lift and drag divergent number. Since the lift and drag divergent Mach numbers occur at an increment above the theoretical critical, this parameter can be used as a guide to establish the Mach number for the lift and

drag divergence.

To establish the lift and drag divergent Mach numbers for all the airfoil sections considered, the theoretical critical value was therefore established using the method outlined in Reference 22. Then the increment in Mach number above the peak critical value was established using the experimental data given in References 23, 24 and 28. An example is shown on Figure 67 as a comparison of the critical Mach number along with the lift and drag divergent Mach numbers established using the available experimental data.

From Figure 67 it will be noted that the range of lift coefficients before the lift and drag divergent Mach numbers rapidly decreases and is much higher than predicted based on the theoretical critical Mach number. Therefore, the critical Mach number as determined by theory is a poor measure of the end of the subsonic range, and test data are required to find the lift and drag divergent Mach numbers. It should be noted that today, with the availability of transonic wind tunnels, it is possible to determine exactly the lift and drag divergent numbers by test with good accuracy.

The subsonic values of $C_L$ and $C_D$ obtained from the cross plots were plotted vs. Mach number. When this was done, some of the differences between the plots at constant values of Mach number were faired out.

The variation of available $C_L$ and $C_D$ data up to the Mach number for lift and drag divergence was plotted as a function of Mach number. Where lift coefficient data as a function of Mach number was lacking, the Kármán-Tsien equation developed in Reference 29 was used to extend the low-speed $C_L$ data up to the lift divergence point. This equation may be written in the form

$$C_{L_M} = \frac{C_{L_O}}{\sqrt{1 - M^2} + C_{L_O} M^2 / \left[1 - \sqrt{1 - M^2}\right]^2} \qquad (118)$$

where $C_{L_O}$ = the low-speed lift coefficient
$C_{L_M}$ = the lift coefficient at Mach number equal to M

Equation (118) was used to determine the variation of the lift coefficient with changes in Mach number rather than the Prandtl-Glauert equation, as a better fit was obtained with the existing experimental data than with the P - G equation, which is

$$C_{L_M} = \frac{C_{L_O}}{\sqrt{1 - M^2}} \qquad (119)$$

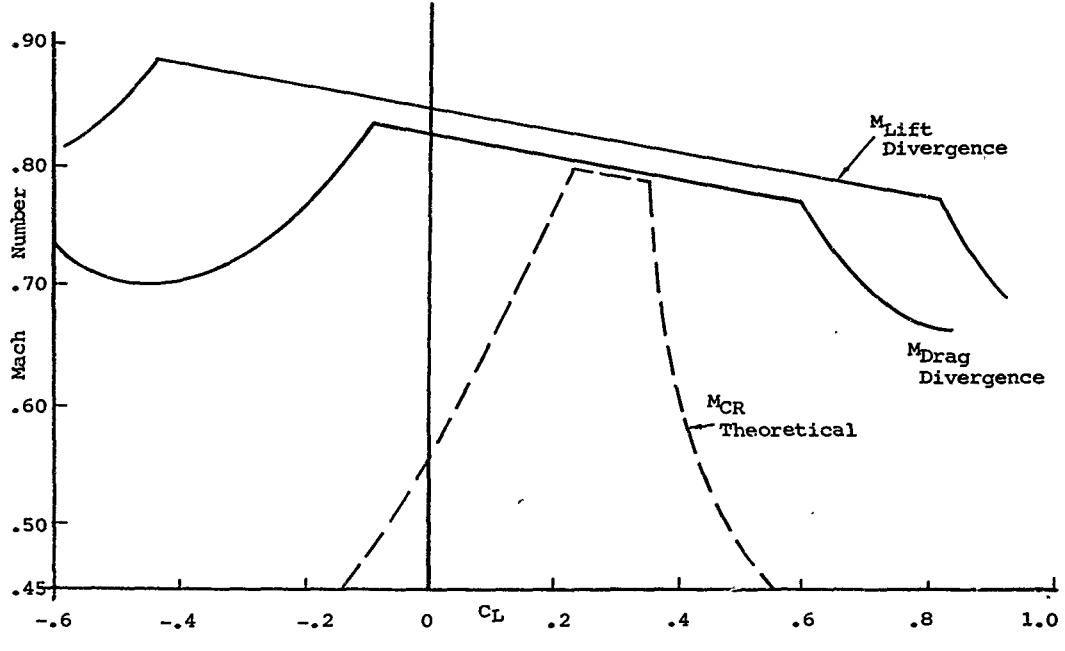


Figure 67. Comparison of $M_{CR}$ With Lift and Drag Divergence, NACA 16-206 Section.

Equation (118) was developed for the pressure coefficient $C_p$ on the airfoil, but can be used in the form given above as $C_L$ is integrated value of $C_p$. Thus, if the low-speed value of $C_L$ is known, it is possible to extend the $C_L$ vs Mach number curve for a constant angle of attack up to the lift divergence Mach number. As Equation (118) was developed using the linearized theory, its accuracy for thick airfoils operating at high angles of attack may be questionable. It was found, however, that for the majority of cases where $C_L$ data was available, the agreement is excellent. When using Equation (118) for extending the $C_L$ vs Mach number data, it must be realized that this equation does not apply after the critical Mach number of the section has been exceeded.

The subsonic values of $C_D$ obtained from the cross plots were replotted vs Mach number for lines of constant values of operating lift coefficient for all the airfoils listed and in Figures 84 to 133 in Volume III. The available $C_D$ data at Mach numbers above .6 was also used. It was noted from Figures 84 to 133 (Volume III) that as the Mach number increased, there was usually a small reduction of $C_D$ for those values of operating $C_L$ close to the design $C_L$ of the airfoil before the point for drag divergence was reached. This reduction of the drag coefficient with increasing Mach number has been explained in a number of reports (see, for instance, Reference 21) and is caused by a delay of the point of separation on the airfoil which results in a reduction of the profile drag. The point of separation is delayed by the increase of speed over the airfoil as the Mach number is increased. The above effect may occur at other operating lift coefficients than those near the design lift coefficient. However, the magnitude of the reduction is generally not quite as large.

For those airfoils which have not been tested, it was necessary to extrapolate the values of $C_D$ obtained from the cross plots to the drag divergence Mach number. This was done following the trends shown by the test data. As in most cases, the change of drag coefficient with increasing Mach number is small and the error involved in the above extrapolation is small. Furthermore, the drag divergence Mach number approaches .6 as h/b and $C_{Li}$ increases; thus the length of the extrapolation becomes progressively smaller.

Data Correlation - Supersonic Range

To establish lift and drag coefficient data at section Mach numbers above the critical, the transonic range, the performance of the airfoils was first found for the supersonic range. This was done by assuring that NACA 16 series airfoils had essentially the same lift/drag characteristic as circular arc sections. The lift and drag of these sections were then

calculated as a function of Mach number using the Ackeret method (Reference 30) and the method developed by the NACA (Reference 31). These methods are based on the theory of small disturbances and determine the lift and pressure drag.

The friction drag in the supersonic range was assumed to be constant and equal to .008 and added to the calculated pressure drag. Although the friction drag is a function of Reynolds number, the value of .008 is an average value, and is of sufficient accuracy in view of the high level of the overall drag in the range. The results of these calculations are given on Figures 84 to 133 in Appendix II, Volume III.

Data Correlation - Transonic Range

At the time of the development of the airfoil data, little experimental or theoretical data was available for estimating the performance of airfoils operating in the transonic range. Most of the wind tunnels were limited by blocking, as the porous or slotted walls had not been developed. The only data, therefore, for estimating the performance of airfoils in the transonic region was that from drop and bump tests. These data were three dimensional in nature and severely limited in scope.

Because of the lack of airfoil data in the transonic range, a considerable number of propeller tests were run by the NACA. These data included force test and pressure distribution measurements on rotating propeller sections. With these test data, it was possible to check by strip analysis the airfoil data extrapolations in the transonic range. Before these checks could be accomplished, however, it was necessary to develop consistent procedures for extrapolating the airfoil data from the Mach numbers for the critical lift and drag divergence to the supersonic condition.

The procedure used to develop consistent extrapolation throughout the transonic depended on locating the maximum and minimum lift coefficients for a given angle of attack as a function of thickness ratio, design $C_L$, and Mach number. These points were estimated from the available drop and bump test data.

The extrapolation of the drag coefficient in the transonic range was based on determining the peak and its location with respect to Mach number. From this point it was relatively easy to extrapolate from the drag divergence Mach number to the supersonic case.

After the lift and drag coefficients were established in the transonic range, the data was checked by many calculations of the performance of propellers and comparisons with wind tunnel test data. Based on the checks, the airfoil data was modified

to improve the accuracy. This process was carried out until satisfactory agreement was obtained.

As it is now possible to test airfoils throughout the transonic range, the procedure described above would not have to be used again to develop the necessary data.

As shown in the section Accuracy of Calculation, the performance of propellers can be calculated with good accuracy when operating in this range, considering the methods that had to be used to establish the basic data. If the performance of propellers becomes important when the sections are operating above the critical, it would be desirable to modernize the data in the transonic range to improve the accuracy of predicting performance and designing new propellers.

The airfoil data developed for propeller strip analysis calculations as described above for NACA 16 series sections is given on Figures 34 to 133 in Volume III. These data are of sufficient scope for most strip analysis calculations at the normal flight conditions, and thus serve as the base data. However, when the propeller is operating at high lift coefficients and section angles of attack above the stall, additional airfoil data is required.

In the development of the base airfoil data for NACA 16 series sections, data of NACA 6 series sections were used where NACA 16 series data was not available. The NACA 6X series data used was the data with the most rearward peak pressure point available. A comparison of the data, when operating at conditions below the maximum lift coefficient, and the lift and drag divergence Mach numbers indicates there are no important differences. Therefore, at these conditions, that data in Appendix II, Volume III, can be used for NACA 16, 66, 65 or 64 series airfoils.

The critical Mach number of NACA 6 series sections is below that for the NACA 16 series sections. Therefore, the data in Appendix II, Volume III, should be adjusted for the 6 series sections when operating above the critical Mach number.

Data at High Angles of Attack

When the propeller is operating at high blade loadings, airfoil data are required to find the section characteristics at high angles of attack, including angles well above the stall. Data are also needed to find the lift/drag characteristics of NACA 6 series airfoils as well as NACA 16 series. These data are required especially when evaluating propellers operating at the condition of zero advance or when operating at high section angles of attack.

To determine the performance of airfoils operating at high angles of attack, including those angles up to and beyond the stall, it is necessary to establish the stall angle and the associated value of $C_{L\ max}$. Airfoils operating in straight rectangular flow develop flow separation after $C_{L\ max}$, which causes a loss of lift as the angle of attack is increased. This causes a reduction of lift, the magnitude of which depends on the leading-edge radius, the thickness ratio, and the section type.

The application of uncorrected two-dimensional airfoil data to propellers operating at high section angles of attack indicated that the reduction of $C_L$ above $C_{L\ max}$ as measured in the wind tunnel is not obtained. Due to the lack of a suitable theory for calculating the inflow velocity, it is not known exactly how the lift varies above the stall angle. However, based on the work done in reducing the propeller test data, it is apparent that the lift of sections on a propeller operating above the stall is considerably above that measured on two-dimensional airfoils.

When the airfoil is operating on the propeller blade, the tendency of the flow to separate appears to be reduced by the centrifugal flow field. As the air tends to separate in the boundary layer, it is energized by the centrifugal field, thus reducing separation and allowing the airfoil to maintain lift. This reduced tendency for the flow to separate results in an increase in $C_{L\ max}$ for sections operating on a propeller compared with that measured in two-dimensional flow.

The variation of lift above the stall angle was estimated for propeller sections from whirl test data. This was done by calculating the lift and drag coefficients necessary to satisfy the propeller test data for only those sections operating above the two-dimensional stall angle. These values of $C_L$ and $C_D$ above the stall angle were calculated by a step-by-step procedure, as only part of the blade will operate above the stall angle with a small increase in blade angle. The induced angle of attack was calculated using a modified Theodorsen theory.

It was found that the variation of the lift coefficient with angle of attack above the stall as determined by this method depends only on the actual two-dimensional $C_{L\ max}$ of the section; see Figure 154, Volume III . From this figure it will be noted that the lift continues to increase when operating above the stall until a new maximum value is obtained, after which it remains essentially constant with increasing angle of attack.

The airfoil data obtained from the reduction of the propeller test data as described above has been formulated into a series

of plots so that, with the data of Appendix II, Volume III, as a base, the performance of any section can be found at high angles of attack above the stall. The procedure and data for finding the lift and drag coefficients of propeller airfoil sections operating at angles above the stall are also given in Appendix II, Volume III. It should be noted that these data also allow the characteristics of NACA 65 and 66 airfoils to be found at high angles as well as those of NACA 16 series sections.

Performance of Thick Airfoils

For structural reasons, blade thickness ratios in excess of 21% are often found on the inboard blade sections. If neither a spinner nor a blade fairing is used, thickness ratios approaching 1.0 can be encountered. Thus airfoil data at thickness in excess of 21% are required to calculate the characteristics of these sections.

The aerodynamic properties of sections having thickness ratios in the range of .25 to 1.0 depend mainly on the thickness ratio and such parameters as maximum thickness location, maximum camber location, and leading-edge radius. In addition, Reynolds number and Mach number influence the performance. In the case of thick airfoils, no systematic set of data has been developed; therefore, it was necessary to review and average the available data to develop consistent trends suitable for propeller calculations.

Originally the airfoil data developed for thick sections was set up to account for a number of different parameters including a large range of Reynolds number. At the time the work was done, it was considered necessary to cover the entire range, as propellers were operating in front of large reciprocating engines with thick airfoil sections used quite far outboard. Today propellers would be designed with thinner inboard sections to prevent large losses in ram recovery when operating on turboprop engines. Further, any thick sections would be used farther inboard, where the drag losses would have a small

overall effect on the performance.

For these reasons and the questionable accuracy of some of the corrections developed, the thick airfoil data presentation has been simplified where possible. These simplifications were made in the area of the effects of Reynolds number on the lift and drag coefficients when operating at angles of attack above zero. The corrections for angle of attack were set up for the range of Reynolds number normally associated with propellers, and no loss of accuracy of the results is anticipated.

Tables II and III in Volume III illustrate the methods for determining the lift and drag coefficients of thick airfoils. The necessary curves for the calculations shown are presented in Volume III, Figures 134 to 145.

When using Tables II and III of Volume III to find the lift and drag coefficients, the data for the symmetrical airfoils are used as a base. These data were set up for symmetrical NACA 00xx-63 sections. Corrections to the data are used to determine the performance of the cambered and elliptic sections. It should be noted that the camber is expressed in percentage of the total section chord.

Trailing-Edge Extension

Due to the high cost of developing a hollow steel propeller blade, trailing-edge strips were added when it became desirable to increase blade activity factor. It was found feasible to add a trailing-edge strip up to 20% of the original airfoil chord.

To find the performance of airfoils so modified, Theodorsen and Stickle, Reference 32, developed theoretical charts for determining the change of design $C_L$ and angle of attack as a function of the trailing-edge strip angle.

Generally when trailing-edge strips are added to a blade, it is necessary to maintain the design $C_L$ of the section. To maintain the design $C_L$ of a section, the tailing-edge strip is applied to the airfoil at the angle shown in Figure 68. With the trailing-edge strip extension added to the airfoil at the angle indicated, the angle of zero lift decreases. Thus, to obtain the same lift coefficient as determined from the two-dimensional airfoil data, it is necessary to increase the angle of attack by the increment shown on Figure 69. This angle-of-attack increase is applied as a blade angle correction. Also, when the trailing-edge strip is applied to the propeller blade at the angles shown in Figure 68, two-dimensional airfoil data may be used to calculate the performance if the change in angle of attack shown on Figure 69 is used to correct the apparent blade angle.

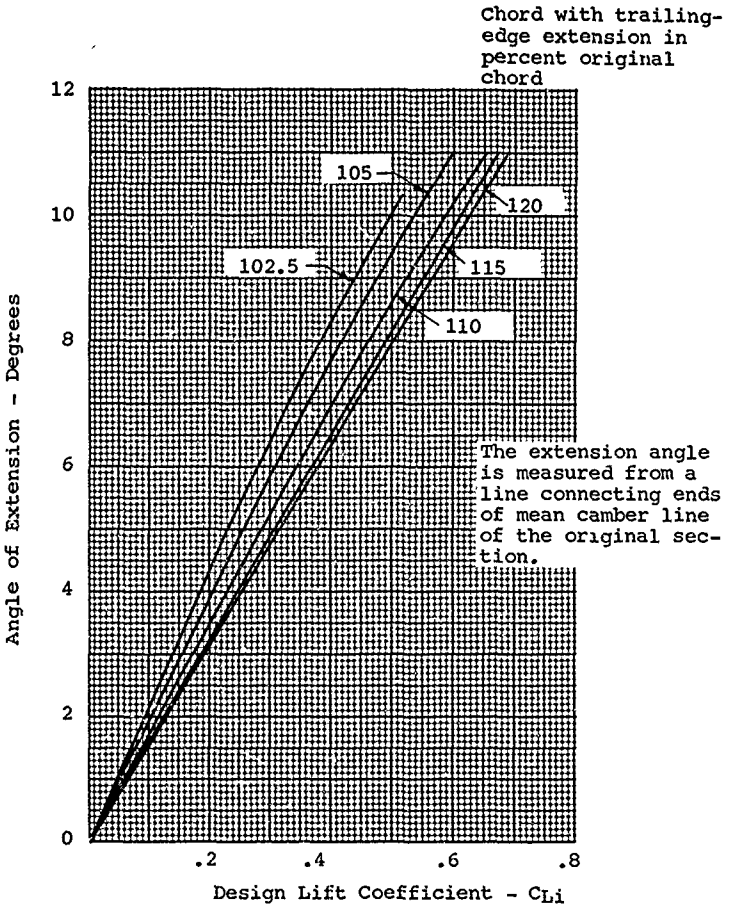


Figure 68. Angle of Extension vs. Design $C_L$
NACA 16 Section.

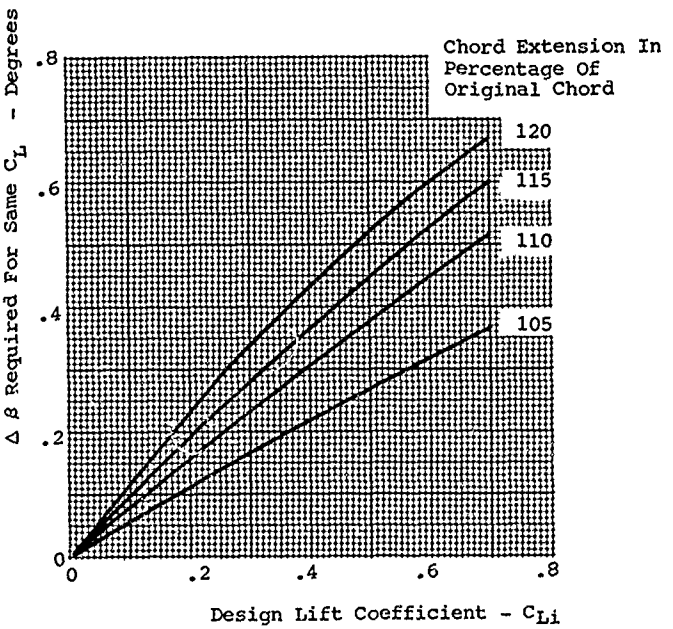


Figure 69. Change in Blade Angle due to Addition of Trailing-Edge Strip.

Propellers built using trailing-edge strip have developed high levels of efficiency at both the takeoff and cruise conditions. In fact, early tests of the trailing-edge blades indicated a higher level of takeoff performance than would have been expected, based on the increase of solidity alone. An analysis of the airfoil showed that NACA 16 series sections with trailing-edge strips were very much like NACA 65 series sections. Thus the trailing-edge strip can be added to blades without losses in performance due to compromises in the section.

Airfoil Moment Data

When calculating the power requirements for the blade pitch change mechanism, accurate data is required. The torque required for changing the blade angle is the sum of the aerodynamic moment produced by the blade sections and the blade centrifugal twisting moment. As the blade centrifugal twisting moment due to mass can be calculated with good accuracy, it is necessary to develop the data for finding the aerodynamic moment. The position of the center of lift and hence the aerodynamic twisting moment is dependent on the airfoil load distribution. At low and moderate angles of attack, the two-dimensional airfoil data appears to give good results when used to calculate the aerodynamic moment. However, when operating at high lift coefficients, the aerodynamic twisting moment calculated for a propeller blade using two-dimensional airfoil data does not agree with test data.

As was previously noted when operating at high powers, the blade sections stall at a higher angle than would be expected from two-dimensional airfoil data. This change in stall angle and level of $C_L$ apparently changes the moment coefficient from that measured in two-dimensional flow, probably due to centrifugal boundary layer effects.

To find the center of pressure of NACA 16 series airfoils under actual operating condition, the pressure distribution data was obtained on rotating blade sections of operating propellers, References 33 to 38. Blades of five designs using NACA 16 series airfoils were used, and measurements were made at nine radial stations so that a useful range of section thickness ratio and design lift coefficients was evaluated. The data covered a large range of operating lift coefficients and Mach numbers.

The pressure distribution data was integrated at each station and condition, and the results were presented in the form of normal force coefficient, $C_n$, and moment coefficient at the quarter chord, $C_{mc/4}$. From these coefficients the location of the center of pressure in terms of percent chord was determined, and results were plotted as functions of operating $C_L$ in Figures 70

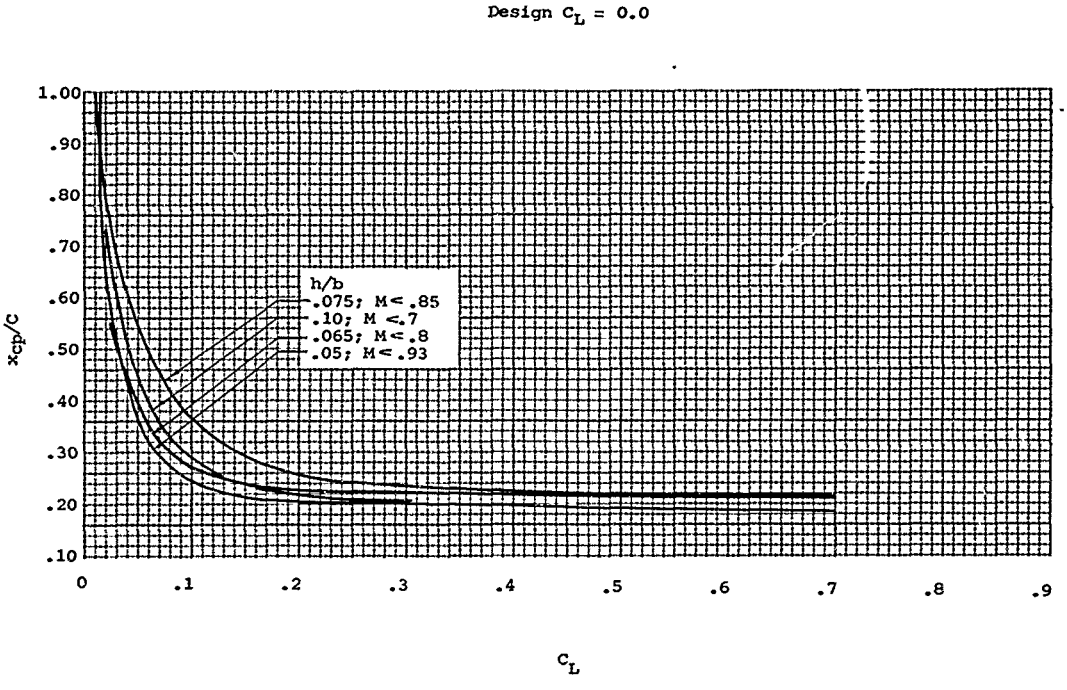


Figure 70. Airfoil Center of Pressure Location, NACA 16 Sections $C_{Li}$ = 0.0.

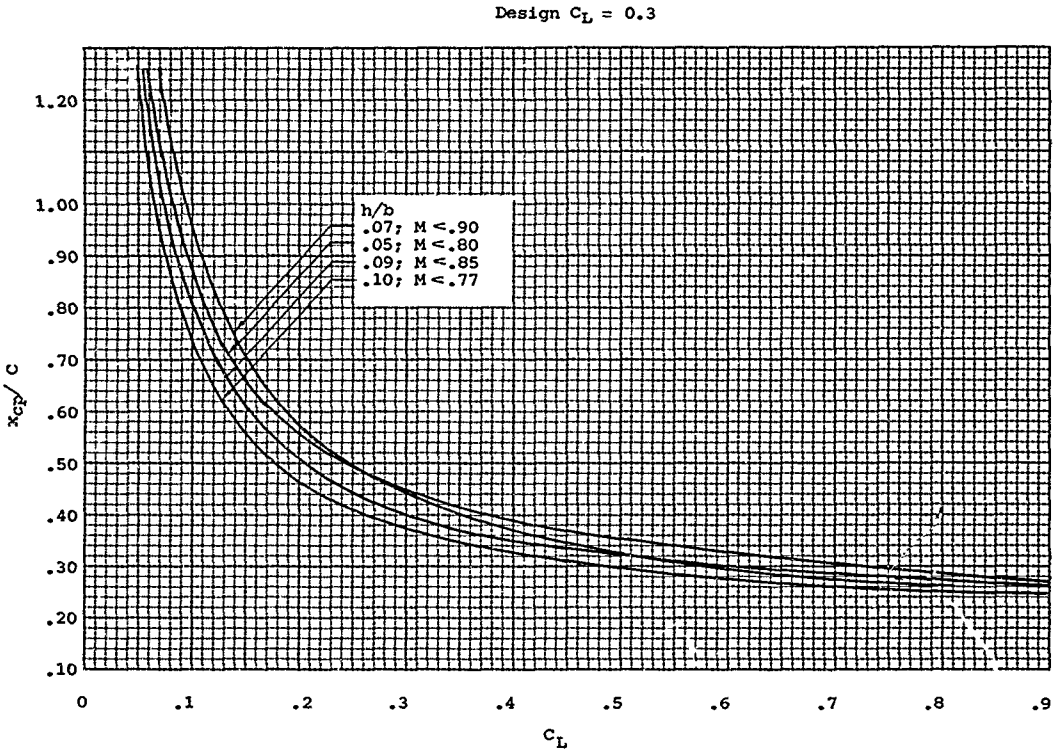


Figure 71. Airfoil Center of Pressure Location, NACA 16 Sections $C_{L1}$ = 0.3.

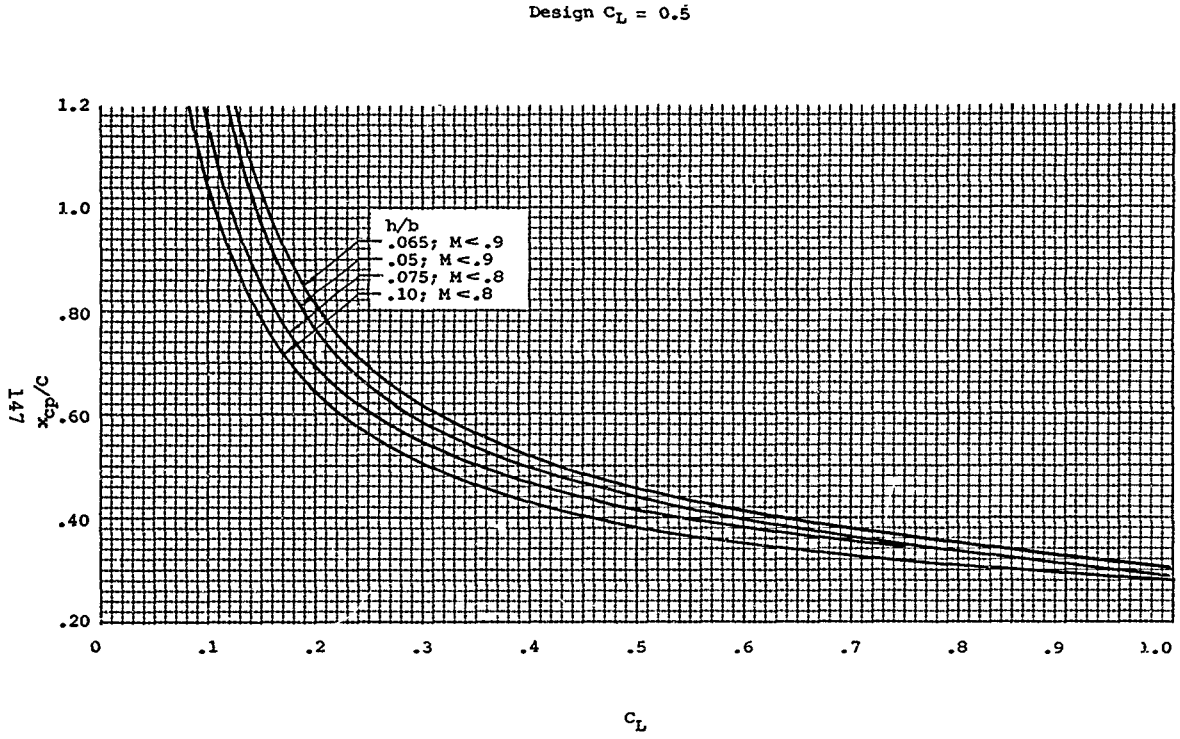


Figure 72. Airfoil Center of Pressure Location, NACA 16 Sections $C_{Li}$ = 0.5.

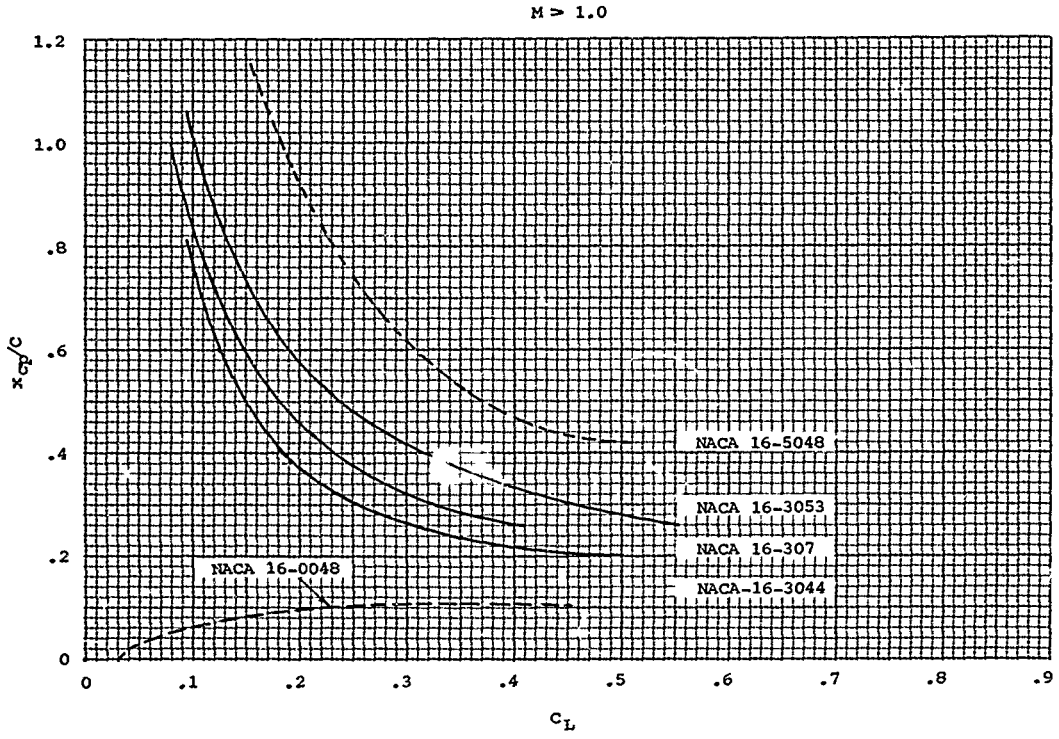


Figure 73. Airfoil Center of Pressure Location NACA 16 Sections Effect of Thickness Ratio.

to 73 . Although the inflow angle was not known exactly, the error of assuming $C_n = C_L$ is small at the low angles of attack of these tests. The data given on Figures 70 to 73 allows the center of lift to be found as a function of h/b and design $C_L$ up to the Mach number for lift divergence.

When the Mach number approaches and exceeds that for lift divergence, a normal shock is formed on the upper surface of the airfoil. Under these conditions the flow is not steady, and difficulty was encountered in establishing the location of the center of pressure. The available data indicates that the center of pressure moves after the lift divergence Mach number is exceeded. Further data are needed to confirm this.

## PROPELLER PERFORMANCE CALCULATION PROCEDURES

### Introduction

The performance of a propeller must be predicted over a wide range of operating conditions to evaluate its suitability in any given installation. The range of operation must include the velocity range from zero to the maximum dive speed of the airplane as well as off-design conditions, including negative thrust operating conditions. It is also necessary to be able to predict the performance at the feather condition and, in the case of a V/STOL airplane, at conditions involving high shaft angles of attack.

The performance must be predicted at any of the above conditions for any combination of propeller geometry. For instance, it must be possible to predict the performance of propellers with two to twelve or more blades and single or dual rotation. Blades differing in solidity, camber, blade angle, and thickness ratio have to be evaluated to find the best propeller for a given installation. Further, methods must be available to establish the optimum distribution of these parameters as a function of blade radius for a given operating condition.

Suitable calculation procedures are necessary, as the large range of operating conditions as well as the extensive range of design parameters makes any systematic test program for developing charts suitable for establishing the performance of any propeller highly impractical. Therefore, suitable calculation procedures are required for designing and evaluating propellers. The accuracy of these procedures must be high to be suitable for design purposes; therefore, the methods and data are evaluated against test data and modified where necessary to obtain the desired accuracy.

When the propeller is producing positive thrust with a given power input, the performance can be found from test data, by single-point methods or by strip analysis procedures, using the vortex theory to calculate the induced velocity and efficiency and two-dimensional airfoil data to calculate the profile losses. If the performance is determined from test data, the blade geometry of the desired propeller must be similar to that of the test propeller. Also, the test data must cover the range of loading, Reynolds number and Mach number required for analysis. Using the vortex theory of propellers developed in the previous sections, certain corrections can be made to propeller test data that extend its usefulness. However, it is generally unusual to have the exact test data required to calculate the performance of the desired propeller with the same accuracy as is possible with the other methods.

Single-point methods for calculating the performance have been developed which can be used with test data for determining the profile losses, or the profile losses may be calculated by strip analysis theory. Thus, when calculating the performance of propellers using single-point methods, the induced losses are determined based on theoretical vortex theory results, and the profile or drag losses are found from the test data or by integrating the drag losses using airfoil data. Although this method of calculating the performance is limited to blades where the data is available with the same thickness ratio, camber, and blade angle distribution, the procedure is of sufficient accuracy to be very valuable for initial propeller selection procedures.

For the normal range of propeller operation, the strip analysis method of calculation is the best method available for analyzing a given propeller or designing a new propeller. This method of performance calculation is based on determining the lift and drag at a series of blade stations from two-dimensional airfoil data and resolving these quantities in the thrust and torque direction and integrating to find the total thrust torque and efficiency. The propeller vortex theory for correcting conditions at the blade to correspond to two-dimensional conditions and the necessary airfoil data have been presented. These theories and data are the basis for all strip analysis performance calculations in the full range of operation.

The strip analysis procedure also allows the use of the actual velocity distribution in the plane of the propeller as determined by the geometry of the airplane for finding the force coefficients. Thus the true efficiency of the propeller as installed on the airplane may be found.

The normal range of operation is that where the propeller is producing positive thrust and the shaft angle is between 0 and approximately 10 degrees. At normal operating conditions, the flow into the propeller is essentially axial with no sudden change due to blockage, for instance. Normal propeller operation is also that where the blade loading is near the optimum so that the theoretical values of induced velocity can be used.

The methods for calculating the performance of the propeller at all the conditions required using the theory and airfoil data previously presented are given in the following sections. The methods will cover strip analysis procedures, single-point methods, off-design conditions, optimization procedures, failure conditions, and supersonic propellers. Where possible, the accuracy of the results found using methods of calculation will be compared with test data.

## Installed Propeller Efficiency

When the propeller is installed on an airplane, the velocity at the propeller disc may be different from the free-stream velocity due to the influence of other parts of the airplane. For instance, if the propeller were installed in front of a large radial reciprocating engine, the velocity on the inboard section of the propeller would be less than the free stream. On the other hand, if the propeller were installed on a large spinner, the velocity at the inboard sections would exceed the free-stream velocity. On some of the older airships, the propellers operated completely within the boundary layer and the velocity in the propeller plane was much less than free stream.

The velocity in the propeller disc determines the forces on the blades. If the velocity is less than free stream, the thrust is higher than if the section were operating at free-stream conditions. Thus if the efficiency were calculated using the free-stream velocity, the level would exceed the actual value by the ratio of the integrated velocities. This fact has been demonstrated by flight tests of a P-47 airplane equipped with a thrust meter, where, with measured thrust and free-stream velocity, an efficiency of over 100% was obtained.

If the efficiency is calculated using a proper integration of the velocity in the place of the disc, the values will not exceed 100%. In this case the true efficiency of the propeller is determined. Thus if the true efficiency is quoted, it is necessary to know the velocity in the plane of the disc to determine the thrust available for propulsion.

Unfortunately, the propeller and airplane designer may not use exactly the same velocity for determining the conditions in the plane of the disc, so that differences in thrust are calculated for the same values of efficiency. To eliminate this problem, it has become standard to quote the efficiency based on the free-stream velocity. This value of efficiency is defined as the apparent efficiency and is used to calculate the actual thrust. The procedure for calculating the performance by strip analysis is based on the use of the free-stream velocity for determining the efficiency.

## Strip Analysis Procedure - Single Rotation, V = 0

The strip analysis calculating procedure for finding the performance of single-rotation propellers at the static condition V = 0 is given in detail on Tables IV and V. This procedure was developed from Equations 109 to 117 previously derived. When calculating the performance, the geometric characteristics of the propeller must be known, including the blade number, diameter, and detailed blade characteristics. The power to be

TABLE III. STRIP ANALYSIS CALCULATION PROCEDURE
FORWARD VELOCITY = 0

GIVEN = H.P. = _____ RPM PROP = N = _____

BLADE NO.B__ ALTITUDE = _____ TEMP.= _____ DIAMETER= _____

Find: $\rho$ = ___ $\rho/\rho_0$ = ____ Speed of sound - a___ From ATS Tables

Calculate: Req'd $C_p = .0005\,hp \Big/ \left[\left(\rho/\rho_0\right)(N/1000)^3\ (D/10)^5\right]$

| ITEM NO. | PROCEDURE |
|---|---|
| 1 $x = r/R$ | Spinner & x = .2,.3,.4,.5,.6,.7, .8,.9,.95 & .975 |
| 2 $\pi$ NDx | Know D,x,N Cal. $\pi$ nDx = $\pi$NDx/(60) |
| 3 $M_s = \pi nDx/a$ | Calculate |
| 4 b = Blade Chord | From blade characteristics |
| 5 RN = $(\rho/\mu)b\pi$ nDx | Calculate |
| 6 $C_{li}$ = Design $C_L$ | From blade characteristics |
| 7 h/b = Thickness Ratio | From blade characteristics |
| 8 $\beta$ = Blade Angle Dist. | From blade characteristics - value assumed |
| 9 $\sigma = bB/\pi xD$ | Calculate |
| 10 $\sigma \Delta x$ | Calculate |
| 11 $\tan\gamma$ | Step 24 Table IV |
| 12 $\cos\phi$ | Step 3 Table IV |
| 13 $\cos^2\phi$ | Calculate |
| 14 $\sin\phi$ | Tables |
| 15 $C_L$ | Step 20 Table IV |
| 16 $x^4\pi^3/8$ | Calculate |
| 17 $x\sigma C_L x^4$ | Calculate |
| 18 $\Delta C_Q/\Delta x$ | $\Delta x \sigma C_L \frac{x^4\pi^3}{8} \cos^2\phi(\sin\phi + \tan\gamma\cos\phi)$ |
| 19 $x^3\pi^3/4$ | Calculate |
| 20 $\Delta C_T/\Delta x$ = | $\Delta x \sigma C \frac{(x\pi)^3}{8} \cos^2\phi(\cos\phi - \tan\gamma\sin\phi)$ |
| 21 $C_Q$ = | $\Sigma \Delta C_Q/\Delta x$ |
| 22 $C_p = 2\pi C_Q$ | Calculate Cp; item 22 must agree with req'd Cp within 3%; otherwise, repeat calculation at new |
| 23 $C_T$ | $\Sigma \Delta C_Q/\Delta x$ |
| 24 k' | Figure 65 contraction ratio |
| 25 FM = | $.565\ C_p^{3/2}/Cpk'$ |

TABLE IV. PROCEDURE FOR CALCULATING $C_L$ & $C_D$
FORWARD VELOCITY = 0

B = ___ From Table III
$C_P$ = ___ From Table III
$\pi$ nD ___

| | ITEM | PROCEDURE |
|---|---|---|
| 1 | x = r/R | From Table III |
| 2 | $\phi$ | Assume |
| 3 | tan $\phi$ | Tables (Trig) |
| 4 | w/nD | $\pi$x tan $\phi$ |
| 5 | K(x) | From Figures 8 to 12 |
| 6 | $\epsilon$ | From Figure 19 |
| 7 | k | From Figure 7 |
| 8 | $(\epsilon + k/2)/\epsilon$ | Calculate |
| 9 | $\sigma C_L$ | $2\,K(x)((\epsilon + k/2)/\epsilon)^2$ |
| 10 | b | Table III |
| 11 | $\sigma$ | $bB/\pi$ xD |
| 12 | $C_L$ | $\sigma C_L/\sigma$ |
| 13 | $\beta$ | Table III |
| 14 | $\alpha = \beta - \phi$ | Calculate |
| 15 | $C_{Li}$ | Table III |
| 16 | h/b | Table III |
| 17 | Section Type | Table III |
| 18 | RN | Table III |
| 19 | $M_S$ | Table III |
| 20 | $C_L$ | Operating $C_L$ @ $\alpha$, M Appendix II |
| 21 | $C_L \neq C_L$ | $C_L(12) \neq C_L(20)$ Repeat steps 2 to 21 |
| 22 | $C_L = C_L$ | $C_L(12) = C_L(20)$ Complete calculation |
| 23 | $C_{D_{-1}}$ | From airfoil data Appendix @ $C_L$(22 ) |
| 24 | $\tan\gamma = C_D/C_L$ | Calculate |

absorbed, the rotational speed, and the ambient conditions must also be known.

The procedure given in Table III is based on incompressible flow theory for finding the induced velocity. However, compressibility effects are considered with the use of the airfoil data which accounts for Mach number effects. If the propeller is operating at tip Mach numbers in excess of one, the tip corrections given on Figures 57 to 63 should be applied to correct the lift and drag data.

The lift and drag characteristics at each blade station are found based on Equation(117)and two-dimensional airfoil data. Equation(117)relates the induced angle to the loading, $\sigma C_L$. With the induced angle and blade angle known, the two-dimensional angle of attack is determined by Equation(51). The lift and drag coefficients are found from the two-dimensional airfoil data given in Appendix II, Volume III, at the angle of attack for the specified airfoil section and operating condition. The $\sigma C_L$ determined from the airfoil data must match the $\sigma C_L$ used to find the induced angle; otherwise, further iterations must be made until agreement is obtained.

The design $C_L$ and thickness ratio of the airfoils specified for the propeller at each blade station will not match those presented in Appendix II, Volume III. Therefore, when finding the lift and drag coefficients, it is necessary to use linear interpolation. Thus, if the lift of a section with a design $C_L$ of .5 and a thickness ratio of 7.5% were required, the lift would be read at thickness ratios of 6% and 9 degrees, and desired value would be halfway between the two values.

The differential torque and thrust coefficients at each station are determined based on Equations (62) and (63). The procedure outlined in Table III uses the method of integration given and Equations (110)and(111)to determine the total thrust and torque coefficients. If the performance of the propeller is to be found at given power, the power found from the integrated torque coefficient must agree within ±3%. If this level of accuracy is not obtained, the blade angle setting must be adjusted until agreement is obtained.

The results of the calculation are presented in terms of Figure of Merit. The Figure of Merit is determined knowing the thrust and power coefficients using the Theodorsen contraction ratio found as a function of the power coefficient from Figure 65.

Strip Analysis Procedure - Single Rotation, $V > 0$

The strip analysis procedure for calculating the performance of propellers at a forward velocity above zero is similar to that described for the static condition. The main difference in the two procedures is the effect of forward velocity. The procedures used are given in Tables V to VII and are developed from Equations (44) to (58).

Table V contains the basic information needed for the analysis, the calculation of the fixed constants, and the final results. The detailed blade data required, including the distributions of blade chord, design $C_L$ and blade angle, are given in Table V, along with the detailed procedure for calculating the torque and thrust coefficients at each station. The calculation of the operating lift coefficient depends on the matching of the induced loading and the lift and drag characteristics of the airfoils from Appendix II, Volume III, and presented on Table VII.

Before starting the strip analysis calculation, it is necessary to establish the operating blade angle that will closely match the power specified. If many calculations are planned to develop an efficiency map, this is not necessary. However, when the power is specified, the calculated value should check that given within 3 percent. If no other data is available for estimating the blade angle, the single-point method given on page 182 may be used. The operating blade angle at $x = .75$ may be found as follows:

1. Calculate power coefficient Cp and advance ratio J, Table VI.
2. From short single-point method, find drag/lift ratio $\gamma$ and efficiency knowing activity factor and integrated design $C_L$.
3. Calculate $\tan \phi = J/.75x$.
4. Find $\tan (\phi + \gamma) = \tan \phi_o/\eta$.
5. Knowing $\gamma$, read $\phi$.
6. Using the airfoil data of Appendix II, Volume III, read $\alpha$ operating $C_L$ @ $\gamma$ for the section corresponding to the $x = .75$.
7. Knowing $C_L$, read $\alpha$.
8. $\beta .75 = \phi + \alpha$.

TABLE V. STRIP ANALYSIS CALCULATION, SINGLE-ROTATION PROPELLERS

DATA GIVEN

Velocity, $V_o$____fps Shaft Horsepower _____rpm____

Altitude _____Feet, Temp.____Pressure_____psi

Propeller_____No. of Blades____Blades Des._____

Diameter_____ AF _____J $C_{Li}$ _____

CONSTANTS FOUND

Density Ratio $\sigma$ =____ Density $\rho$ = _____ $\rho/\mu$= ___

Speed of Sound a =____fps Mach No.,$M_a = V_o/a$ =____

$C_p = .0005hp/\sigma\left(\frac{N}{1000}\right)^3\left(\frac{D}{10}\right)^5$ =___ Advance Ratio=$\frac{60V_o}{ND}$

$\pi nD = \pi ND/60$ =___ Tip Speed fps R = D/2

$\rho/\rho_o = \sigma$, and $\rho/\mu$ Read from standard atmosphere Tables

INTEGRATED RESULTS

$C_Q = \Sigma \Delta C_Q$ = _____

$C_P = 2\pi C_Q$ = _____

$C_T = \Sigma \Delta C_T$ = _____

$\eta = J\ C_T/C_P$ = _____

TABLE VI. STRIP ANALYSIS CALCULATION PROCEDURE, SINGLE-ROTATION PROPELLERS, $V > 0$

| | | |
|---|---|---|
| 1 | $x = r/R$ | Use $x_s$ and $x = .3, .4, .5, .6, .7, .8, .9, .95$ & $.975$ |
| 2 | $\Delta x$ | $(.3 - x_s)/2$, $(.4 - x_s)/2, .1 \cdots .1, .075, .0375$ & $.025$ |
| 3 | $V/V_o$ | Given for installation |
| 4 | $\csc \phi_o$ | $\phi_o = \tan^{-1} J/\pi x$, Tables (Trig) |
| 5 | $M = M_a \csc \phi_o V/V_o$ | Calculate |
| 6 | b, ft | Given blade characteristics |
| 7 | $RN = baM \rho/\mu$ | Calculate |
| 8 | Design $C_L$ | Given blade characteristics |
| 9 | h/b | Given blade characteristics |
| 10 | $\beta$ | Given blade characteristics-assumed |
| 11 | $\sigma$ | $bB/\pi xD$ |
| 12 | $\sigma \Delta x$ | (11) (2) |
| 13 | $C_L$ | Calculate per Table VII item 27 |
| 14 | $C_D$ | From airfoil data - Appendix |
| 15 | $\phi$ | From Table VII |
| 16 | $\sin \phi$ | Trig Tables |
| 17 | $(1 - \sin^2\phi)$ | Calculate |
| 18 | $\pi x^2 J^2/8$ | Calculate |
| 19 | $(1 + w/2)$ | Table VII |
| 20 | $\left\lvert \frac{(1 + \bar{w}/2)(1 - \sin^2\phi)}{\sin^2\phi} \right\rvert$ | Calculate |
| 21 | Z | Calculate = (16) (18) (20) |
| 22 | $\sigma \Delta x Z$ | Calculate |
| 23 | $\cot \phi$ | Trig Tables |
| 24 | $\tan\gamma$ | Table VII |
| 25 | $1 + \cot \phi \tan\gamma$ | Calculate |
| 26 | $C_L \sigma \Delta x Z$ | Calculate |
| 27 | $\Delta C_Q$ | (20) (21) |
| 28 | $\cot \phi - \tan\gamma$ | |
| 29 | (21) (23) | $C_L \sigma \Delta x Z(\cot \phi - \tan\gamma)$ |
| 30 | $\Delta C_T$ | (24)/(x/2) |

TABLE VII. PROCEDURE FOR CALCULATING $C_L$ & $C_D$, SINGLE-ROTATION PROPELLERS, FORWARD VELOCITY V> 0

$V_o$ = ____ fps D= ____ ft n ____ rps J = ____ $V_o/nD$ = ____

Blade No. B ____

| | ITEM | PROCEDURE |
|---|---|---|
| 1 | x = r/R | From Table VI |
| 2 | $V/V_o$ | Table |
| 3 | $J_L$ | $J(V/V_o)$ |
| 4 | $\beta$ | Table VI |
| 5 | b | Table VI |
| 6 | RN | Table VI |
| 7 | M | Table VI |
| 8 | $\sigma$ | $bB/\pi xD$ |
| 9 | $\bar{w}$ | Assume = .3, first iteration, $\bar{w}=0$ when $M_a>1.0$ |
| 10 | $1 - \bar{w}/2$ | Calculate |
| 11 | $\phi$ | $= \tan^{-1}(J/\pi x)(1 + \bar{w}/2)$ |
| 12 | $\cos \phi$ | From Tables |
| 13 | $\cos^2\phi$ | Calculate |
| 14 | $\sin^2\phi$ | From Tables (Trig) |
| 15 | $1 + \bar{w}$ | 1 + (9) |
| 16 | $J_W$ | $J_L(1 + \bar{w})$ |
| 17 | K(x) | Read from Figure 8 to 12 @ B,x & $J_W$ |
| 18 | $\sin^2\phi/\cos \phi$ | Calculate (14)/(12) |
| 19 | F(w) | $(1 + \bar{w})/(1+\bar{w}/2)(1 + \bar{w}/2 \cos^2)$ |
| 20 | $\sigma C_L$ | F(w)2WK(x)(18) |
| 21 | $\bar{w}_c/\bar{w}_i$ | Read Figures 27 to 56 @ $M_a$, J and x |
| 22 | $\bar{w}_c/2$ | $\bar{w}_c/2(w_c/w_L)$ |
| 23 | $\phi_c$ | $\tan^{-1}(J/x)(1 + \bar{w}_c/2)$ |
| 24 | $\alpha$ = (4)-(23) | $\beta - \phi_c$ |
| 25 | $C_{Lu}$ | From airfoil data Appendix II |
| 26 | $K_1$ | Read from Figures 57 to 63 |
| 27 | $C_L$ | $= K_1 C_{Lu}$ |
| 28 | $\sigma C_L$ | Must agree with $\sigma C_L$ item 20 or repeat (9 to 28) |
| 29 | $C_{Du}$ | From airfoil data |
| 30 | $C_D$ | $K_1 C_{Du}$ |

With the blade angle setting as determined above, the blade angle at each station is determined and the calculation is made as outlined in Tables VII and IX. When matching the induced loading $\sigma C_L$ with the loading determined from the airfoil data of Appendix II, Volume III, it is convenient with the hand calculations to cross plot $C_L$ versus angle of attack to determine the true operating lift coefficient. When the lift and drag coefficients are found from the airfoil data, linear interpolations with respect to design $C_L$ and thickness ratio are used for sections between those for which data are available. After the lift and drag coefficients are established, the differential torque and thrust coefficients are found and the results integrated. If the power is within 3 percent of the specified value, the efficiency is found; otherwise, other iterations are required until the power is within limits.

The procedures outlined above for calculating the efficiency are for a propeller with specified characteristics. Procedures have also been developed for modifying the distribution of blade angle, design lift coefficient, and blade chord to obtain the optimum loading, and therefore, the optimum performance. The theory and procedures for these calculations are presented in the section entitled "Optimum Propeller Design".

The basic procedure for calculating the performance of propellers operating at a velocity greater than zero has been set up for high-speed computers, as these calculations are very time consuming and many points are received in the course of selecting a propeller for a given installation. The basic method with the input and output requirements is given in Appendix III. This computation method depends on a "Tape" which has the basic airfoil data and the coefficients for establishing the induced characteristics. The tape setup is also given and could be generated from the airfoil data of Appendix II and the induced data given on Figures 7 to 20. With the procedure shown in Appendix III, it is possible to write the required program in computer language.

Strip Analysis Procedure - Single Rotation, $V \geq 0$, $M < 1.0$

The preceding strip analysis methods apply only when the propeller is operating at tip Mach numbers less than one. From the data presented, it was shown that compressibility effects did not influence the induced losses as long as the tip Mach number is less than 1.0. However, if the tip Mach number exceeds 1.0, the rule of forbidden signals becomes important, and modifications to the induced velocity must be made as shown on Table IX. When applying the data for correcting the induced velocity for compressibility effects, it should be noted that there are two effects that are considered. The

first correction reduces the inflow velocity due to the blockages of the induced flow by the shock waves. The second correction is localized at the tip within the Mach cone and effectively reduces the lift and drag coefficients from that read for two-dimensional flow.

Strip Analysis Procedure - Single Rotation, M > 1

When calculating the performance of propellers operating at forward Mach number above 1.0 (supersonic propellers), the procedures are much simpler. Because of the rule of forbidden signals, induced velocity is zero. Thus $\phi = \phi_o$ and the angle of attack of the section can be found directly. The only correction to the data that is necessary is that due to tip effects given on Figures 57 to 63 . Table VII is used to determine the lift and drag characteristics, and Tables V and VI are used for calculating thrust and torque coefficients and the final efficiency.

Strip Analysis Procedures - Dual Rotation, V> 0

The procedure for calculating the performance of dual-rotation propellers by strip analysis is given on Tables VII to XI. The procedure was developed from Equations (66) to (78) and also used the two-dimensional airfoil data of Volume III.

The calculation procedure is similar to that for single-rotation propellers. The main difference is the effect of the front unit on the rear and the length of the calculation. Because of the mutual interaction of the front and rear units the blade angles must be different for equal power absorption. Equal power absorption between units is necessary for peak efficiency and to minimize gearbox loads.

TABLE VIII. STRIP ANALYSIS CALCULATION,
DUAL-ROTATION PROPELLERS

DATA GIVEN

Velocity, $V_o$ = ___ fps, Shaft Horsepower ____ Prop.rpm = ___

Altitude = ____ Feet, Temp. ___ ° Pressure ___ psi

Propeller= ____ No. of Blades = ____ Blade Des. _____

Diameter = _____ Blade AF _____ $IC_{Li}$ _____

CONSTANTS FOUND

Density Ratio $\sigma$ ____ Density _____

Speed of Sound, a ____ fps Mach No., $V_o/a$ = _____

$$C_P = \frac{.0005\ HP}{\sigma \left(\frac{N}{1000}\right)^3 \left(\frac{D}{10}\right)^5}$$ Advance Ratio $\frac{60V_o}{nD}$ = ____ J

$\pi nD = \pi ND/60$ ____ Tip Speed ___ fps $R = D/2$

INTEGRATED RESULTS

$C_P = C_{PF} + C_{PR}$ = $\Sigma(27)$ = _____

$C_T = C_{TF} + C_{TR}$ = $\Sigma(32)$ = _____

TABLE IX. STRIP ANALYSIS CALCULATION PROCEDURE, DUAL-ROTATION PROPELLERS

| | | PROCEDURE |
|---|---|---|
| 1 | $x = r/R$ | Use $x_s$ & x .3,.4,.5,.6,.7,.8,.9, & .95, .975 |
| 2 | $\Delta x$ | $(.3 - x_s)/2$, $(.4 - x_s)/2$,.1 ···.1, .075,.0375 & .025 |
| 3 | $V/V_o$ | Given for installation |
| 4 | csc $\phi_o$ | $\phi_o$ $\tan^{-1} J/\pi x$ Tables |
| 5 | $M = Ma(4)(3)$ | Ma csc $\phi$ $V/V_o$ |
| 6 | b | Given - Blade Characteristic Curves |
| 7 | $RN = a(5)(6)\rho/\mu$ | a b M $\rho/\mu$ |
| 8 | $\beta$ | Given - Blade Characteristic Curves |
| 9 | Design $C_L$ | " " " " |
| 10 | h/b | " " " " |
| 11 | $\sigma$ | $bB/2\pi xD$ |
| 12 | $J^2M^2/Ma$ | Calculate |
| 13 | $(\pi^2x^2/4)\Delta x$ | " |
| 14 | $(\pi x/4)\Delta x$ | " |
| 15 | $\sigma(11)(12)(13)$ | $\sigma J^2M^2/Ma$ $(\pi^2x^2/4)\Delta x$ |
| 16 | (11)(12)(14) | $\sigma J^2M^2/Ma$ $(\pi x/4)\Delta x$ |

| | DETERMINE FOR | FRONT PROP | REAR PROP |
|---|---|---|---|
| 17 | $\bar{w}$ | Table X | Table XI |
| 18 | $C_L$ | Table X | Table XI |
| 19 | $C_D$ | Table X | Table XI |
| 20 | $G_F$ or $G_R$ | Table X | Table XI |
| 21 | (18)(20) | Calculate | Calculate |
| 22 | $\tan\gamma = C_L/C_D$ | Calculate | Calculate |
| 23 | sin $\phi$ | Table X | Table XI |
| 24 | (22)(28) | Calculate | Calculate |
| 25 | (23)+(24) | Calculate | Calculate |
| 26 | (15)(21) | " | " |
| 27 | $\Delta C_p = (25)(26)$ | " | " |
| 28 | cos $\phi$ | Table X | Table XI |
| 29 | (22)(23) | Calculate | Calculate |
| 30 | (28)-(29) | " | " |
| 31 | (16)(21) | " | " |
| 32 | $\Delta C_T = (16)(30)$ | " | " |

TABLE X. PROCEDURE FOR CALCULATING $C_L$ & $C_D$, DUAL-ROTATION PROPELLERS, VELOCITY V> 0, $M_T$<1.0

FRONT COMPONENT

$V_O$= ___ fps  D = ___ ft  n = ___ rps  $J = V_O/nD$ = ____

Blade No. _____  B = _____

| | ITEM | PROCEDURE |
|---|---|---|
| 1 | x = r/R | Table 1X |
| 2 | $V/V_O$ | Table 1X |
| 3 | $J_L$ | $J \cdot V/V_O$ |
| 4 | $\beta_F$ | Table 1X |
| 5 | b | Table 1X |
| 6 | RN | Table 1X |
| 7 | M | Table 1X |
| 8 | $\bar{w}$ | Assume = .3, First iteration |
| 9 | $1 + \bar{w}$ | Calculate |
| 10 | $J_L/\pi x$ | Calculate |
| 11 | $\phi_O$ | $\tan^{-1} J_L/\pi x$ |
| 12 | $\sin \phi_O$ | Tables |
| 13 | $\sin^2\phi_O$ | Calculate |
| 14 | J = (3)(9) | $J_L(1 + \bar{w})$ |
| 15 | k | Figure 18 |
| 16 | K(x,Θ) | Figure 13 to 17 |
| 17 | 1 +1/4[(15)(13)(8)] | $1 + 1/4\,(k\,\bar{w}\,\sin^2\phi_O)$ |
| 18 | (8)(9)/(17) | Calculate |
| 19 | $\sigma C_{L_F}$ = (10)(18)(16) | From Equation 71 |
| 20 | $G_F = \sqrt{17}$ | Calculate |
| 21 | $\phi$ | $\tan^{-1}[J/\pi x](1 + \bar{w}/2)$ |
| 22 | $\phi_F$ | $\tan^{-1}\left[J/\pi x\right]\left[1 + \bar{w}/2\,(1 + \tfrac{1}{2}k \tan^2\phi)\right]$ |
| 23 | $\alpha_F = \beta_F - \phi_F$ | Calculate |
| 24 | $C_L$ | From airfoil data -Appendix II,Vol.III |
| 25 | $\sigma C_L$ | Must agree with item 19 or steps 6 to 19 must be repeated |
| 26 | $C_D$ | From airfoil data -Appendix II, Vol. III |

TABLE XI. PROCEDURE FOR CALCULATING $C_L$ & $C_D$, DUAL-ROTATION PROPELLERS, VELOCITY $V>0$, $M_T<1.0$

REAR COMPONENT

$V_O$= ___ fps, D ___ ft n= ___ rps $J = V_O/nD$ = _____

Blade No. _____

| | ITEM | PROCEDURE |
|---|---|---|
| 1 | x | Table IX |
| 2 | $J_L$ | Table X |
| 3 | $\bar{w}$ | Assume = .3, First iteration |
| 4 | $i + \bar{w}$ | Calculate |
| 5 | $J_I/\pi x$ | Table X |
| 6 | $\phi_o$ | Table X |
| 7 | $\sin \phi_o$ | Table X |
| 8 | $\sin^2\phi_o$ | Calculate |
| 9 | $J_W$ = (2)(4) | $J_L(1 + \bar{w})$ |
| 10 | k | Figure 18 |
| 11 | $G_F$ - 1 | $1/4(k\ \bar{w}\ \sin^2\phi_o)$ |
| 12 | 3(11) | Calculate |
| 13 | $\sqrt{G_R}$ | $\sqrt{1 + 12}$ |
| 14 | $G_F/\ G_R$ | Calculate |
| 15 | $C_{LF}$ | Table X |
| 16 | $C_{LR} = C_{LF}(14)$ | Calculate |
| 18 | $\phi$ | $\tan^{-1}\left[J/\pi x\right](1 + \bar{w}/2)$ |
| 19 | $\phi_R$ | $\tan^{-1}\left[J/\pi x\right]\left[1 + \bar{w}/2\ \ (1 - \frac{1}{2}k\ \tan^2\phi)\right]$ |
| 20 | $\beta_R$ | Table X |
| 21 | $\alpha_R = \beta_R - \phi_R$ | Calculate |
| 22 | $C_L$ | From airfoil data - Appendix II, Volume III, must agree with item 16 or steps 3 to 16 must be repeated |
| 23 | $C_L$ | From airfoil data = Appendix II, Volume III |

## OPTIMUM PROPELLER DESIGN

For purposes of designing propellers, it is necessary to know the blade planform, blade loading, and/or design $C_L$ distribution which results in maximum efficiency for a given design flight condition. Previously the blades have been designed on the basis of a Betz type loading, on a maximum lift-drag ratio loading, or on a combination of the two loadings. In general, the results obtained by these loadings are near maximum efficiency. However, the true maximum is obtained when the combination of profile and induced losses is a minimum. To determine this optimum condition, the theory of "Calculus of Variation" is used.

The application of the Calculus of Variations to the propeller problem was developed by Haines and Diprose, Reference 39. The solution to the problem as given requires considerable time for the calculation. For the solution to a specific case, simplifications to the general solution may be made which greatly reduce the calculating time.

### Optimum Blade Loading

In the following discussion it is assumed that the design flight condition and the propeller configuration with the exception of the blade planform, blade loading, and/or design $C_L$ distribution are specified. The problem is to define these three unknown distributions to produce maximum propeller efficiency at the given design condition. Obviously the condition of maximum efficiency will be realized if these distributions are selected such that the power loss for the given power input is minimum. The solution then requires that one integral (power loss) shall be minimized for a constant value of a second integral (power input). This is a problem which may be solved by the theory of "Calculus of Variations".

The problem is to determine a distribution or distributions, depending upon the number of variable quantities, such that the power loss integral is minimized for a constant value of the power input. The general solution as given in Reference 40 is

$$\frac{\gamma A}{\gamma \mu} = 0 \qquad (120)$$

where $A = \frac{d \Delta C_p}{dx} + \frac{\lambda \, dC_p}{dx}$

$\lambda$ = arbitrary constant (with x) so chosen that the power input integral is the desired value

$\mu$ = independent variable and the subscript refers to the particular independent variable as $C_L$, $C_{Li}$ or b.

Equation (120) must be satisfied for each station along the blade. Note that an equation must be written for each independent variable. Consequently, for n independent variables, there will be n conditions to be satisfied. With Equation (120) as the basic equation, various specific cases will now be considered.

Case 1: Variable blade planform and blade loading.

Since there are two independent variables in this problem, two equations must be written. In Reference 39, it was shown that one condition is that L/D must be maximum. Consequently, the lift and drag coefficients are known (from airfoil data), and the problem is reduced to a single variable -- blade planform. It was also shown in Reference 39 that the solution for a single variable requires that

$$\frac{d \Delta \dot{C}_p}{d \dot{C}_p} = \lambda \tag{121}$$

where $\Delta \dot{C}_p \equiv \frac{d \Delta C_p}{dx}$

$\dot{C}_p \equiv \frac{dC_p}{dx}$

$\lambda$ = arbitrary constant as previously defined.

Equation (121) is not dependent upon any particular integrals defining $\Delta C_p$ and $C_p$ and, therefore, it applies to any strip analysis equation. Since $\Delta \dot{C}_p / \dot{C}_p$ is the element efficiency loss,

$$\Delta \dot{C}_p = \dot{C}_p - J \dot{C}_T \tag{122}$$

and

$$d \Delta C_p = d\dot{C}_p - J d\dot{C}_T \tag{123}$$

Thus, Equation (121) becomes

$$\frac{d\dot{C}_T}{d\dot{C}_P} = \lambda, \tag{124}$$

where $\lambda$, is a constant, but has a value different from $\lambda$. Thus, the solution to case 1 may be determined by the following steps:

1. From suitable airfoil data, determine at each station the $C_L$ and $C_D$ for maximum L/D.

2. At each station, assume several values of solidity and calculate by the strip analysis method the corresponding $\Delta x\dot{C}_T$ and $\Delta x\dot{C}_P$.

3. Plot $\Delta x\dot{C}_T$ versus $\Delta x\dot{C}_P$ and determine graphically the slope $d\dot{C}_T/d\dot{C}_P$.

4. At each x, plot $\lambda = d\dot{C}_T/d\dot{C}_P$ versus $\Delta x\dot{C}_P$.

5. Assume a value of $\lambda$, such that $\Sigma \Delta x\dot{C}_P$ is equal to the desired power coefficient.

6. The blade angle may be determined from airfoil data since the $C_L$ and therefore $\alpha$ are known from step 1.

7. The solidity may be determined from a plot of $\sigma$ versus $\Delta x\dot{C}_P$.

8. The efficiency may be determined from $\eta = JC_T/C_P$, where $C_T = \Sigma \Delta x C_T$, and $\Delta x\dot{C}_T$ may be found from the plot in step 3.

Note that this procedure would be the same if the blade planform were fixed and the $C_L$ distribution desired. In this case various values of $C_L$ instead of $\sigma$ at each station would be assumed and corresponding calculations performed.

The method described above is exact. However, the time required is considerable, and the accuracy is affected somewhat by the graphical determination of the slope, item 3 above. In the following equations, the basic strip analysis equation given in the previous section will be used, and several simplifying assumptions made to reduce the time required for the calculation.

The necessary equations for the profile and induced losses are derived from Equations 39 to 65.

$$\frac{d\,\Delta C_P}{dx} = \Delta \dot{C}_{PD} = \frac{\pi x}{4} \sigma C_D \left(\frac{W}{nD}\right)^3 \tag{125}$$

$$\frac{d\,\Delta C_{Pi}}{dx} = \Delta \dot{C}_{Pi} = \frac{\pi x}{4} \sigma C_L \left(\frac{W}{nD}\right)^2 J\frac{\overline{W}}{2} \cos \phi \tag{126}$$

$$\frac{dC_P}{dx} = \dot{C}_P = \frac{\pi^2 x^2}{4} \sigma C_L \left(\frac{W}{nD}\right)^2 \sin \phi \left(1 + \frac{\tan\gamma}{\tan \phi}\right) \tag{127}$$

Therefore,

$$\Delta \dot{C}_P = \Delta \dot{C}_P + \Delta \dot{C}_{PD} \tag{128}$$

$$\dot{C}_P = \frac{\pi x}{4} C_L \left(\frac{W}{nD}\right)^2 \tan\left[\frac{W}{nD} + J\frac{\overline{W}}{2} \cos \phi\right] \tag{129}$$

Thus, from Equation (120),

$$A = \Delta \dot{C}_P + \Delta \dot{C}_P \tag{130}$$

$$A = \frac{\pi x}{4} \sigma C_L \left(\frac{W}{nD}\right)^2 \left[\tan\gamma \frac{W}{nD} + J\frac{\overline{W}}{2} \cos \phi\right] + \lambda \frac{\pi^2 x^2}{4} \sigma C_L \left(\frac{W}{nD}\right)^2 \sin \phi \left(1 + \frac{\tan\gamma}{\tan \phi}\right) \tag{131}$$

Since $C_L$ and $C_D$ are fixed by the condition of maximum L/D, the only independent variable is the solidity, $\sigma$. It will be assumed that at a given station, a change in $\sigma$ changes the value of $\overline{w}$, but does not change the angle $\phi$ which is assumed equal to $\phi_o$. It would appear that the resulting solution would apply only to light loadings. However, exceptionally good accuracy has been found even at very high loadings. From Equation (131),

$$\frac{\lambda A}{\lambda \mu} = \frac{\delta A}{\delta \sigma} = \frac{\pi x}{4} \left(\frac{W}{nD}\right)^2 C_L \left[\tan\gamma \frac{W}{nD} + J\frac{\overline{W}}{2} \cos \phi_o\right] + \frac{\lambda \pi^2 x^2}{4} C_L \left(\frac{W}{nD}\right)^2 \sin \phi_o \left(1 + \frac{\tan\gamma}{\tan \phi_o}\right) + \frac{\pi x}{4} \sigma C_L \left(\frac{W}{nD}\right)^2 \frac{J}{2} \cos \phi_o \frac{\delta \overline{W}}{\delta \sigma} = 0 \tag{132}$$

Therefore,

$$\frac{W}{nD}\tan\gamma + J\frac{W}{2}\cos\phi_o + \lambda\pi x \sin\phi_o\left(1 + \frac{\tan\gamma}{\tan\phi_o}\right)$$

$$+ \frac{J}{2}\cos\phi_o \sigma \frac{\delta\bar{w}}{\delta\sigma} = 0 \qquad (133)$$

Since it was assumed that $\phi = \phi_o$, $W/nD = J/\sin\phi_o$. Also, if $\bar{w}$ is below about .4, a plot of $\sigma C_L$ versus $\bar{w}$ is essentially a straight line passing through 0 at $\bar{w} = 0$.

Consequently,

$$\sigma C_L = a\,\bar{w} \qquad (134)$$

or $$\frac{\delta\bar{w}}{\delta(\sigma C_L)} = \frac{1}{a} \qquad (135)$$

Since $C_L$ is a fixed value, for this case $\sigma\,\delta\bar{w}/\delta\sigma = \bar{w}$. Substituting these values into Equation (133),

$$\frac{\tan\gamma}{\sin\phi_o\cos\phi_o} + \bar{w} + \lambda\left(1 + \frac{\tan\gamma}{\tan\phi_o}\right) = 0 \qquad (136)$$

Since

$$\frac{1}{\sin\phi_o\cos\phi_o} = \tan\phi_o + \cot\phi_o = \frac{J}{\pi x} + \frac{\pi x}{J} \qquad (137)$$

$$\bar{w} = -\lambda - \frac{\tan\gamma}{J/\pi x}\left[\lambda + 1 + \left(\frac{J}{\pi x}\right)^2\right] \qquad (138)$$

It is of interest to note that if the drag coefficient is zero, Equation (138) reduces to the condition that $\bar{w}$ must be constant along the blade. This is the Betz condition for optimum loading. As a matter of fact, where both blade chord and loading are variables, the efficiency determined by the exact solution will differ only slightly from that obtained by using the conditions of maximum L/D and constant $\bar{w}$, provided there is no rapid variation of $\tan\gamma$ with x. It should be emphasized here that the condition of max. L/D applies only to the case where both solidity and loading may vary along the span. No such simplification is possible if either of these quantities is fixed.

Case 2: Fixed solidity - variable $C_L$ (or $\beta$ )

The solution of this case may be obtained in exactly the same manner as that used to obtain Equation 138. Again, using Equations 120 and 131,

$$\frac{\delta A}{\delta C_L} = \frac{\delta C_D}{\delta C_L}\frac{W}{nD} + J\frac{\delta\left(C_L \frac{\overline{W}}{2}\cos\phi\right)}{\delta C_L} + \lambda\pi x \frac{\delta(C_L \sin\phi)}{\delta C_L}$$

$$+ \lambda\pi x \frac{\delta(C_D \cos\phi)}{\delta C_D}\frac{\delta C_D}{\delta C_L} = 0 \qquad (139)$$

or

$$\frac{C_D}{C_L} = -\frac{\frac{J}{\pi}\frac{\delta\left(C_L \frac{\overline{W}}{2}\cos\phi\right)}{\delta C_L} + \lambda\frac{\delta(C_L \sin\phi)}{\delta C_L}}{\frac{W}{\pi nD} + \lambda x \frac{\delta(C_D \cos\phi)}{\delta C_D}} \qquad (140)$$

Making the same substitution as before,

$$\frac{\delta(C_L \sin\phi)}{\delta C_L} = \sin\phi_o \qquad (141)$$

$$\frac{\delta(C_D \cos\phi)}{\delta C_D} = \cos\phi_o \qquad (142)$$

$$\frac{\delta\left(\frac{\overline{W}}{2}C_L \cos\phi\right)}{\delta C_L} = \frac{\overline{W}}{2}\cos\phi_o \qquad (143)$$

Equation (140) becomes

$$\frac{\delta C_D}{\delta C_L} = -\frac{\frac{J}{\pi}\frac{\overline{W}}{2}\cos\phi_o + \lambda x \sin\phi_o}{W/\pi nD + \lambda x \cos\phi_o} \qquad (144)$$

Simplifying,

$$\frac{\delta C_D}{\delta C_L} = -\frac{\frac{1}{2}\sin 2\phi_o\left(\frac{\overline{W}}{2} + \lambda\right)}{1 + \lambda\cos^2\phi_o} \qquad (145)$$

Case 3: Fixed solidity, variable $C_L$ and $C_{Li}$.

Obviously one of the two equations necessary for the solution of this case is that given by Equation (140), (144), or (145), depending upon the accuracy required. The second equation may be obtained by setting the partial of A with respect to $C_{Li}$ equal to zero.

Thus,

$$\frac{\delta A}{\delta C_{Li}} = \frac{\pi x}{4} \sigma \left(\frac{W}{nD}\right)^2 \left[\frac{\delta C_D}{\delta C_{Li}} \frac{W}{nD}\right] = 0 \qquad (146)$$

Consequently,

$$\frac{\delta C_D}{\delta C_{Li}} = 0 \qquad (147)$$

Therefore, at a fixed operating $C_L$ the design $C_L$ must be one that gives minimum drag. In other words, the L/D must be maximum. Thus, the solution is defined by Equations (145) and (147), which must be satisfied simultaneously. This is most easily accomplished by plotting for each station curves of $C_D$ versus $C_L$ for lines of constant $C_{Li}$ for the airfoil with the given thickness ratio and type from the data of Appendix II, Volume III. An envelope of this family of curves may then be drawn which represents the minimum drag for any given operating $C_L$. The operating $C_L$ at each station is then determined by use of Equation (140), (144), or (145), in conjunction with the envelope curve of $C_D$ versus $C_L$. The design $C_L$ is obtained directly from the $C_D$ versus $C_L$ plots.

It follows that if the solidity, $C_L$ and $C_{Li}$ are all variable, the solution is identical to that of case 1. The $C_{Li}$ is again determined for maximum L/D.

Aerodynamic Balancing - Strip Analysis

Strip analysis procedures may also be used to set the blade angle of production propeller blades to obtain equal loading or balance. This is done by measuring the blade length, chord and angle at each station and then computing the change in blade angle setting required to obtain equal loading as compared to a master blade operating at the design flight condition. This change in blade angle is known as the blade balancing angle increment and may be calculated by strip analysis procedures, shown in Tables V to VII. Experience has shown that this procedure is very effective for aerodynamically balancing propeller blades.

## SHORT OR SINGLE-POINT METHODS OF ANALYSIS

When a propeller is sized for a new installation, a large amount of data is required to evaluate changes in performance due to changes of both propeller and aircraft design variables. The effects of changes of the propeller diameter, blade number, blade camber, and solidity must be found as well as changes in the operating conditions of the airplane. These data are then used for parametric analysis leading to the propeller selection.

The complete design data necessary to find the physical characteristics of propellers required for performance calculation needed for these initial parametric studies is generally not available because of the interaction of the propeller and airplane design parameters. Thus, complete strip analysis calculations cannot be done without making a number of assumptions with regard to the blade design variables. Because of this lack of design data and the cost of complete strip calculations, single-point methods which permit the rapid calculation of performance based on the overall, or effectively integrated, characteristics of propellers have been developed. These methods are based on the blade characteristics at the 75% station and other design factors such as blade number and diameter. When the propeller is operating in the normal range, the accuracy of the single-point methods is generally excellent. Further, the time required to calculate propeller performance is small, thus making it possible to find the effects of a large range of parameterss for a number of operating conditions without the need of high-speed computers.

The single-point methods of analysis are also useful for analyzing and applying propeller test data and calculating performance for off-design conditions where the strip theory no longer applies. In this way at least an approximation can be made to find the off-design propeller performance using at least the gross effects.

### Single-Point Method - Efficiency Maps

There are several single-point methods of analysis for finding the performance of propellers. One of the simplest methods depends on the use of numerous efficiency maps for presenting the basic data. For instance, a series of maps of advance ratio as a function of power coefficient are developed for lines of constant efficiency for a series of different propellers. To cover the necessary range, maps are required for a range of blade number, activity factor, and design lift coefficient. The maps must be prepared for geometrically similar blades. However, the blade thickness ratio and blade angle distribution can be adjusted to agree with the camber and activity factor selected. Because of the number and range of

variables necessary to cover the range, a large number of efficiency maps are required to obtain reasonable accuracy.

To calculate the efficiency of a propeller using the efficiency maps, it is only necessary to calculate the standard power coefficient and advance ratios knowing power, diameter, rotational speed, and density from the equations

$$C_P = \frac{.0005\ hp}{\sigma(N/1000)^3\ (D/10)^5} \tag{148}$$

$$J = \frac{60V}{ND} \tag{149}$$

where $C_P$ = power coefficient
hp = horsepower
N = rotational speed, rpm
D = propeller diameter, ft
$\sigma$ = density ratio
V = velocity, fps
J = advance ratio

The maps corresponding to the proper blade number activity factor and design lift coefficient are then entered at the power coefficient and advance ratio found from Equations (135) and (136). Straight-line interpolations are used to correct for values of activity factor and design lift coefficient between the efficiency maps. Thus, if the efficiency is required for a three-bladed propeller with blades having a design $C_L$ of 0.5 and an activity factor of 130, the efficiency would be read at the 0.5 design $C_L$ for three-bladed propellers at activity factors of 120 and 140, for instance. The desired efficiency would be halfway between the values read at 120 and 140 activity factors.

Efficiency maps can be developed to account for compressibility losses, or factors can be found to correct to the basic maps. These corrections for compressibility should cover the effects of camber and thickness ratio for a wide range of helical tip Mach number.

The main difficulty with the above procedure is the large number of basic charts required and its lack of flexibility. Further, the source of the efficiency losses is not described, and thus it is not known if high induced or high profile losses are encountered at a given operating condition.

To eliminate the number of efficiency charts required, other procedures have been formulated to develop corrections for determining the effects of changes of activity factor or design lift coefficient. These corrections are developed and presented in a number of ways, and the accuracy of the procedure

is good only within the area for which the corrections were developed. For instance, corrections for activity factor developed for one range of power coefficients may not apply at another range. For this reason this procedure is not a satisfactory single-point method of analysis, and has been eliminated as a suitable method for calculating performance.

The large number of efficiency maps needed for calculating performance by single-point methods can be eliminated by the application of propeller theory. This is done by separating the profile and induced losses as is done in strip theory. By calculating these losses separately, it is possible to develop the basic data that applies over the entire range of propeller design and operating parameters. The procedure also has the advantage of identifying the losses separately, and shows the modifications necessary to improve the performance.

Single-Point Method Theory - V>0

The basic theory for calculating the performance of propellers by a single-point method depends on the assumption that the conditions described by the 75% station represent or describe the conditions for the rest of the propeller. Thus, if the propeller is operating at a given blade loading, the operating lift coefficient at the 75% radius completely describes the lift/drag ratio of the blade. The lift/drag ratio thus depends only on the effective operating lift coefficient for blades of a given camber level and is independent of the blade solidity and operating condition at speeds below the critical Mach number. Compressibility correction can be developed to correct the lift/drag ratio as a function of the operating Mach number and advance ratio.

The induced losses developed by a propeller are assumed to be independent of the blade lift/drag ratio and are dependent on the total loading on the blade, the blade number, and the advance ratio. The induced efficiency can be developed as a function of blade number, total loading, and advance ratio from theory for propellers with an optimum blade distribution. Since the propeller desired for a given installation will be operating near the peak efficiency, the optimum load distribution assumption is valid.

The basis for calculating the performance of propellers by a single-point method of analysis as described above is developed from the equations previously derived for strip analysis calculations.

Since

$$C_p = 2\pi C_Q \tag{150}$$

Equation (46) becomes

$$\frac{dC_p}{dx} = \sigma C_L \left(\frac{\pi x}{4}\right)^2 \left(\frac{W}{nD}\right)^2 (\sin \phi + \tan\gamma \cos \phi) \tag{151}$$

If the drag is zero, $\tan^{-1} C_D/C_L = \gamma$ is also zero and Equation (151) becomes

$$\frac{dC_{pi}}{dx} = \sigma C_L \left(\frac{\pi x W}{4nD}\right)^2 \sin \phi \tag{152}$$

An integration of Equation 152 over the blade radius gives the induced power coefficient.

The thrust coefficient is also calculated by integrating the equation

$$\frac{dC_T}{dx} = \sigma C_L \left(\frac{W}{nD}\right)^2 \frac{\pi x}{4} (\cos \phi - \tan\gamma \sin \phi) \tag{153}$$

When the drag is zero, Equation (153) becomes the equation for the induced thrust coefficient and is equal to

$$\frac{dC_{Ti}}{dx} = \sigma C_L \left(\frac{W}{nD}\right)^2 \frac{\pi x}{4} \cos \phi \tag{154}$$

Equations (153) and (155) may be integrated by assuming the propeller has the optimum load distribution as defined by Theodorsen, Reference 19, and Equation (120). The values of the induced power and thrust coefficients, $C_{pi}$ and $C_{Ti}$, found from integration with the corresponding advance ratio give the ideal efficiency. Thus,

$$\eta i = \frac{C_{Ti}}{C_{pi}} J \tag{155}$$

For the actual case where the drag is greater than zero, Equations (151) and (153) may be integrated for the case of the optimum load distribution with the drag found at each station for the corresponding value of lift. Thus, the total power and thrust coefficients are found and the total efficiency is equal to

$$\eta = \frac{C_T}{C_p} J \tag{156}$$

From Equations (151) and (153) it will be noted that the thrust and power coefficients can be broken into two parts: the induced and profile components, respectively. Thus,

$$C_P = C_{Pi} + C_{PP} \tag{157}$$

$$C_T = C_{Ti} - C_{TP} \tag{158}$$

and

$$C_P = C_{Pi}(1 + \tan\gamma \tan \phi) \tag{159}$$

$$C_T = C_{Pi}(1 - \tan\gamma \cot \phi) \tag{160}$$

where $C_{PP}$ = the power coefficient due to profile drag

$C_{TP}$ = the thrust coefficient due to profile drag

$\gamma = \tan^{-1} C_D/C_L$

$\phi$ = the true wind angle = $(V + \frac{W}{2})/ \pi nDx$

Since both the induced and total thrust and power coefficients can be found, the profile component is also easily determined.

A very useful expression for efficiency results from Equations (152), (153) and (156), thus:

$$\eta = \frac{dC_t/dx}{dC_P/dx} J \tag{161}$$

which becomes, on substitution of Equations (160) and (161) and reducing,

$$\eta = \frac{\tan \phi_o}{\tan(\phi + \gamma)} \tag{162}$$

From Equations (161) and (162) it is also noted that the induced components of the thrust and power coefficient are not influenced by the profile drag or the value of the drag/lift ratio. Also, it should be noted that the induced power and thrust coefficients are only dependent on the total loading $\sigma C_L$ and the advance ratio. For these reasons, the variation of the induced thrust and power coefficients and efficiency can be determined for the optimum load distribution independently as a function of blade number and advance ratio. The variation of the induced efficiency for propellers with 2, 3 and 4 blades, and as a function of advance ratio and power coefficient, is shown on Figures 81, 84 and 87.

The lift/drag ratio of any airfoil section depends only on the section type, camber, thickness ratio, operating conditions, and the operating lift coefficient. Thus, for a propeller of

a given camber and thickness ratio at a given condition, the drag/lift ratio will depend on the operating lift coefficient only. From Equation (151), it will be noted that

$$C_L = f\left(\frac{C_p}{\sigma}\right) \tag{164}$$

The activity factor of a blade is a measure of the solidity and is defined by Equation (165):

$$AF = \frac{100,000}{15} \int_{.2}^{1.0} \frac{b}{D} \left(\frac{1}{R}\right)^3 d\left(\frac{r}{R}\right) \tag{165}$$

For rectangular blades, the activity factor equals

$$AF = 1562 \frac{b}{d} \tag{166}$$

where b = the blade chord

D = the propeller diameter.

Since the solidity $\sigma = bB/2\pi r$ at any blade station, the activity factor and blade number terms may be substituted for $\sigma$ in Equation (151), which becomes

$$C_L = f\left(\frac{C_p}{BAF}\right) \tag{167}$$

For a blade with a given camber and blade angle distribution, the equivalent drag/lift ratio is a function of $C_p/BAF$ since this is a function of the operating $C_L$. Thus, knowing the variation of the drag/lift ratio with power coefficient of a propeller with blades of a given activity factor, the drag/lift ratio can be found for any other propeller with a given activity factor of the same camber and blade angle distributions. Thus, for a blade with varying activity factors but with a given camber or design $C_L$ distribution, the profile drag characteristics can effectively be reduced to one line.

With the breakdown of the thrust and power coefficient equations into their induced and profile components as discussed above, the elements are available to formulate a single-point method for calculating the performance of any propeller.

Since the total efficiency is a function of the power coefficient, drag/lift ratio, blade number, and advance ratio charts are developed of efficiency as a function of these variables. These charts are found for propellers with blades operating

at optimum load distribution and typical variations of lift/drag ratio.

To develop the data necessary for determining the profile losses, the drag/lift ratio is found as a function of 400 $C_p/BAF$ for variations of blade camber, which is measured in terms of the integrated design lift coefficient described by Equation (168):

$$IC_{Li} = 4\int_{.2}^{1.0} C_{Li}\left(\frac{r}{R}\right) d\left(\frac{r}{R}\right) \qquad (168)$$

where $IC_{Li}$ = the integrated design lift coefficient

$C_{Li}$ = the blade section design lift coefficient

$r$ = radius at a blade station

$R$ = total blade radius.

The drag/lift ratio must also be determined as a function of advance ratio and Mach number to cover the complete range of operation. If the propeller is operated at tip Mach numbers below the critical, these effects may be neglected.

The variation of drag/lift coefficient on the blade is defined by the $\gamma$, which is

$$\gamma = \tan^{-1}\frac{C_D}{C_L} \qquad (169)$$

To find the variation of $\gamma$ as a function of the necessary variables, complete performance data is used. These data may be determined from detailed strip analysis calculations or test results. In either case, $\gamma$ is found from the charts of total efficiency, Figures 81 to 89, knowing the efficiency and advance ratio. This was done from strip analysis calculations, and results are then presented as a function of 400 $C_p/BAF$ J for a series of blade integrated design lift coefficients (see Figures 78 to 80).

These charts can be modified for any blade configuration using the same procedure and the complete test or calculated data available.

Single-Point Method Theory, V = 0

A short single-point method for calculating the performance at the static condition can also be developed based on the procedures as described for the flight condition. At the static condition, the total thrust and power coefficients can be broken down into the induced and profile components. Also, the drag/lift ratio is found as a function of Cp/BAF for propellers varying in blade number and blade camber level. As before, this reduces the variation of $\gamma$ to a single line for a series of activity factors at a given blade camber and blade number. The profile losses can thus be found independent of the induced losses.

The induced losses can be found as a function of the induced power coefficient using the procedure developed by Theodorsen for the optimum loading, as shown in Reference 19.

$$C_{Ti} = \frac{\pi^3}{4} \frac{k'^4}{\mu_o^2} ( \epsilon + \tfrac{1}{2}k) \qquad (170)$$

$$C_{Pi} = \frac{\epsilon}{4} \frac{4}{\mu_o^3} \left|k'\right|^5 \qquad (171)$$

where $C_{Ti}$ = the induced thrust coefficient static condition

$C_{Pi}$ = the induced power coefficient static condition

$\epsilon$ = energy function @ $\mu_o$

$k'$ = contraction ratio

$k$ = mass coefficient @ $\mu_o$

$\mu_o = r/w_p = 1/\lambda$, helix angle in final wake

$\lambda$ = tan of the angle of wake spiral.

For a series of values of $\mu_o$, Equations (170) and (171) can be solved using the coefficients of Reference 19 and Figures 7 and 65. From Equations (159) and (160), the total thrust and power coefficients can be found knowing the induced value and the drag/lift ratio. When solving Equations (166) and (167) at the static condition, the true wind angle $\phi$ is found at the 75% radius knowing $\mu_o$ from the Equation

$$\phi_{.75} = \cot^{-1}\left[\left(\frac{\epsilon + \frac{1}{2}k}{\epsilon}\right)\frac{\mu_o}{k'} .75\right] \qquad (172)$$

where $\phi_{.75}$ = the wind angle at the 75% radius at the propeller disc.

Assuming values of the drag/lift ratio at the .75 station, the total thrust and power coefficients are calculated by modifying the induced coefficients found with Equations (170) & (171). This has been done for 2-, 3- and 4-bladed propellers and is presented on Figures 75 to 77 in the form of $C_T/C_p$ as a function of $\gamma$ for lines of constant $C_p$. When $\gamma = 0$, $C_T/C_p$ corresponds to the induced value and represents the maximum or ideal for that power.

The profile performance in terms of $\gamma = \tan^{-1} C_D/C_L$ was determined as a function of 400 $C_p$/BAF from propeller test data by using Figures 81 to 89. Thus, with the known values of $C_T/C_p$ and $C_p$ from the test data, $\gamma$ may be read as a function of $C_p$ from the appropriate figure based on the blade number. Since the operating $C_L$ is a function of the power coefficient over total activity factor, BAF, Equation (167), the data was normalized by plotting the results in the form of 400 $C_p$/BAF as a function of $\gamma$ and integrated design $C_L$; see Figure 74.

Application of the Single-Point Method

The charts necessary to calculate the performance of 2-, 3- and 4-bladed single-rotation propellers at the static and flight conditions are given on Figures 74 to 89. The charts for calculating the thrust and efficiency are given on Figures 81 to 89. The profile performance is determined from Figure 74 for the static condition and Figures 78 to 80 for the flight cases. The charts for finding the profile performance were set up for representative type blades for use at Mach numbers below the critical. Integrated design lift coefficients from 0 to 0.5 are covered.

Method - Static Condition

To calculate the performance at the static condition, use the following procedure:

1. Knowing hp, diameter, D, density ratio, $\sigma$, and rpm, N, calculate $C_p$:

$$C_p = \frac{.0005\ hp}{\sigma\left(\frac{N}{1000}\right)^3\left(\frac{D}{10}\right)^5} \qquad (173)$$

2. Knowing or assuming activity factor, AF, and blade number, B, calculate 400 $C_p$/BAF.

3. Knowing or assuming integrated design $C_L$, $IC_{Li}$, and 400 $C_p$/BAF, read $\gamma$ , $\tan^{-1} C_D/C_L$, Figure 74.

4. Knowing $\gamma$ , $C_p$, and B, read $C_T/C_p$, Figures 75 to 77. Note ideal $C_T/C_p$ read at $\gamma = 0$.

5. Calculate T:

$$T = \frac{C_T}{C_p} \frac{hp}{\pi nD} 1728 \qquad (174)$$

Method - Flight Conditions

The efficiency at the flight condition is calculated by the single-point method with the following procedures:

1. Knowing hp, diameter, D, density ratio, and rpm, N, calculate

$$C_p = \frac{.0005\ hp}{\sigma \left(\frac{N}{1000}\right)^3 \left(\frac{D}{10}\right)^5}$$

2. Knowing or assuming activity factor, AF, and blade number, B, calculate 400 $C_p$/BAF.

3. Calculate advance ratio J = V/nD.

4. Knowing or assuming integrated design $C_L$, $IC_{Li}$, 400 $C_p$/BAF and advance ratio, read $\gamma$, Figures 78 to 80. Use linear interpolation to find $\gamma$ at $IC_{Li}$s' between plotted values.

5. Knowing $\gamma$ , $C_p$, B, and J, read $\eta$, Figures 81 to 89 . Use linear interpolation to find $\eta$ at values of $\eta$ . Note the ideal or induced efficiency is found at $\gamma = 0$.

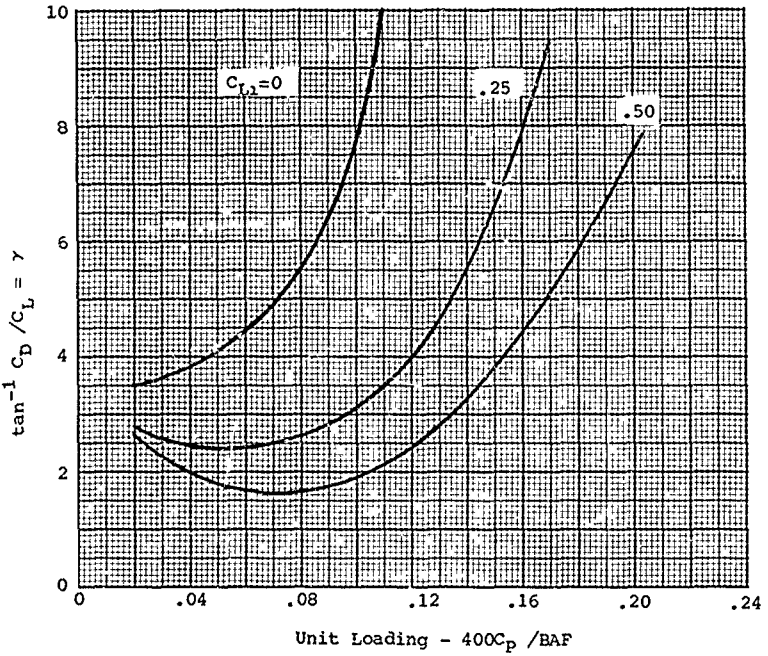


Figure 74. Propeller Profile Loss Chart, V = 0.

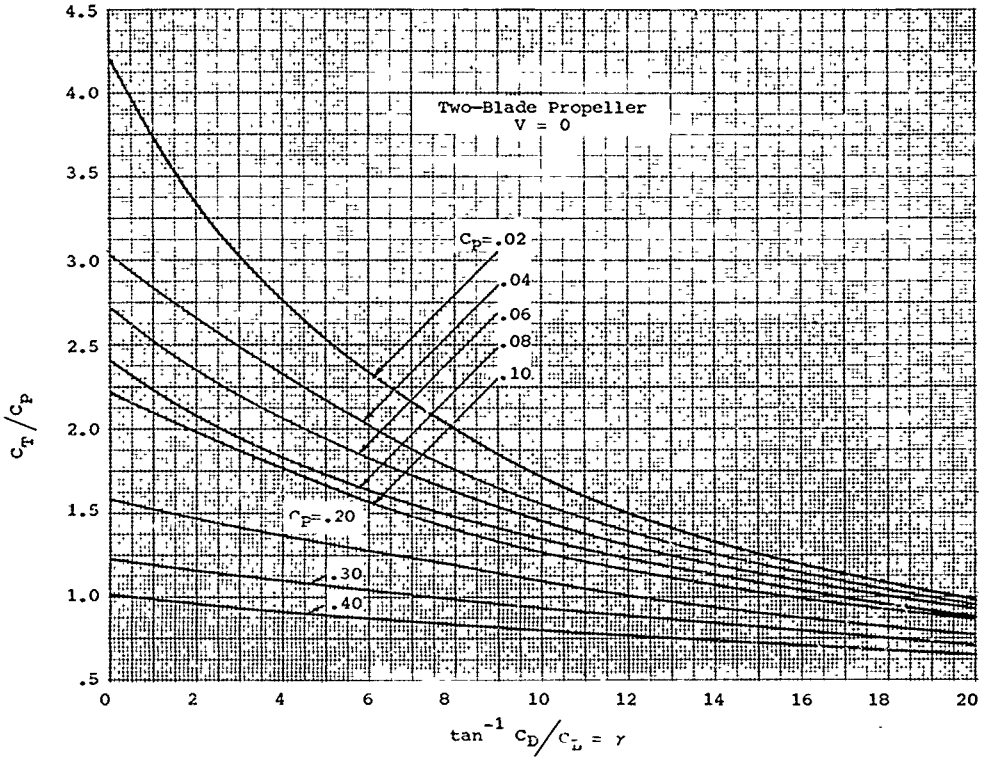


Figure 75. Propeller Thrust to Power Coefficient Ratio, Static Condition - Two Blades.

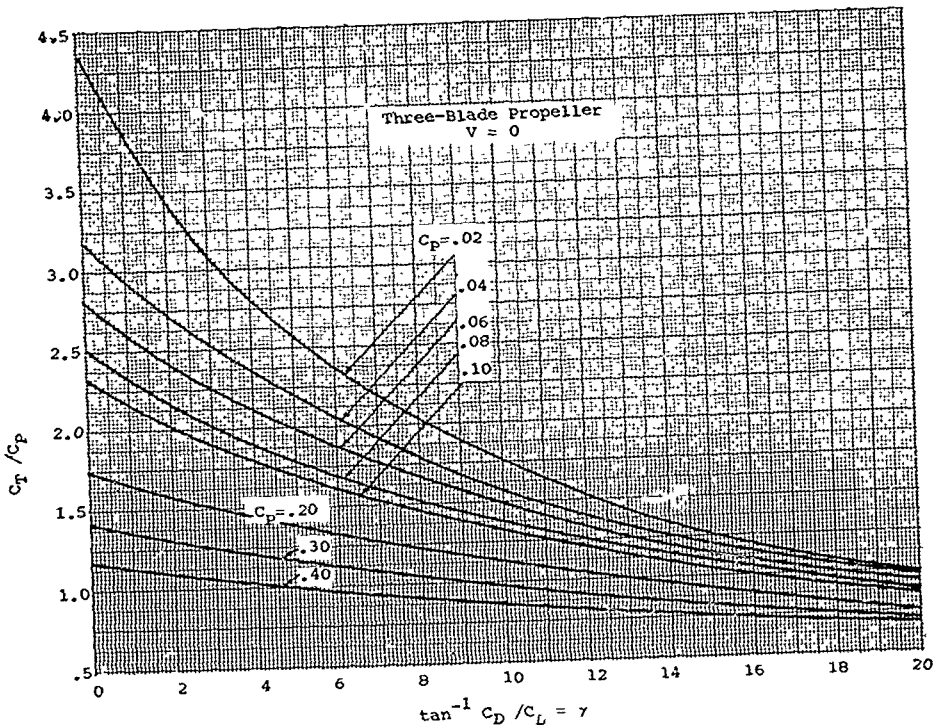


Figure 76. Propeller Thrust to Power Coefficient Ratio, Static Condition - Three Blades.

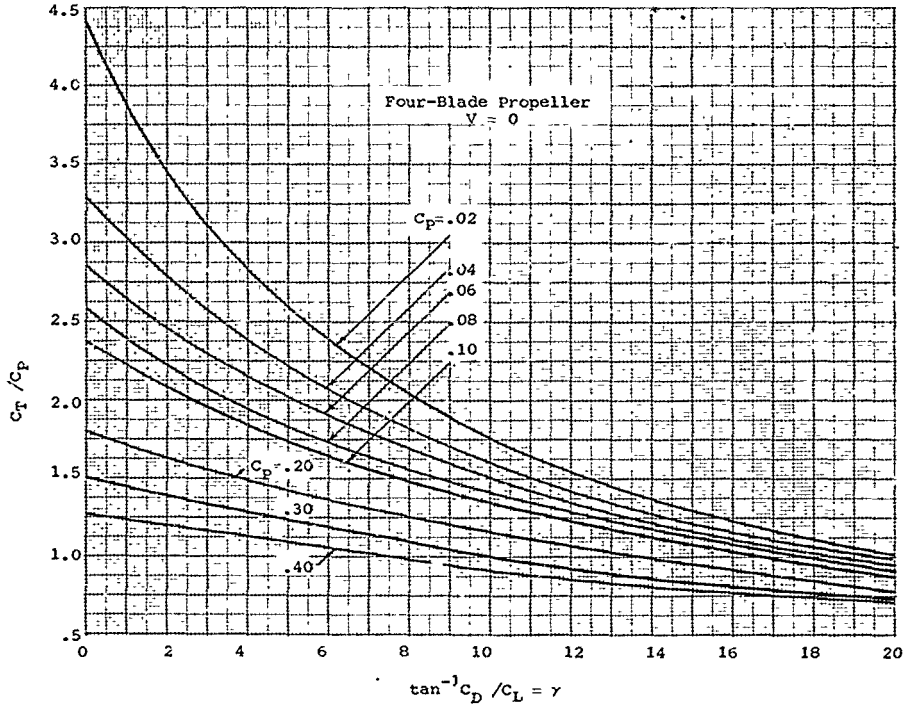


Figure 77. Propeller Thrust to Power Coefficient Ratio, Static Condition - Four Blades.

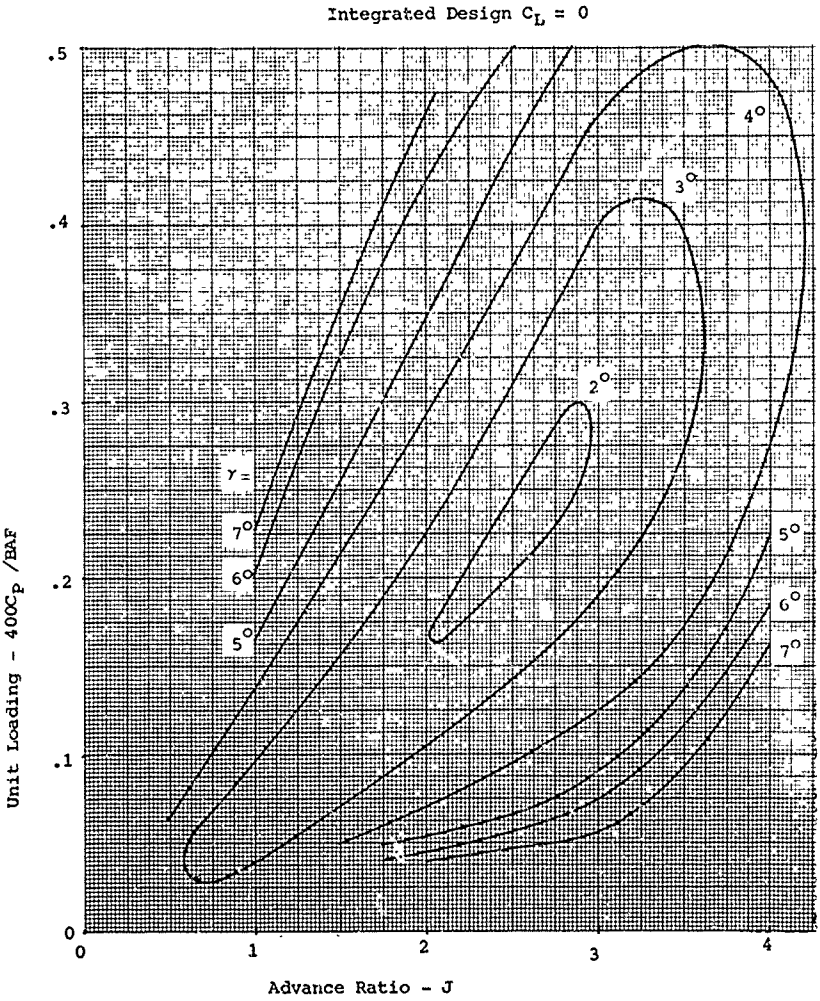


Figure 78. Propeller Unit Loading - $C_{Li}$ = 0.

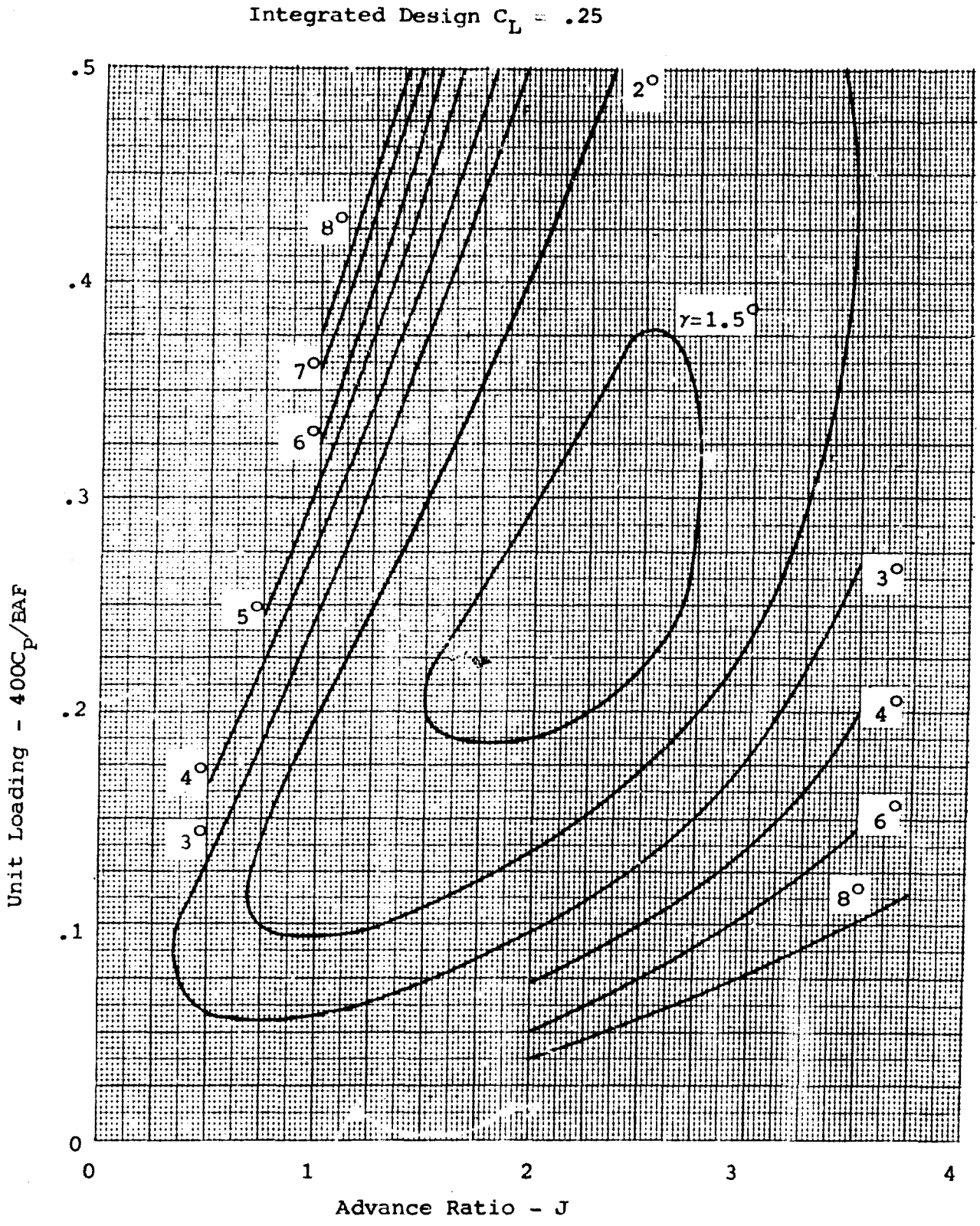


Figure 79. Propeller Unit Loading - $C_{Li}$ = .25.

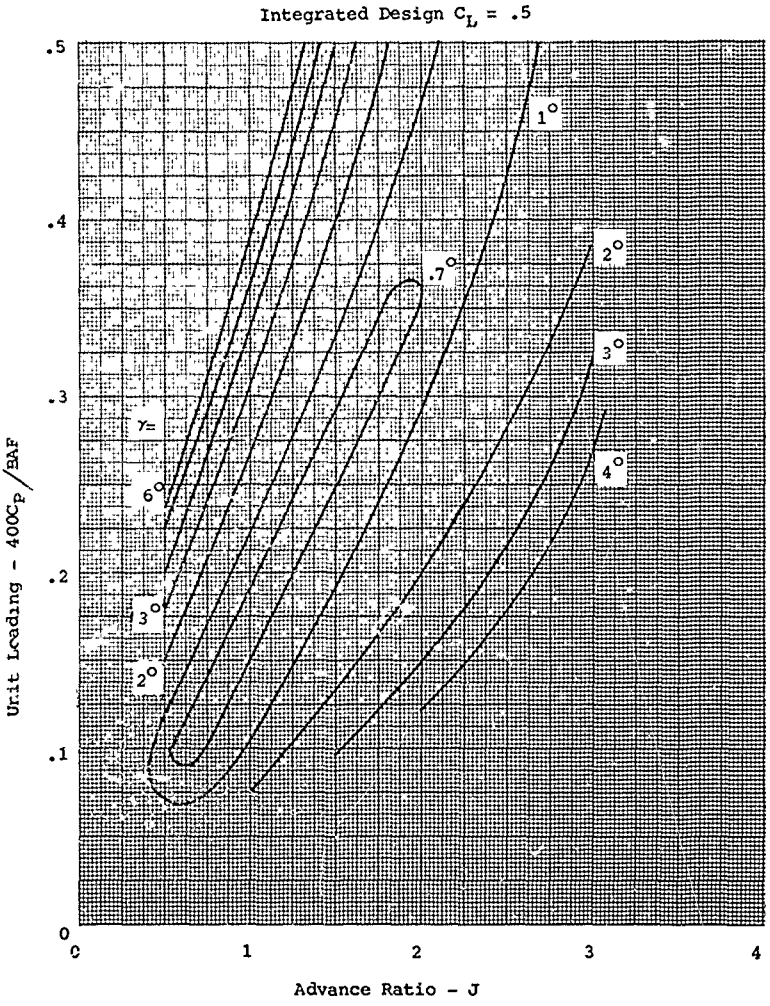


Figure 80. Propeller Unit Loading - $C_{L1}$ = .5.

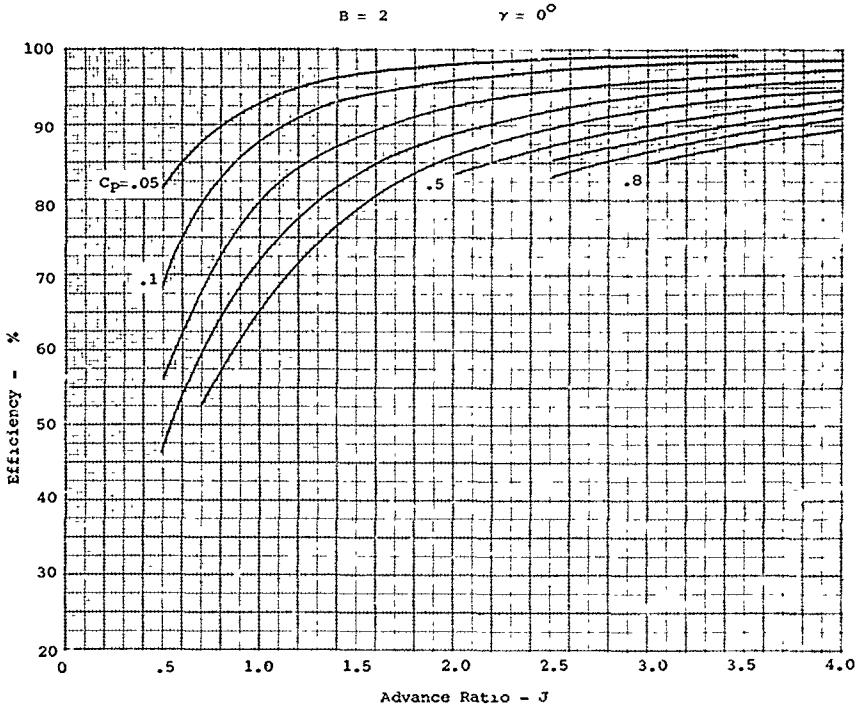


Figure 81. Propeller Efficiency, B = 2, $\gamma$ = 0°.

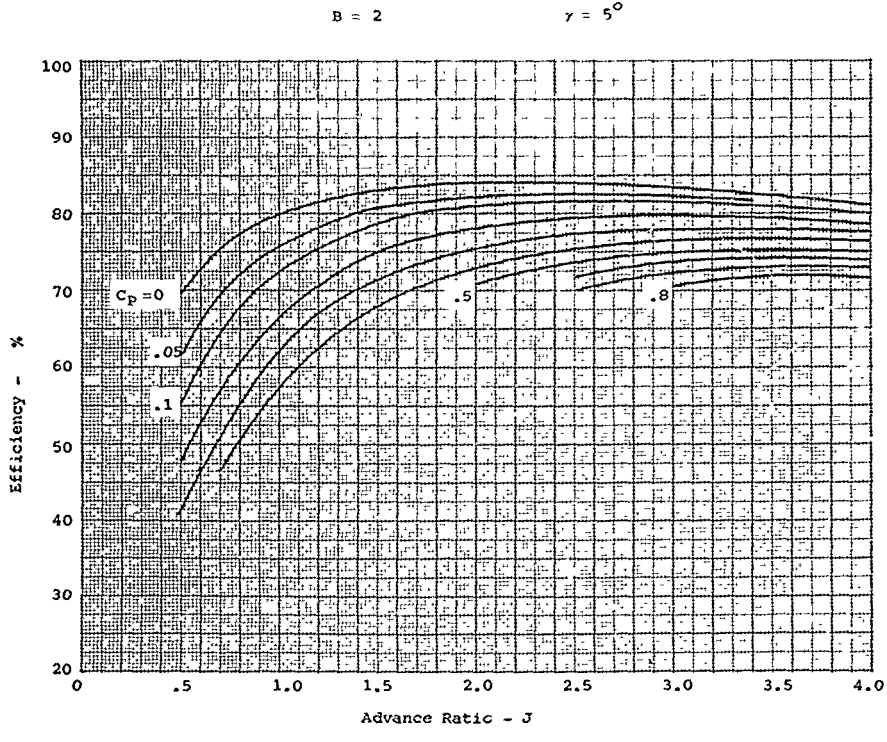


Figure 82. Propeller Efficiency, B = 2, γ = 5°.

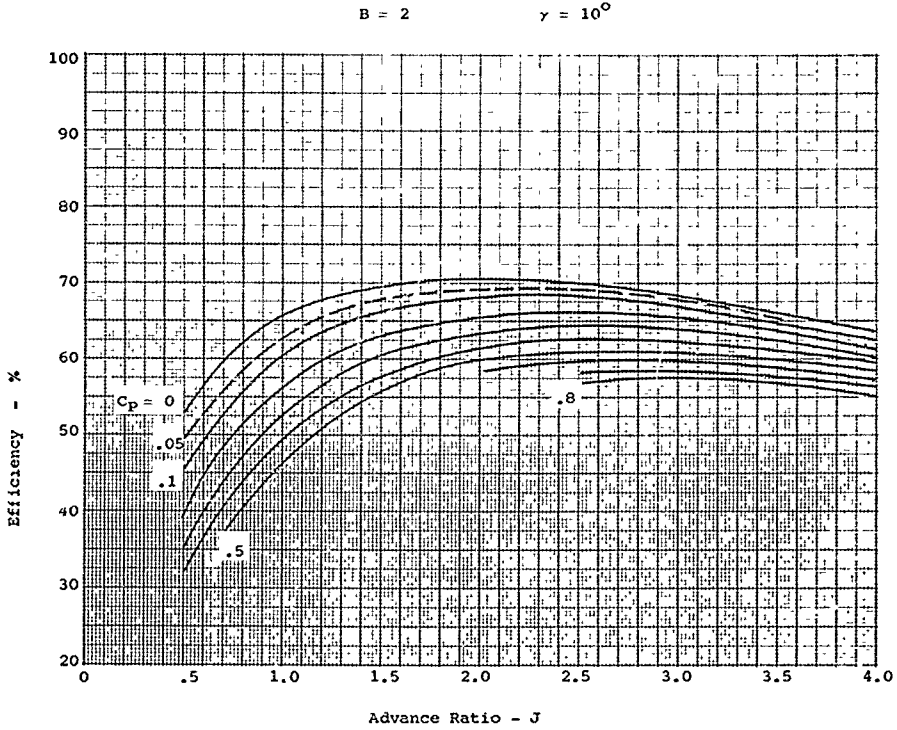


Figure 83. Propeller Efficiency B = 2, $\gamma = 10^{\circ}$.

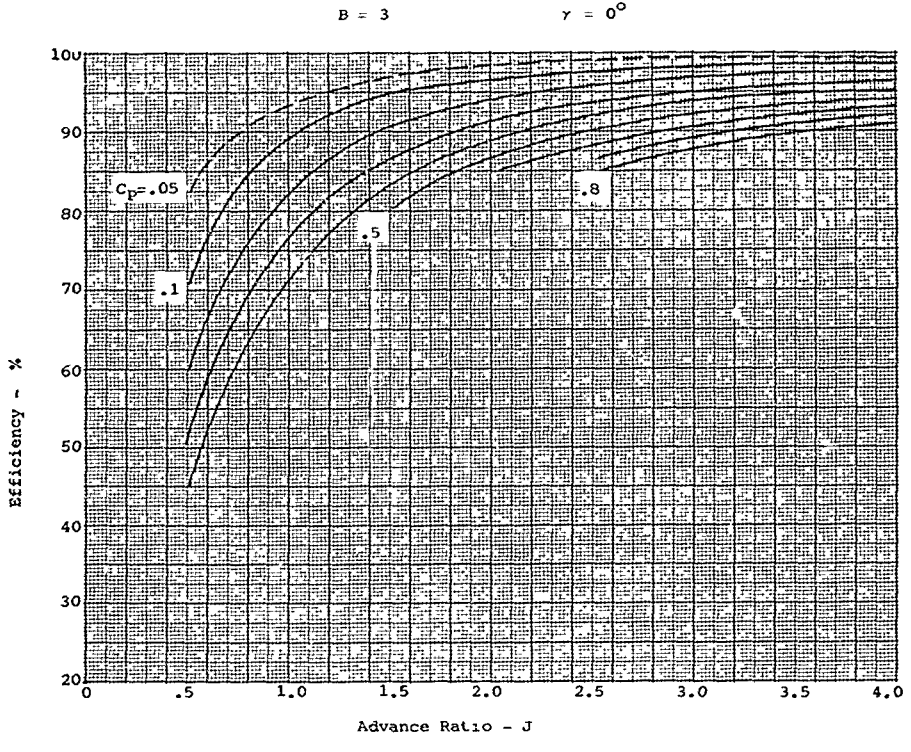


Figure 84. Propeller Efficiency, B = 3, $\gamma$ = 0.

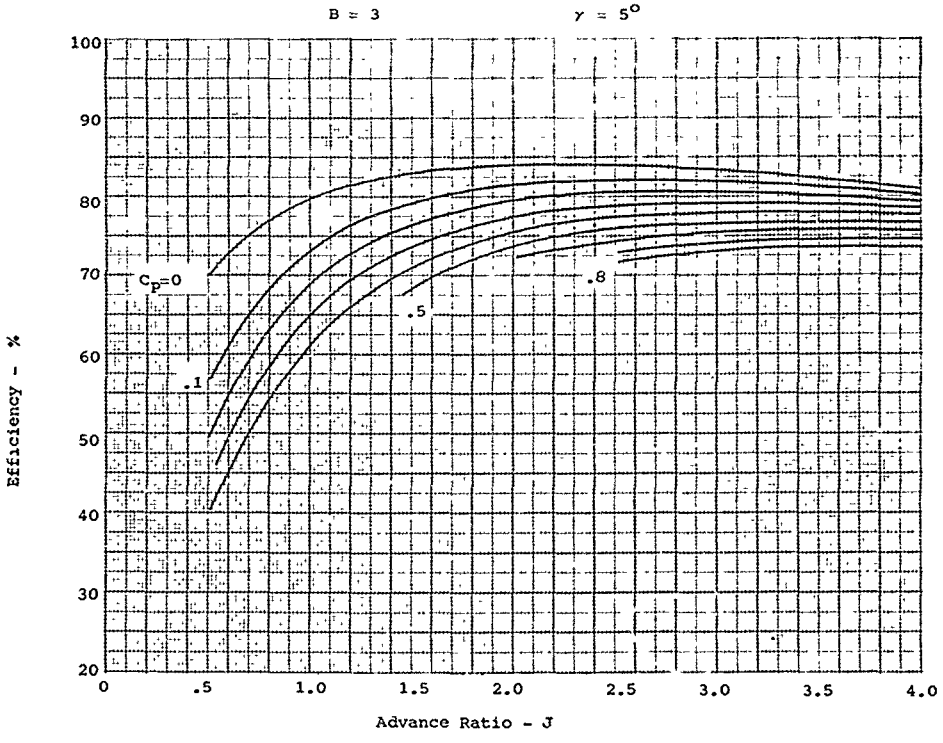


Figure 85. Propeller Efficiency, B = 3, $\gamma = 5^{\circ}$.

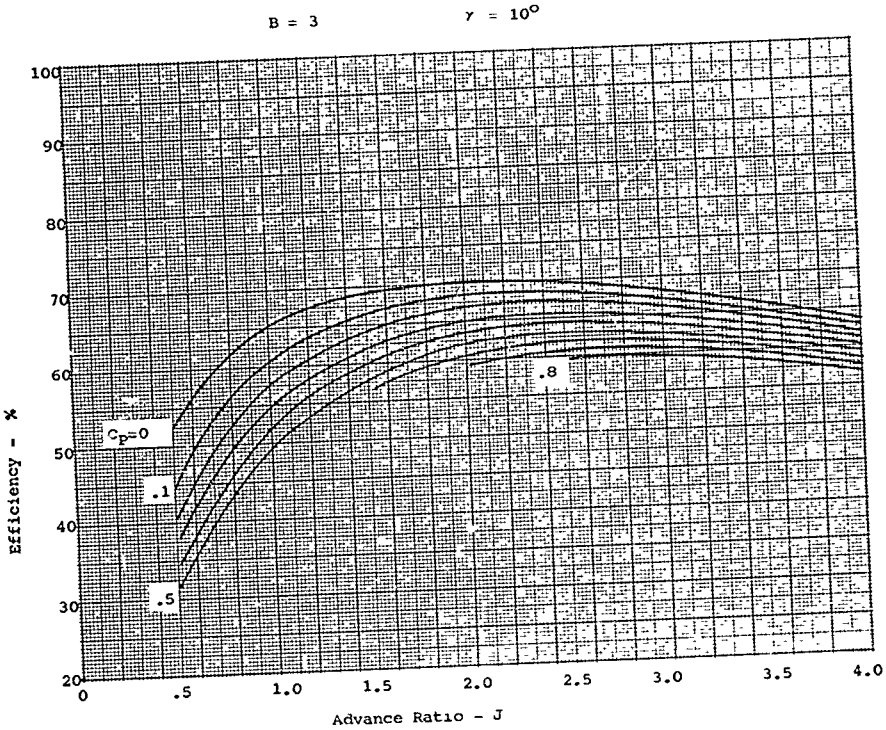


Figure 86. Propeller Efficiency, B = 3, $\gamma = 10^{\circ}$.

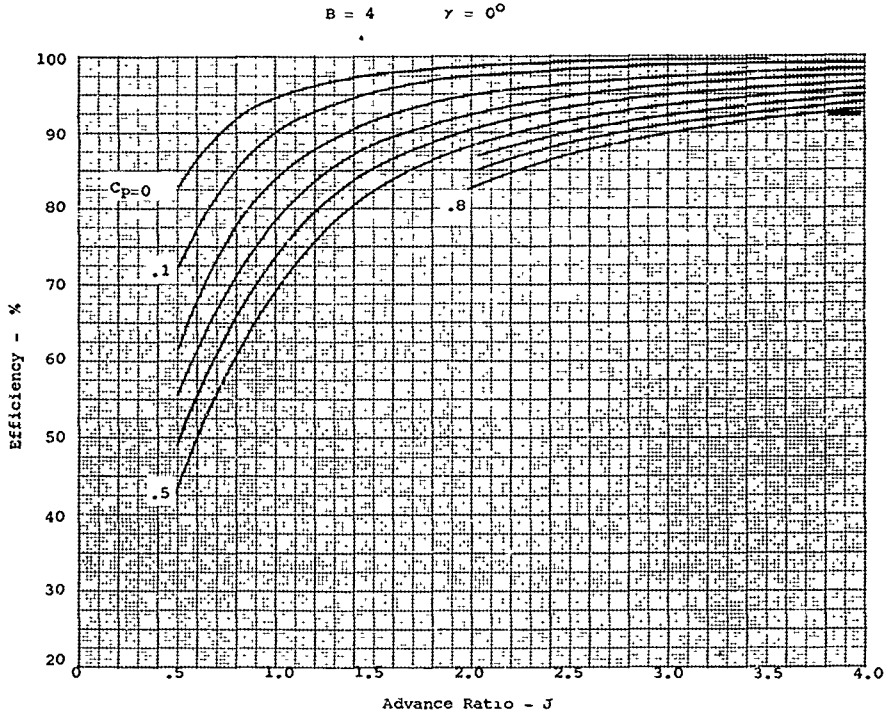


Figure 87. Propeller Efficiency, B = 4, $\gamma = 0^{\circ}$.

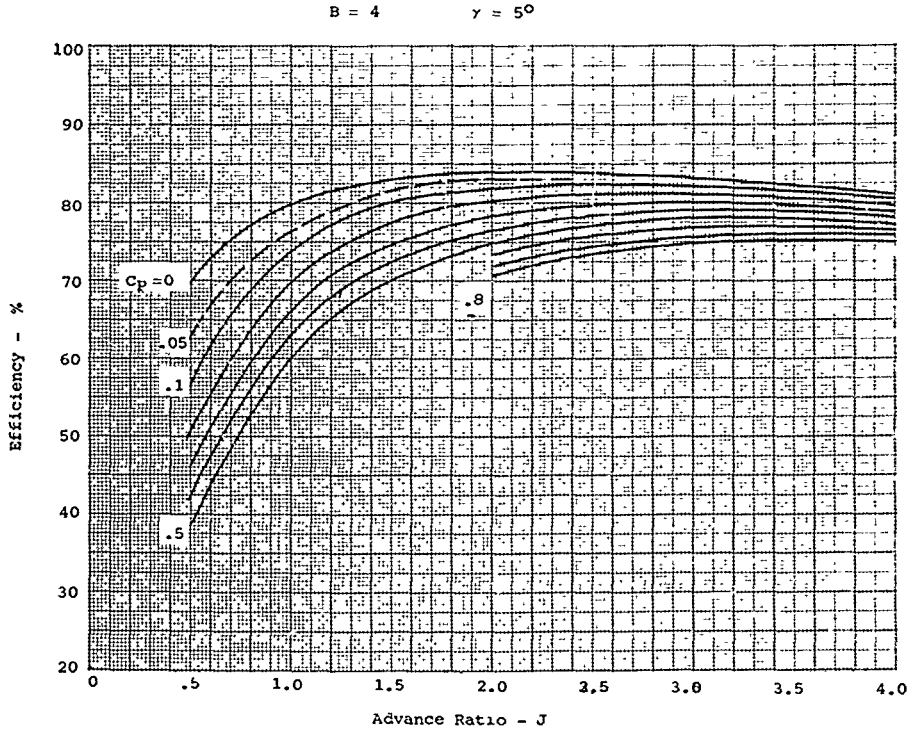


Figure 88. Propeller Efficiency, B = 4, $\gamma = 5^{\circ}$.

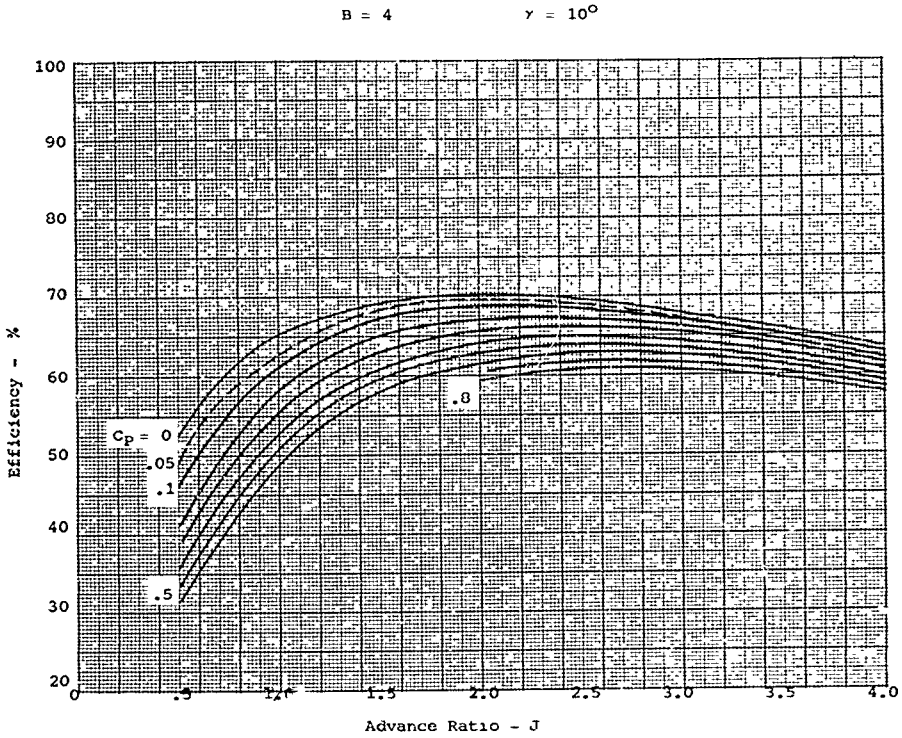


Figure 89. Propeller Efficiency, B = 4, $\gamma = 10^{\circ}$.

## OFF-DESIGN AND FAILURE CONDITIONS

When the propeller is operating at conditions other than normal, the blade sections are generally producing negative lift. When this occurs, the propeller is producing negative thrust and either is producing negative torque, is windmilling, or is absorbing engine power, depending on the mode of operation. Generally the propeller is intentionally operated at the negative thrust condition to reduce landing distances and to control the speed of the airplane. Under these conditions this characteristic of the propeller is desirable.

As the propeller can be a powerful means of generating negative thrust, it is often used to reduce landing roll distances. At touchdown, for instance, on a typical transport airplane, the negative thrust produced by a propeller can be as high as the positive static thrust at takeoff power. This high level of negative thrust decreases as the speed decreases and reaches a value of 30 to 40% of the takeoff thrust at the zero speed condition. The propeller operating at negative blade angles absorbs up to full engine power at these conditions.

At the approach condition, it is desirable to have the airplane operating at high drag so that the descent angle can be increased. For this condition the propeller is generally set at a relatively low pitch condition and is operating at a positive blade angle windmilling condition. The negative thrust produced by the propeller at this condition is low, but because the blade angle is not much below that required for positive thrust, an increase in power will give positive thrust with a small time delay. This is important from safety considerations.

Propellers have been operated at negative blade angles for developing high values of negative thrust for producing high rates of descent. For instance, it was demonstrated on a DC-4 airplane that with a level airplane and the propellers operating at a negative blade angle, a rate of descent of over 10,000 feet per minute could be obtained under full control. The propellers operating at this condition not only produce large values of negative thrust but also spoil the wing lift. Thus, if such a system were to be used, it would be imperative to have complete reliability in the pitch change mechanism to assure that positive blade angles are available prior to landing so that the wing would have its normal lift. Although the use of propellers operating at negative blade angles is very effective, the system was never operational because of safety considerations.

The use of dive brakes to reduce speed of fighter type airplanes operating in a dive imposed severe weight penalties. To reduce the weight penalties of a dive brake and also have

a more effective system, tests were made of propellers operating at the negative blade angle. These tests again confirmed the effectiveness of the propeller operating at negative blade angles for producing negative thrust. On one airplane, for instance, the negative thrust produced was equal to the weight of the airplane.

Unfortunately, the propeller operating at high values of negative thrust also produces a large and high-energy wake that tends to shake the airframe. In one case the energy in the propeller wake was so high the horizontal elevator was shaken off. This high-energy air in the propeller wake and safety considerations were sufficient to eliminate any further consideration of this dive brake concept.

In the case of an engine failure, the propeller is feathered to eliminate the high windmilling drag. Feathering is accomplished by increasing the blade angle to approximately 87 degrees at the 75 percent blade radius. At this angle the rotation is stopped and the drag of this system is a minimum. The feather angle for zero torque varies somewhat with speed, so that with turbine engines where rotational torque is low, it may be necessary to use a brake to stop rotation or use a control system that varies the blade angle automatically to prevent rotation.

## Malfunction Conditions

In the case of failures of the propeller control system, large values of negative thrust can be developed. This is especially true in the case of propellers installed on coupled turboprop engines. These engines can absorb large values of negative torque which will result in very high values of negative thrust. The level of negative thrust obtained increases with speed.

When a propeller is installed on a free-turbine engine, the problem of a malfunctioning control system is much less severe. However, because of low power absorption characteristics of this engine, the malfunctioning propeller may achieve a much higher rotational speed than in the case of the coupled engine, with the potential of blade failure at the higher speeds.

## Negative Thrust Propeller Calculations

A comparison of the positive and negative operating conditions of a typical blade section and the corresponding flow conditions are shown on Figure 90. In comparing the modes of operation, it is noted that the torque produced by the windmilling propeller increases with the lift/drag ratio and the

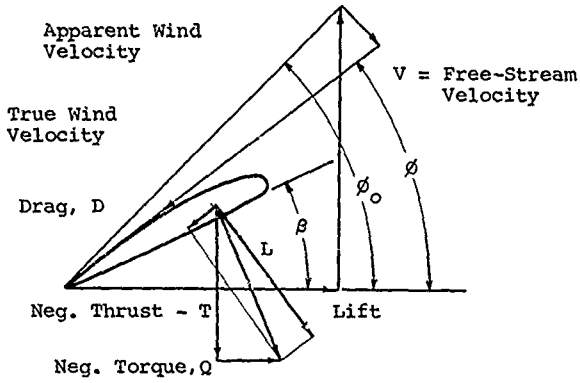


Propeller Section Operating at Negative Torque and Thrust

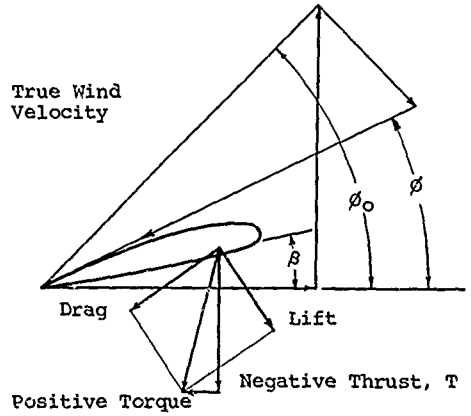


Propeller Section Operating at Positive Torque and Negative Thrust

Figure 90. Force and Velocity Diagrams for a Windmilling Propeller.

wind angle. At a given operating condition, it is possible for the blade to be operating in both the windmilling state and the positive torque condition while producing negative thrust. The actual torque of the propeller operating at this condition then depends on the integrated value of torque along the blade.

If the advance ratio of the propeller becomes negative or the combination of the advance and induced velocity is negative, the propeller can enter the vortex ring state. The propeller flow diagram for this condition is shown on Figure 91. The vortex ring state, generally very unstable, will occur in the descent condition.

When a propeller is operating at the negative thrust condition, the blade load distribution is far from the optimum. In certain cases the load distribution on the blade may be both positive and negative, with the total being negative. This type of load distribution will produce a nonrigid vortex system which has not been solved, and so it is not possible to find the induced velocity at each blade station. For this reason, strip analysis procedures are not useful for analyzing propellers operating at negative thrust conditions.

To find the performance of propellers operating at the negative thrust condition, it is therefore necessary to depend on test data and single-point techniques for converting the test data to the desired propeller. There is a considerable amount of test data on propellers operating at the negative thrust and positive advance ratio conditions; References 40 to 43. These data can be used to estimate the negative thrust with sufficient accuracy for most practical purposes, as the accuracy requirements are not as critical as in the normal flight conditions.

When using test data to find the performance of a given propeller operating at the negative thrust flight condition, the thrust and power coefficients are read directly from the test data knowing the advance ratio, blade angle, and blade number. If possible, the test data used for analysis should have been run for blades geometrically similar to the blade being analyzed. That is the blade chord, angle, and thickness ratio, and design $C_L$ distribution should be identical. Since this is unlikely, the data must be corrected to apply for the blade being considered.

One of the most complete sets of propeller negative thrust data was that of Reference 43; it covers tests of three- and four-bladed single-rotation propellers as well as tests of four-, six- and eight-bladed dual-rotation propellers. The tests reported in Reference 43 were run with blades using Clark Y sections of activity factor equal to 90 and 135. These blades were designated as the narrow and wide blades respectively. The

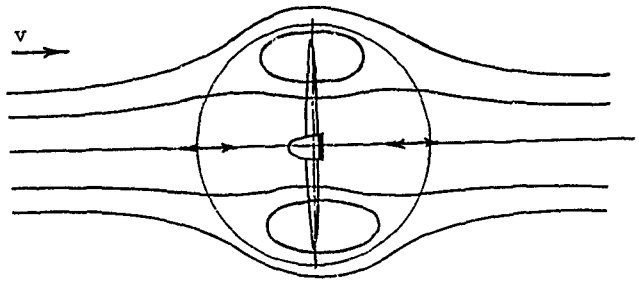


Flow Diagram Vortex Ring State

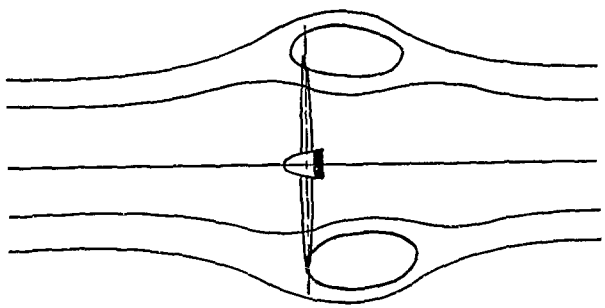

Flow Diagram End of Vortex Ring State

Figure 91. Flow Diagrams, Propeller in Vortex Ring State.

tests covered the negative thrust conditions at blade angles from 25 degrees to 125 degrees.

The data of References 41 through 43 can be used to determine the performance of propellers at off-design conditions with sufficient accuracy for most purposes. If, however, the propeller is to be used to produce negative thrust during approach or landing, the method will not have sufficient accuracy to properly set any blade angle stops. In this case it will be necessary to use model or flight test data to obtain the desired information.

To determine the characteristics of a new specified propeller at the negative thrust/positive advance ratio operating conditions, the following single-point procedures may be used.

Given:

Activity Factor AF, blade number B, advance ratio J, altitude and blade angle at 75% radius station $\beta$ s. The subscript s refers to the specified propeller and t refers to the propeller test data

Find:

$T_S$ and H.P.$_S$

Procedure:

1. From two-dimensional airfoil data for the proper section at 75% radius, find the angle of attack at zero lift for both the test and specified props.

2. Correct $\beta_s$ to $\beta_t$, $\beta_t = \beta_s + \alpha_t - \alpha_{os}$.

3. If $AF_S$ is between the higher and lower blade test, read $C_{T_t}$ and $C_{P_t}$ for both values of $AF_t$ and linearly interpolate to find $C_{T_S}$ and $C_{P_S}$.

4. If $AF_S$ is above or below $AF_t$, read $C_{T_S}$ and $C_{P_t}$ at $AF_t$ close to $AF_S$.

5. From item 4, correct $C_{Tt}$ and $C_{Pt}$ to $C_{T_S}$ and $C_{P_S}$ by multiplying by the factor $AF_S/AF_t$.

6. Knowing rpm, diameter, and density ratio, calculate $T_S$ or H.P.$_S$ from $C_{T_S}$ or $C_{P_S}$, steps 3 or 4.

Find blade angle required to absorb the power:

1. Calculate $C_{P_S}$ knowing diameter, power, density

ratio, and rpm.

2. Find $C_{pt} = C_{ps}\ AF_t/AF_s$.

3. Knowing advance ratio and $C_{pt}$, read $\beta_t$.

4. Read angle of zero lift $\alpha_{os}$ & $\alpha_{ot}$ as in step 1, case 1.

5. Find $\beta_s = \beta_t + \alpha_{os} - \alpha_{ot}$.

Feathered Propeller Performance

When an engine fails, the propeller will generate large values of negative thrust due to windmilling, especially if connected to a coupled turboprop engine. On multiengine aircraft this will cause large aircraft trim changes unless the propeller is promptly feathered. Even if large trim change were not obtained, it is desirable to feather the propeller to eliminate propeller and engine rotation and prevent possible further engine damage. Also, the feathered propeller has much less drag than either a locked or rotating propeller, so that the power required for flight is much reduced.

When the propeller is operating at blade angles near feather, part of the blade will be at a positive lift and part at negative lift. This lift distribution is far from the ideal case, so that the usual wing theory does not give satisfactory results for determining the induced angle of attack. For this reason, the strip theory does not yield satisfactory results when the propeller is operating near the feather condition, and it will be necessary to use test data to find the performance at this condition.

There is no available published data to determine the torque and thrust characteristics of a propeller at zero rotation and blade angles near feather. The only data available for finding the thrust and torque are unpublished data by NACA which was run in the 16-foot high-speed tunnel and data run for the Air Force in conjunction with the Douglas C-124B program. These data are presented on Figure 92 in terms of the thrust and torque coefficients $Q_c$ and $T_c$ for a range of blade angles at the 75% radius of 70 to 125 degrees. The coefficients $Q_c$ and $T_c$ are used, as the rotational speed is zero, and are defined as follows:

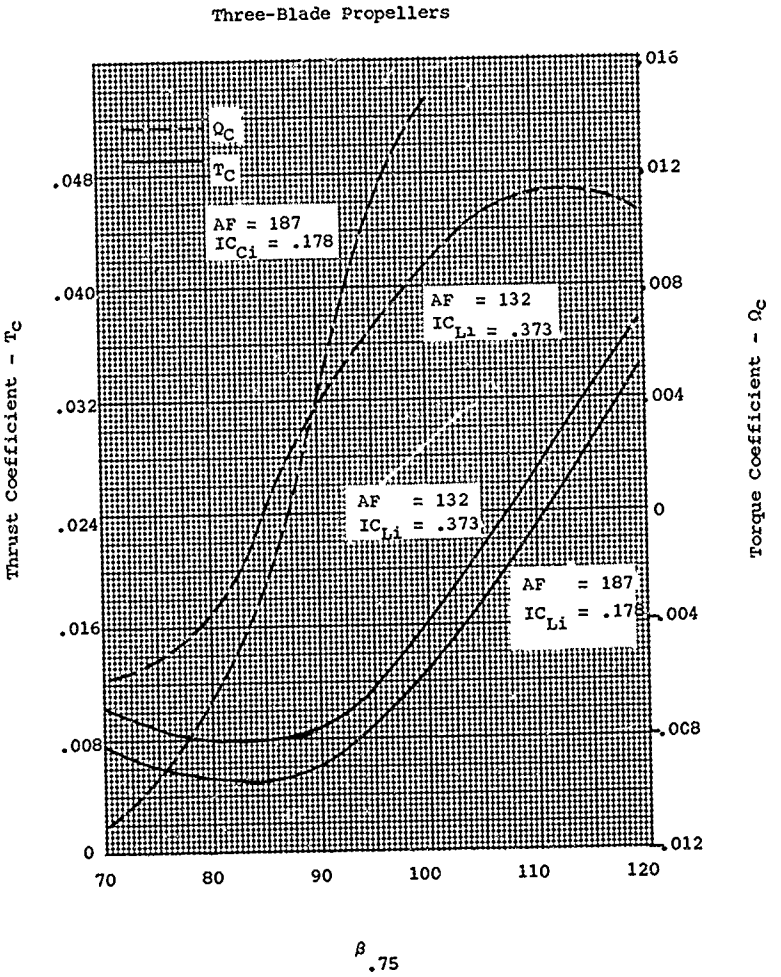


Figure 92. Propeller Performance at 0 Rotation.

$$Q_c = \frac{Q}{\rho V^2 D^3} = \frac{Q}{2qD^3} \quad (175)$$

$$T_c = \frac{T}{\rho V^2 D^2} = \frac{T}{2qD^2} \quad (176)$$

where $Q$ = propeller torque
$\rho$ = density ratio, slugs/cu ft
$V$ = free-stream velocity, ft/sec
$D$ = propeller diameter, ft
$T$ = thrust, lb
$q$ = dynamic pressure.

The data presented on Figure 92 are for three-bladed propellers having blades with activity factors of 132 and 182. The integrated design lift coefficient of the blades is .373 and .178 respectively. These data can be used to estimate the characteristics of other propellers operating at blade angles near feather by correcting the data for total solidity. Thus, using the subscripts t and s to denote the test and specified propellers respectively, the thrust and torque coefficients for a new specified propeller would be found from the equations

$$Q_{cs} = Q_{ct} \frac{B_s AF_s}{B_t AF_t} \quad (177)$$

$$T_{cs} = T_{ct} \frac{B_s AF_s}{B_t AF_t} \quad (178)$$

The test data corresponding the closest to the specified blade should be used in estimating the performance of the specified blade.

If more precise data is required than can be estimated from the above, it will be necessary to run wind tunnel tests with the actual or model propellers.

Feather Blade Angle

On reciprocating engines, a feather blade angle could be chosen so that no rotation would be encountered, as the breakaway torque of the engine was sufficient to lock the engine and prevent rotation. On free-turbine installations, the engine torque resisting rotation is low so that the propeller will tend to rotate at low speeds at certain flight conditions. To prevent this rotation, a propeller brake may be used, or the propeller can be equipped with a sensing system that changes

blade angle to seek zero rotation. The data given on Figure 92 and the correction of Equations (177) and (178) should be of sufficient accuracy to allow the design of either system.

Vortex Ring State

When VTOL airplanes and helicopters descend vertically with the propellers or rotors developing thrust, an unstable operating condition known as the vortex ring state is encountered. This condition will be found when the induced velocity produced is of the same order of magnitude as the descent velocity. The flow produced by the propeller or rotor operating in the vortex ring state is highly unstable and oscillatory in nature. The lift produced by the propeller actually decreases when operating at this condition even with increasing power and descent velocity (Reference 44).

Smoke pictures taken of a propeller operating in the vortex ring state showed the propeller generates a large "donut" of air in its plane. After a short period of time, this "donut" is shed from the propeller, after which another "donut" is formed. The period between the initial formation of the "donuts" is from 3 to 5 seconds and depends on the loading. This type of operation is extremely unstable and must be avoided with VTOL aircraft and helicopters.

Sufficient testing of propellers and helicopter rotors has been accomplished so that the conditions at which the vortex ring state are encountered can be identified. The region of operation where the vortex ring state is encountered is shown on Figure 93 and is a function of the rate of descent and disc loading. When the parameter $J_V/C_T^{\frac{1}{2}}$ is between -.2 and approximately -1.5, the rotor will be operating in the vortex ring state. Above $J_V/C_T^{\frac{1}{2}}$ of -1.5, the windmill brake state of operation is encountered and the flow is again stable.

The parameter $J_V/C_T^{\frac{1}{2}}$ can be written in terms of the disc loading or

$$\frac{J_V}{C_T^{\frac{1}{2}}} = .05502 \frac{V_V}{\left(\frac{T}{A_p \sigma}\right)^{\frac{1}{2}}} \qquad (179)$$

Note the advance ratio $J_V$ and the velocity $V_V$ are positive when opposite to the thrust.

The limit or start of the vortex ring state can be plotted in terms of the rate of descent, Figure 94, and shows that if high vertical rates are required, the disc loading should be higher than used with normal helicopters.

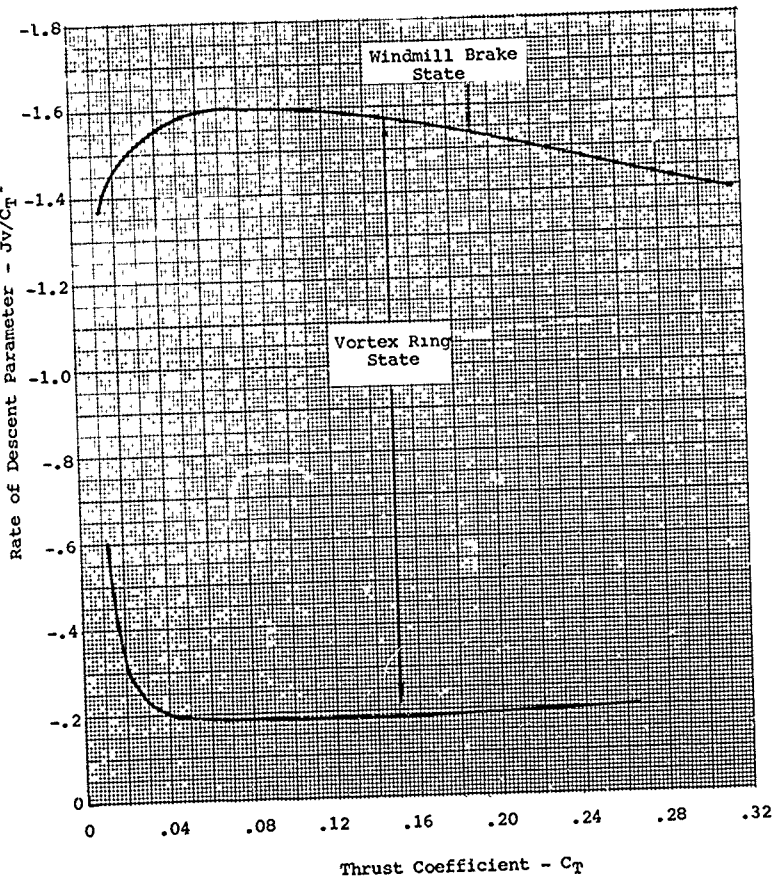


Figure 93. Vortex Ring and Windmill Brake State - Propellers and Rotors.

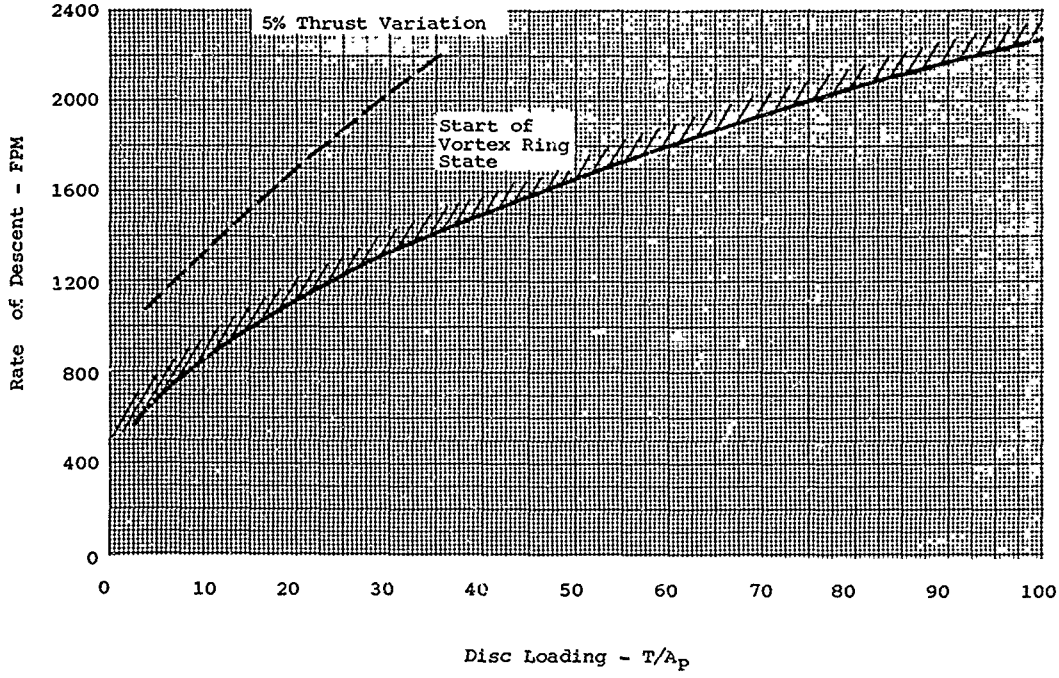


Figure 94. Rate of Descent for a Propeller for Start of Vortex Ring State.

Performance at Shaft Angles Above Zero

Propellers installed on conventional aircraft seldom operate at shaft angles in excess of 20 degrees. Although the forces and moments produced by the propeller at these conditions are important, especially in terms of aircraft stability and the blade structure, precise information was not required until the advent of VTOL airplanes. In the case of tilt-wing or tilt-propeller VTOL airplanes, propeller operation is encountered at angles up to 95 to 100 degrees. At these high angles of attack all the forces and moments developed are of primary import to find the performance, stability, and control of the airplane. See Reference 45 for test data.

The force and moment produced by a propeller operating at a shaft angle of attack above zero degrees are shown on Figure 95 . It will be noted from this figure that in addition to the thrust force and torque, an in-plane force, a normal force, and a pitch and yawing moment are obtained. The normal force and moment produced by the propeller become significant at the higher shaft angles and must be accurately evaluated.

When the propeller is operating at a shaft angle of attack with respect to the free-stream velocity vector, the flow into the disc is not symmetrical and the blade angle is effectively increasing and decreasing as the blade rotates. This causes an increase and decrease in the resulting blade force which may be resolved into the force and moment coefficients shown on Figure 96 . The side force and moments generated are believed to be produced due to the lag of the blade forces with changes in angle of attack.

Although thrust and the normal forces on each blade increase and decrease once during each revolution, the total forces remain nearly constant at a given flight condition for propellers with three or more blades. The forces produced by a two-bladedpropeller become periodic, increasing and decreasing for each revolution.

The propeller thrust and normal forces produced when operating at a shaft angle of attack can be reduced to coefficients similar to the lift and drag coefficients of a wing instead of the usual propeller thrust and normal force coefficients. These coefficients become

$$C_{L_p} = \frac{T \sin A + N \cos A}{q A_p} \qquad (180)$$

and

$$C_{x_p} = \frac{T \cos A - N \sin A}{q A_p} \qquad (181)$$

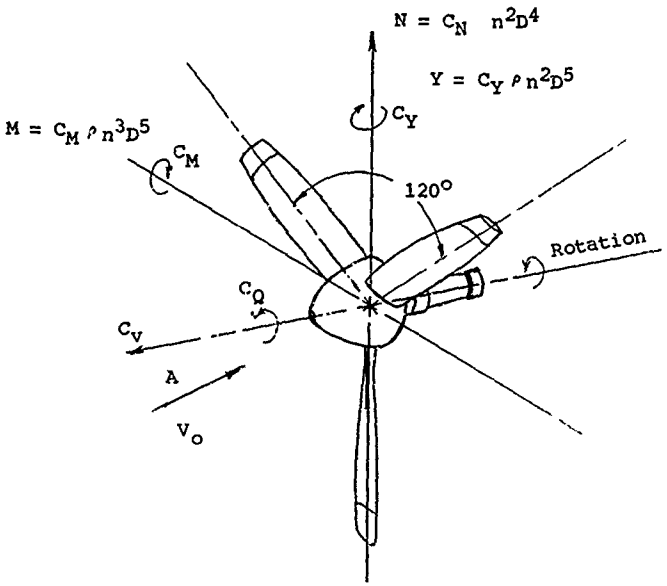


Y = Yawing Moment

M = Pitching Moment

N = Normal Force

Q = Torque - Shaft

S = Side Force

T = Thrust

A = Shaft Angle of Attack

Figure 95. Propeller Force and Moment Diagram, Shaft Angle Greater Than Zero.

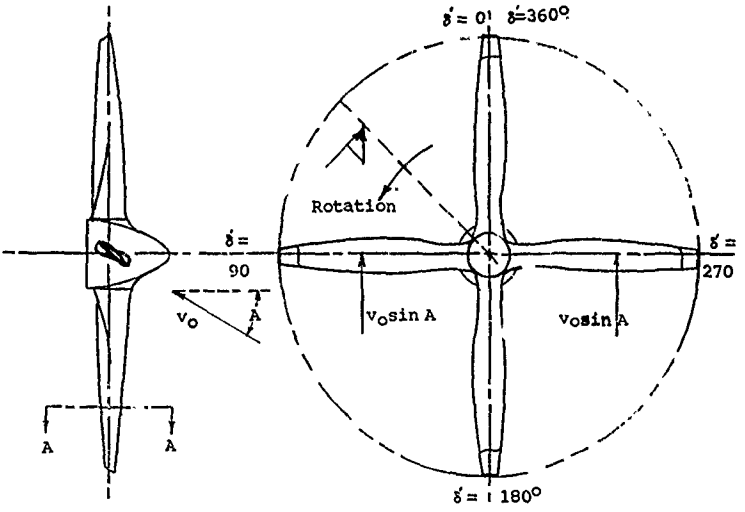


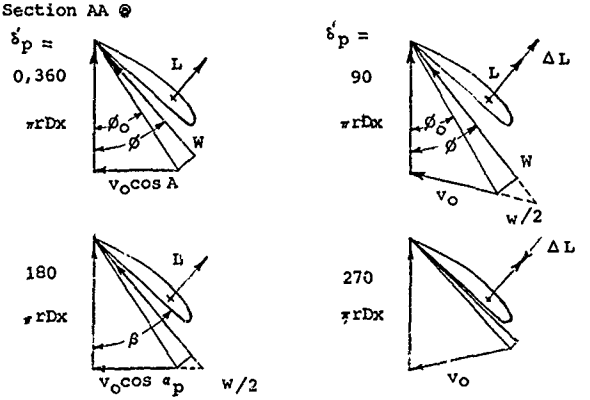


Figure 96. Propeller Velocity Diagram at Shaft Angles Above Zero.

where $T$ = shaft thrust
$N$ = normal force
$q$ = dynamic pressure = $\frac{1}{2}\rho V_o^2$
$A_p$ = disc area
$A$ = shaft angle of attack.

When the combined coefficients are plotted as a function of angle of attack at a fixed power coefficient and advance ratio, the results resemble that of an airfoil, Figure 96. From Figure 96 it is noted that $C_{Lp}$ is a straight line up to very high angles of attack, without encountering a sharp force break. The axial force coefficient remains positive with changes of angle of attack.

Method of Calculation - Shaft Angle > 0

Strip analysis methods and data may again be used to calculate the forces and moments produced by a propeller operating at a shaft angle of attack above zero. At this condition the forces and moments must be integrated as a function of blade azimuth position as well as blade station due to the variation of the effective blade angle with rotation.

Consider a propeller operating at a shaft angle of attack A. The free-stream velocity is $V_o$, the rotational velocity at any blade station x is $\pi nDx$, and the blade angle relative to the disc is constant. When the blade is at the vertical position, the azimuth angle $\delta'$ is 0 or 360 degrees. As the blade rotates, the angle $\delta'$ is 90 degrees at the horizontal position on the down stroke and 270 degrees on the up stroke. From Figure 97, it will be noted that the apparent resultant velocity at a given blade station $W_o$ increases to a maximum at 90 degrees and decreases to a minimum at 270 degrees. The section angle of attack has the same variation as the blade rotates through the angle $\delta'$ from 0 to 360 degrees.

The lift and drag of each blade section with the corresponding thrust and torque vary in the same manner as the resultant velocity and angle of attack as the propeller rotates. Thus, to find the total forces and moments, the section lift and drag forces must be integrated over a complete revolution.

Since the thrust and torque forces and moments lie in the plane of the propeller disc, Equations (46) and (50) developed for the zero angle case may be used to find $dC_Q$ and $dC_T$ at any blade position $\delta'$. To use these equations for the case where the propeller shaft angle is other than zero, it is necessary to establish an effective free-stream velocity and advance ratio. The effective velocity and advance ratio vary with blade position $\delta'$ and are used in place of the actual free-stream

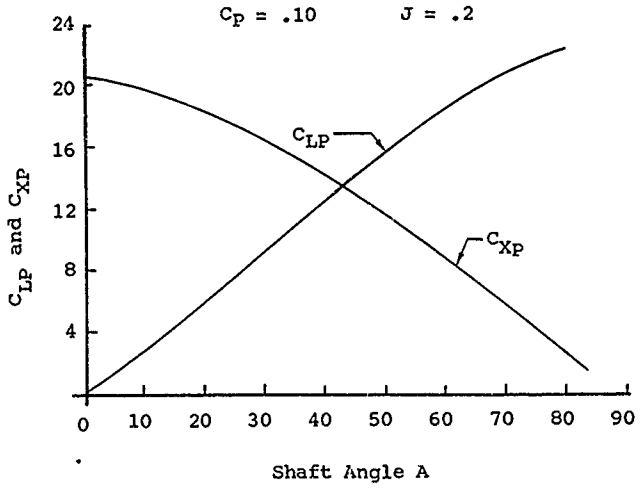


Figure 97. Propeller Total Lift and Thrust Force, A = 0 to 90°.

velocity and advance ratio in Equations (46) and (50).

To find the lift and drag forces at a blade station, the apparent velocity component normal to the blade centerline must be known. This velocity is made up of the rotational component, the free-stream velocity component normal to the blade centerline, and the induced component. At the blade position $\delta'$ equal to 0 degrees, the effective velocity is equal to

$$V_e = V_o \cos A \tag{182}$$

where $\delta' = 90$ degrees

$$V_e = V_o \tag{183}$$

At all other blade positions, the effective velocity is found from the equation

$$V_e = V_o \sqrt{\cos^2 A + \sin^2 A \sin^2 \delta'} \tag{184}$$

The corresponding effective advance ratio is

$$J_e = \frac{\pi V_e}{\pi nD + V_o \sin A \sin \delta'} \tag{185}$$

and

$$\tan \phi_o = \frac{V_e}{\pi nDx + V_o \sin A \sin \delta'} \tag{186}$$

where $J_e$ = the effective advance ratio
$V_o$ = the free-stream velocity - ft/sec
$A$ = shaft angle of attack - deg
$\delta'$ = blade azimuth position
$x$ = fractional radius
$n$ = rotational speed - rps
$D$ = diameter - ft

The true wind angle at any blade position is equal to

$$\phi = \tan^{-1} \frac{V_e + w/2}{\pi nDx + V_o \sin A \sin \delta'} \tag{187}$$

where $w/2$ = the induced velocity at the blade position.

It will also be noted from Figure 97 that the apparent wind velocity W at any station is

$$W = \frac{V_e + w/2}{\sin \phi} - \frac{w}{2} \sin \phi \qquad (188)$$

Unlike the zero shaft angle case where the propeller can be considered to have a rigid wake, the strength of the shed vortices is continuously increasing and decreasing as the blade rotates. For this reason, the induced velocity is not the same as would be calculated using $J_e$, assuming steady-state conditions. Also, as the propeller is producing a lift force normal to the free stream, the vortices will no longer be parallel to the shaft as a result of the downwash velocity.

Although there is no solution available for calculating the induced velocity for the case when the shaft angle is greater than zero, engineering approximations are available that give satisfactory results at angles up to approximately 50 degrees. From Figure 97, it will be noted that the average angle of attack and apparent velocity are approximately equal to those at $\delta' = 0$ and 180 degrees. Since the induced velocity is made up of the effects of all the conditions in the wake from the propeller disc to infinity, to the first approximation the induced velocity at any blade position should be based on the average conditions. With this approximation, the induced velocity is calculated at the effective advance ratio at $\delta' = 0$ degrees using the equation

$$J_e \text{ @ } \delta' = 0 = \frac{V_o \cos A}{nD} \qquad (189)$$

The induced velocity is found at the advance ratio noted above using the same procedure outlined for the case where $A = 0$.

At each blade station and blade position, the differential thrust and torque coefficients are thus found from the equations

$$C_Q = \int_0^{2\pi} \int_0^1 C_L Z \left(1 + \frac{\tan \gamma}{\tan \phi}\right) dx \, d\delta' \qquad (190)$$

$$C_T = \int_0^{2\pi} \int_0^1 C_L \frac{2Z}{x} (\cot \phi - \tan \gamma) \, dx \, d\delta' \qquad (191)$$

When the propeller is operating at a shaft angle of attack, it is noted from Figure 97 that the lift increases over the average at $\delta' = 0$ and 180 degrees on the down-going blade. Also, as the blade returns to the vertical position, the lift decreases. Thus the total force on one side of the disc is greater than the other and a yaw moment is produced. At high angles, this moment can be high and must be considered in control analysis of any airplane.

This moment can be found from the Equation (192) which is derived in the same manner as Equations (190) and (191).

$$C_Y = \int_0^{2\pi} \int_0^1 \sigma C_L Z (\cot \phi - \tan \gamma) dx \, d\delta' \qquad (192)$$

$$C_Y = \frac{V}{\rho n^2 D^5} \qquad (193)$$

Also from Figure 97, it will be noted that the excessive lift produced by the down-going blade adds to the like decrement of lift of the up-going blade to give the normal force in the plane of the propeller. This force may be found from Equation (194), which is derived in the same manner as Equation (189). Thus,

$$C_N = \int_0^{2\pi} \int_0^1 \sigma C_L Z \frac{2}{\pi} \left(1 + \frac{\tan \gamma}{\tan \phi}\right) dx \, d\delta' \qquad (194)$$

where $$C_N = \frac{N}{\rho n^2 D^5} \qquad (195)$$

Both Equations (194) and (195) are solved in the same manner as the thrust and torque equations for the case where the shaft angle is at an angle of attack A. That is, at each blade position, the effective advance ratio $J_e$ is found for calculating Z and the inflow velocity is determined at $J_e$ at $\delta' = 0$.

In addition to the thrust, torque, normal force, and the yawing moment, the propeller produces a side force and a pitch-up moment when operating at an angle of attack. The pitch-up moment is caused by the induced up-wash velocity in the propeller plane. This moment and force are small at A angles below 30 degrees. At angles above this, the moment must be determined by either test or procedures developed for helicopters.

## ACCURACY OF ANALYSIS METHODS

The methods and data presented for calculating the performance of propellers are based on a combination of theoretical and empirical data arranged so that the performance can be calculated for any propeller operating at any flight condition. The methods and data are valuable to the designer only if the results are of sufficient accuracy to allow for the selection of the optimum propeller for a given airplane. With accurate drag predictions of the airplane, either from wind tunnel data or standard prediction techniques, the propeller performance data must be of sufficient accuracy to predict airplane performance within the guarantee limits.

The direct measurement of the performance of propellers on an airplane is complicated by the difficulty of measuring thrust, power, and the proper free-stream velocity. Difficulty is also encountered in accurately determining the velocity distribution in the plane of the propeller disc. Since the velocity at which the blade sections are operating is not exactly known, the results cannot be compared accurately with the calculated performance results. Thus, direct propeller testing on aircraft is not used for assessing propeller performance.

To determine the accuracy of propeller performance calculations, comparisons are made with wind tunnel test data. The performance of the propellers tested is calculated for the same set of operating conditions as were tested, and the results are compared.

The performance was calculated using the method and data of the vortex theory of strip analysis and the two-dimensional airfoil data presented in Appendix II, Volume III. The wind tunnel data used for the evaluation is presented in References 46 to 52. The test data used for the comparisons were run in the 8-foot and 16-foot high-speed Langley wind tunnels during the period of 1945 to 1950. The test data was run with two-bladed 4-foot and 10-foot-diameter propellers with blades varying in thickness ratio, integrated design lift coefficient, and solidity. The design lift coefficients varied from zero to .5, and the thickness ratios varied from .03 to .12 at the 75% blade station.

The system for identifying the blades tested and their characteristics is illustrated by the following example. Blade No. 10-3-08-03 is 10 feet in diameter, has a design $C_L$ of .3, a thickness ratio of .08, and a solidity of .03, all at the 75% blade station. This system is very useful for identifying the blades tested.

The blades were tested at forward Mach numbers from .3 to .925. Several of the blades were tested in both the 8-foot and

16-foot high-speed wind tunnels, and the results were identical for blades of the same geometric design. The effects of wind tunnel walls on the results are also considered to be minimal. As the tests of the 4-foot-diameter propeller agree with the results of the 10-foot-diameter propeller, the data reported for both diameters is considered to be representative of full-scale results.

References 46 to 51 present force test and section thrust coefficient test data over the range of operating conditions. Thus, systematic propeller tests showing the variation of blade loading with blade station are available for evaluating the accuracy of the calculated results. On Figures 98 to 107, the thrust loading as measured is compared with the value as calculated using strip analysis procedures. From Figures 98 to 106, it will be noted that the load distribution as calculated by strip analysis corresponds closely to that measured at Mach numbers from .35 to .6. It will be noted that the correlation of the efficiency as calculated and measured at these conditions is also good. As the Mach number is increased above 0.6, the correlation between the test and calculated values is generally quite good, although the accuracy is poorer than at the lower speed operating conditions. The shape of the curves is, in general, the same as the shape measured in the wind tunnel with the exception of a few stations where there may have been some difficulty with the pressure measurement deviations. At forward Mach numbers of .8 and .925, the accuracy o the results further deteriorates. However, the overall s ape of the curves seems to be nearly the same.

On Figure 108, the variation of propeller efficiency with advance ratio is shown for test and calculated results. It will be noted that the accuracy of the data is within 1% over a large portion of the range of operation. At very high loadings corresponding to the advance ratio conditions, the deviation in performance is as high as 7%. This change in performance could be caused by optimistic drag values at the higher lift coefficient.

On Figures 109 to 119, the results are shown of the comparison of the test and calculated performance for the 10-(3)(05)-045 and the 10-(3)(12)-03 blades. The comparison is given as a function of power coefficient and advance ratio at either a fixed rotational speed or a fixed Mach number.

For the 10-(3)(05)-(045) blade, the calculated performance agrees closely at all advance ratios above 1.0, with the test data including those conditions up to forward Mach number of 0.603. At a forward Mach number of 0.65, the calculated data is 4% higher than test. At this condition the tip Mach number equals 1.13, and it is possible that the losses due to compressibility are higher than calculated.

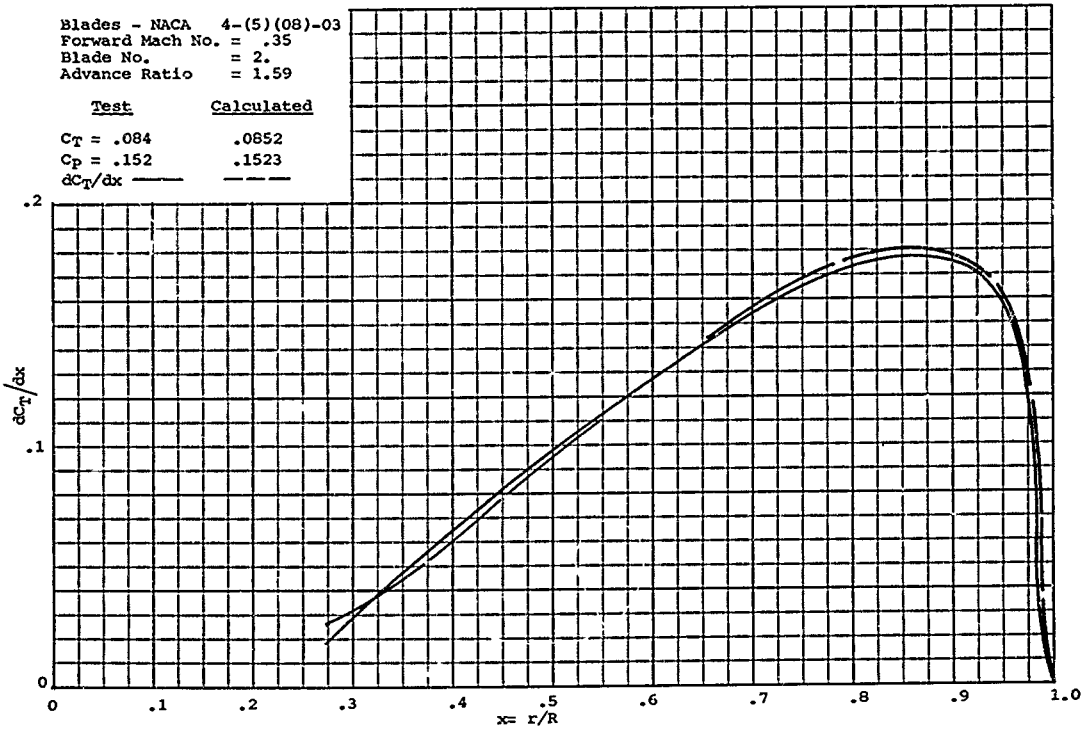


Figure 98. Comparison of Test and Calculated Propeller Loading, M = .35.

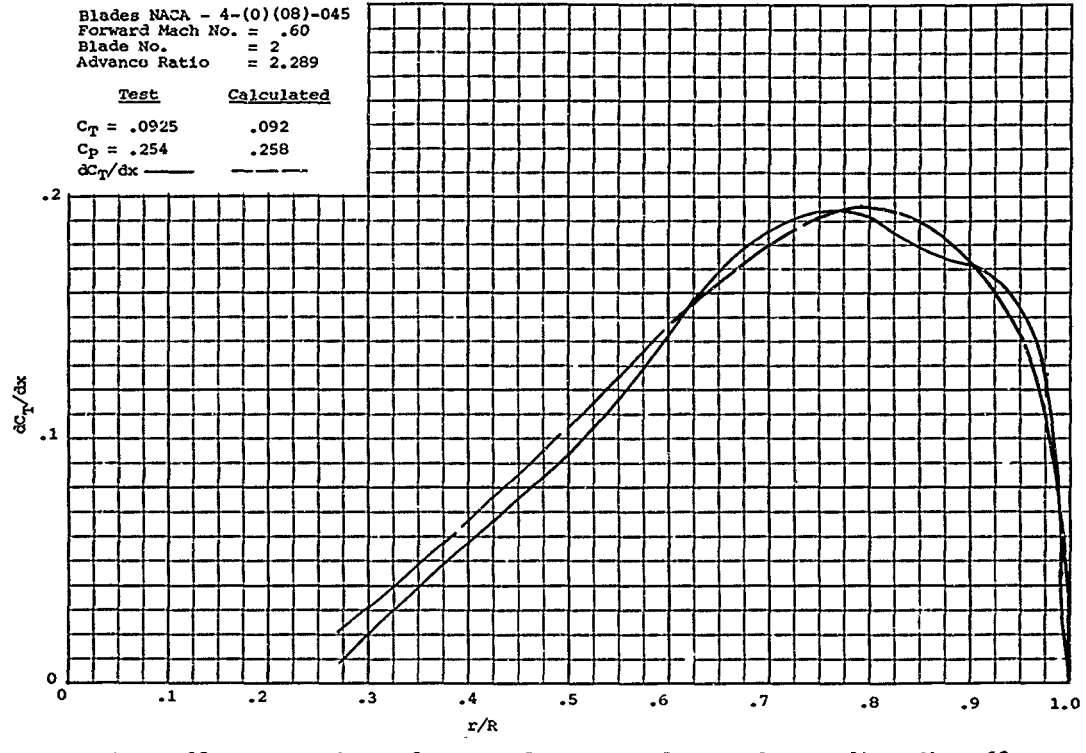


Figure 99. Comparison of Test and Calculated Propeller Loading, M = .60.

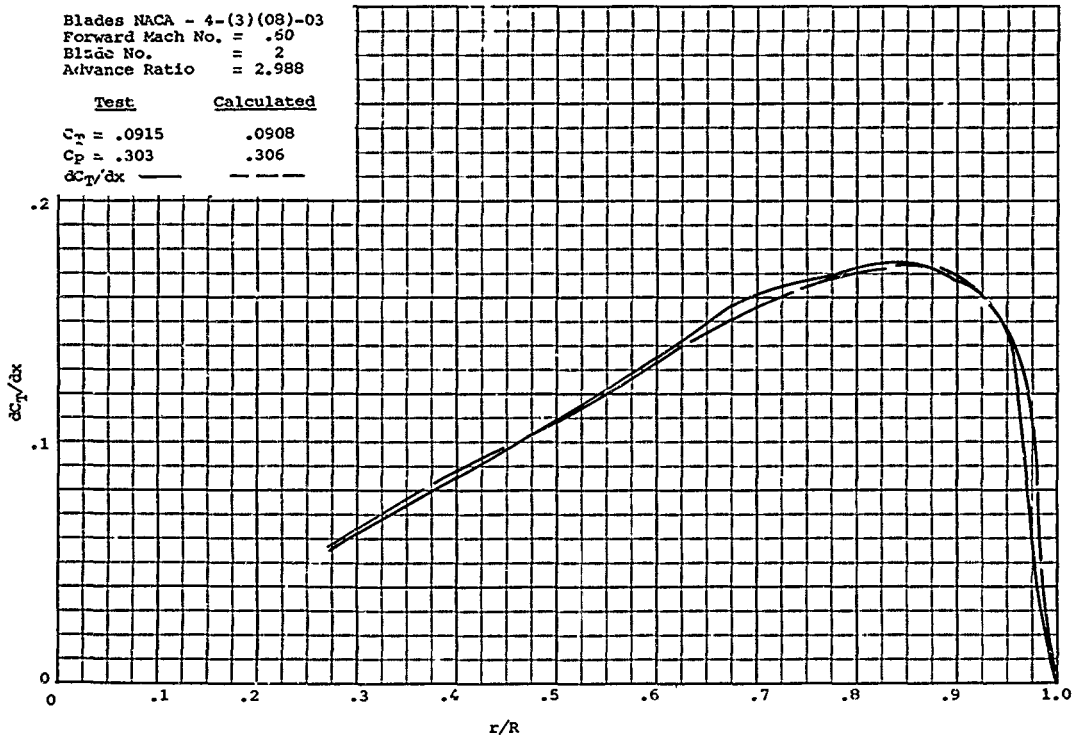


Figure 100. Comparison of Test and Calculated Propeller Loading, M = .60.

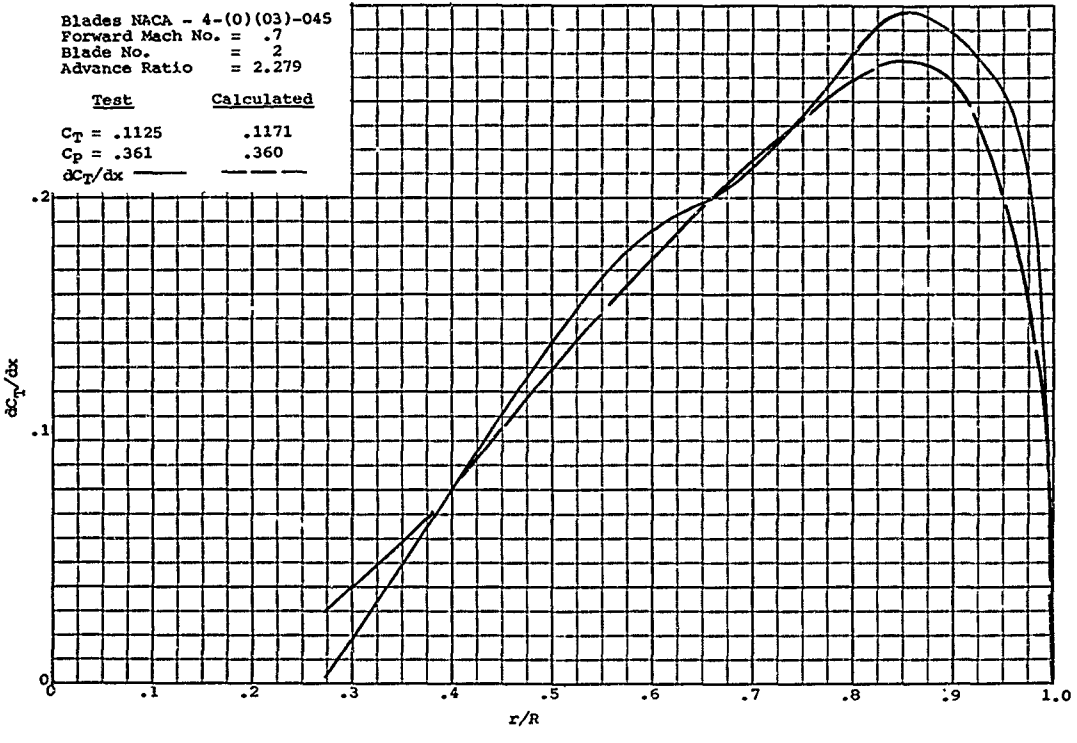


Figure 101. Comparison of Test and Calculated Propeller Loading, M = .70.

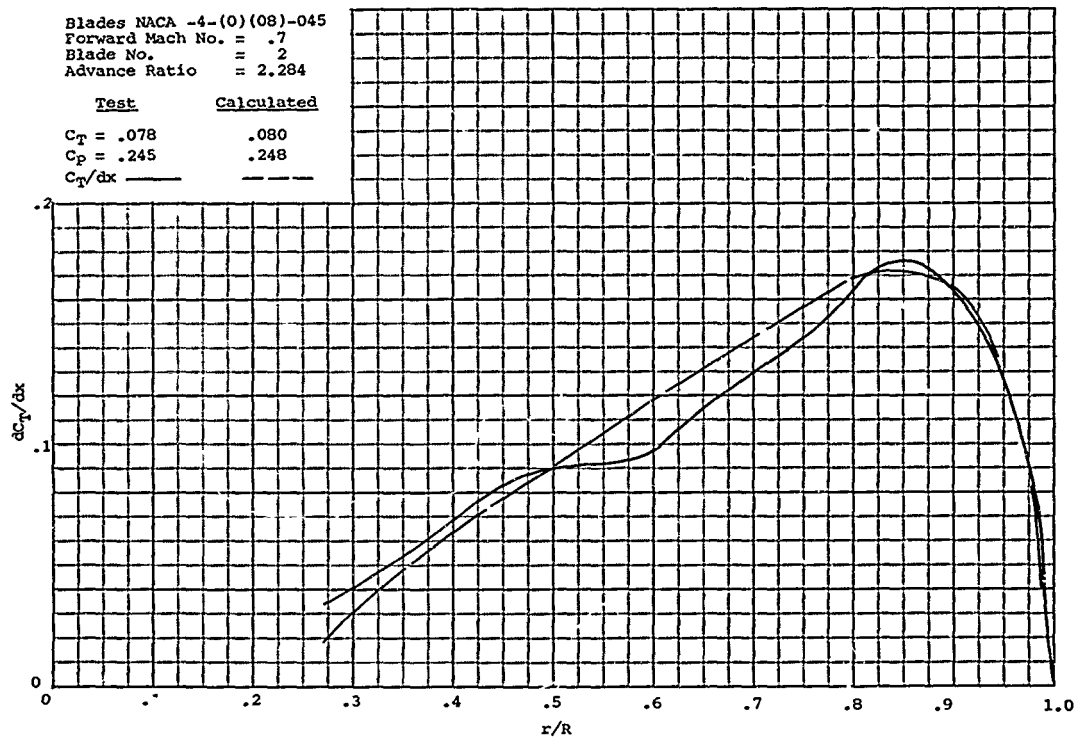


Figure 102. Comparison of Test and Calculated Propeller Loading, M = .7.

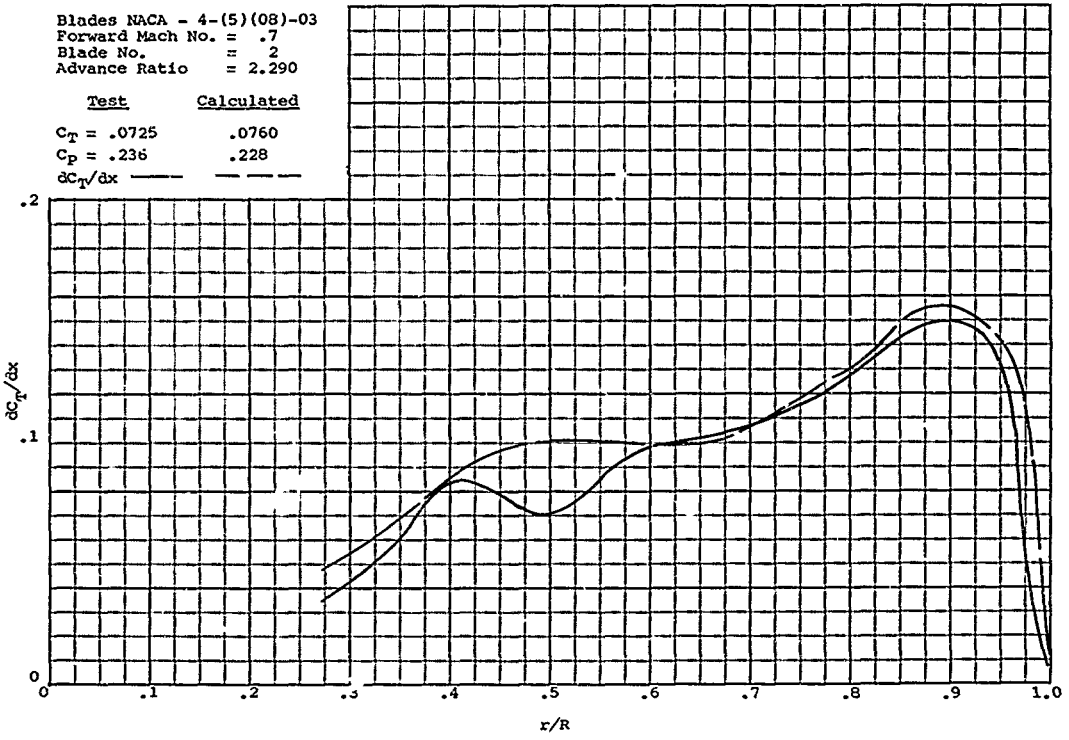


Figure 103. Comparison of Test and Calculated Propeller Loading, M = .7.

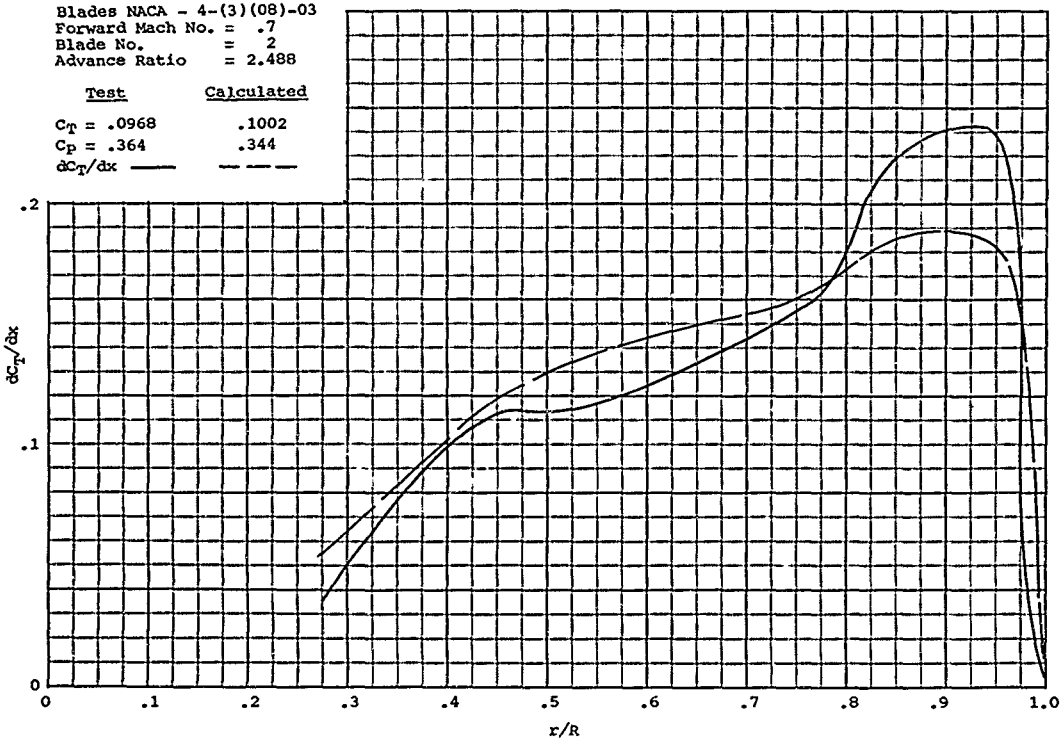


Figure 104. Comparison of Test and Calculated Propeller Loading, M = .7.

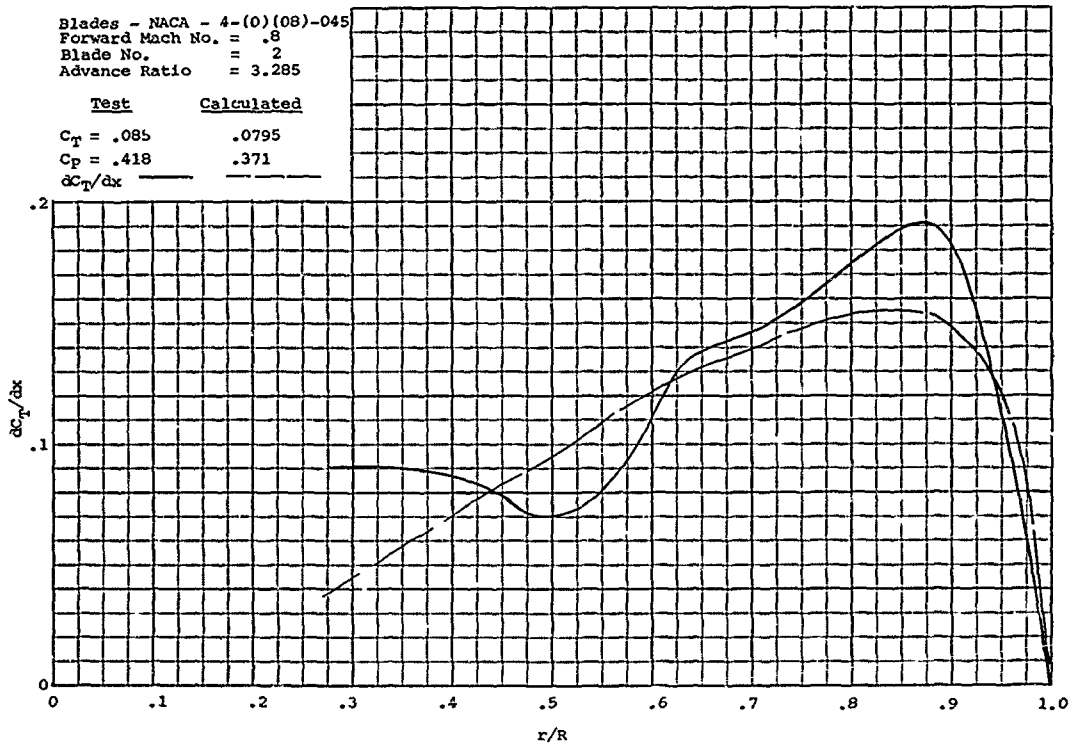


Figure 105. Comparison of Test and Calculated Propeller Loading, M = .8.

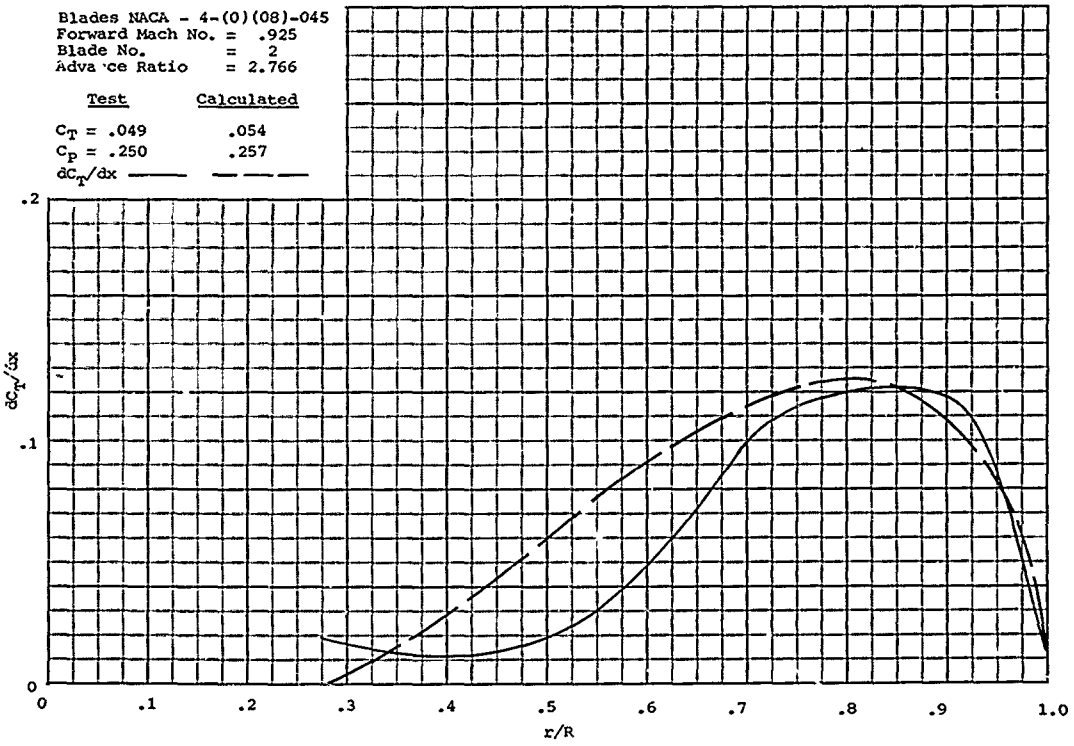


Figure 106. Comparison of Test and Calculated Propeller Loading, M = .925.

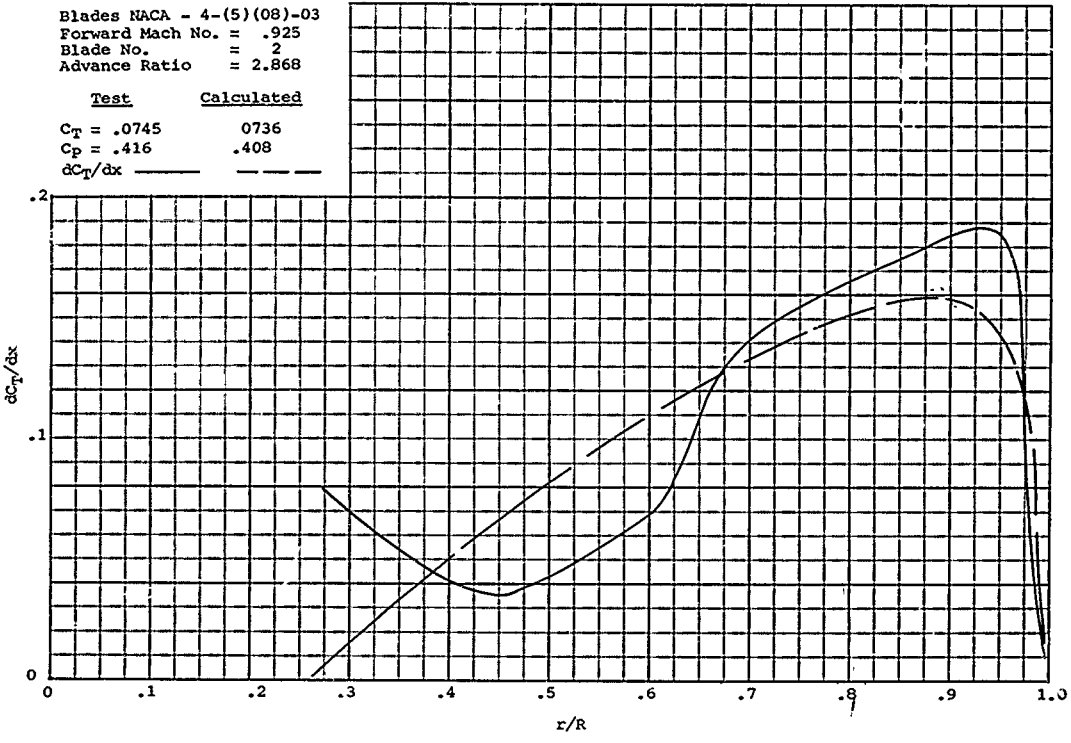


Figure 107. Comparison of Test and Calculated Propeller Loading, M=.925.

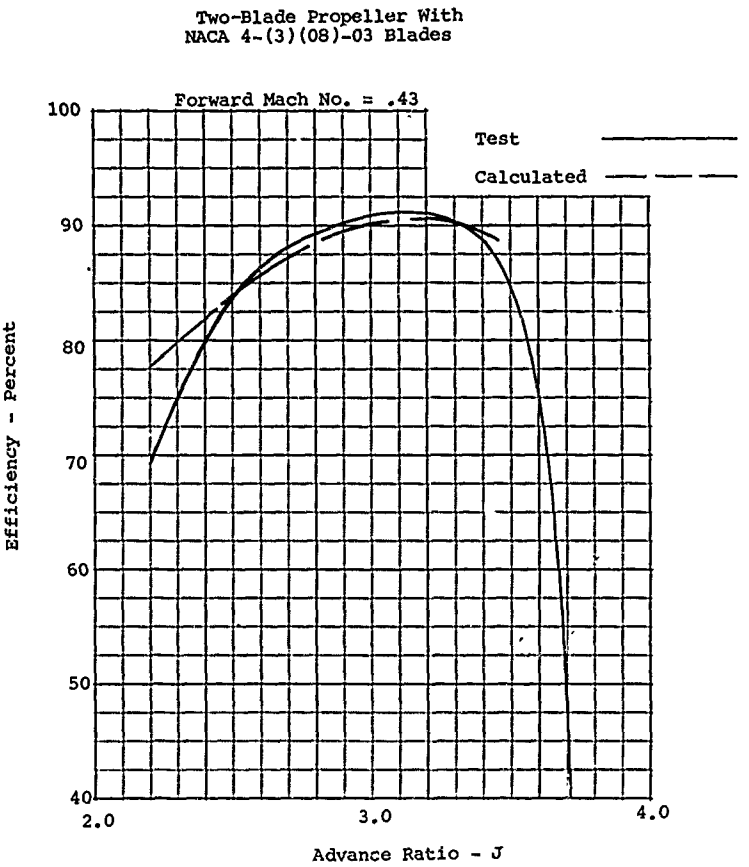


Figure 108. Comparison of Test and Calculated Efficiency.

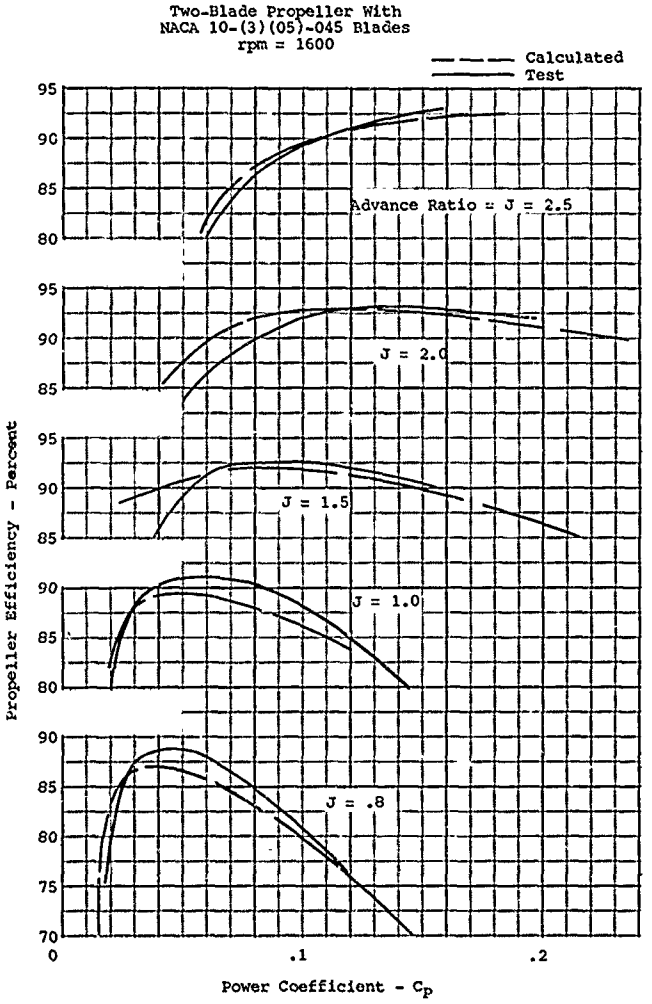


Figure 109. Comparison of Propeller Wind Tunnel Test and Calculated Performance.

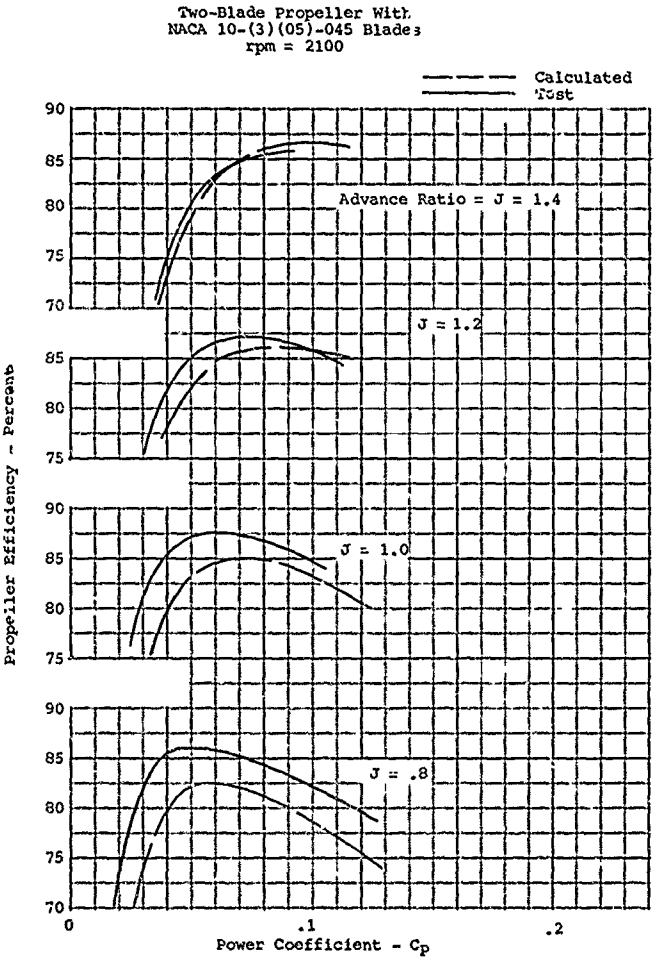


Figure 110. Comparison of Propeller Wind Tunnel Test and Calculated Performance.

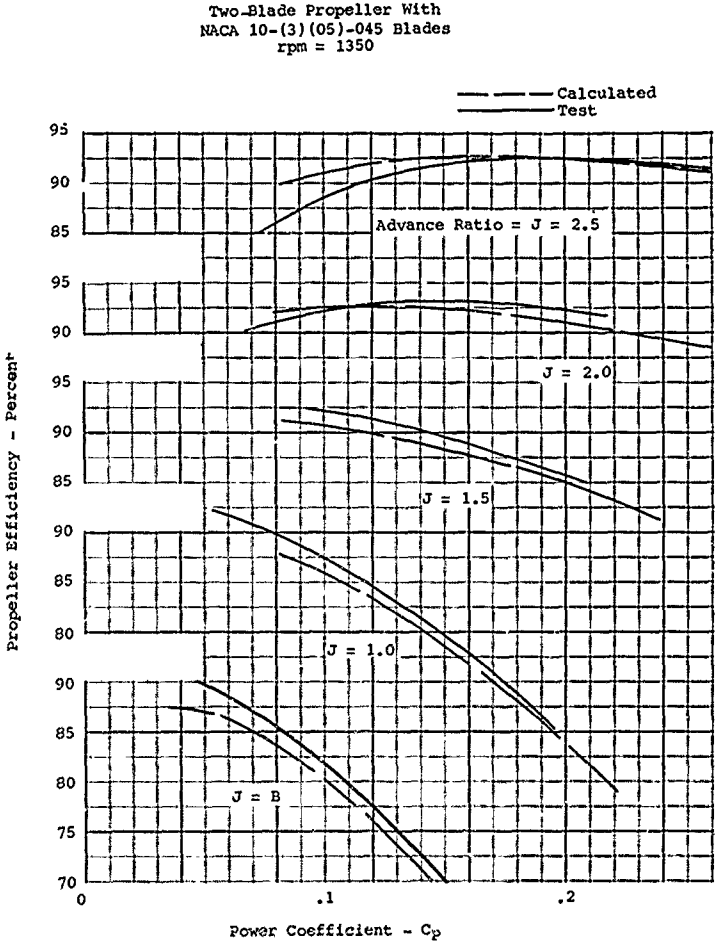


Figure 111. Comparison of Propeller Wind Tunnel Test and Calculated Performance.

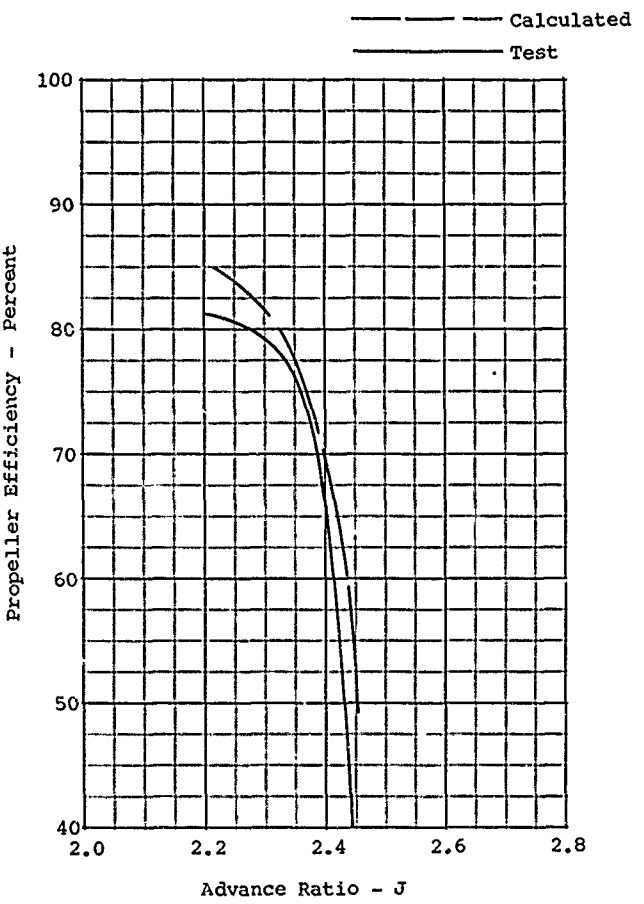


Figure 112. Comparison of Propeller Wind Tunnel Test and Calculated Performance.

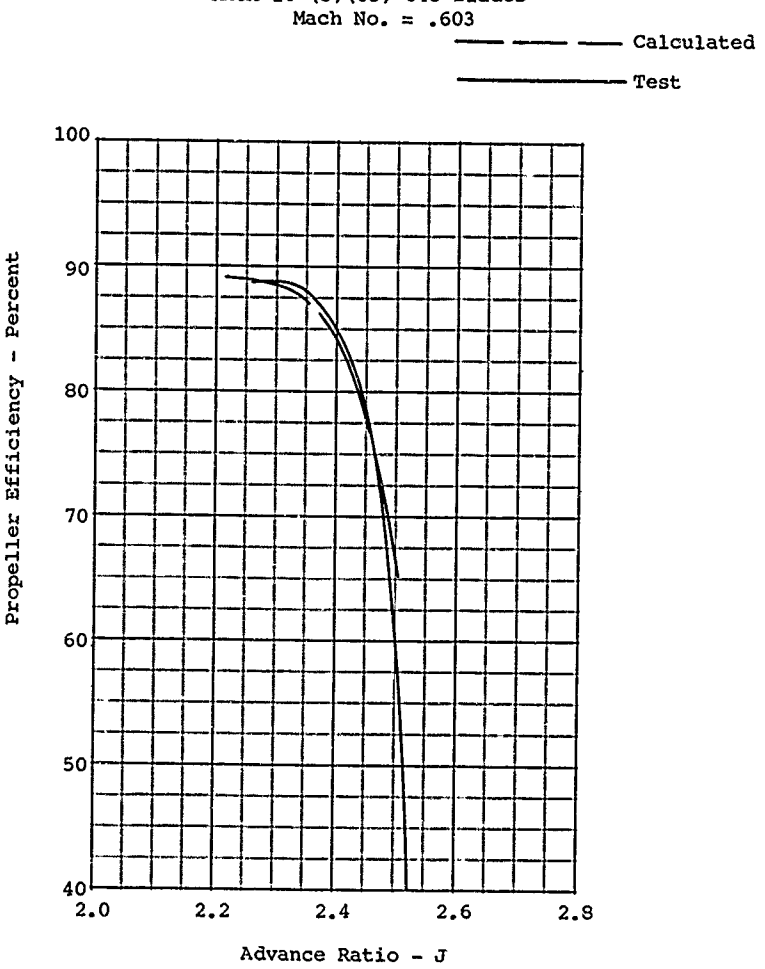


Figure 113. Comparison of Propeller Wind Tunnel Test and Calculated Performance.

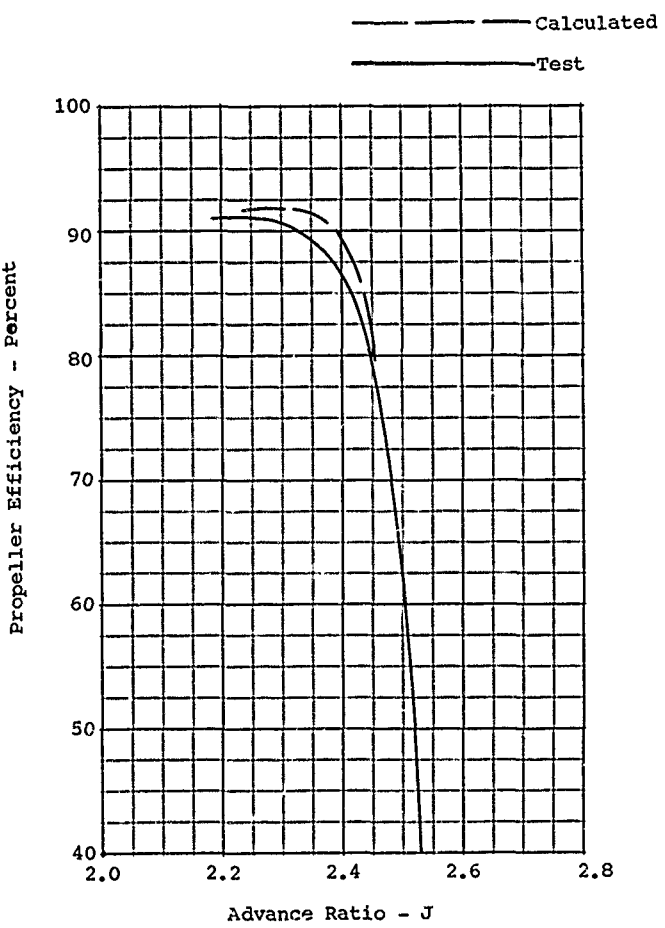


Figure 114. Comparison of Propeller Wind Tunnel Test and Calculated Performance.

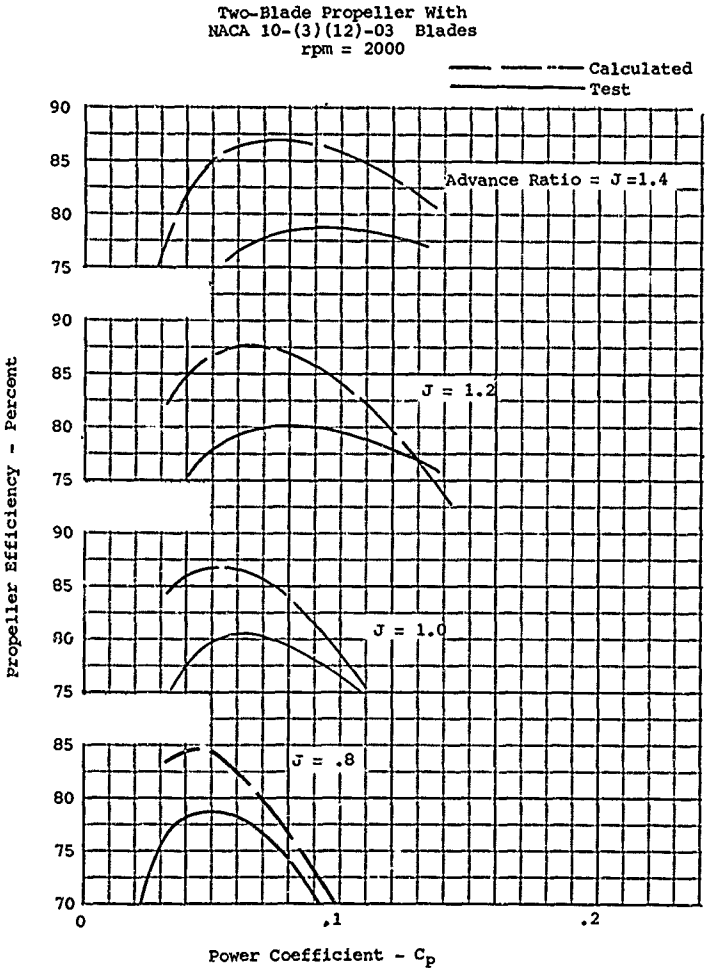


Figure 115. Comparison of Propeller Wind Tunnel Test and Calculated Performance.

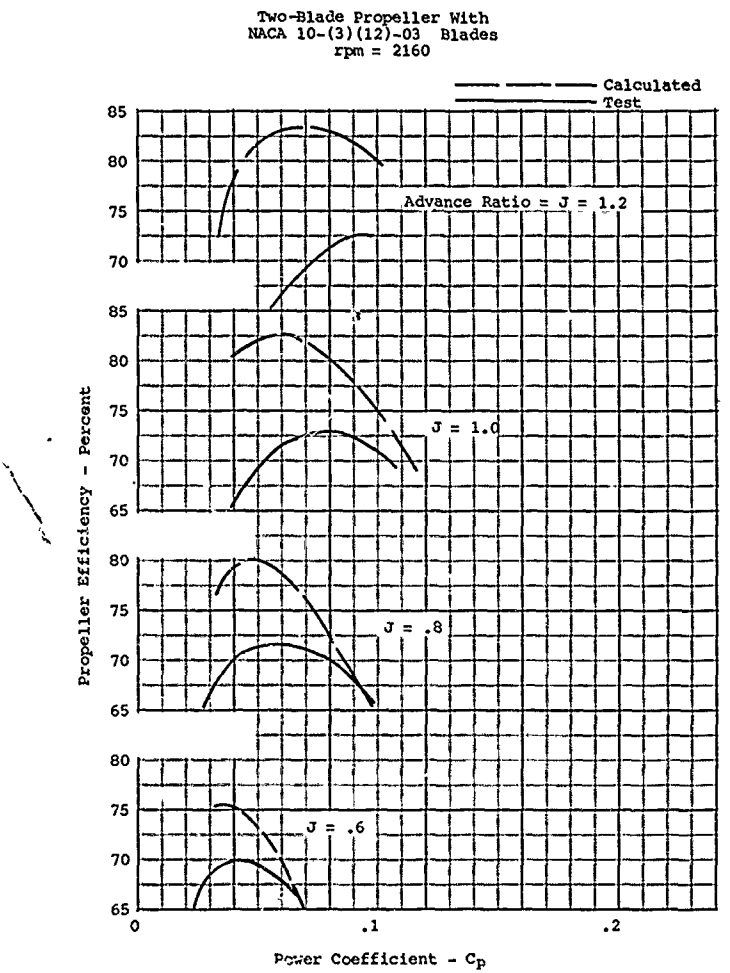


Figure 116. Comparison of Propeller Wind Tunnel Test and Calculated Performance.

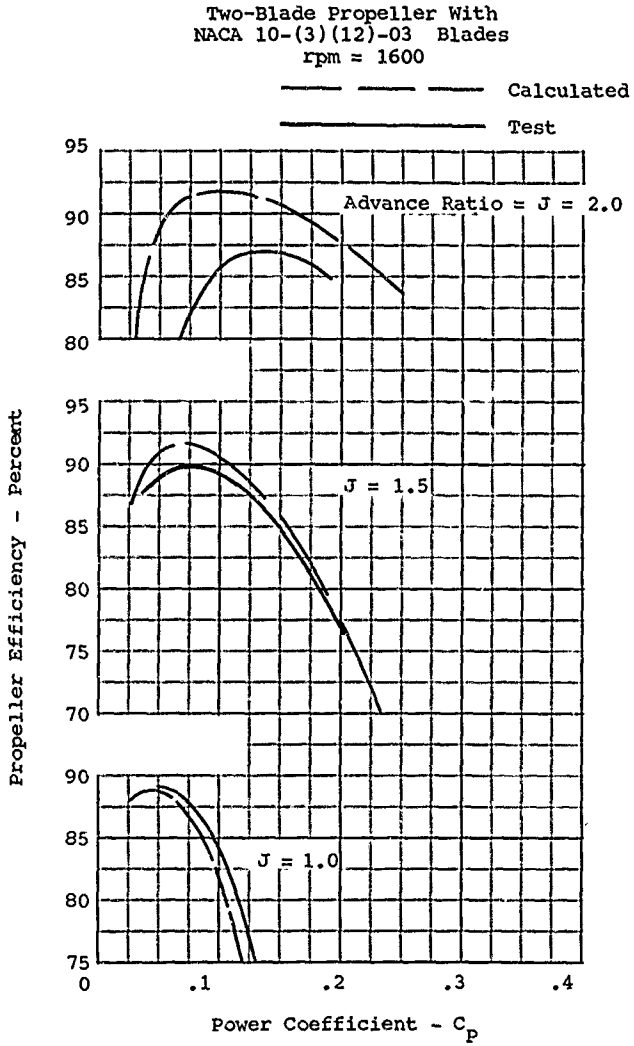


Figure 117. Comparison of Propeller Wind Tunnel Test and Calculated Performance.

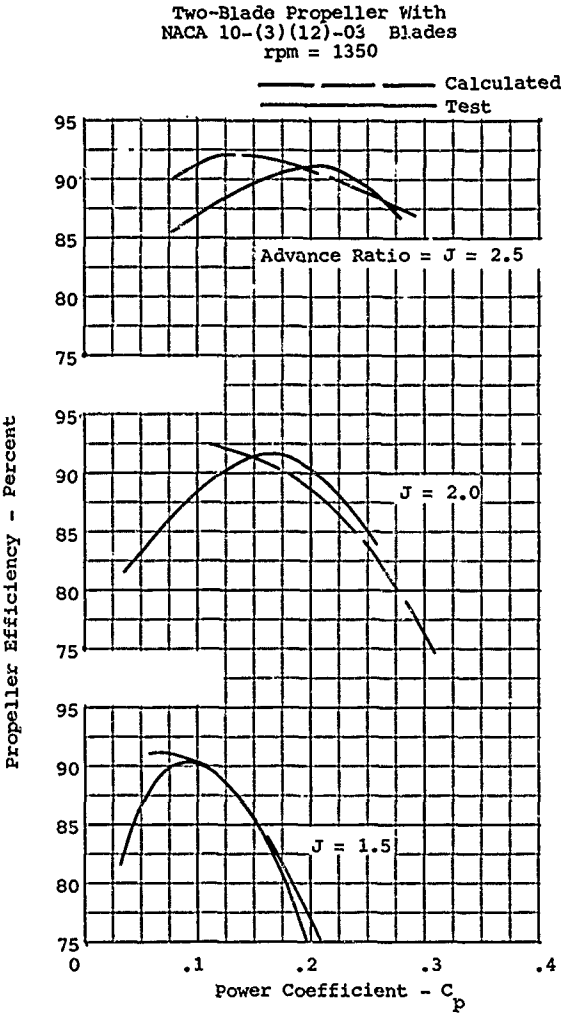


Figure 118. Comparison of Propeller Wind Tunnel Test and Calculated Performance.

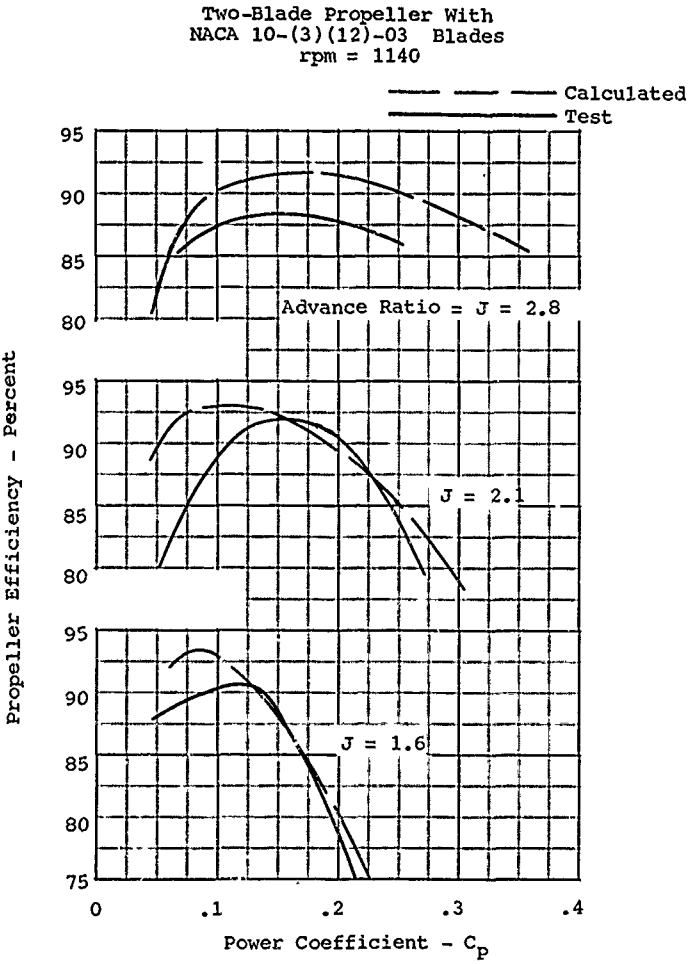


Figure 119. Comparison of Propeller Wind Tunnel Test and Calculated Performance.

At 1600 propeller rpm, the correlation is good at J = .8, being generally within $\pm$ 2° in efficiency. At 2160 rpm, the calculated efficiency is as much as 4% below the measured value. The tip Mach number at this condition also approaches 1.0, indicating that in this case the compressibility losses are overestimated. As the blades are operating at different lift coefficients at these two conditions, it is possible that a correction to the airfoil data could be made to improve the accuracy at both conditions.

The results of similar comparisons of test and calculated performance for the 10-(3)(12)-03 blade are shown on Figures 115 to 119. With this thick low-camber blade, the results of the comparison are much poorer than the other blades examined. For instance, at propeller rpm's of 1140-1350, the calculated efficiency is 4 to 5% higher than test values, especially at low values of power coefficients. At the test rpm of 1600, good agreement is obtained for the advance ratios of 1.0 and 1.5; whereas at J = 2.0, the correlation is poor, the calculated efficiency being 8 to 7% higher than that measured.

At the condition of 1600 rpm, the tip Mach number is actually the lowest at J = 2. Therefore, it would appear that the reason for poor correlation is not compressibility effects. In this particular case, the correlation of the test data appears to be poor, and therefore it is believed that the poor correlation is due to the test data.

At the 2000 and 2160 propeller rotational speed test conditions, the correlation of the calculated performance with test data is also poor. At these conditions, the tip Mach number is in excess of 0.8, and it would therefore appear that the drag rise used in the strip analysis calculations is optimistic.

The available comparisons of calculated performance and test data indicate that the accuracy of the predicted performance is good at those conditions where the propeller is operating in incompressible flow. The comparisons of the calculated and test load distributions are excellent in the incompressible flow range, thus giving further proof of the good accuracy. It appears, however, that when the tip Mach number approaches one, the predicted performance is high, especially for the propellers with the thicker blade sections.

During the time when the procedures and data for calculating propeller performance were developed, the data for establishing compressibility effects was in question due to wind tunnel blockage effects. The procedures for determining the proper free-stream Mach number in the tunnel and the corresponding flow at the test section were not known. The result of this was felt to be a premature measurement of the lift and drag divergence on airfoils. Some of the propeller test results

were believed to be affected by the same problem.

As was previously noted, an attempt was made to adjust the airfoil data to eliminate the effects of using premature lift and drag divergence Mach numbers. However, the propeller test data was not corrected for any blockage problems, and it is therefore possible that the comparison at high tip Mach numbers may not be valid. Thus, the performance comparison may be more accurate at the higher Mach numbers than the comparison given on Figures 109 to 119 would indicate.

For those propeller / rotor installations where the high-speed performance is critical, the procedures and data given in this report should be reviewed and refined to establish the necessary accuracy. As the induced losses are small at the high-speed conditions, the accuracy problems associated with predicting performance are most probably associated with the prediction of the profile losses. Thus, the problem is associated with establishing accurate airfoil data, especially at and above the lift and drag divergence Mach numbers.

The available airfoil data obtained since the compilation of the data of Appendix II, Volume III, should first be reviewed in relationship to these data. Only data obtained in transonic wind tunnels where blockage problems have been eliminated should be used in this review. Based on the available data and the difference between it and the data of Appendix II, Volume III, a program can be developed testing two-dimensional airfoils to obtain the necessary improvements of accuracy.

Along with the program for evaluating the newer airfoil data and establishing the data requirements should be a program to reassess the propeller test data. This is considered to be desirable to establish the data suitable for establishing the accuracy of the calculated performance, and take advantage of the considerable amount of high-speed propeller test data that has been run.

PROPELLER TEST DATA : A = 0 TO 180°

When analyzing propellers for use on V/STOL airplanes, data are needed for a large variation of operating conditions. It is necessary to cover a large range of shaft angles of attack as well as the usual range of power, advance ratio, and velocity, as angles in excess of 90 degrees can be encountered, especially when operating at or near the hover condition. For instance, as the airplane decelerates to the hover condition, the shaft angle of attack will often exceed 90 degrees.

The available test data for propellers operating at shaft angles above 90 degrees is very limited, and no consistent set of

data is available covering the full range of angles. Tests were therefore run to cover the range of operation from 0 to 180 degrees for low-advance-ratio operating conditions. These tests were run for a conventional type three-bladed propeller model originally designed for use on a Lockheed Constellation airplane. The blade characteristics curves showing the variation of thickness ratio, design lift coefficient, blade angle, and chord as a function of radius are shown on Figure 120.

Propeller Tests

The model propeller had a 30-inch diameter and was tested in the University of Maryland wind tunnel. The model was powered by a dynamometer with sufficient power to allow tests to be conducted to power coefficients of .16. This range is considered adequate for most propeller-driven V/STOL airplanes.

To cover the range of angles of attack, the propeller axis was turned in the horizontal plane or yaw direction. This minimized tunnel wall effects, as the tunnel width is greater than its height, thus reducing flow blockage effects. The propeller dynamometer was designed so that the centerline of the propeller remained essentially in the center of the tunnel.

A strain gage balance system was used to measure the forces and moments. The forces and moments measured and their sign convention are shown on Figure 96. The forces and moments all have the same sign convention with respect to the propeller disc and the axis of rotation. The propeller rotated to the right. That is, the propeller rotated clockwise as viewed from the rear.

RESULTS

The results of the tests are given on Figures 121 to 141 for thrust, power, normal and side force coefficients. Figures 142 to 162 cover the moment coefficient data. The data covers blade angles measured at the 70% radius of 8 to 20 degrees.

Although the data presented on Figures 121 to 163 is believed to be accurate, it should be used only as an indication of trends. This is necessary as the data was never fully analyzed and checked. However, the points that were checked appeared to be reasonable. It is considered desirable to run and analyze further data of this type to establish the performance at the higher shaft angles. Detailed comparisons with the full-scale data of Reference 45 would be desirable.

Blade Activity Factor - AF = 115  Integrated Design $C_{Li}$ = .5

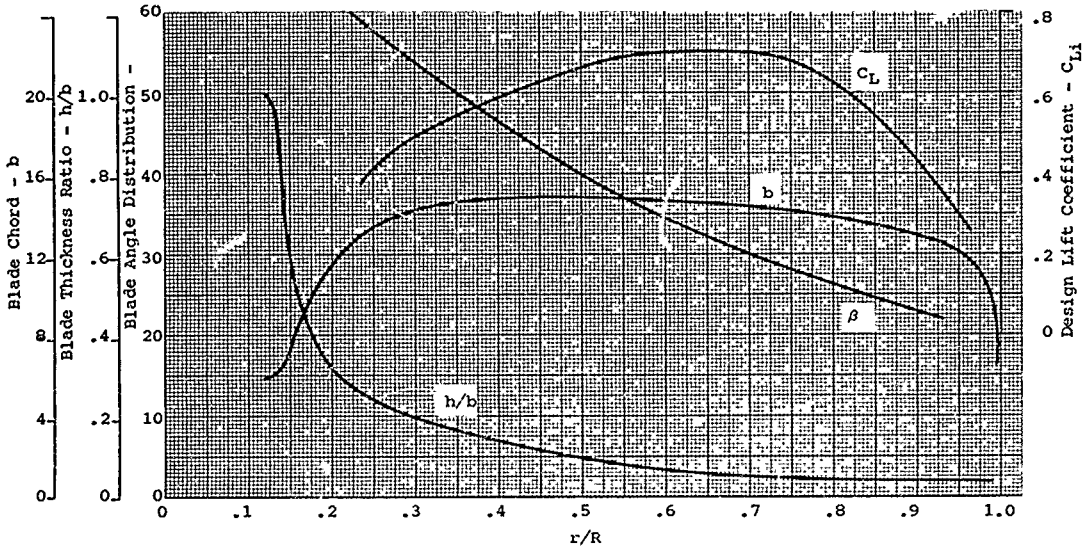


Figure 120. Characteristic Curves - 109652 Blade.

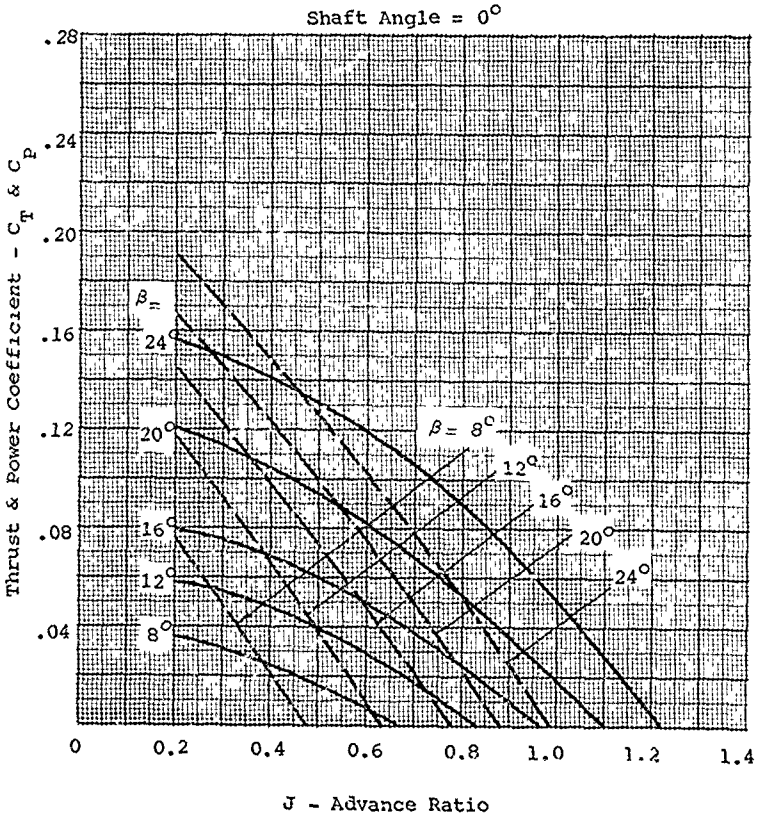


Figure 121. Performance at 0-Degree Shaft Angle - Three-Blade Propeller, Blade No. 109652.

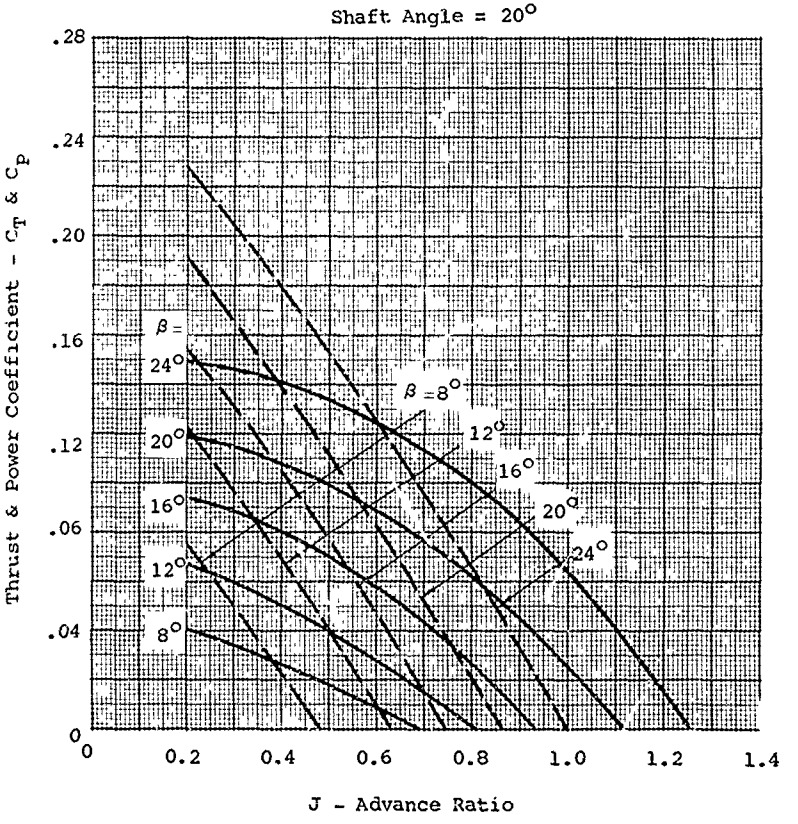


Figure 122. Performance at 20-Degree Shaft Angle - Three-Blade Propeller, Blade No. 109652.

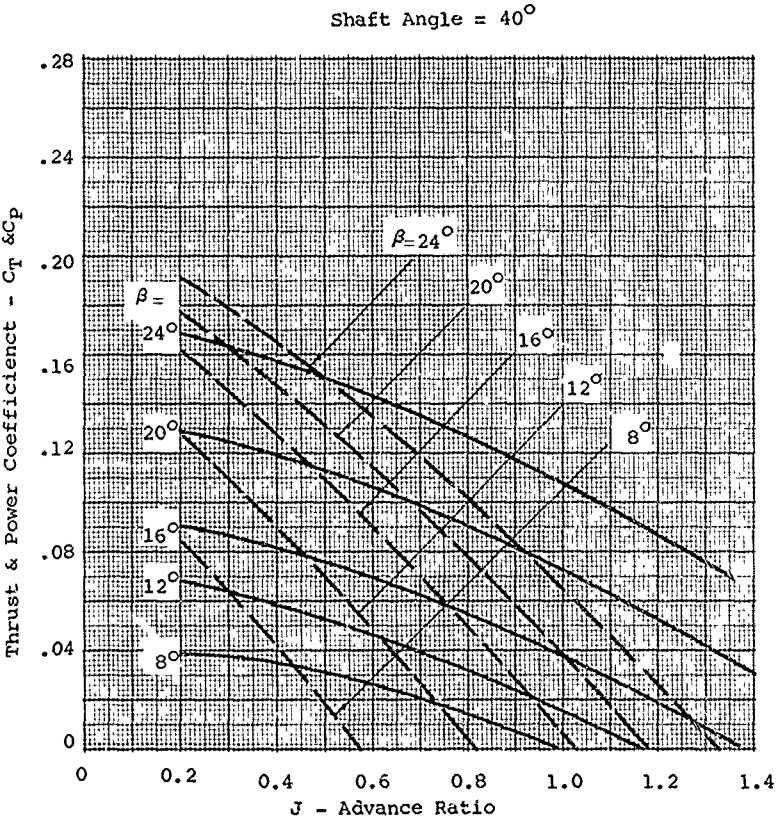


Figure 123. Performance at 40-Degree Shaft Angle - Three-Blade Propeller, Blade No. 109652.

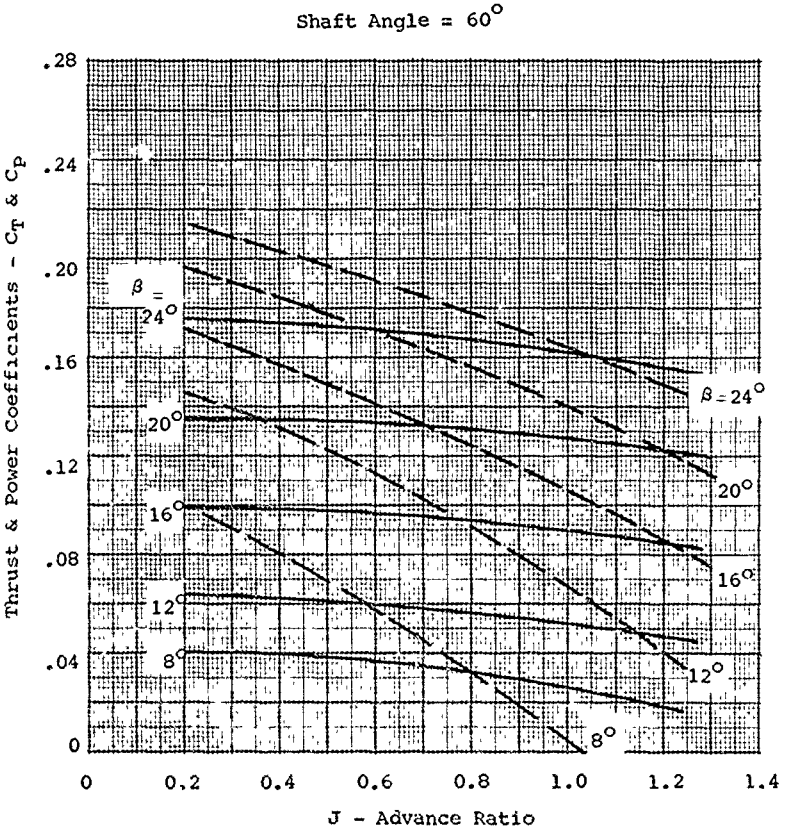


Figure 124. Performance at 60-Degree Shaft Angle - Three-Blade Propeller, Blade No. 109652.

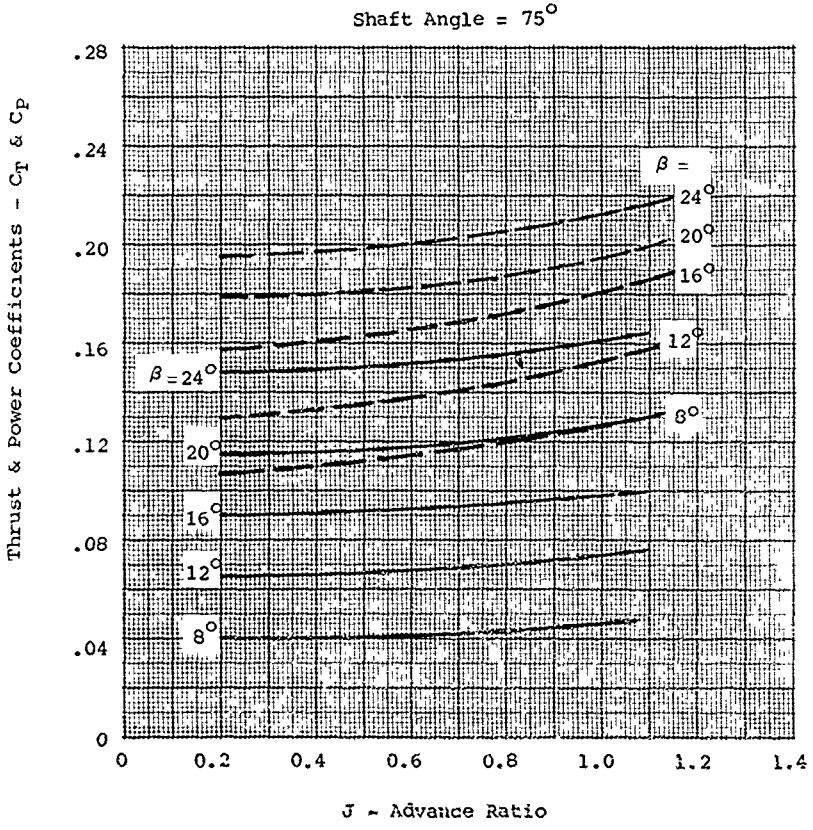


Figure 125. Performance at 75-Degree Shaft Angle - Three-Blade Propeller, Blade No. 109652.

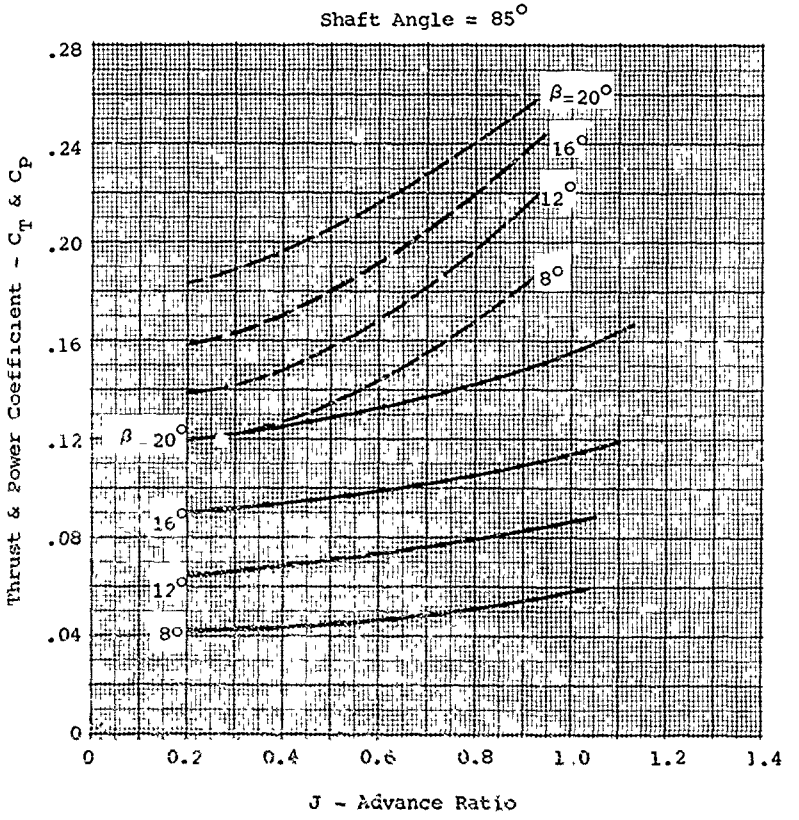


Figure 126. Performance at 85-Degree Shaft Angle - Three-Blade Propeller, Blade No. 109652.

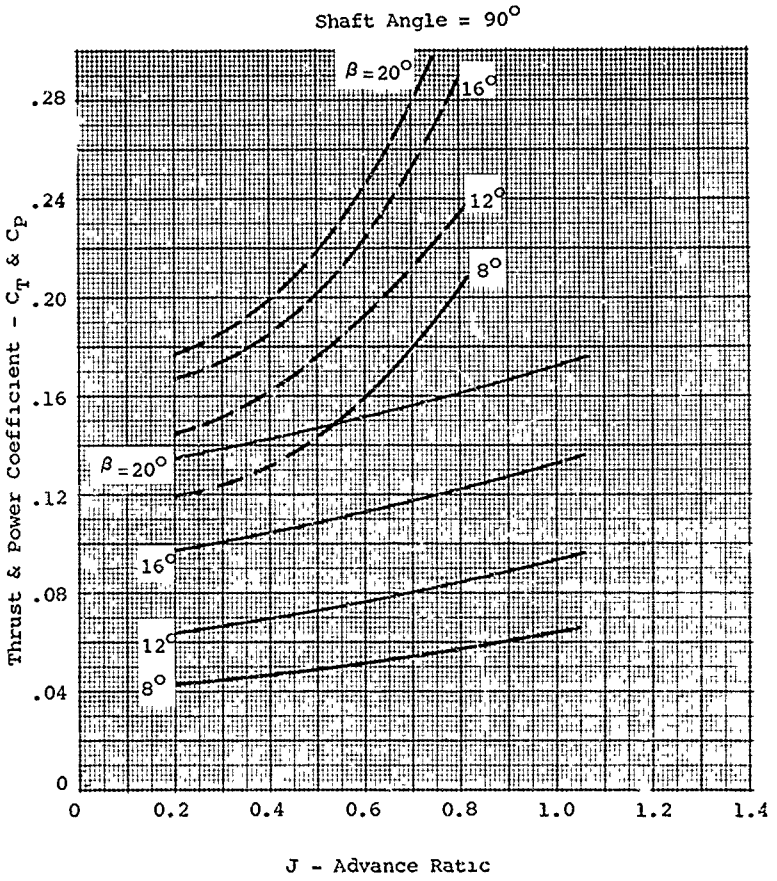


Figure 127. Performance at 90-Degree Shaft Angle - Three-Blade Propeller, Blade No. 109652.

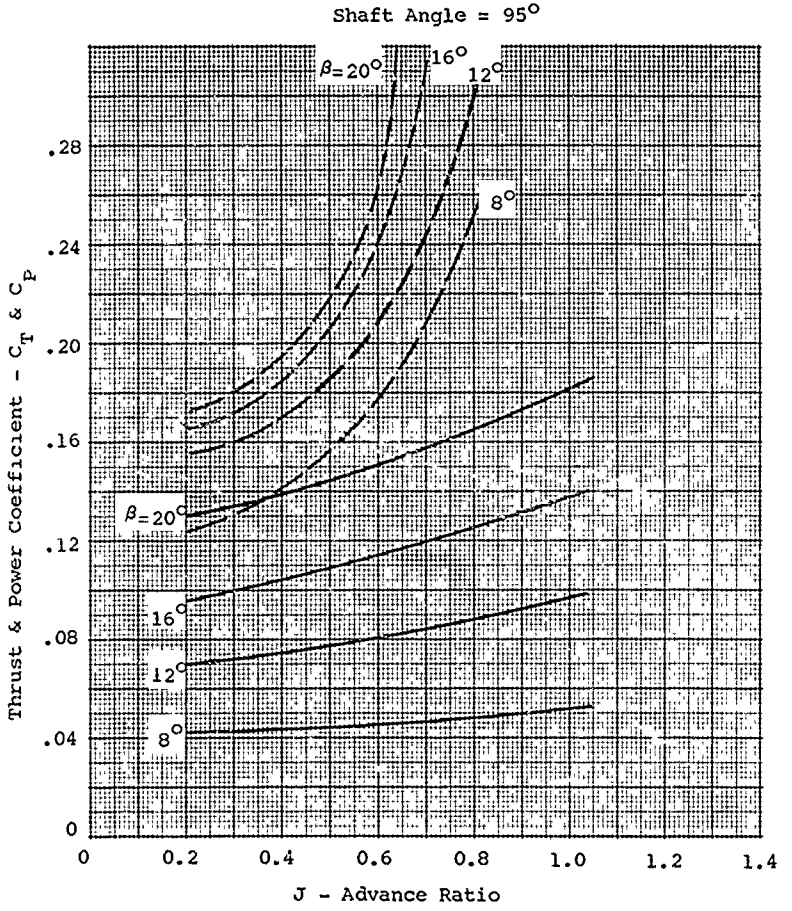


Figure 128. Performance at 95-Degree Shaft Angle - Three-Blade Propeller, Blade No. 109652.

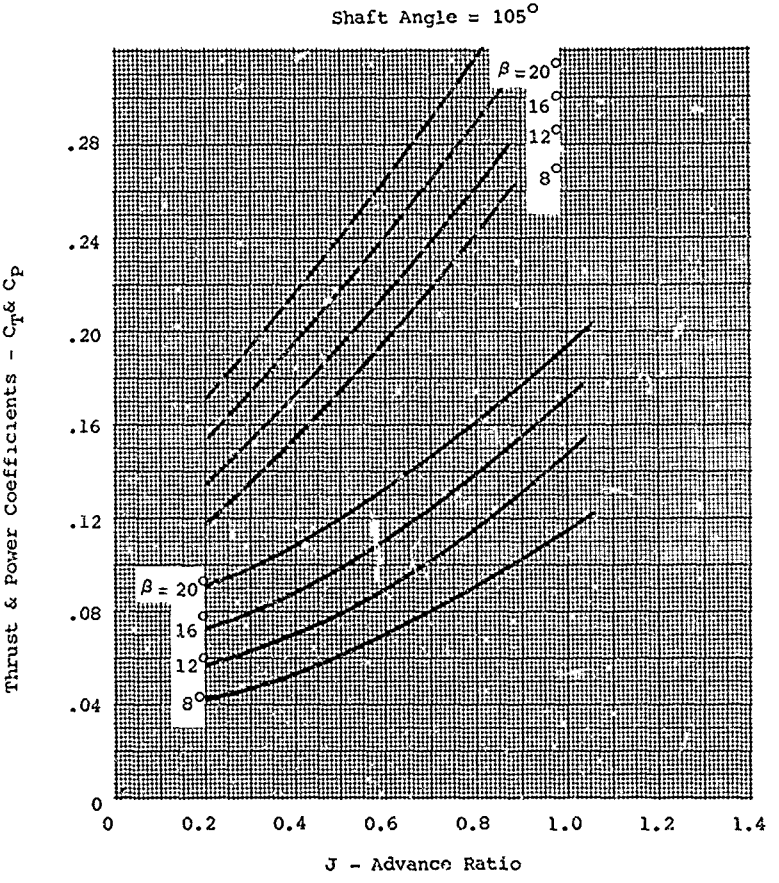


Figure 129. Performance at 105-Degree Shaft Angle - Three-Blade Propeller, Blade No. 109652.

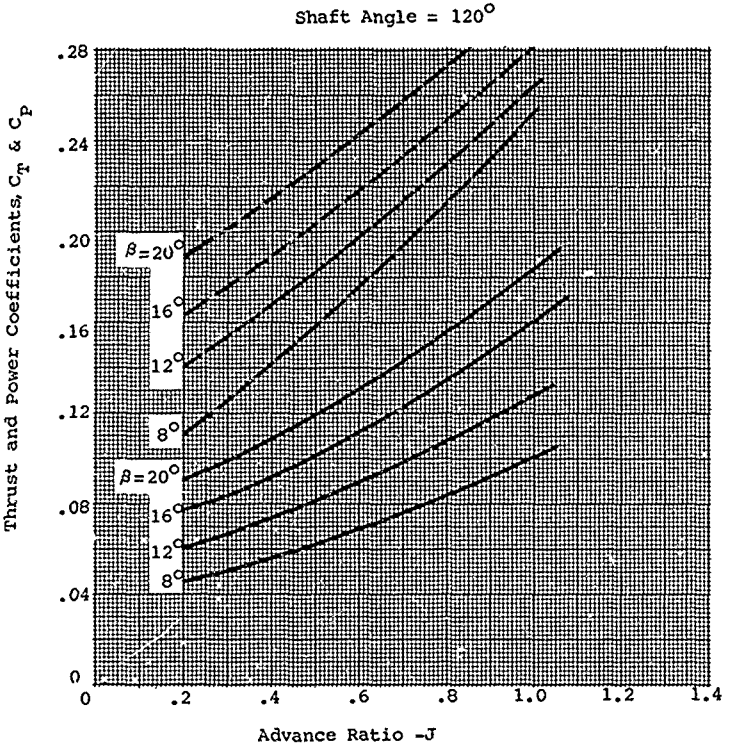


Figure 130. Performance at 120-Degree Shaft Angle - Three-Blade Propeller, Blade No. 109652.

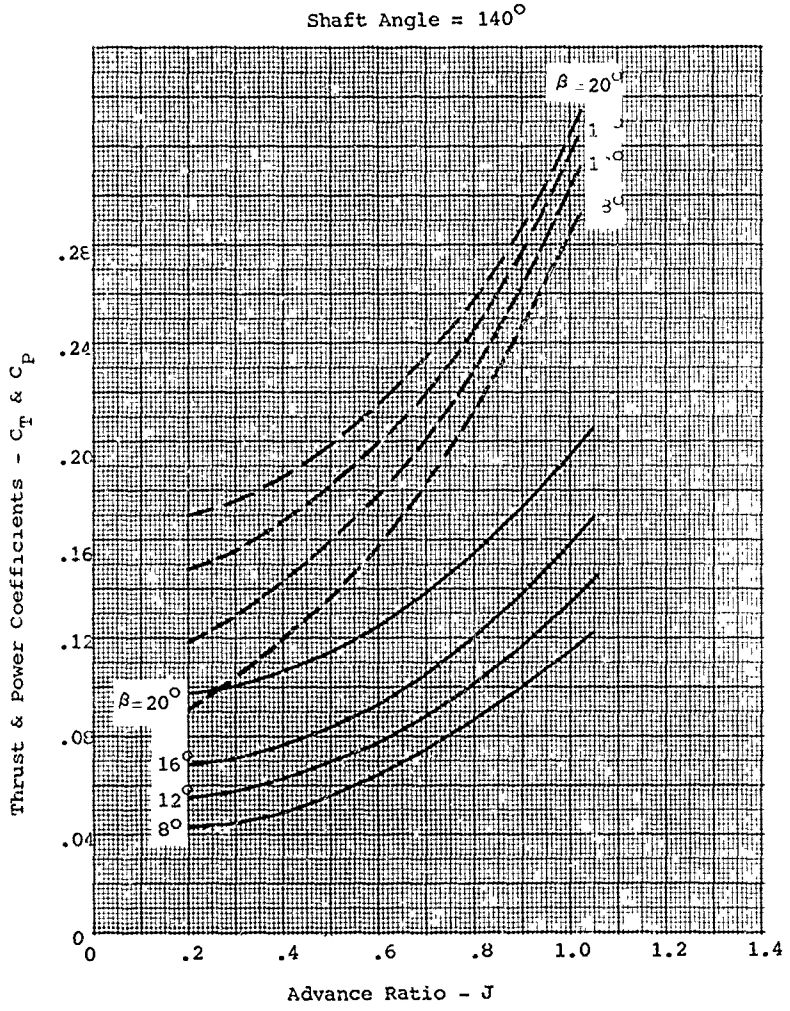


Figure 131. Performance at 140-Degree Shaft Angle - Three-Blade Propeller, Blade No. 109652.

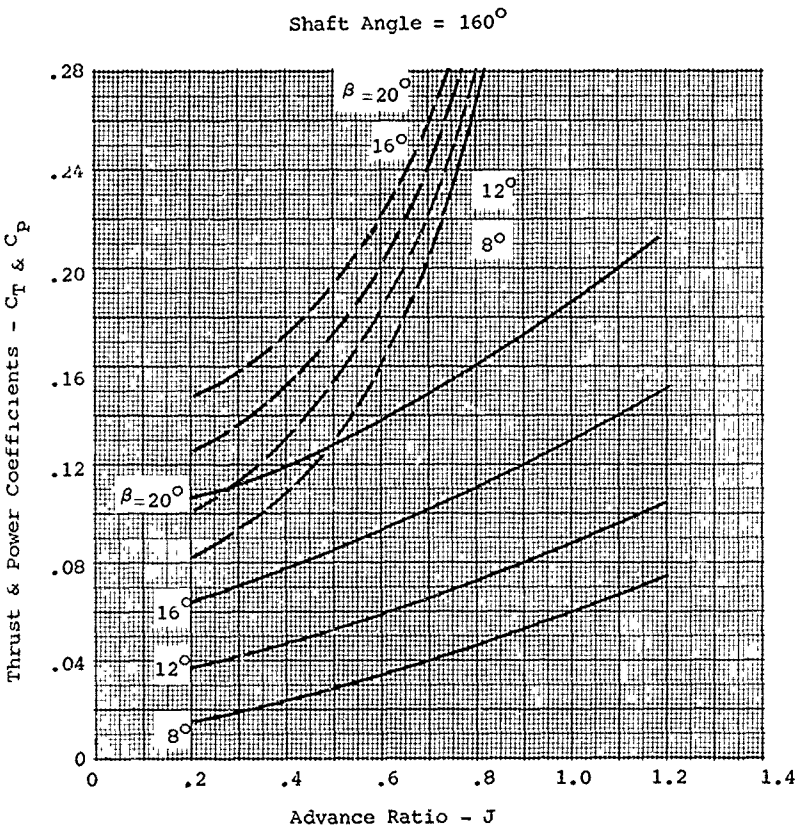


Figure 132. Performance at 160-Degree Shaft Angle - Three-Blade Propeller, Blade No. 109652.

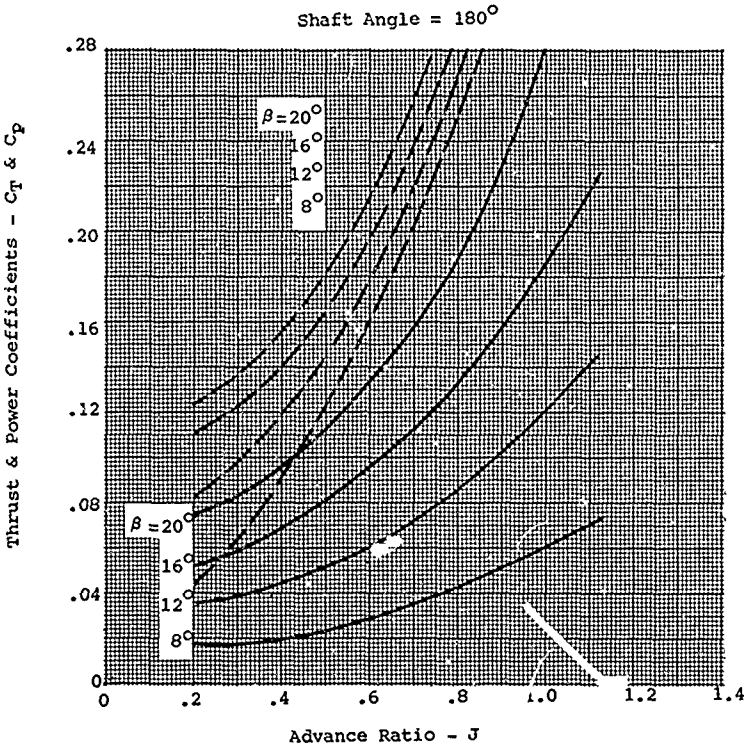


Figure 133. Performance at 180-Degree Shaft Angle - Three-Blade Propeller, Blade No. 109652.

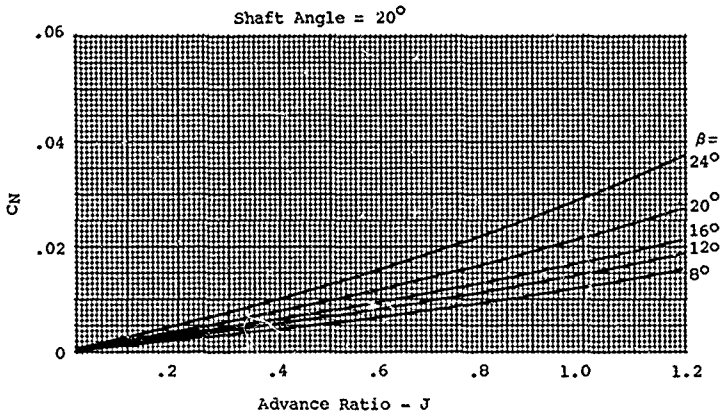


Figure 134. Normal Force at 20-Degree Shaft Angle - Three-Blade Propeller, Blade No. 109652.

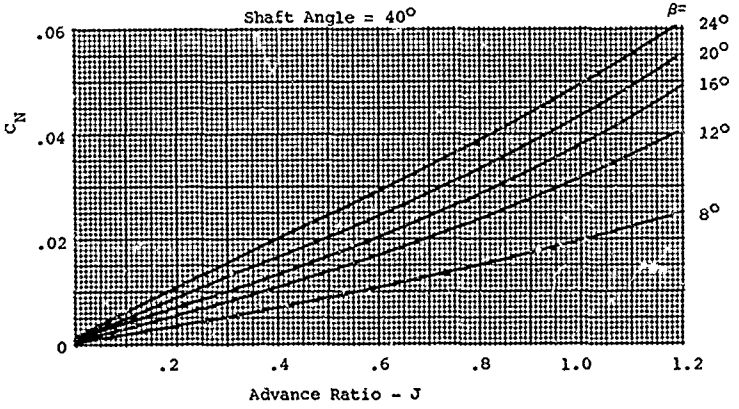


Figure 135. Normal Force at 40-Degree Shaft Angle - Three-Blade Propeller, Blade No. 109652.

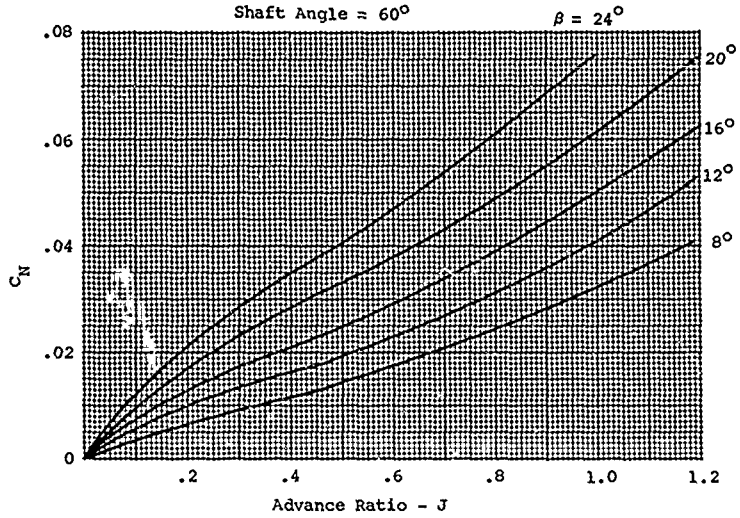


Figure 136. Normal Force at 60-Degree Shaft Angle - Three-Blade Propeller, Blade No. 109652.

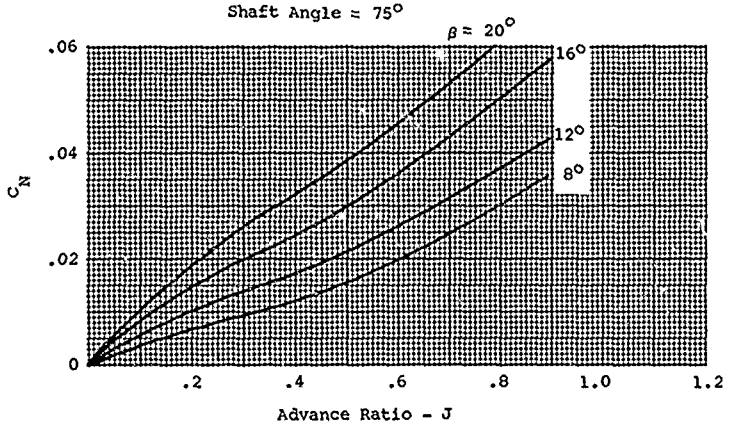


Figure 137. Normal Force at 75-Degree Shaft Angle - Three-Blade Propeller, Blade No. 109652.

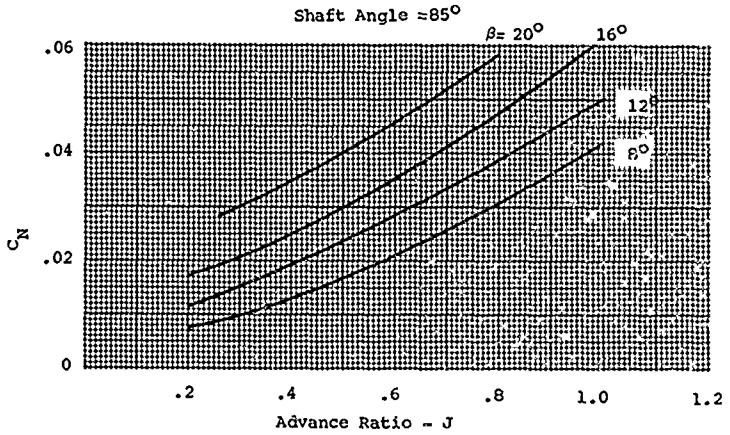


Figure 138. Normal Force at 85-Degree Shaft Angle - Three-Blade Propeller, Blade No. 109652.

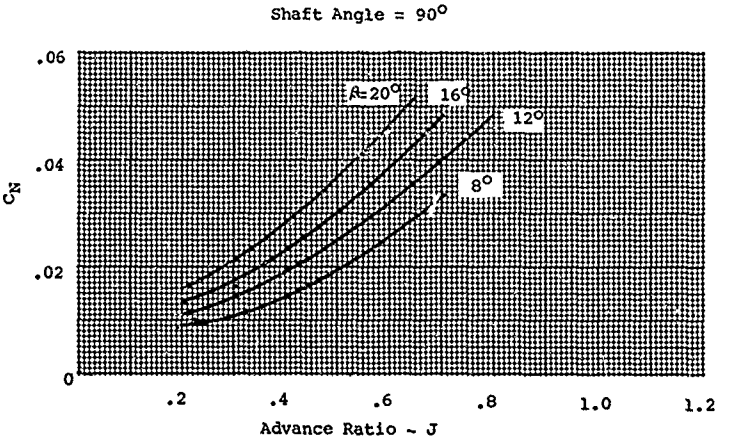


Figure 139. Normal Force at 90-Degree Shaft Angle - Three-Blade Propeller, Blade No. 109652.

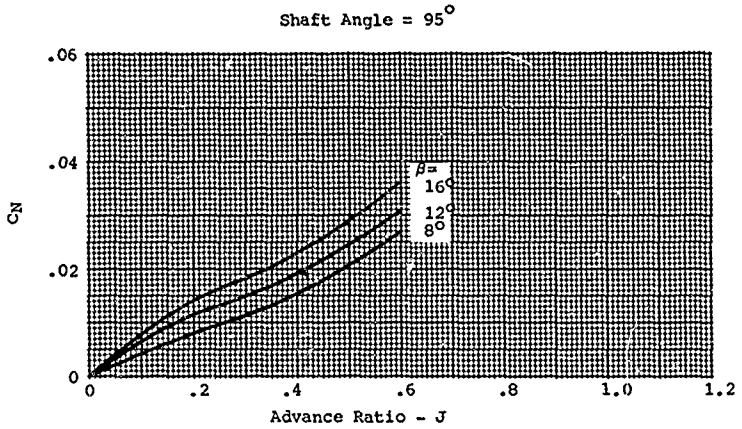


Figure 140. Normal Force at 95-Degree Shaft Angle - Three-Blade Propeller, Blade No. 109652.

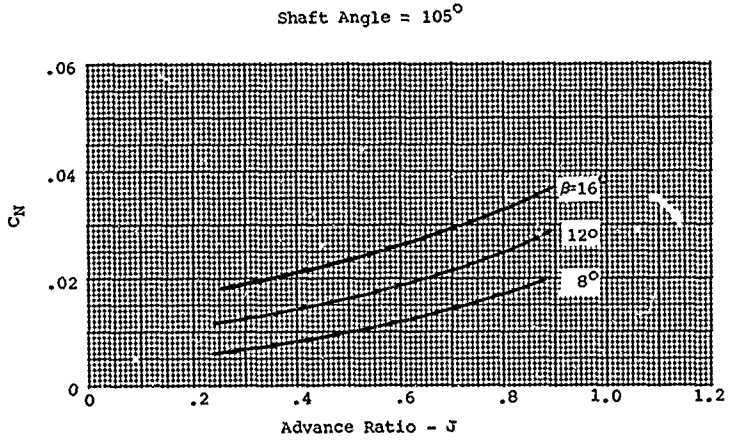


Figure 141. Normal Force at 105-Degree Shaft Angle - Three-Blade Propeller, Blade No. 109652.

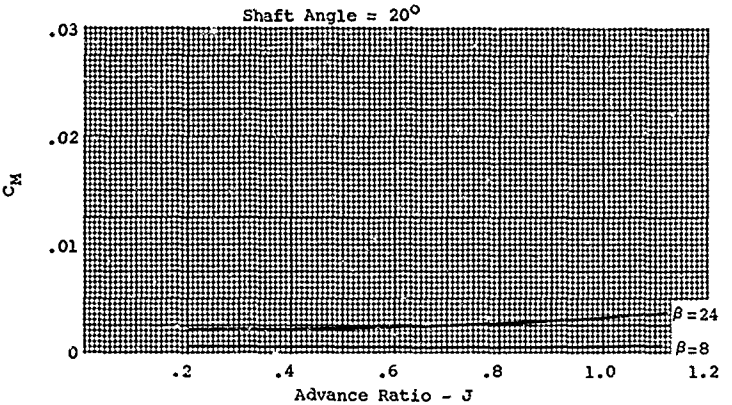


Figure 142. Pitching Moment at 20-Degree Shaft Angle - Three-Blade Propeller, Blade No. 109652.

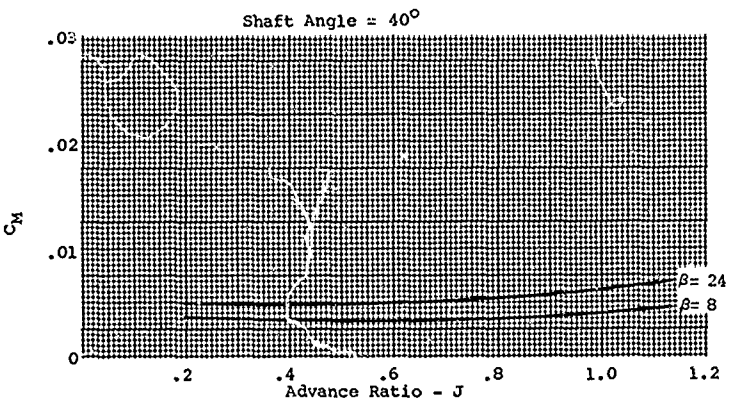


Figure 143. Pitching Moment at 40-Degree Shaft Angle - Three-Blade Propeller, Blade No. 109652.

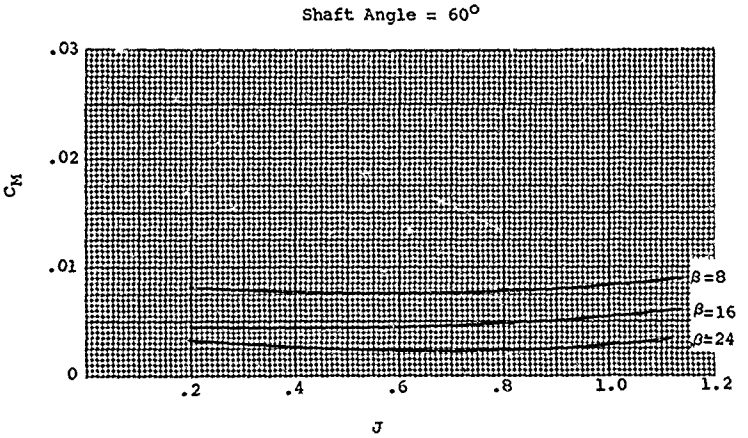


Figure 144. Pitching Moment at 60-Degree Shaft Angle - Three-Blade Propeller, Blade No. 109652.

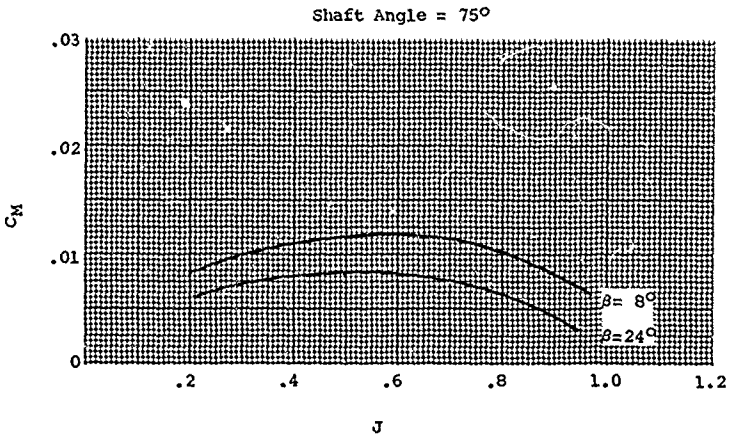


Figure 145. Pitching Moment at 75-Degree Shaft Angle - Three-Blade Propeller, Blade No. 109652.

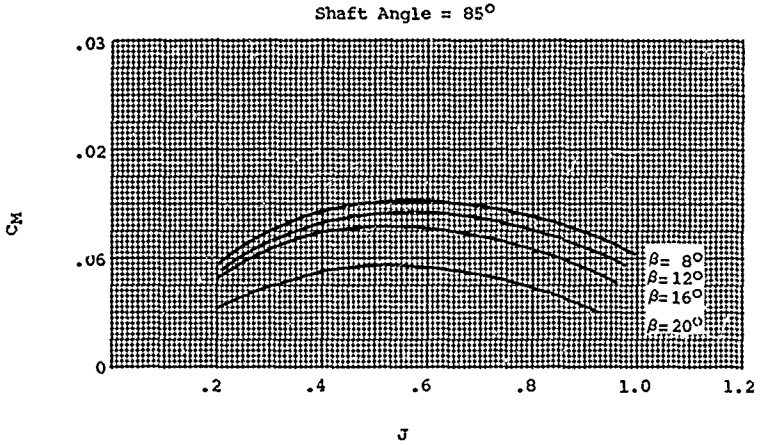


Figure 146. Pitching Moment at 85-Degree Shaft Angle - Three-Blade Propeller, Blade No. 109652.

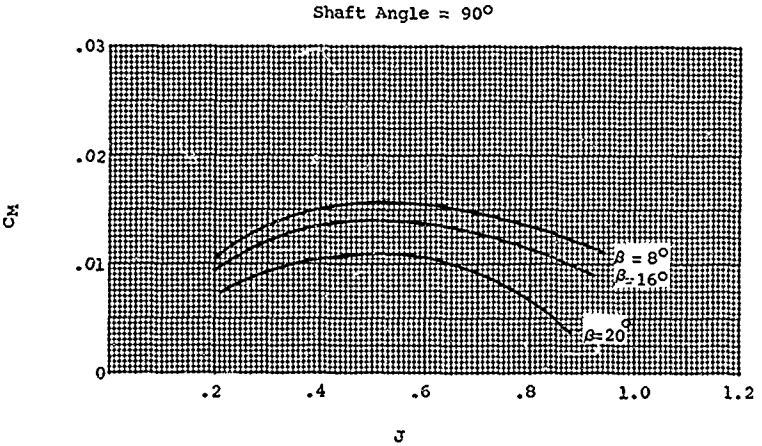


Figure 147. Pitching Moment at 90-Degree Shaft Angle - Three-Blade Propeller, Blade No. 109652.

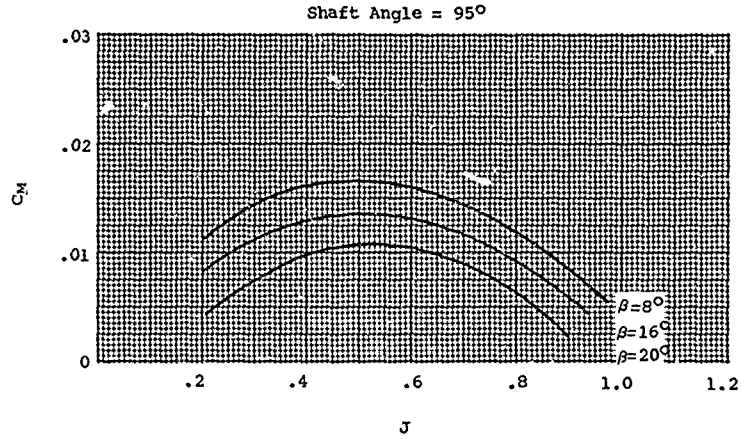


Figure 148. Pitching Moment at 95-Degree Shaft Angle - Three-Blade Propeller, Blade No. 109652.

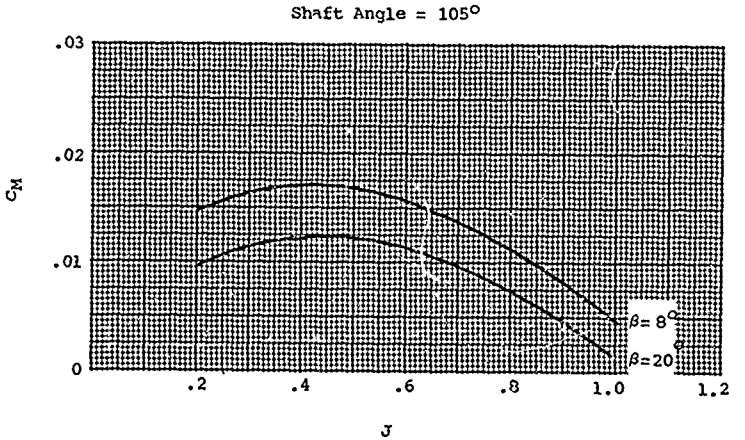


Figure 149. Pitching Moment at 105-Degree Shaft Angle - Three-Blade Propeller, Blade No. 109652.

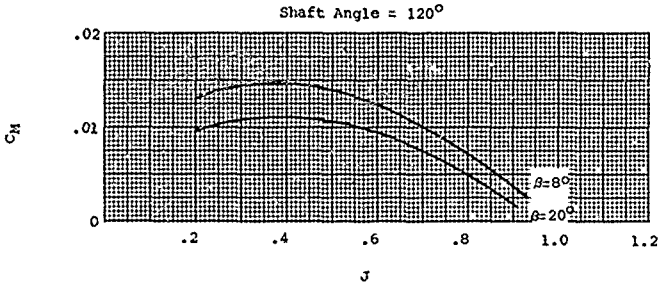


Figure 150. Pitching Moment at 120-Degree Shaft Angle - Three-Blade Propeller, Blade No. 109652.

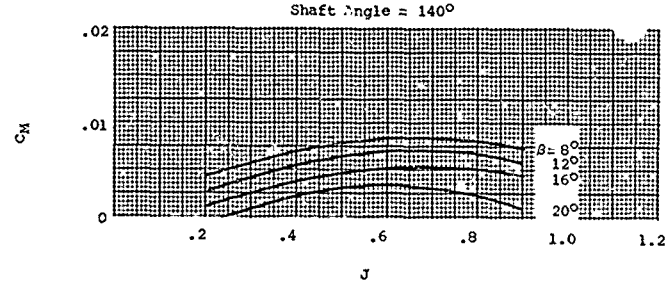


Figure 151. Pitching Moment at 140-Degree Shaft Angle - Three-Blade Propeller, Blade No. 109652.

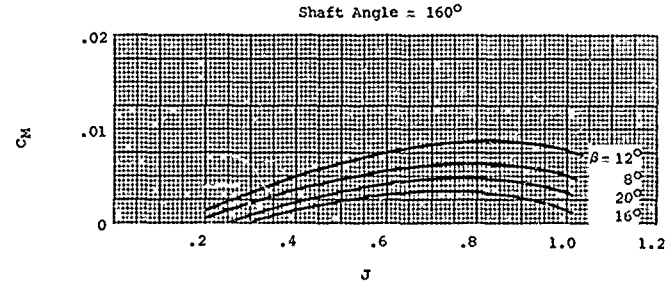


Figure 152. Pitching Moment at 160-Degree Shaft Angle - Three-Blade Propeller, Blade No. 109652.

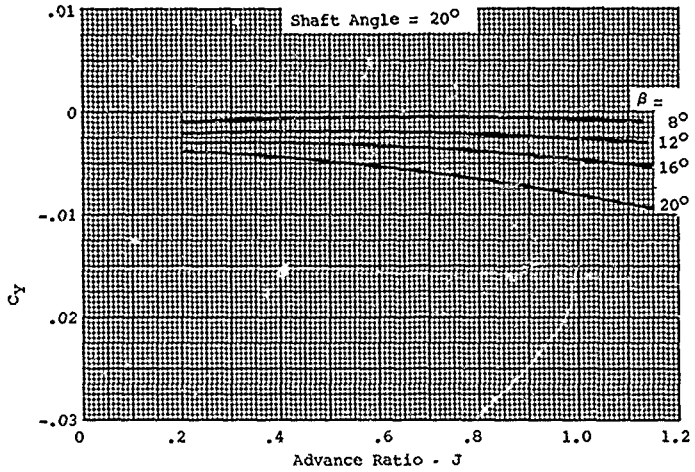


Figure 153. Yawing Moment at 20-Degree Shaft Angle - Three-Blade Propeller, Blade No. 109652.

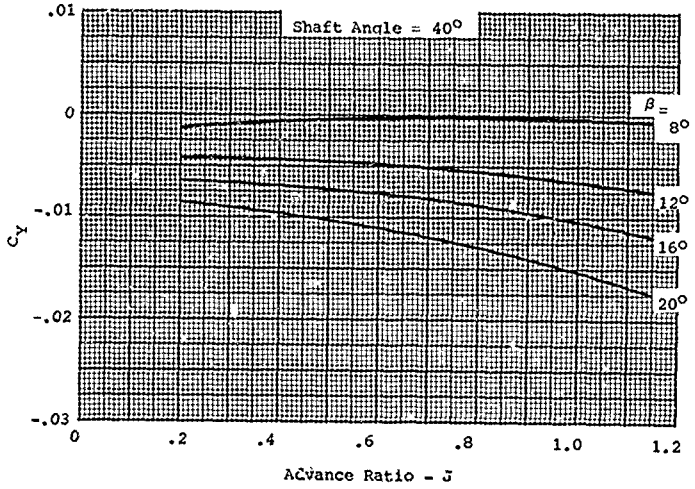


Figure 154. Yawing Moment at 40-Degree Shaft Angle - Three-Blade Propeller, Blade No. 109652.

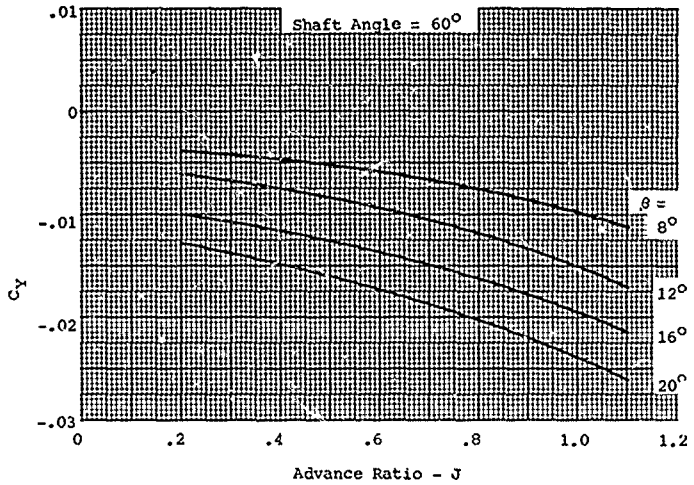


Figure 155. Yawing Moment at 60-Degree Shaft Angle - Three-Blade Propeller, Blade No. 109652.

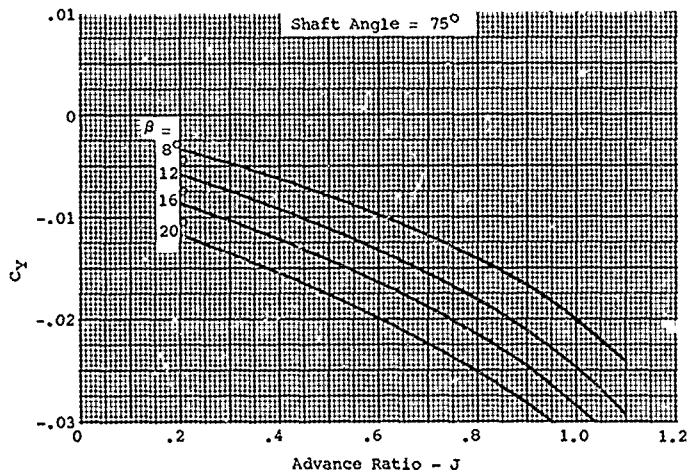


Figure 156. Yawing Moment at 75-Degree Shaft Angle - Three-Blade Propeller, Blade No. 109652.

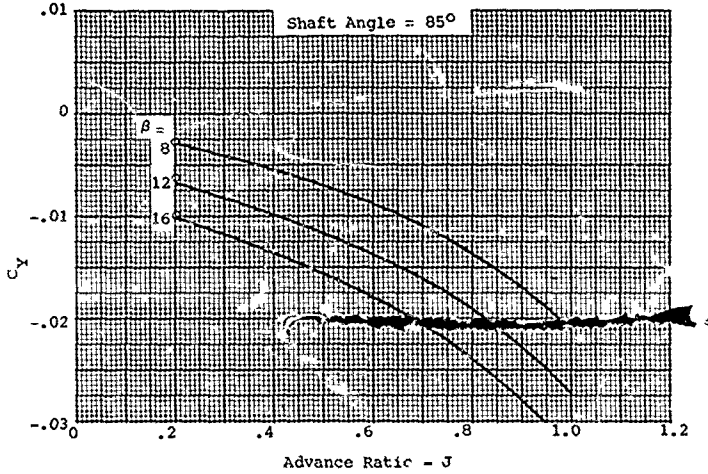


Figure 157. Yawing Moment at 85-Degree Shaft Angle - Three-Blade Propeller, Blade No. 109652.

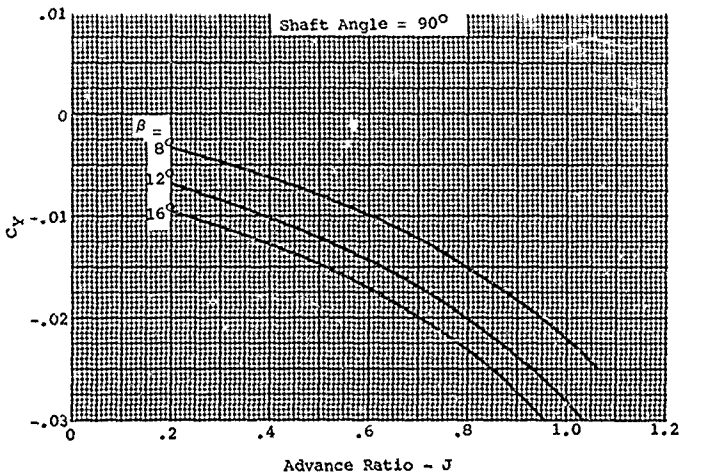


Figure 158. Yawing Moment at 90-Degree Shaft Angle - Three-Blade Propeller, Blade No. 109652.

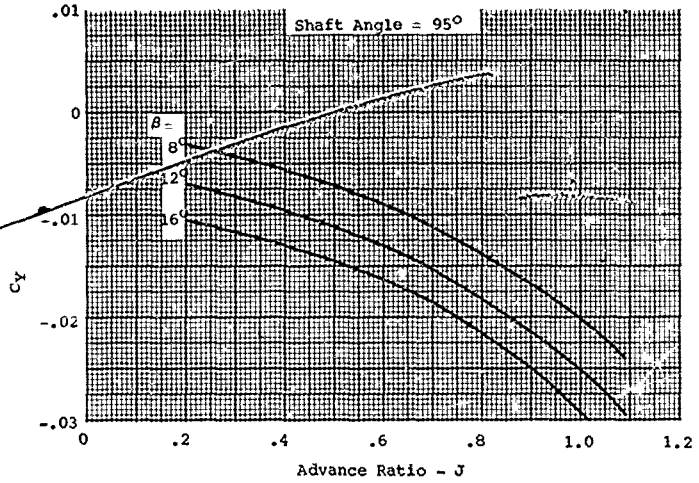


Figure 159. Yawing Moment at 95-Degree Shaft Angle - Three-Blade Propeller, Blade No. 109652.

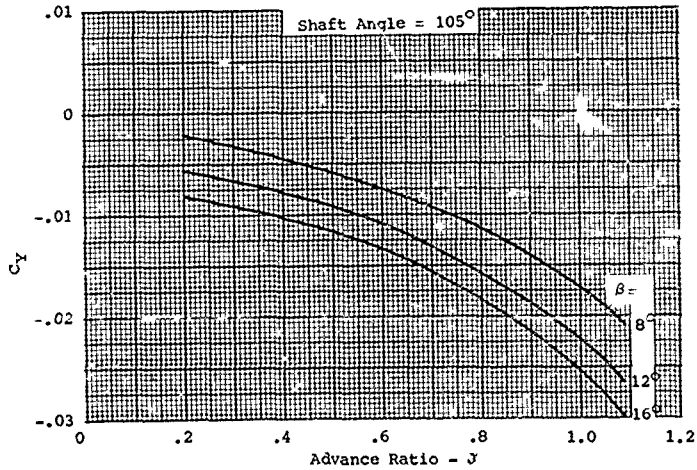


Figure 160. Yawing Moment at 105-Degree Shaft Angle - Three-Blade Propeller, Blade No. 109652.

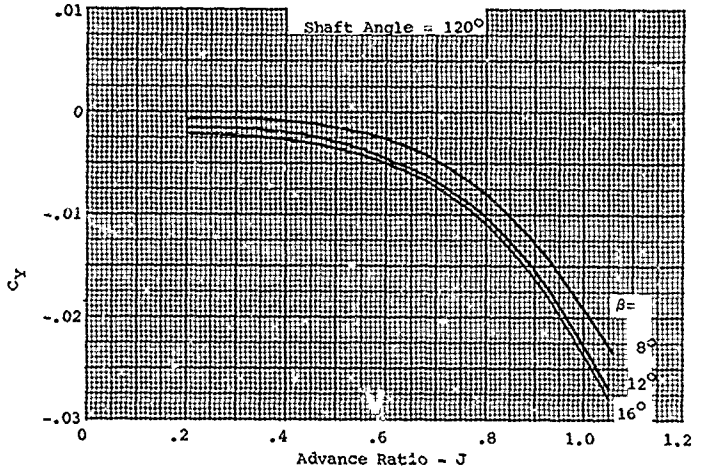


Figure 161. Yawing Moment at 120-Degree Shaft Angle - Three-Blade Propeller, Blade No. 109652.

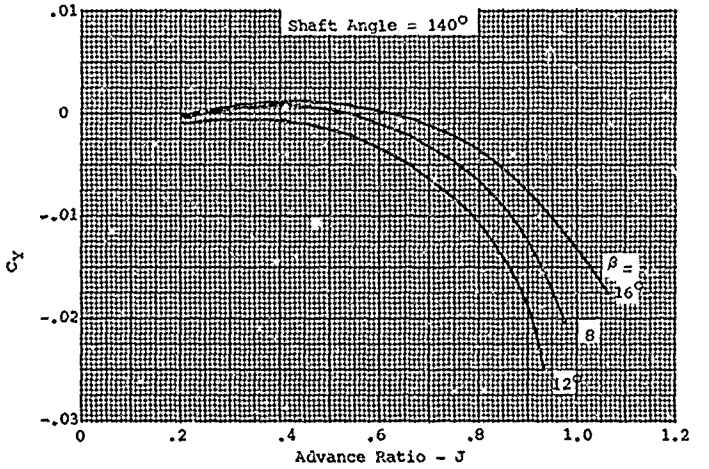


Figure 162. Yawing Moment at 140-Degree Shaft Angle - Three-Blade Propeller, Blade No. 109652.

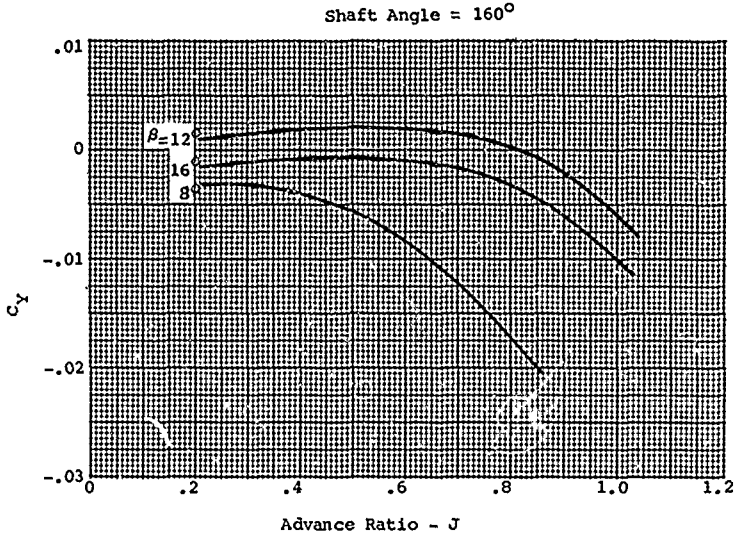


Figure 163. Yawing Moment at 160-Degree Shaft Angle - Three-Blade Propeller, Blade No. 109652.

## COWLINGS AND PROPELLER SPINNERS

Cowlings and spinners are used on propeller airplanes to provide a low-drag nacelle air induction system for cooling radial reciprocating engines. Streamline nose installations are used for liquid-cooled engines. In each of these installations, it is necessary to provide low external drag and, in the case of the radial engine, to have adequate cooling air at low drag. The importance of obtaining engine carburetor air at high ram pressure levels, in order to obtain maximum engine economy, is a separate item from cowl and spinner problems. A small scoop for carburetor air could be situated conveniently to the carburetor.

With the advent of the turboprop engine, however, comparatively large quantities of charge air must be handled for the engine at generally higher ram pressures. Now the entire cowling inlet or large scoop must be used to handle engine charge air, and great care must be taken in the cowling spinner selection to provide an air inlet that will give as high a ram pressure recovery as possible. Figure 164 shows the effect of ram pressure loss on SHP (shaft horsepower) and S.F.C. (specific fuel consumption) for a typical turboprop engine (300 mph @ 30,000 ft at about 2,000 SHP). For the older round-shank propellers, the ram pressure loss was sometimes on the order 10-25%. Thus, if these propeller shanks operated in front of the engine air inlet, a severe penalty in both power and specific fuel consumption could arise, as shown in Figure 164. For this reason, it is important to integrate the design on the cowling, spinner, and blade shank so that the best overall performance is obtained on the turboprop installation. The following discussion deals with the design concepts briefly and presents a working chart from which a preliminary cowling spinner design can be evaluated.

### Spinner Types and Selection

For the subsonic turboprop airplane, there are several nacelle configurations which have been used. These are shown in Figure 165. Arrangement (a) is an "E" or open-nose spinner used primarily for high-speed operation where propeller blade shanks cannot be made thin enough to give efficient operation. Very high ram pressure recovery may be obtained here, with the disadvantages of weight and maintenance. Configuration (b) indicates a "D" cowl and spinner. This configuration allows high ram efficiency if the cowl inlet width is sufficiently large to minimize spinner boundary layer effects, and blade shanks are operating with unseparated flow. The streamline nose type (c) is used where the turbine engine has an extension shaft. Wing engine air inlets used here are affected by propeller slipstream and generally can be designed for high ram recovery.

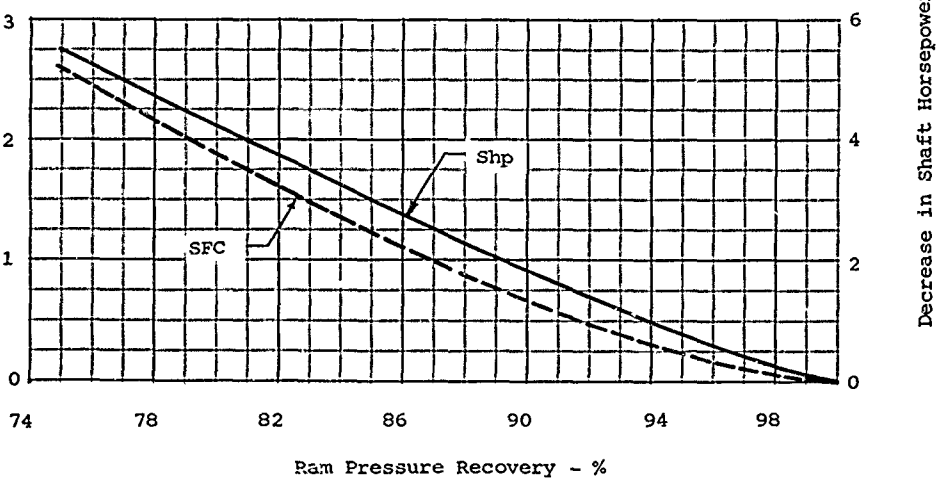


Figure 164. Ram Pressure Recovery Effects on Shaft Horsepower and Specific Fuel Consumption for a Typical Turboprop Engine.

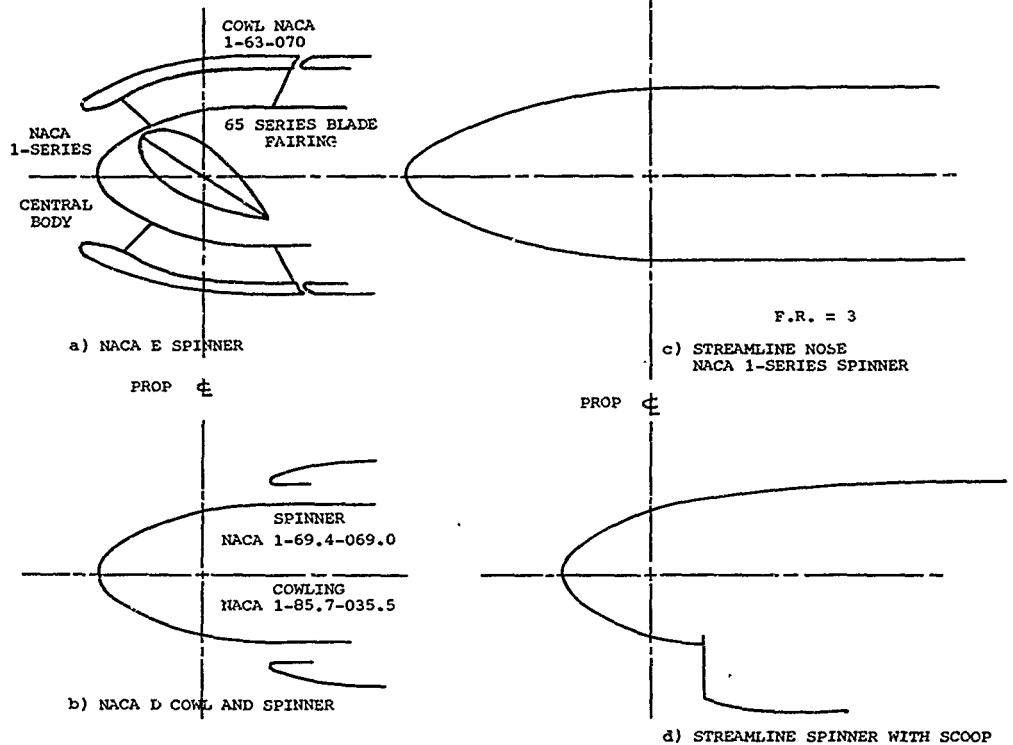


Figure 165. Typical Symmetrical Cowling and Spinner Types.

The underslung scoop type (d) may be used where the engine is offset from the propeller gearbox, allowing practically straight flow into the engine but beneath the streamline nose spinner. This arrangement allows high ram efficiency due to large depth of scoop. The scoop type inlet can also be placed above the centerline of the propeller for an over-wing engine installation. At high angles of attack, the ram recovery is generally less than with the underslung scoop inlet.

Selection of the actual body contours for an optimum cowling and spinner arrangement for a propeller turbine installation may be made analytically using one of a family of cowling and spinners evolved by the NACA and referred to as NACA 1-series bodies, reported in Reference 54 . These NACA 1-series bodies are cylindrical and have a contour derived by calculation and test to give a flat pressure distribution so desired for a high critical Mach number. Systematic testing of over 88 NACA 1-series cowling and spinner combinations was accomplished, and a cowling selection technique using this series-1 contour body was reported in Reference 55 . A complete table of coordinates and a cowl-spinner drawing showing their use are given in Figure 166. The NACA 1-series ordinates are always given in a form, for example, as NACA 1-85-050, where the 85 stands for diameter ratio d/D in % and d = cowl inlet or spinner maximum diameter and D = cowl diameter, and the 50 stands for length ratio x/D in % where x = cowl or spinner length.

Cowling and spinner selection charts for cowl angle of attack, $\alpha = 0^{o}$, are presented in Figures 167 and 168, from Reference 55. As an example of their use, assume that an E spinner is to be designed using Figure 167. The required information for spinner selection is the desired critical Mach number, $M_{cr}$, the cowl diameter D and desired length x, the engine air requirement m, and air inlet area. Assume the flight Mach number, $M_o = .75 = M_{cr}$ @ 35,000' and m = 45 lb/sec. A cowl diameter may be selected to clear the engine, or if the propeller hub is large with respect to the engine, a selection is made on the basis of hub and blade clearance requirements so that the net spinner duct area at the blade centerline is equal to or greater than the compressor or engine air inlet area. This will allow a straight or convergent duct aft to the engine which minimizes the duct loss. The inner spinner selected to cover the hub may be an NACA 1-series type. Blade fairings are used to cover round propeller shanks and to enclose the struts from inner spinner bulkhead to outer spinner shell. Symmetrical airfoil shapes are selected whose thickness is distributed on the local relative flow helix in the duct as determined by the duct local axial velocity and the rotational velocity at the particular sectional radius. Let the spinner diameter D = 50 inches and length X = 35 inches, or X/D = .70. We find the mass flow coefficient

$$X = \left(\frac{X}{D}\right)D \qquad X_S = \left(\frac{X_S}{D}\right)D$$

$$Y = \frac{D - d}{2} - r$$

For $r = 0.025Y$:

$$Y_S = \frac{D_S}{2} = \frac{\left(\frac{D_S}{D}\right)D}{2}$$

$$Y = \frac{D - d}{2.05} = \frac{D\ 1 - \frac{d}{D}}{2.05}$$

| ORDINATE RATIOS IN PERCENT | | | | | | | |
|---|---|---|---|---|---|---|---|
| $x/X$ or $x_S/X_S$ | $x/X$ or $y_S/Y_S$ | $x/X$ or $x_S/X_S$ | $x/X$ or $y_S/Y_S$ | $x/X$ or $x_S/X_S$ | $x/X$ or $y_S/Y_S$ | $x/X$ or $x_S/X_S$ | $x/X$ or $y_S/Y_S$ |
| 0 | 0 | 13.0 | 41.94 | 34.0 | 69.08 | 60.0 | 89.11 |
| .2 | 4.80 | 14.0 | 43.66 | 35.0 | 70.08 | 62.0 | 90.20 |
| .4 | 6.63 | 15.0 | 45.30 | 36.0 | 71.05 | 64.0 | 91.23 |
| .6 | 8.12 | 16.0 | 46.88 | 37.0 | 72.00 | 66.0 | 92.20 |
| .8 | 9.33 | 17.0 | 48.40 | 38.0 | 72.94 | 68.0 | 93.11 |
| 1.0 | 10.38 | 18.0 | 49.88 | 39.0 | 73.85 | 70.0 | 93.95 |
| 1.5 | 12.72 | 19.0 | 51.31 | 40.0 | 74.75 | 72.0 | 94.75 |
| 2.0 | 14.72 | 20.0 | 52.70 | 41.0 | 75.63 | 74.0 | 95.48 |
| 2.5 | 16.57 | 21.0 | 54.05 | 42.0 | 76.48 | 76.0 | 96.16 |
| 3.0 | 18.31 | 22.0 | 55.37 | 43.0 | 77.32 | 78.0 | 96.79 |
| 3.5 | 19.94 | 23.0 | 56.66 | 44.0 | 78.15 | 80.0 | 97.35 |
| 4.0 | 21.48 | 24.0 | 57.92 | 45.0 | 78.95 | 82.0 | 97.87 |
| 4.5 | 22.96 | 25.0 | 59.15 | 46.0 | 79.74 | 84.0 | 98.33 |
| 5.0 | 24.36 | 26.0 | 60.35 | 47.0 | 80.50 | 86.0 | 98.74 |
| 6.0 | 27.01 | 27.0 | 61.52 | 48.0 | 81.15 | 88.0 | 99.09 |
| 7.0 | 29.47 | 28.0 | 62.67 | 49.0 | 81.99 | 90.0 | 99.40 |
| 8.0 | 31.81 | 19.0 | 63.79 | 50.0 | 82.69 | 92.0 | 99.65 |
| 9.0 | 34.03 | 30.0 | 64.89 | 52.0 | 84.10 | 94.0 | 99.85 |
| 10.0 | 36.13 | 31.0 | 65.97 | 54.0 | 85.45 | 96.0 | 99.93 |
| 11.0 | 38.15 | 32.0 | 67.03 | 56.0 | 86.73 | 98.0 | 99.98 |
| 12.0 | 40.09 | 33.0 | 68.07 | 58.0 | 87.95 | 100.0 | 100.00 |
| Cowling nose radius: 0.025Y | | | | | | | |

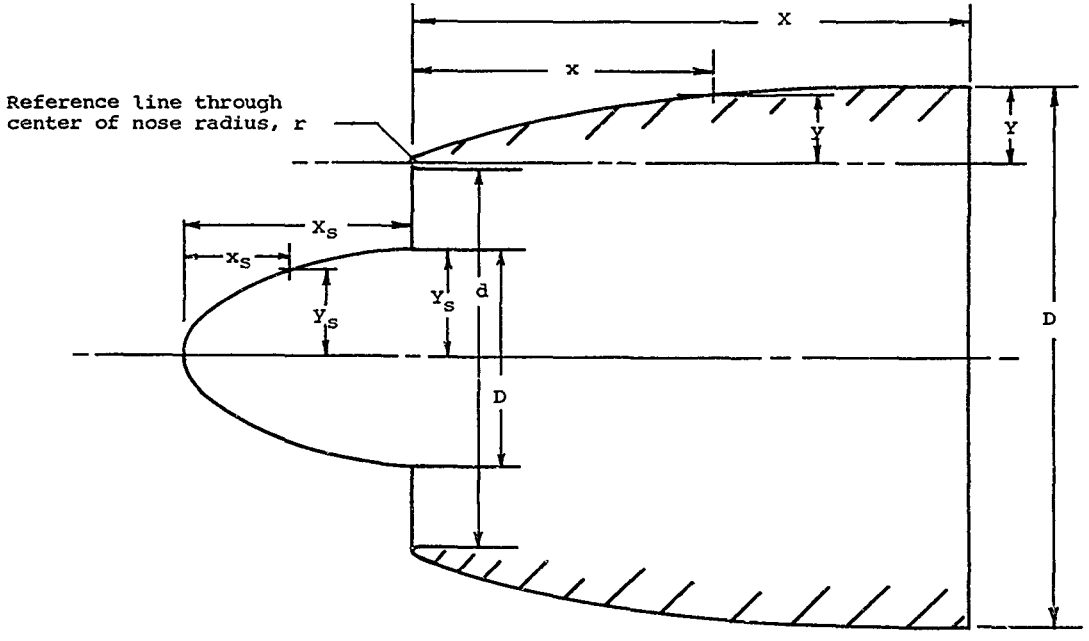


Figure 166. NACA Series 1 Cowling Ordinates.

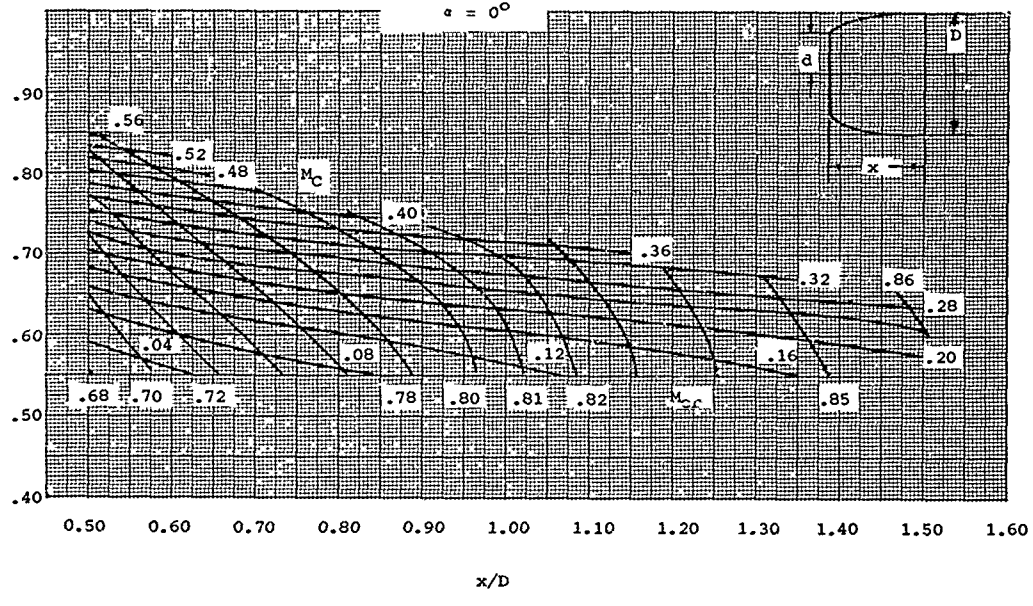


Figure 167. Selection Chart for NACA 1-Series Cowlings.

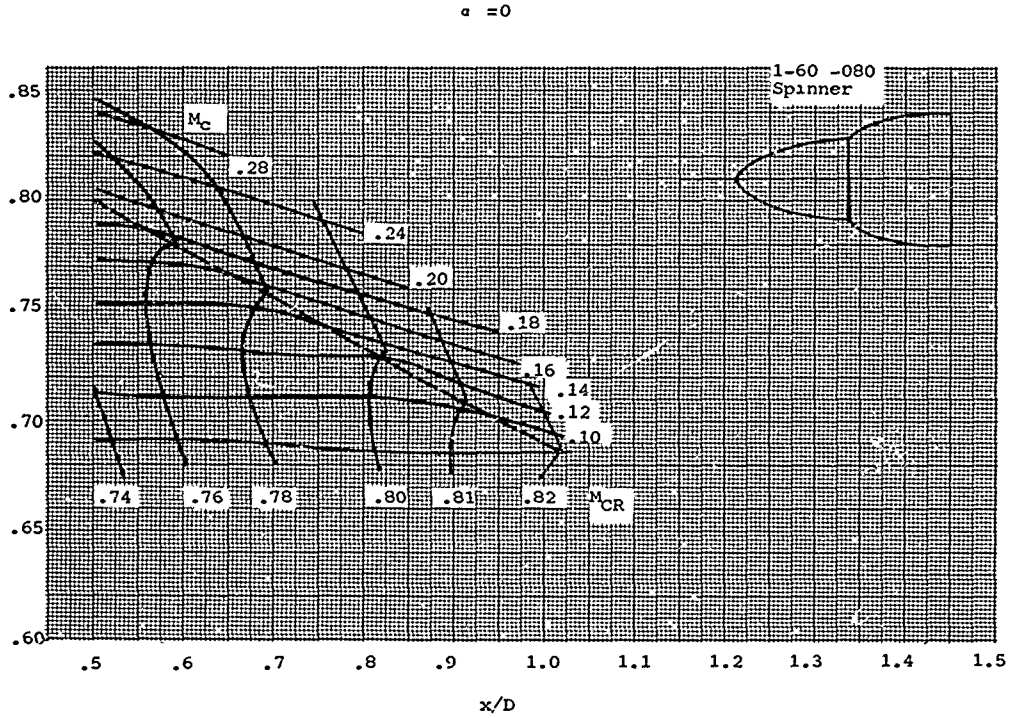


Figure 168. Selection Chart for NACA 1-Series Cowlings With NACA 1-60-080 Spinner Propeller Removed.

$$m_c = (m/\rho_o F V_o) = .191 \qquad (196)$$

where $M$ = required engine mass flow, slugs/sec
$\rho_o$ = air density, slugs/ft$^3$
$V_o$ = airplane velocity, fps
$F = \pi D^2/4$ = frontal area of nacelle, ft$^2$

Then, from Figure 167, we have d/D = 62.5 or the inlet diameter d = 31.25 inches. The spinner contour determined is designated NACA 1-62.5-070. This spinner will have $M_{cr} = 0.75$ @ $\alpha = 0^o$. The drag rise Mach number will be of the order .05 higher or $M_{dr}$ approximately 0.80. For angles of attack $\alpha > 0^o$, a larger d/D is required.

A similar procedure is followed in determining a "D" cowl and spinner combination for a turboprop engine. First, a spinner diameter is selected that will clear the propeller hub. The cowl lip and end of spinner are then assumed to be located between 1 and 2 inches behind the most rearward position of the propeller blade trailing edge. The cowling diameter to match the spinner is usually selected to be as small as possible for drag reasons and yet to give at least .075D inlet width to minimize spinner boundary layer effects, and generally allow matching the engine air inlet and cowl inlet areas. Assume, for example, the same conditions as for the E cowl above, and an NACA 1-60-080 spinner to cover the propeller hub. Then, using Figure 168 with x/D = 50 and $m_c = .191$, a d/D = 80 is obtained. The cowl-spinner designation is then NACA 1-60-080 spinner with NACA 1-80-050 cowling. This will give $M_{cr} = .75$ without propeller slipstream effects.

The procedure indicated above for selection of both E and D cowl spinner configurations neglects propeller effects. In general, the propeller increases the air velocity over the spinners and cowlings. This increase in velocity is a function of the propeller thrust being produced on an annular segment of air passing over the cowling or spinner. Propeller strip analysis using the proper local velocity field due to the nacelle body is used to calculate the thrust produced. The velocity increase due to the thrust is calculated using momentum theory, Equation (196).

For subsonic propellers, the slipstream effects on an E cowl are in general small, and the decrease in $M_{cr}$ is usually negligible. For the D cowl spinner configuration, the change in $M_{cr}$ is small but may be obtained at higher angles of attack due to the slipstream tending to reduce the effective inflow angle at the cowl lip. For typical supersonic propellers, slipstream effects may be appreciable. Here the slipstream velocities may $M_{cr}$ by as much as .05, depending of course on the blade loading.

In designing a streamline nose propeller installation, an NACA 1-series spinner is used that has proper hub clearance characteristics and a critical Mach number, $M_{cr}$. The procedure for determining $M_{cr}$ is given in Reference 56, where the surface pressure coefficients may be calculated by means of line or point source distributions representing the body in a potential flow. Corrections for compressibility are made by use of the Prandtl-Glauert rule by stretching the body in the stream direction by the factor $(1/\sqrt{1 - M^2})$, finding an incompressible pressure distribution for the stretched body, then correcting this pressure distribution back to compressible flow by the Prandtl-Glauert factors once again.

A streamline spinner body with a scoop design may be handled in two parts: first as a streamline nose to determine the desired characteristics of that portion of the installation, and then with the scoop handled as though it were an NACA D cowl and spinner combination. If the scoop operates with a thick surface boundary layer, special precautions must be taken in bleeding this low-energy air away from the scoop. Some indication of the proper design of the width-to-height ratio and edge contour characteristics is shown in Reference 58.

The design of an open-nose spinner having arbitrary shape to obtain a desired $M_{cr}$ and/or a particular velocity distribution at the propeller plane may be handled by methods indicated by Kuchemann, References 59-63. This method concerns the use of axially located ring source distributions duplicating the body with vortex rings of constant density over a stream surface extending to infinity, producing the required circulation. The design of a streamline nose spinner of arbitrary shape may be handled quite well by a method indicated above; Reference 58.

## Ram Pressure Recovery for Propeller Spinners

Ram pressure coefficient referred to previously is defined as $(H - P_o)/(H_o - P_o)$, where H is the total pressure at the station of interest, and $H_o - P_o$ are free-stream total and static pressures respectively. The significance of attaining high ram pressure coefficient is that the turbine engine compressor efficiency drops in direct ratio to a drop in ram pressure coefficient. This drop in compressor efficiency is transmitted through the remainder of the engine and appears as shown in Figure 164 as a drop in SHP and increase in S.F.C. Other effects may be associated with low ram pressure coefficients, such as large dissymmetry of flow at the compressor face causing compressor blade flutter.

Calculation of ram recovery at the engine air inlet may be made for these spinner configurations. For the E spinner designed in the prescribed manner and shown in Reference 54,

the duct losses arise mainly from skin friction. Possibility of flow separation from the blade fairings is minimized by keeping the sections reasonably thin (not over 35% h/b) using generous fillets, designing the fairing for operation at zero lift by laying its axis along the relative helical flow of duct air, and keeping the net duct area from diverging.

For the D cowl and spinner designed as indicated by NACA procedure, spinner losses will arise from skin friction alone. Propeller effects may be found by strip analysis of the portion of the blade operating in the charge air annulus. Here the flow-field velocities must be considered. Generally it is satisfactory to consider the velocity at the blade centerline. However, if the velocity gradient into the cowling is severe, flow separation may occur over the rear portion of the blade section. The cowl inlet losses back to the engine may be handled using standard duct loss calculations.

Ram pressure recovery for the scoop type installation may be analyzed by assuming that all forebody boundary layer air has been eliminated by suitable bleed or scoop. The importance of eliminating the boundary layer to maintain high ram recovery is shown on Figure 169. The ram pressure at the inlet will then be that due to free stream plus that effect due to the propeller, which may be obtained as indicated above by strip analysis. Generally, the scoop is deep enough to allow the propeller to give some pumping action.

Nacelle Flow Field and Propeller Design

The axial velocity field at or about the propeller plane for a cruise condition is affected for the most part by the forward portion of the nacelle or spinner. For certain spinners, the radial variation in axial velocity may be of sufficient magnitude to require its inclusion in propeller strip analysis.

Typical radial velocity distributions in the propeller plane are shown on Figure 169. For the E spinner and D cowl and spinner shown in Figure 170, the operating conditions are zero angle of attack and $M_o$ = .7 @ 35,000'. From Figure 170 it may be seen that it is possible to obtain a substantial velocity increase over the inboard portions of a propeller blade operating with an E spinner. These velocity variations spanwise on a propeller require a blade pitch different from that for free-stream operation as well as a possible change in h/b to allow more efficient operation of the blade shank at higher local velocities.

The flow fields shown in Figure 170 have been calculated by methods and data of Reference 58, using ring vortex sheets to represent the body in a potential flow. Compressibility

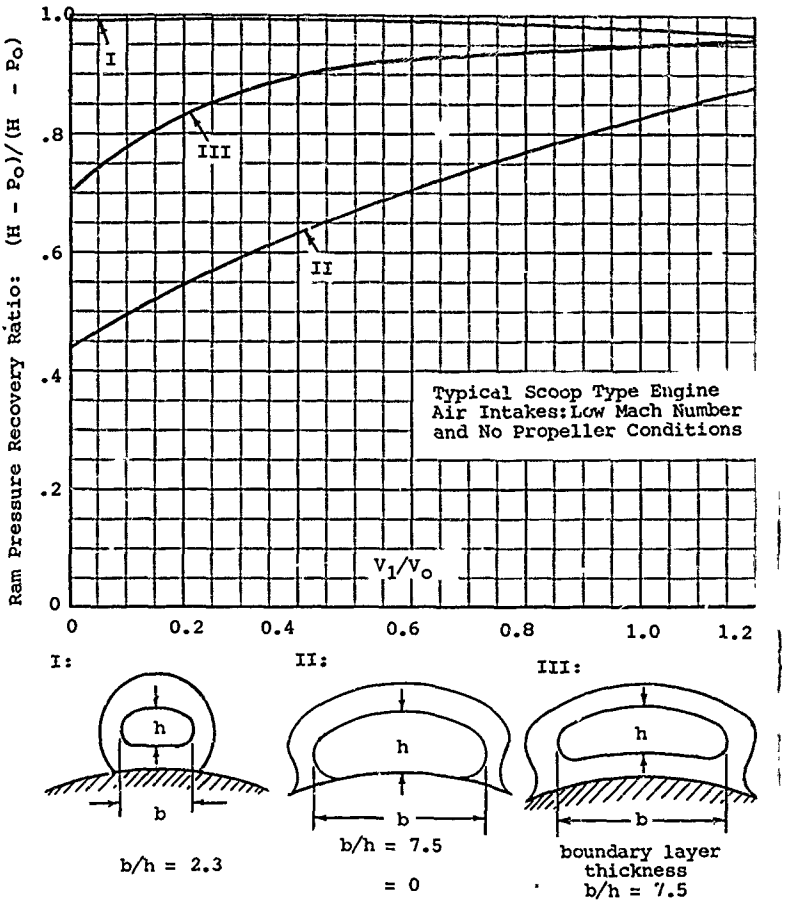


Figure 169. Pressure Recovery at Cowl Inlet.

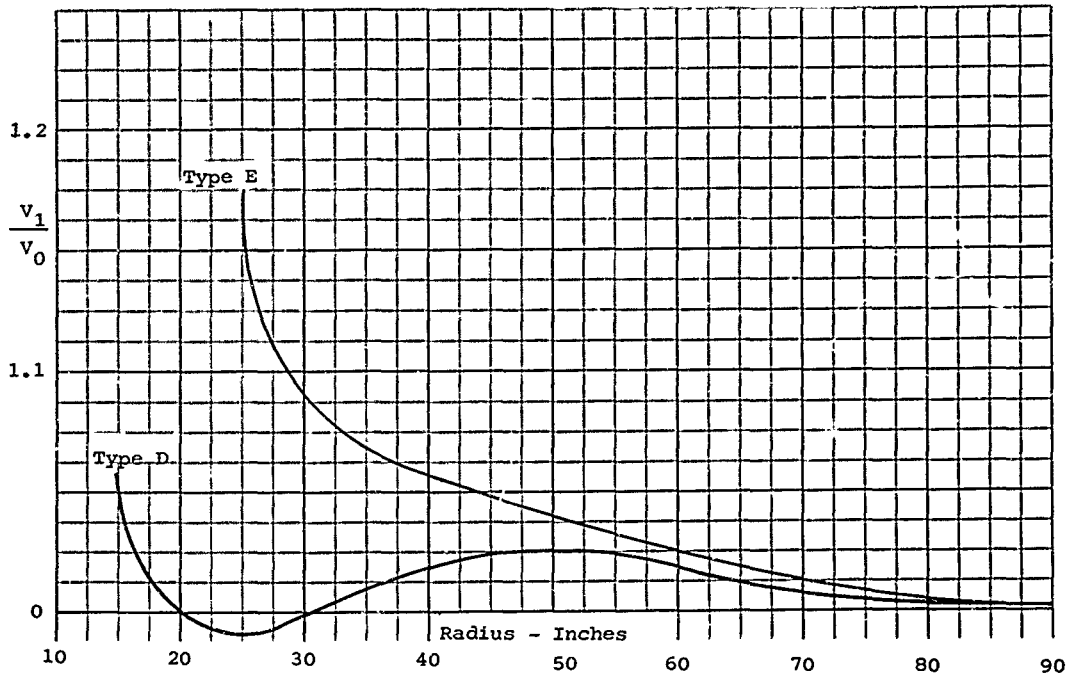


Figure 170. Radial Variation of Axial Velocity at Propeller Plane For "D" and "E" Type Cowls .

is taken into account by use of the Prandtl-Glauert rule. This method of determining axial velocity at the propeller plane has been checked at low Mach numbers by test; Reference 68.

From the preceding, it may be seen that the spinner flow field may seriously affect propeller operation. Thus, it becomes evident that this effect must be accounted for, either by altering spinner design or propeller pitch and h/b distribution, in order to arrive at an optimum configuration.

## CONCLUSIONS

From a review of the material presented in this volume, it is concluded that:

1. The technology is available to design high-performance propellers for subsonic conventional installations.

2. To achieve the desired performance, it is important to establish the proper criteria for the installation of the propeller.

3. The present propeller qualification procedures should be improved to assure a more adequate and reliable installation.

4. For high subsonic speeds of .7 Mach number or above, further work is necessary to improve calculation accuracy.

5. Further work is necessary to develop and refine the methods of designing and calculating the performance of V/STOL propellers operating at the zero velocity or hover condition.

6. With the application of some of the advanced airfoils, important reductions of propeller size, weight, and normal force can be realized. These reductions are especially important for propellers designed for STOL and V/STOL aircraft.

## REFERENCES CITED


1. Holford, F. R., and Kasley, J. H., FLIGHT TEST COMPARISON OF PROPELLERS WITH 836-14C2-18R1, 109390, 109394 AND 109498 BLADES IN LEVEL FLIGHT CONDITIONS, Curtiss Wright Corp., Propeller Division, C-1799, 6 March 1947, AT1-163-675.

2. Military Specification MIL-P-26366A, PROPELLER SYSTEMS, AIRCRAFT, GENERAL SPECIFICATION FOR, 15 November 1962.

3. CODE OF FEDERAL REGULATIONS, TITLE 14 - AERONAUTICS AND SPACE PARTS, 1-39, Revised as of January 1972.

4. Glauert, H., THE ELEMENTS OF AEROFOIL AND AIRSCREW THEORY, New York, The Macmillan Company, 1944.

5. Erickson, J. C., Jr., and Ordway, D. E., A THEORY FOR STATIC PROPELLER PERFORMANCE, Proceedings, CAL/USAAVLABS Symposium, Aerodynamics Problems Associated with V/STOL Aircraft, Volume I - Propeller and Rotor Aerodynamics 22, 24 June 1966.

6. Goldstein, Sydney, ON THE VORTEX THEORY OF SCREW PROPELLERS, Proceedings of the Royal Society of London, Ser. AV123, 1929.

7. Lock, C. N. H., APPLICATION OF GOLDSTEIN'S AIRSCREW THEORY TO DESIGN, R & M 1377.

8. Theodorsen, T., THEORY OF PROPELLERS, McGraw-Hill Book Company, 1948.

9. Crigler, J. L., APPLICATION OF THEODORSEN'S THEORY TO PROPELLER DESIGN, NACA Research Memorandum Number L8F30, 1948.

10. Frankl, THEORY OF THE AIRSCREW WITH A FINITE NUMBER OF BLADES IN CASE OF HIGH ADVANCE AND ROTATIONAL SPEEDS Part I, SUBSONIC VELOCITY OF THE AIRSCREW BLADE TIP, CAHI (Moscow), Technical Note (secret) Number 36 (1939).

11. Ginzel, J., THE AIRFOIL THEORY OF AIRSCREWS IN COMPRESSIBLE SUBSONIC FLOW FB 1915, March 1944, and AWA Report 44/A/05. British Reports and Translation Number 248.

12. Kondo, Kazuo, ON THE POTENTIAL-THEORETICAL FUNDAMENTALS OF THE AERODYNAMICS OF SCREW PROPELLERS AT HIGH SPEED, Journal of the Faculty of Engineering, University of Tokyo, Volume XXV, Number 1

13. Von Kármán, T., SUPERSONIC AERODYNAMICS - PRINCIPLES AND APPLICATIONS, Journal of the Aeronautical Sciences, 1947.

14. Kawada, S., CALCULATION OF INDUCED VELOCITY BY HELICAL VORTICES AND ITS APPLICATION TO PROPELLER THEORY. Report of the Aeronautical Research Institute Tokyo Imperial University Number 172, 1939.

15. Moriya, T., CALCULATION CHARTS OF INDUCED VELOCITY AND CALCULATION METHOD OF AERODYNAMIC CHARACTERISTICS OF PROPELLERS. The Journal of the Society of Aeronautical Science of Nippon, Volume 3, Number 9, January 1936.

16. Evvard, J. C., DISTRIBUTION OF WAVE DRAG AND LIFT IN THE VICINITY OF WING TIPS AT SUPERSONIC SPEEDS. NACA TN 1382.

17. Erickson, N. C., Ladden, R. M., Borst, H. V., and Ordway, D. E., A THEORY FOR VTOL PROPELLER OPERATION IN A STATIC CONDITION, Curtiss-Wright Corp., USAAVLABS Technical Report 65-69, U.S. Army Aviation Materiel Laboratories, Ft. Eustis, Virginia, October 1965, AD 623527.

18. Erickson, J. C., THEORETICAL AND EXPERIMENTAL INVESTIGATIONS OF V/STOL PROPELLER OPERATION IN STATIC CONDITION, Therm Advanced Research, Inc., USAAVLABS Technical Report 69-55, U.S. Army Aviation Materiel Laboratories, Ft. Eustis, Virginia, October 1969, AD 864117.

19. Theodorsen, T. T., THEORY OF STATIC PROPELLERS AND HELICOPTER ROTORS, 25th Annual Forum, American Helicopter Society, No. 326, May 1969.

20. Stack, John, "TESTS OF AIRFOILS DESIGNED TO DELAY THE COMPRESSIBILITY BURBLE, NACA T.R. 763.

21. Lindsey, W. F., Stevenson, D. B., and Daley, Bernard N., AERODYNAMIC CHARACTERISTICS OF 24 NACA SERIES AIRFOILS AT MACH NUMBER BETWEEN 0.3 AND 0.8. NACA T.N. 1546.

22. Abbott, Ira H., von Doenhoff, A. E., and Stivers, L. S., SUMMARY OF AIRFOIL DATA, Wartime Report Number L-560.

23. Van Dyke, Milton D., and Wibbert, Gordon A., HIGH-SPEED AERODYNAMIC CHARACTERISTICS OF 12 THIN NACA 6 SERIES AIRFOILS, NACA Report MR Number A5F27.

24. Ganzer, V. A., HIGH-SPEED TWO-DIMENSIONAL WIND TUNNEL TEST OF A SERIES OF RELATED AIRFOILS, Vol. I, and Bowes, G. M., Supplemental High-Speed Two-Dimensional BWT84, Volume I, Boeing Aircraft Company Reports Numbers D-7052 and D-8218.

25. Hood, Manley J., TESTS ON NACA 66, 2-420 AIRFOIL OF 5 FOOT CHORD AT HIGH SPEED, NACA ACR, September 1942.

26. Ilk, Richard J., HIGH-SPEED AERODYNAMIC CHARACTERISTICS OF FOUR THIN NACA 63 SERIES AIRFOILS.

27. Lindsey, Daley, and Humphreys, THE FLOW AND FORCE CHARACTERISTICS OF SUPERSONIC AIRFOILS AT HIGH SUBSONIC SPEEDS, NACA TN Number 1211.

28. Ferri, A., COMPLETED TABULATION IN UNITED STATES OF TESTS OF 24 AIRFOILS AT HIGH MACH NUMBERS (DERIVED FROM INTERRUPTED WORK AT GUIDONIA, ITALY IN THE 1.31 BY 1.74 FOOT HIGH SPEED TUNNEL).

29. Von Kármán, T., COMPRESSIBILITY EFFECTS IN AERONAUTICS, Journal of the Aeronautical Sciences, July 1941.

30. Ackeret, J., AIR FORCES ON AIRFOILS MOVING FASTER THAN SOUND, NACA TM No. 317.

31. Ivey, H. Reese, Stickle, George W., and Schuttler, Alberta, CHARTS FOR DETERMINING THE CHARACTERISTICS OF SHARP-NOSE AIRFOILS IN TWO DIMENSIONAL FLOW AT SUPERSONIC SPEEDS, NACA TN Number 1143.

32. Theodorsen, T., and Stickle, G. W., EFFECT OF A TRAILING-EDGE EXTENSION ON THE CHARACTERISTICS OF A PROPELLER SECTION, NACA Report ACR L4121.

33. Evans, A. J., and Liner, George, PRELIMINARY INVESTIGATIONS TO DETERMINE PROPELLER SECTION CHARACTERISTICS BY MEASURING THE PRESSURE DISTRIBUTION ON AN NACA 10 - (3)(08)(03) PROPELLER UNDER OPERATING CONDITIONS, 14 July, 1948.

34. Maynard, J. D., and Murphy, M. P., PRESSURE DISTRIBUTIONS ON THE BLADE SECTIONS OF THE NACA 10-(3)(066)-033 PROPELLER UNDER OPERATING CONDITIONS, 24 January 1950.

35. Gray, W. H., and R. M. Hunt, PRESSURE DISTRIBUTIONS ON THE BLADE SECTIONS OF THE NACA 10-(3)(049)-033 PROPELLER UNDER OPERATING CONDITIONS, RML9L23, 14 February 1950.

36. Johnson, P. J., PRESSURE DISTRIBUTIONS ON THE BLADE SECTIONS OF THE NACA 10-(3)(090)-03 PROPELLER UNDER OPERATING CONDITIONS, RM L50A26, 22 March 1950.

37. Evans, A. J., and Luchuk, W., PRESSURE DISTRIBUTIONS ON THE BLADE SECTIONS OF THE NACA 10-(5)(066)-03 PROPELLER UNDER OPERATING CONDITIONS, RM L50B21, 18 April 1950.

38. Steinberg and Milling, PRESSURE DISTRIBUTIONS ON THE BLADE SECTIONS OF THE 10-(0)(066)-03 PROPELLER UNDER OPERATING CONDITIONS, NACA RML50C03.

39. Haines & Diprose, THE APPLICATION OF THE CALCULUS OF VARIATIONS TO PROPELLER DESIGN WITH PARTICULAR REFERENCE TO SPITFIRE VII WITH MERLIN 61 ENGINES, RM 2083, 1943.

40. Wilson, ADVANCE CALCULUS, Ginn & Company.

41. Hartman, E. P., NEGATIVE THRUST AND TORQUE CHARACTERISTICS OF AN ADJUSTABLE PITCH METAL PROPELLER, NACA Report Number 464, 1933.

42. Hartman, E. P., and Biermann, D., THE NEGATIVE THRUST AND TORQUE OF SEVERAL FULL SCALE PROPELLERS AND THEIR APPLICATION TO VARIOUS FLIGHT PROBLEMS, NACA Report Number 641, 1938.

43. Gray, W. H., and Gilman, Jean, Jr., CHARACTERISTICS OF SEVERAL SINGLE AND DUAL ROTATION PROPELLERS IN NEGATIVE THRUST, NACA MR L5C07, March 1945, WR L-634.

44. Yaggy, Paul F., and Mort, Kenneth W, NASA TN D-1766, WIND TUNNEL TESTS OF TWO VTOL PROPELLERS IN DESCENT.

45. Yaggy, Paul F., and Rogallo, Vernon L., NASA TN D-318, A WIND-TUNNEL INVESTIGATION OF THREE PROPELLERS THROUGH AN ANGLE-OF-ATTACK RANGE FROM 0° TO 85°.

46. Delano, James B., and Morgan, Francis G., Jr., INVESTIGATION OF THE NACA 4-(3)(08)-03 TWO-BLADE PROPELLER AT FORWARD MACH NUMBERS TO 0.925, NACA RM L9106, T.F. 6048.

47. Delano, James B., and Carmel, Melvin M., INVESTIGATION OF THE NACA 4-(5)(08)-03 TWO-BLADE PROPELLER AT FORWARD MACH NUMBERS TO 0.925, NACA RM L9G06a, T.F. 5992.

48. Carmel, Melvin M., Morgan, Francis G., Jr., and Coppolino, Domenic A., EFFECT OF COMPRESSIBILITY AND CAMBER AS DETERMINED FROM AN INVESTIGATION OF THE NACA 4-(3)(08)-03 AND 4-(5)(08)-03 TWO-BLADE PROPELLERS UP TO FORWARD MACH NUMBERS OF 0.925, NACA RM L50D28, T.F. 6371.

49. Delano, James B., and Carmel, Melvin M., INVESTIGATION OF NACA 4-(0)(03)-045 AND NACA 4-(0)(08)-045 TWO-BLADE PROPELLERS FORWARD MACH NUMBERS TO 0.925, RM L9L06a. T.F. 6126.

50. Harrison, Daniel F., and Millilo, Joseph R., THE EFFECT OF THICKNESS RATIO ON SECTION THRUST DISTRIBUTION AS DETERMINED FROM A STUDY OF WAKE SURVEYS OF THE NACA 4-(0)(03)-045 AND 4-(0)(08)-045 TWO-BLADE PROPELLERS UP TO FORWARD MACH NUMBERS OF 0.925, NACA RM L51B05, T.F. 6831.

51. Carmel, Melvin M., and Millilo, Joseph R., INVESTIGATION OF THE NACA 4-(0)(03)-045 TWO-BLADE PROPELLER AT FORWARD MACH NUMBERS TO 0.025, NACA RM L50A31a, T.F. 6208.

52. Maynard, J. D., and Steinberg, S. THE EFFECT OF BLADE-SECTION THICKNESS RATIOS ON THE AERODYNAMIC CHARACTERISTICS OF RELATED FULL SCALE PROPELLERS AT MACH NUMBERS UP TO 0.65, NACA RM L9D29, June 6, 1949.

53. Gray, W. H., and Allis, A. E., AERODYNAMIC CHARACTERISTICS OF A TWO-BLADE NACA 10-(3)(12)-03 Propeller, NACA RM No. L8D01, August 1948.

54. Baals, Donald D., Smith, N. F., and Wright, J. B., THE DEVELOPMENT AND APPLICATION OF HIGH-CRITICAL-SPEED NOSE INLETS, NACA ACR No. L5F30a, L. MAL, 1945.

55. Nichols, Mark R., and Keith, Arvid L., INVESTIGATION OF A SYSTEMATIC GROUP OF NACA L-SERIES COWLINGS WITH AND WITHOUT SPINNERS, NACA RM No. L8A15.

56. Von Kármán, T., CALCULATION OF PRESSURE DISTRIBUTION ON AIRSHIP HULLS, NACA TM No. 574, July 1930.

57. Matthews, C. W., A COMPARISON OF THE EXPERIMENTAL SUBSONIC PRESSURE DISTRIBUTIONS ABOUT SEVERAL BODIES OF REVOLUTION WITH PRESSURE DISTRIBUTIONS COMPUTED BY MEANS OF THE LINEARIZED THEORY, NACA RM L9F28.

58. Smith, N. F., and Baals, D. D., WIND TUNNEL INVESTIGATION OF A HIGH-CRITICAL-SPEED FUSELAGE SCOOP INCLUDING THE EFFECTS OF BOUNDARY LAYER, NACA ACR No. L5B01a.

59. Kuchemann, D., and Weber, J., M.A.P. Volkenrode AVA Monographs, POWER UNIT DUCTS, PART 3, THE INFLOW, CADO ATI 49335.

60. Kuchemann, Dietrich, CONCERNING THE FLOW ABOUT RING-SHAPED COWLINGS OF FINITE THICKNESS, PART I, NACA TM 1325.

61. Kuchemann, Dietrich, and Weber, J., CONCERNING THE FLOW ABOUT RING-SHAPED COWLINGS PART II ANNULAR BODIES OF INFINITE LENGTH WITH CIRCULATION FOR SMOOTH ENTRANCE, NACA TM 1326.

62. Kuchemann, Dietrich, and Weber, J., CONCERNING THE FLOW ABOUT RING-SHAPED COWLINGS PART VI FURTHER MEASUREMENTS ON INLET DEVICES, NACA TM 1327.

63. Kuchemann, Dietrich, and Weber, J., CONCERNING THE FLOW ABOUT RING-SHAPED COWLINGS, PART IX, THE INFLUENCE OF OBLIQUE ONCOMING FLOW ON THE INCREMENTAL VELOCITIES AND AIR FORCES AT FRONT PART OF CIRCULAR COWLS, NACA TM 1329.

64. Reynolds, Robert M., and Sammonds, Robert I., SUBSONIC MACH AND REYNOLDS NUMBER EFFECTS ON THE SURFACE PRESSURES, GAP FLOW, PRESSURE RECOVER, AND DRAG OF A NON-ROTATING NACA 1-SERIES E-TYPE COWLING AT AN ANGLE OF ATTACK OF 0°, NACA RM No. A51E03.

65. UNPUBLISHED NACA AMES DATA 12'VDT WITH NACA 1-62.8-070 COWL AND NACA 1-46.5-047 SPINNER TOGETHER WITH NACA 4-(5)(05)-041 PROPELLER.

66. Keith, Arvid L., Bingham, G. J., and Rubin, Arnold J., EFFECTS OF PROPELLER-SHANK GEOMETRY AND PROPELLER-SPINNER-JUNCTURE CONFIGURATION ON CHARACTERISTICS OF AN NACA 1-SERIES COWLING-SPINNER COMBINATION WITH AN EIGHT-BLADE DUAL-ROTATION PROPELLER, NACA RM L51F26.

67. Shields, R. T., and Addams, D. H., PRESSURE MEASUREMENTS ON TWO PROPELLER BLADE ROOTS, R.A.E. T.N. No. Aero 1719.

68. Nichols, Mark R., and Pendley, Robert E., NACA Conference Report on High Speed Airplan Aerodynamics, A Compilation of Papers presented, Dec. 4-5, 1951, Part B, PERFORMANCE OF AIR INLETS AT TRANSONIC AND LOW SUPERSONIC SPEEDS.